GAP JUNCTION INTERCELLULAR COMMUNICATION PATHWAYS IN NORMAL AND DISEASED HUMAN VENTRICULAR MYOCARDIUM

NICHOLAS S PETERS

A thesis submitted to the University of London for the degree of Doctor of Medicine

Department of Cardiac Medicine,
National Heart and Lung Institute,
Dovehouse Street, London SW3 6LY
and
Department of Anatomy
and Developmental Biology,
University College London.

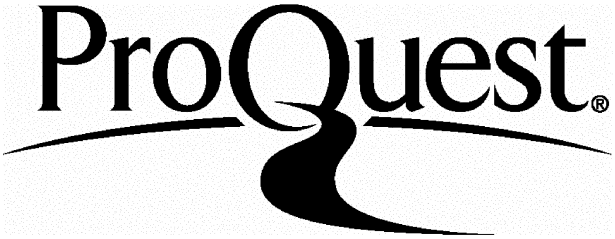

ACKNOWLEDGEMENTS

I would like to express my thanks to the following:

Dr. Nicholas J Severs (NHLI), whose expertise, unfailing encouragement and objective criticism guided me through this study.
Dr. Colin R Green (UCL), for his inspiration, guidance and willingness to assist.
Professor Philip A Poole-Wilson (NHLI), for his expert advice and enthusiastic support throughout.
Mr. Stephen Rothery (NHLI), whose excellent and diverse technical skills and his ability to teach me were fundamental to this work.
Messrs. John Pepper, Graeme Bennett, Christopher Lincoln and Sir Magdi Yacoub (Royal Brompton Hospital & NHLI), and to their patients, for their willingness to help and provide the tissue for examination.
Mr. Tim Robson (UCL), for technical assistance.
Drs. Federica Del Monte and Kenneth McLeod (NHLI), for their help with the guinea pig model, and Dr. Del Monte and Mr. Peter O'Gara for the myocyte isolation.
Drs. Eckhardt Olsen and Robert Anderson (NHLI), for their assistance with interpretation of experimental findings.
Dr. Robert Gourdie (UCL), for his inspiration, discussion and ideas.
The late Mr. Victor Aber (NHLI), for his willingness to give statistical advice.
Professor Andrew Wit (Columbia University, New York, USA) for his support and Mr. Issy Sanchez (Columbia Univ.) for technical assistance.

The British Heart Foundation for funding this project.
The National Heart, Lung and Blood Institute of the United States of America, and The Wellcome Trust for funding, and giving me the opportunity of working at Columbia University, New York, USA.

This work would not have been completed without the enthusiasm and support of my family and all my dear friends. My wife, Charlotte, was, and will remain, my greatest inspiration.

STATEMENTS

I confirm that the work presented herein is my own and forms part of a broader approach to the study of gap junctions by Nicholas J Severs and Colin R Green. Study 1 in Chapter 2 and the study in Chapter 5 were performed in collaboration with other members of the laboratory. The immunogold labelling was performed with the help of S Rothery, who took the original immunogold electron micrographs. The confocal micrographs were all taken by myself, and all the processing, examination and analysis of the human tissue, the analysis of the statistical data, and the micrograph printing were undertaken by myself. Assistance with the animal models used is acknowledged in the text.

The thesis submitted was written by me under the supervision of Dr NJ Severs and Professor PA Poole-Wilson.

Nicholas S Peters

PUBLICATIONS ARISING FROM THIS WORK

Peters NS, Green CR, Poole-Wilson PA, Severs NJ. Reduced content of connexin43 gap junctions in ventricular myocardium from hypertrophied and ischemic hearts. *Circulation* 1993;88:864-875.

Green CR, Peters NS, Rothery S, Severs NJ. Validation of immunohistochemical quantification by confocal laser scanning microscopy: a comparative assessment of gap junction size using confocal and ultrastructural techniques. *J Histochem Cytochem* 1993;41:1339-1349.

Severs NJ, Gourdie RG, Harfst E, Peters NS, Green CR. Intercellular junctions and the application of microscopical techniques: the cardiac gap junction as a case model [Review]. *J Microsc* 1993;169:299-328.

Smith JH, Green CR, Peters NS, Rothery S, Severs NJ. Altered patterns of gap junction distribution in Ischemic Heart Disease. An immunohistochemical study of human myocardium using laser scanning confocal microscopy. *American Journal of Pathology* 1991;139:801-821.

Papers submitted and in press:

Peters NS. The cardiac gap junction in myocardial ischemia. *Microscopy Research and Technique*; in press (1994).

Peters NS, Rowland E, Bennett GR, Green CR, Anderson RH, Severs NJ. The Wolff-Parkinson-White Syndrome: Cellular substrate for conduction in accessory atrioventricular pathways.

Peters NS, Severs NJ, Rothery S, Lincoln C, Yacoub M, Green CR. Changing distribution of intercellular junctions during postnatal human ventricular myocardial growth.

Abstracts:

Peters NS, del Monte F, MacLeod KT, Green CR, Poole-Wilson PA, Severs NJ. Increased cardiac myocyte gap-junctional membrane early in renovascular hypertension. *J Am Coll Cardiol* 1993;21:58A.

Peters NS, Severs NJ, Lincoln C, Yacoub M, Green CR. Changes in ventricular myocardial gap junction distribution in man throughout childhood. *J Am Coll Cardiol* 1993;21:219A.

Gourdie RG, Green CR, Thompson RP, Rothery S, Peters NS, Severs NJ. Confocal scanning laser microscopy applied to quantify gap junction expression and discriminate different connexin isoforms. *Proc. Microscopy Society of America* 1993;266-267.

Peters NS, Green CR, Poole-Wilson PA, Severs NJ. Gap junction quantification in normal, ischemic and hypertrophied human ventricular myocardium. *Circulation* 1992;86(suppl):I-425.

Peters NS, Rowland E, Bennett GR, Green CR, Anderson RH, Severs NJ. Cellular morphology and basis for conduction in accessory atrioventricular pathways in the Wolff-Parkinson-White Syndrome. *Circulation* 1992;86(suppl):I-425.

Peters NS, Green CR, Severs NJ. Changes in ventricular myocardial gap junction distribution in man throughout childhood. *Eur Heart J* 1992;13(suppl):406.

Peters NS, Green CR, Severs NJ, Poole-Wilson PA. Gap junction quantification in normal, ischaemic and hypertrophied human ventricular myocardium. *Eur Heart J* 1992;13(suppl):31.

Peters NS, Rowland E, Bennett GR, Green CR, Anderson RH, Severs NJ. Cellular morphology and basis for conduction in accessory atrioventricular pathways in the Wolff-Parkinson-White Syndrome. *Eur Heart J* 1992;13(suppl):80.

Severs NJ, Peters NS, Gourdie RG, Harfst E, Green CR. Cytochemical labelling of gap junctions in ischaemic heart disease - correlative investigation by laser scanning confocal microscopy and electron microscopy. In Megias-Megias L, Rodriguez-Garcia MI, Rios A, Arias JM (eds): Electron Microscopy 1992, vol 1. Secretariado de Publicaciones de la Universidad de Granada, 1992, 627-638.

Peters NS, Green CR, Poole-Wilson PA, Severs NJ. Altered gap junction distribution in ischemic heart disease. *Circulation* 1991; 84:II-497.

Peters NS, Smith JH, Green CR, Severs NJ. Altered patterns of gap junction distribution in ischaemic heart disease. *Eur Heart J* 1991;12(suppl):211.

AWARDS

2nd Prize - Young Investigator's Award, British Cardiac Society, 1992.
Gap junction quantification in normal, ischaemic and hypertrophied human ventricular myocardium.

ABSTRACT

The gap junction is the plasma membrane specialisation responsible for electrical and chemical coupling of cardiac myocytes. Despite increasingly recognised significance, there is a paucity of data on gap junctions in the human heart. This thesis reports studies in which confocal microscopic immunohistochemistry of the principal gap-junctional protein, connexin43, and electron microscopy, were used to characterise gap-junctional organisation in developing and adult human ventricular myocardium, and to investigate altered gap-junctional organisation as a possible contributing factor to electromechanical dysfunction in congenital, ischaemic and hypertrophic myocardial diseases.

In the adult left ventricle, connexin43-gap junctions occupy a surface area of 0.0051 $\mu m^2/\mu m^3$ myocardial volume, and are confined to the intercalated disks. In the neonate, connexin43-gap junctions are distributed over the entire surface of ventricular myocytes, with a progressive (linear) change to the adult pattern by six years of age.

Recurrently ischaemic adult ventricular myocardium has gap junctions confined to intercalated disks of normal number and appearance, but with a reduced gap-junctional surface area (0.0027 $\mu m^2/\mu m^3$), as also found in chronically hypertrophied ventricular myocardium (0.0031 $\mu m^2/\mu m^3$). When expressed **per myocyte**, there is a 30% reduction in gap-junctional content in ischaemic ventricle compared with normal. The pattern of junction distribution is grossly disturbed at the surviving borders of myocardial infarcts, both early and after healing. In the early hypertrophic response to acute renovascular hypertension in an animal model, left ventricular myocytes show a 35% increase in gap-junctional surface area per unit myocyte volume.

Hearts with congenitally anomalous morphology are not associated with abnormal gap junction distribution. The cells comprising accessory atrioventricular pathways have a junction distribution suggestive of ventricular myocytes, and of efficient coupling, despite vestigial contractile apparatus.

Although the pattern of myocardial gap junction distribution is severely disrupted at infarct borders, the site of origin of many clinical arrhythmias, there are no widespread disturbances of gap-junctional distribution patterns, in the diseases investigated. Quantitative alterations of gap-junctional expression, however, may be a hitherto unrecognised determinant of mechanical and arrhythmic dysfunction in diseased hearts.

SUMMARY OF CONTENTS

	page
Title page	1
Acknowledgements	2
Statements	3
Publications and Awards	4
Abstract	6
Contents table	7
List of tables	14
List of figures	16
PART I — Introduction	
Chapter 1: The gap junction	22
Chapter 2: General methodology and initial studies	54
PART II — Gap junctions in normal human ventricular myocardium	
Chapter 3: Gap junctions in adult human ventricular myocardium	75
Chapter 4: Changing distribution of intercellular junctions during human infancy	91
PART III — Alterations of gap junctions in myocardial disease	
Chapter 5: Gap junction distribution in surviving myocardium bordering healed infarcts	113
Chapter 6: Gap junction quantification per myocyte in intact ventricular myocardium	134
Chapter 7: Gap junction content of well-preserved ischaemic and hypertrophied myocardium	142
Chapter 8: Gap junction organisation and ultrastructure of myocytes of accessory AV pathways	158
PART IV - Animal studies	
Chapter 9: Gap junction distribution in surviving myocytes bordering canine four-day old infarcts	169
Chapter 10: Left ventricular myocardial gap-junctional content in response to acute renovascular hypertension in guinea pigs	177
Final Discussion and Conclusion	184
Appendix	186
References	199

CONTENTS

page

PART I - INTRODUCTION

CHAPTER 1: THE GAP JUNCTION 22

1.1 **The history of the study of gap junctions** 22
1.2 **Structural model of gap junctions in ventricular myocardium** 25
1.2.1 The ventricular myocyte 25
1.2.2 The intercalated disk 25
1.2.2a *The intercalated disk as part of the ventricular myocyte* 27
1.2.2b *The anchoring junctions* 28
1.2.3 The gap junction 29
1.2.3a *Distribution of gap junctions* 31
1.2.3b *Quantitative morphometry of gap junctions* 33
1.2.3c *Gap junction assembly and turnover* 36
1.2.3d *Packing of gap-junctional connexons* 37
1.2.4 Methods of study of the structure of cardiac gap junctions 38
1.3 **Physiological properties of gap junctions** 39
1.3.1 Permeability 40
1.3.1a *Regulation of gap junction permeability* 40
1.3.2 Direct measurements of cardiac gap-junctional conductance 41
1.3.2a *Factors affecting gap-junctional conductance* 43
- Cytosolic [Ca^{2+}] and pH
- Hypoxia
- Cytosolic ATP
- Transjunctional voltage
- n-Alkanols and volatile anaesthetics
- Fatty acids

1.4 **Molecular biology of gap junctions** 45
1.4.1 Immunolocalisation of connexins 46
1.5 **Gap junctional coupling and cardiac function** 47
1.5.1 Computer modeling 48
1.5.2 Gap junctions and cardiac electromechanical dysfunction 48
1.5.3 Pathophysiological role of gap junctions 49
1.6 **Clinicopathological basis and hypothesis behind this work** 52
1.6.1 Central hypothesis 52

CHAPTER 2: GENERAL METHODOLOGY AND INITIAL STUDIES 54

2.1 **Patient selection** 54
2.2 **Acquisition of tissue** 54
2.3 **Tissue preparation for immunohistochemistry** 55
2.3.1 Antibodies 55
2.3.2 Immunolocalisation 55
2.4 **Confocal laser scanning microscopy** 57
2.4.1 Quantitative analysis of confocal data 59

page

2.4.1a *Measurements of individual features in the image field* 59
2.4.1b *Automated total-field measurements* 59
2.4.2 Statistical analysis 59
2.5 **Electron microscopy** 60
2.5.1 Thin section electron microscopy 60
2.5.2 Freeze-fracture 60
2.6 **Production and immunolabelling isolated myocytes** 61
2.7 **INITIAL STUDY 1 - Comparing gap junction sizes measured by immunohistochemistry and freeze-fracture electron microscopy** 62
2.7.1 Introduction 62
2.7.2 Materials and methods 63
2.7.2a *Freeze-fracture electron microscopy* 63
2.7.2b *Connexin43 immunohistochemistry* 63
2.7.2c *Analysis of data* 63
2.7.3 Results 64
2.7.4 Interpretation and Conclusions 66
2.8 **INITIAL STUDY 2 - The effects of tissue fixation in Zamboni's solution on gap-junctional ultrastructure at thin section electron microscopy** 67
2.8.1 Introduction 67
2.8.2 Materials and Methods 68
2.8.3 Results 68
2.8.4 Interpretation and Conclusions 69
2.9 **General methodological problems** 69
2.9.1 Biopsy techniques 69
2.9.2 Tissue quantity 70
2.9.3 Glutaraldehyde contaminaton of fluorescence specimens 70
2.9.4 Cold cardioplegic solutions 72
2.9.5 Lipofuscin 72

PART II - GAP JUNCTIONS IN NORMAL HUMAN VENTRICULAR MYOCARDIUM

CHAPTER 3: GAP JUNCTIONS IN ADULT HUMAN VENTRICULAR MYOCARDIUM 75

3.1 **Introduction** 75
3.2 **Materials and methods** 76
3.2.1 "Normal" ventricular myocardium 76
3.2.2 Quantitative connexin43 immunohistochemistry 76
3.2.2a *Sizes of connexin43-gap junctions* 76
3.2.2b *Myocardial gap junction surface area* 77
3.2.2c *Intercalated disks per myocyte & myocardial cell arrangement* 77
3.2.3 Connexon packing density 78

page

3.3 **Results** 79
3.3.1 Histology and General Ultrastructure 80
3.3.2 Immunolabelled Connexin43 Gap Junction Distribution at Confocal Microscopy 80
3.3.3 Quantitative Characterization of Gap Junctions 80
3.3.3a *Analysis of Connexon Density in Freeze-fractured Gap Junctions* 80
3.3.3b *Size of Immunolabelled Gap Junctions* 84
3.3.3c *Gap-junctional Surface Area per Unit Volume of Tissue* 87
3.3.3d *Intercalated Disk Counts* 88
3.4 **Discussion** 88

CHAPTER 4: CHANGING DISTRIBUTION OF INTERCELLULAR JUNCTIONS DURING MYOCARDIAL GROWTH IN HUMAN INFANCY 91

4.1 **Introduction** 91
4.2 **Materials and methods** 92
4.2.1 Human myocardial samples 92
4.2.2 Immunolocalization of gap junctions and fasciae adherentes 93
4.2.2a *Antibodies* 93
- Gap junctions - Connexin43
- Fasciae adherentes - Cadherin
4.2.2b *Immunohistochemical labelling of tissue* 93
4.2.2c *Microscopy of immunolabelled tissue* 93
4.2.2d *Analysis of the Immunohistochemical data* 93
4.2.3 Electron microscopy 94
4.2.3a *Standard thin section electron microscopy* 94
4.2.3b *Electron microscopy of immunocytochemically labelled thin sections* 94
4.3 **Results** 95
4.3.1 Neonate 96
4.3.1a *Gap junctions* 96
4.3.1b *Fasciae adherentes* 97
4.3.2 Age 7 years 98
4.3.3 Intermediate ages 102
4.4 **Discussion** 105
4.4.1 Changing postnatal gap junction distribution 105
4.4.2 Relationship between gap junctions and fascia adherentes 107
4.4.3 Development of the intercalated disk 108
4.4.4 Ventricular growth 109
4.4.5 Potential implications for the timing of surgery in children 110

page

PART III - ALTERATIONS OF GAP JUNCTION ORGANISATION IN DISEASE

CHAPTER 5 - CONNEXIN43 GAP JUNCTION DISTRIBUTION IN SURVIVING MYOCARDIUM BORDERING HEALED INFARCTS. 113

5.1 **Introduction** 113
5.2 **Materials and methods** 114
5.2.1 Data collection from connexin43-immunolabelled tissue 115
5.3 **Results** 116
5.3.1 Histology and General Ultrastructure 117
5.3.2 Immunohistochemistry of connexin43 gap junctions 118
5.3.3 Ultrastructural Correlates of Altered Immunostained Gap Junction Distribution 123
5.3.4 Freeze-fracture of infarct border zone tissue 127
5.4 **Discussion** 128

CHAPTER 6 - DETERMINATION OF GAP-JUNCTIONAL CONTENT PER MYOCYTE IN INTACT VENTRICULAR MYOCARDIUM 134

6.1 **Introduction** 134
6.2 **Theoretical basis of deriving a cell volume index** 135
6.3 **Materials and methods** 137
6.3.1 Cell volume index from whole tissue 137
6.3.2 Cell volume measurement from isolated myocytes 138
6.4 **Results** 140
6.5 **Interpretation and Conclusions** 141

CHAPTER 7 - REDUCED CONNEXIN43 GAP JUNCTION IN WELL-PRESERVED VENTRICULAR MYOCARDIUM FROM ISCHAEMIC AND HYPERTROPHIED HUMAN HEARTS 142

7.1 **Introduction** 142
7.2 **Methods** 143
7.2.1 Myocardial samples 143
7.2.1a *Myocardium from Ischaemic Ventricle* 143
7.2.1b *Hypertrophied left ventricle* 144
7.2.2 Tissue processing 144
7.2.2a *Connexin43 gap junction quantification* 144
7.2.2b *Statistical analysis* 145
7.3 **Results** 145
7.3.1 Histology and General Ultrastructure 146

page

7.3.2 Immunolabelled Connexin43 Gap Junction Distribution at Confocal Microscopy 146
7.3.3 Quantitative Characterization of Gap Junctions 146
7.3.3a *Analysis of Connexon Density in Freeze-fractured Gap Junctions* 146
7.3.3b *Intercalated Disk Counts* 146
7.3.3c *Size of Immunolabelled Gap Junctions* 147
7.3.3d *Gap-junctional Surface Area per Unit Volume of Tissue* 147
7.3.4 Comparative index of myocyte volume in normal, ischaemic and hypertrophied hearts 150
7.3.5 Comparative index of gap-junctional surface area per myocyte 150
7.4 **Discussion** 152
7.4.1 The substrate for abnormal impulse propagation 153
7.4.2 Functional significance: correlating morphology with electrophysiology 154
7.4.3 Implications of results 156

CHAPTER 8 - GAP JUNCTION ORGANISATION AND CELLULAR ULTRASTRUCTURE OF ACCESSORY ATRIOVENTRICULAR PATHWAY IN THE WOLFF-PARKINSON-WHITE SYNDROME 158

8.1 **Introduction** 158
8.2 **Methods** 159
8.3 **Results** 160
8.3.1 Connexin43 immunohistochemistry and cellular morphology of accessory AV pathways 161
8.3.1a *Left-sided* 161
8.3.1b *Right-sided* 161
8.3.2 Ventricular and atrial myocardium 163
8.4 **Discussion** 165

PART IV - ANIMAL STUDIES

CHAPTER 9 - GAP JUNCTION DISTRIBUTION IN SURVIVING MYOCYTES BORDERING CANINE FOUR-DAY OLD INFARCTS 170

9.1 **Introduction** 170
9.2 **Materials and Methods** 170
9.3 **Results** 171
9.4 **Discussion** 172

page

CHAPTER 10 - LEFT VENTRICULAR MYOCARDIAL GAP-JUNCTIONAL CONTENT IN RESPONSE TO ACUTE RENOVASCULAR HYPERTENSION IN GUINEA PIGS 177

10.1 **Introduction** 177
10.2 **Materials and Methods** 178
10.2.1 Renal artery clipping 178
10.2.2 Blood pressure measurement 179
10.2.3 Myocyte isolation and immunolabelling 179
10.2.4 Quantitative analysis of isolated myocytes 179
10.3 **Results** 180
10.3.1 Confocal analysis of gap junctions 181
10.4 **Discussion** 182

11.1 FINAL DISCUSSION AND CONCLUSION 184

LIST OF TABLES

		page
Table 3.1	Details of "normal" ventricular myocardial biopsies.	79
Table 3.2	Mean gap-junctional area per unit myocyte volume in "normal" left ventricles.	88
Table 3.3	Mean gap-junctional area per unit myocyte volume in "normal" right ventricles.	88
Table 4.1	Details of myocardial specimens from infant and child hearts.	95
Table 4.2	Proportion of the total connexin43 label arrayed transversely in each heart.	105
Table 5.1	Details of ventricular myocardial specimens from ischaemic hearts.	116
Table 6.1	Mean myocyte volume measurements from isolated cells and whole tissue from each guinea pig.	141
Table 7.1	Details of hypertrophied left ventricular myocardial specimens.	145
Table 7.2	Mean gap-junctional area per unit myocyte volume in ischaemic left ventricle.	148
Table 7.3	Mean gap-junctional area per unit myocyte volume in hypertrophied left ventricle.	149
Table 7.4	Results of quantitative confocal morphometric analysis of normal, ischaemic and hypertrophied myocardium.	151
Table 10.1	Details of guinea pigs at sacrifice.	180
Table 10.2	Mean confocal measurements made from isolated myocytes.	181
APPENDIX		
Table A1	Confocal data from "normal" LV myocardium.	187
Table A2	Confocal data from "normal" RV myocardium.	188
Table A3	Myocyte volume measurements from isolated cells and whole tissue from each guinea pig.	189
Table A4	Confocal data from ischaemic LV myocardium.	191
Table A5	Confocal data from hypertrophied LV myocardium.	192

		page
Table A6	Confocal derivation of gj area/cell in "normal" LV.	193
Table A7	Confocal derivation of gj area/cell in "normal" RV.	194
Table A8	Confocal derivation of gj area/cell in ischaemic LV.	195
Table A9	Confocal derivation of gj area/cell in hypertrophied LV.	196
Table A10	Cell volume and gj area in control guinea pigs.	197
Table A11	Cell volume and gj area in hypertensive guinea pigs.	198

LIST OF FIGURES

page

Figure 1.1. Light micrograph of toluidine blue-stained normal human ventricular myocardium sectioned longitudinally. 26

Figure 1.2. Diagram of an intercalated disk in mammalian ventricular myocardium 27

Figure 1.3. Thin section electron micrograph of longitudinally-sectioned normal human ventricular myocardium 28

Figure 1.4. Diagram and high power thin section electron micrograph of transected gap junction showing septilaminar structure. 30

Figure 1.5. Diagram of a connexon and the arrangement of the connexin molecule in the cell membrane. 31

Figure 1.6. Diagram of gap junction showing potential lines of membrane cleavage when the tissue is freeze-fractured. 32

Figure 1.7. Electron micrograph of freeze-fracture replica of myocytes in which the fracture plane has penetrated into the cell interiors. 33

Figure 1.8. Freeze-fracture electron micrograph of an entire gap-junctional domain (gj) in the membrane of a myocyte in left ventricular myocardium from a patient with the Wolff-Parkinson-White syndrome. 34

Figure 1.9. Representative traces of whole-cell patch-clamp studies (adapted from Jongsma and Gros, 1991). 42

Figure 1.10. Schematic diagrams showing what is meant by uniform and non-uniform anisotropic propagation of the electrical impulse in ventricular myocardium. 49

Figure 2.1. Summary of the derivation of the "HJ" antibody used for gap-junctional immunolocalisation. 56

Figure 2.2. The principle of confocal technology. 58

Figure 2.3. Diagrammatic illustration of the potential problem of attempting to quantify data in the projection of an image series acquired in an inappropriate plane of section. 64

Figure 2.4. Histograms comparing the frequency distributions of long-axis lengths of gap junctions measured in rat ventricle using freeze-fracture and confocal microscopic techniques. 65

page

Figure 2.5. Thin section electron micrographs of longitudinally-sectioned rat left ventricle fixed by immersion in Zamboni's solution for two hours before fixation in glutaraldehyde. 68

Figure 2.6. Low power thin section electron micrographs of healthy myocardium biopsied by the needle (Trucut) technique. 71

Figure 3.1. The set-up of the confocal microscope to acquire data for quantification. 78

Figure 3.2. Typical light and thin section electron microscopic features of normal ventricular myocardium. 81

Figure 3.3. Immunolocalisation of gap junctions in longitudinally-sectioned normal human left ventricle labelled for connexin43. 82

Figure 3.4. Immunolocalisation of gap junctions in transversely-sectioned normal human left ventricle labelled for connexin43. 83

Figure 3.5. Thin section electron micrograph showing the characteristic long run of gap-junctional membrane at the edge of an intercalated disk. 84

Figure 3.6. A 10-image optical section series acquired from connexin43-labelled transversely-sectioned normal human myocardium for the quantification procedure. 85

Figure 3.7. Electron micrograph of freeze-fracture replica showing the densely packed connexon particles of an entire junctional plaque. 86

Figure 3.8. Plot of connexon surface density vs. gap junction plaque area in plaques up to $1\mu m^2$. 86

Figure 3.9. Frequency distribution of pooled long axis measurements of 860 labelled junctions in normal left ventricle determined by confocal microscopy. 87

Figure 3.10. Laser scanning confocal micrograph of a projection image of a single isolated myocyte labelled for connexin43 89

Figure 4.1. A single confocal optical slice of longitudinally-sectioned connexin43-immunolabelled right ventricular myocardium from a 4 week infant. 96

Figure 4.2. Confocal images of connexin43-immunolabelled right ventricular myocardium from a 4 week infant. 97

Figure 4.3. Standard thin section electron micrographs showing interfaces between longitudinal surfaces of adjacent ventricular myocytes. 98

Figure 4.4. Portion of convoluted plasma membrane from the longitudinal surface of a ventricular myocyte. 99

page

Figure 4.5. Thin section electron micrograph of connexin43 immunogold labelled ventricular myocardium from a 9-week infant 100

Figure 4.6. Confocal micrograph of longitudinally-sectioned ventricular myocardium from a four-week infant immunolabelled for cadherin. 100

Figure 4.7. A single confocal optical slice of longitudinally-sectioned connexin43-immunolabelled right ventricular myocardium from a 7 year old child. 101

Figure 4.8. Confocal micrograph of longitudinally-sectioned ventricular myocardium from a seven-year old child immunolabelled for cadherin. 102

Figure 4.9. Thin section electron micrograph of cadherin immunogold labelled ventricular myocardium 102

Figure 4.10. A single confocal optical slice of longitudinally-sectioned connexin43-immunolabelled right ventricular myocardium from a 4 year old child. 103

Figure 4.11. Low and high power thin section electron micrographs of ventricular myocardium from a 2 year old 104

Figure 4.12. Graph showing the change with age of the proportion of connexin43 gap junction that is distributed at the intercellular abutments lying transverse to the long axis of the myocytes. 106

Figure 5.1. Light micrograph of toluidine-stained interface between partial-thickness infarct scar and surviving epimyocardium 117

Figure 5.2. Thin section electron micrographs showing abnormalities of the contractile apparatus in the myocytes bordering healed myocardial infarcts. 119

Figure 5.3. Gap junction distribution in myocytes bordering healed myocardial infarcts, as seen by laser scanning confocal microscopy of immunolabelled tissue. 120

Figure 5.4. A demonstration of the apparent surface positioning of the abnormal junction distribution at the infarct border zone. 121

Figure 5.5. Low power projection image of longitudinally-sectioned connexin43-immunolabelled myocardium distant from an infarct, containing a transected artery and vein. 122

Figure 5.6. Frequency distribution of immunolabelled junction long-axis lengths pooled from infarct border zone myocytes with disrupted gap-junctional organisation, from well-preserved myocardium distant from infarction, and from normal myocardium. 124

Figure 5.7. Thin section electron micrographs of intercalated disk abnormalities in infarct zone myocytes. 125

page

Figure 5.8. Dissociation of the adhering junctions in intercalated disks of degenerated border zone myocytes. 126

Figure 5.9. Thin section electron micrographs showing abnormal gap-junctional contacts between infarct border zone myocytes. 127

Figure 5.10. Freeze-fracture electron micrograph of an infarct border zone region. 129

Figure 5.11. Higher power freeze-fracture electron micrograph at a site of abutment between myocytes in an infarct border zone region 130

Figure 6.1. Derivation of the cell volume index. 136

Figure 6.2. Laser scanning confocal microscopic images of a single isolated myocyte labelled for connexin43. 139

Figure 6.3. Graph comparing mean cell volumes of single isolated ventricular myocytes with the cell volume index derived from the whole ventricular tissue of each guinea pig. 140

Figure 7.1. Electron micrograph of a freeze-fracture replica showing an entire gap-junctional domain of normal appearance in a small portion of membrane fracture at the tip of a cross-fractured plicate fold of an intercalated disk from an ischaemic heart. 147

Figure 7.2. Plot of connexon surface density vs. gap junction plaque area in plaques up to $1\mu m^2$ in ventricular myocardium from ischaemic hearts. 148

Figure 7.3. Frequency distribution of immunolabelled junction long-axis lengths pooled from ischaemic ventricular myocardium distant from infarction. 149

Figure 7.4. Representation of data produced by groups studying computer models of myocardial electrophysiology 155

Figure 8.1 Light and general electron microscopic features of the accessory atrioventricular pathways. 162

Figure 8.2. Low-power scanning laser confocal micrographs of longitudinally-sectioned ventricular and pathway myocardium, immunolabelled for connexin43. 163

Figure 8.3. Thin-section electron micrographs of longitudinally-sectioned right paraseptal accessory pathway 164

Figure 8.4. Thin section electron micrographs of longitudinally-sectioned myocardium from left ventricle (A) and right atrium (B) from Case 3 165

page

Figure 9.1. Low power confocal micrograph of longitudinally-sectioned connexin43-labelled canine ventricular myocardium from the posterior wall of the left ventricle. 171

Figure 9.2. Subepicardial myocardium sectioned parallel with the epicardium in the region of four-day old infarction. 172

Figure 9.3. Confocal micrographs of infarct border zone. 174

Figure 9.4. Sections perpendicular to the epicardium, showing longitudinally-sectioned subepicardial myocardium in the region of infarction. 175

PART I - INTRODUCTION

CHAPTER 1 - THE GAP JUNCTION

1.1 The history of the study of gap junctions

In the 1870s, the first experiments were described in which frog myocardium dissected into a number of small interconnected pieces was able to transmit an electrical stimulus to all parts (Engelmann, 1875). In a subsequent report, Engelmann (1877) further noted that cells injured during the dissection became rapidly inexcitable, concluding that transmission of the cardiac electrical impulse occurred directly between the myocardial cells, and that injury to a cell caused it to seal off from its neighbours. He supported this conclusion by demonstrating that the injury potential measured at the cut tissue surface, which through cytoplasmic continuity reflected the intracellular potential of adjacent healthy cells, diminished within minutes after cutting. Thus, he described in functional terms how healthy myocardium behaved as an electrically continuous tissue. This evidence was of interest to the histologists of the time, who were discovering that the heart was not a structural syncytium, but consisted of discrete cells (Eberth, 1866), thereby posing an apparent contradiction to Engelman's results. The explanation remained unresolved for more than half a century.

In the 1950s, technological advances enabled detailed investigation of myocardium, both structurally by electron microscopy, and functionally by intracellular microelectrode techniques. The demonstration of the complete and continuous plasma membrane surrounding cardiac myocytes by Sjöstrand and Andersson (1954), in conjunction with the high space constant signifying a low resistance to passive conduction through the cytoplasmic pathway of a sheet of contiguous cells, as demonstrated by Weidmann (1952), only seemed to confirm the contradiction. However, findings such as these led to the necessary concept of a low resistance membrane specialisation responsible for electromechanical coupling in myocardium, with initial experimental investigation of this concept (Loewenstein, 1981) being applied predominantly to membranes derived from mammalian liver.

Investigating the structural properties of this specialised membrane structure has required refinement and development of electron microscopic techniques. Thin section electron microscopy demonstrated regions of close approximation of electron-dense

regions of the plasma membranes of adjacent cells. Careful examination revealed that the extracellular space, although narrow, is not obliterated, hence the name given to this specialised region — the "gap junction" (appearing in the older literature as the "nexus", a word originally defined as early as 1663 as the bond or link between two or more things). Barr, Dewey and Berger (1965) published a paper linking electrical interaction between cardiac myocytes with gap junctions, and work by Revel and Karnovsky (1967) was a landmark in defining the ultrastructure of the cardiac gap junction.

Freeze-fracture electron microscopy, in which membrane lipid bilayers are cleaved apart by a plane of fracture in frozen tissue, demonstrated the integral transmembrane protein particles, named connexons, that exist within gap-junctional regions of the cell membrane viewed en face (Rash and Hudson, 1979). X-ray diffraction showed the hexameric structure of the connexon, which is composed of six subunits (Makowski et al. 1977; Makowski, 1988), each consisting of a single protein molecule, later named a connexin (Zimmer et al. 1987; Milks et al. 1988). The arrangement of the connexins around the central pore has been thought to confer the gating properties of the channel, but the mechanism of gating has never been determined (Makowski, 1988). Unwin and Ennis (1984) suggested that the central pore can be closed simply by a twisting of the connexon within the lipid bilayer.

In parallel with the evolving structural knowledge of the gap junction, the physiological properties were being elucidated. Most of the early characterisation was carried out in invertebrate and non cardiac tissues, with major contributions by Furshpan and Potter (1959), and more recently by Loewenstein (1981), Bennett (1977) and his coworkers (Spray et al. 1985). Before the development of the patch clamp techniques that would enable direct evaluation of gap junction function, these groups and others used tracer molecules and dye transfer (Imanaga, 1974), along with indirect electrophysiological techniques (Weidmann, 1952; Ypey et al. 1979), to determine junctional conductance, selectivity and permeability (Socolar and Loewenstein, 1979). Even at this stage, changes in gap-junctional permeability with the metabolic state of the tissue were demonstrated (Délèze, 1970), and the importance of gap junctions in metabolic coupling of cells became apparent (Spray et al. 1985; Noma and Tsuboi, 1986). Also recognised was another important role played by gap junctions; that is, in development, tissue patterning and regulation of cell growth (Warner et al. 1984; Bode et al. 1987; Fraser et al. 1988; Green, 1988), presumed to be due to intercellular flux of morphogenetic chemical factors via gap-junctional channels.

In the mid 1980s, whole cell patch clamp techniques enabled direct measurement

of the conductance of gap junctions and of single junctional channels (pairs of abutting connexons) (Neyton and Trautmann, 1985; Neyton and Trautmann, 1986; Weingart, 1986), since when, the properties of gap junctions between cells isolated from many tissues throughout the animal kingdom have been characterised.

The consequent discovery of the heterogeneity of gap junction behaviour in different tissues and different animals was parallelled in the 1980s by advances in molecular biology that provided a possible structural basis for the functional variation. Deduction of the amino acid sequence of the 32-kDa liver connexin (so-called connexin32) (Paul, 1986), was followed by identification of what continues to be a growing family of connexin isoforms (Beyer et al. 1987; Kistler et al. 1988; Zhang and Nicholson, 1989; Ebihara et al. 1989; Kanter et al. 1992), with different behavioural properties. The identity of a 43-kDa connexin (connexin43), the principal gap-junctional protein in mammalian heart, was reported in 1987 (Beyer et al.). At the time of starting the work in this thesis in 1991, connexin43 was the only known mammalian cardiac connexin, and although it remains the principal and most abundant connexin in the heart (Kanter et al. 1992), two further cardiac isoforms, connexin40 and connexin45, have recently been reported in canine myocardium (Kanter et al. 1992).

In the late 1980s, knowledge of the DNA sequences of this growing connexin family had greatly enhanced the ability to investigate both morphological and functional properties of gap junctions. Functionally, manipulation of the amino acid sequences in appropriate models is being used to identify the regions of the molecule that confer its different physiological properties (Moreno et al. 1990; Spray et al. 1992). Morphologically, molecular biology has identified the homology that exists between the different connexin types, and the degree to which the basic structure has been conserved in evolution (Zimmer et al. 1987; Beyer et al. 1987). Despite considerable homology, there are distinct differences between different isoforms. By exploiting these differences using antibodies raised to synthetic peptides matching heterologous portions of the connexin molecule, immunohistochemical and immunocytochemical techniques enable study of the arrangement of connexin types within gap junctions, cells and tissues throughout the animal kingdom (Dupont et al. 1988; Milks et al. 1988; Ebihara et al. 1989; Zhang and Nicholson, 1989; Dermietzel et al. 1989). Some connexins for which DNA sequences have been reported, however, have yet to be localised.

A number of recent articles have comprehensively reviewed the extent of knowledge regarding the structure (Forbes and Sperelakis, 1985; Navaratnam, 1987; Severs, 1990;

Page, 1992), function (Spray and Burt, 1990; Jongsma and Gros, 1991; Page, 1992) and molecular biology (Page, 1992) of gap junctions. The current authoritative review on the cardiac gap junction is that of Page (1992). What will follow in this chapter, is a brief review of the salient characteristics of gap junctions, concentrating mainly on the morphological aspects in the mammalian heart.

1.2 **Structural model of gap junctions in ventricular myocardium**

1.2.1 The ventricular myocyte

Working ventricular myocytes (by which is meant the normal contractile ventricular myocyte, as opposed to the more scarce specialised myocytes of the impulse generation and conduction system), are characteristically about 80 to 140 μm in length, and 10 to 40 μm in width (Sommer and Jennings, 1986; Severs, 1989b). The contractile myofibrils that fill the cell are arranged in parallel bundles, accounting for the elongated shape of the cardiac myocyte. However, as the length of the myofibril bundles varies, the myocyte has multiple step-like blunted ends along its length, at which the intercalated disks are found (Fig 1.1), lying predominantly in the plane perpendicular to the long axis of the cell (Sommer and Jennings, 1986; Navaratnam, 1987; Severs, 1989b; Severs et al. 1989). An individual disk may extend over a number of closely-adjacent "steps" (terminations of myofibril bundles) and, therefore, may not lie in a single transverse plane. Each intercalated disk is a site of abutment, mechanical interaction and communication between adjacent cardiac myocytes. The three-dimensional arrangement of such interactions includes apparent side-to-side cell contacts at disks that, although orientated perpendicular to the cell long axis, do so part-way along the cell length (Fig. 1.1. See also Fig 3.10). The geometry of myocyte interactions in mammalian myocardium is therefore complex (Sommer and Scherer, 1985), with an average of about 9 - 11 cells connecting to each individual cell in canine ventricular myocardium (Hoyt et al. 1989; Saffitz et al. 1992).

1.2.2 The intercalated disk

As the structure connecting individual cardiac muscle cells together to form discrete

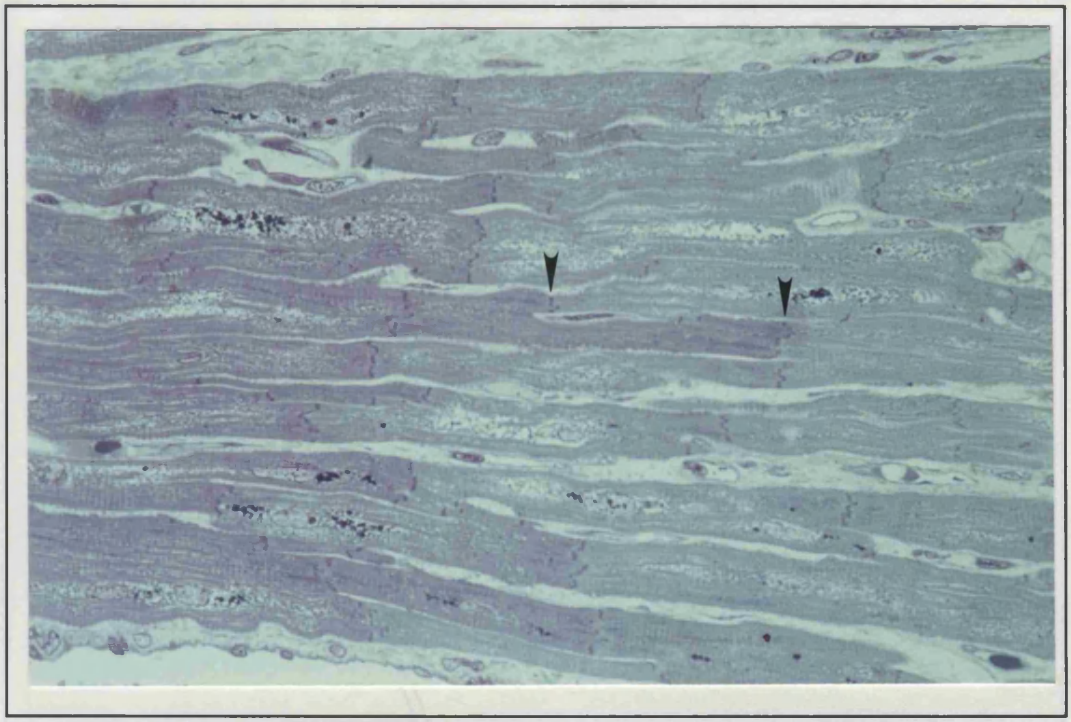

Figure 1.1. Light micrograph of toluidine blue-stained normal human ventricular myocardium sectioned longitudinally. The dark intercalated disks are prominent at the sites of end-on abutment of the interdigitating myocytes (arrows). Note how the intercalated disks are orientated transverse to the long axis of the myocytes, but may exist in this orientation at points along the length of the cells, as well as at their ends, thereby facilitating side-to-side cellular coupling. x440.

fibres which function as coordinated contractile units (Sommer and Scherer, 1985), the intercalated disk incorporates the closely apposed plasma membranes of the abutting cardiac myocytes to form specialised intercellular junctions. These myocardial intercellular junctions, of which there are three types (Fig 1.2), maintain electrical and mechanical integrity between cells, and of myocardium as a whole. Two of these junctions, the fascia adherens and the desmosome (the so called anchoring junctions), are concerned with intercellular adhesion (Severs, 1989b). The third, the gap junction, is responsible for intercellular communication, forming low resistance pathways for passive flow of ions, small molecules and electrical impulses between cells (Page, 1992).

Gap junctions occur in all multicellular tissues in the body, and throughout the animal kingdom, from the sponges to man (Beyer et al. 1990a). In the heart, although typically found in the intercalated disk as described, gap junctions are not necessarily confined the disk. The structural characteristics of different cardiac myocyte types vary; those of the atrioventricular node, for example, have no identifiable intercalated disks even though gap junctions are present (Viragh and Challice, 1973; Severs, 1989b; Gourdie et al. 1992). Working ventricular myocytes, however, which form the bulk of

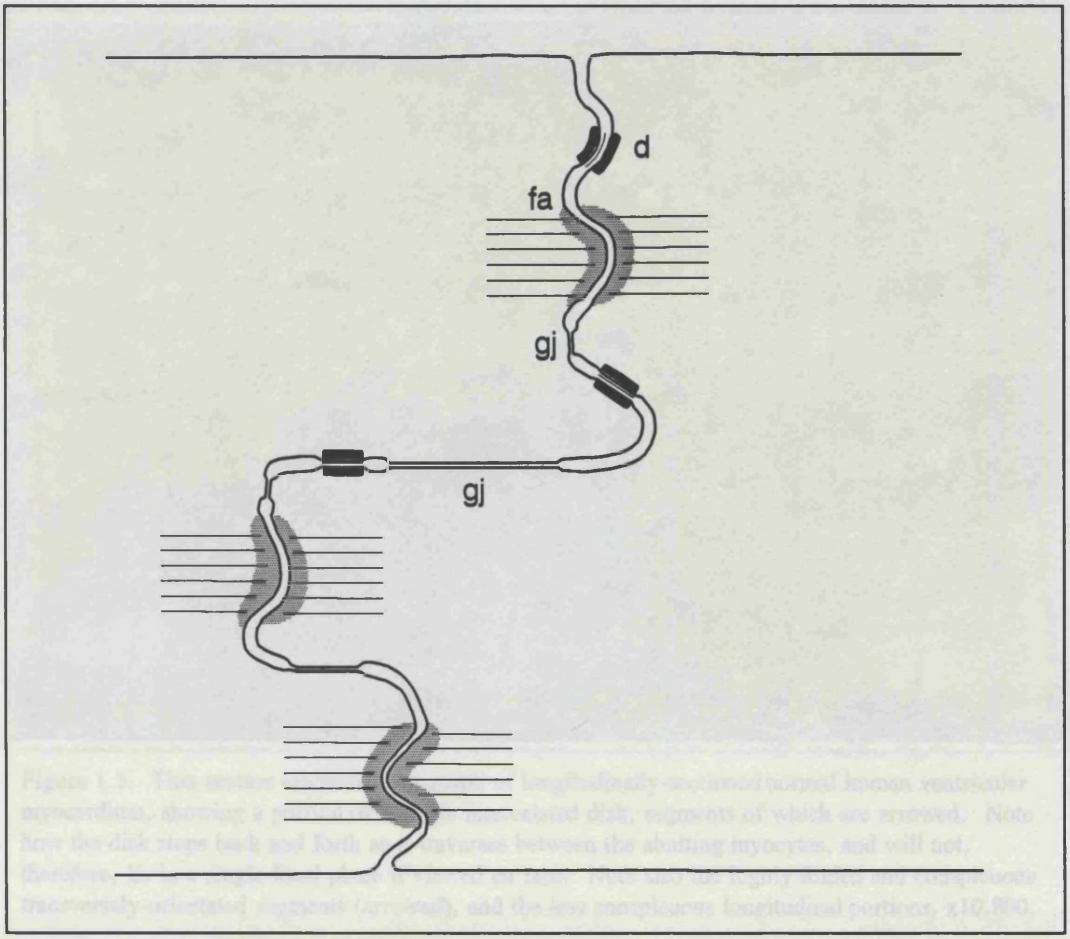

Figure 1.2. Diagram of an intercalated disk in mammalian ventricular myocardium, showing the component specialised junction types, interspersed by ordinary plasma membrane, and the way in which the disk steps back-and-forth on traversing the cell. The fascia adherens (fa) junctions, shown here with the contractile thin filaments inserting into them, are situated in the transverse segments, which are highly folded (plicate). The gap junctions (gj) exist predominantly in the longitudinal (interplicate) segments, although small ones are present in the plicate segments. Desmosomes (d) occur throughout the disk.

the cardiac mass, are interconnected by the most elaborate intercalated disks, the properties of which have been studied in the greatest detail (Forbes and Sperelakis, 1985; Sommer and Jennings, 1986; Severs, 1989a; Severs, 1989b; Page, 1992).

1.2.2a *The intercalated disk as part of the ventricular myocyte*

Thin section electron microscopy reveals the ultrastructural arrangement of the intercalated disk (Fig 1.3), and how the cells abutting at the disk interdigitate such that their paired plasma membranes follow the contour of the myofibril ends (Severs, 1989b). In doing so, the disk steps back and forth across the cell terminal (Figs. 1.2 & 1.3), alternating between approximately parallel (longitudinal) and perpendicular (transverse) to the long axis (Severs, 1990). The size of intercalated disks varies, crossing as few as 2, or up to 20 or more myofibrils in sectional view ("diameter"), and in doing so, a disk

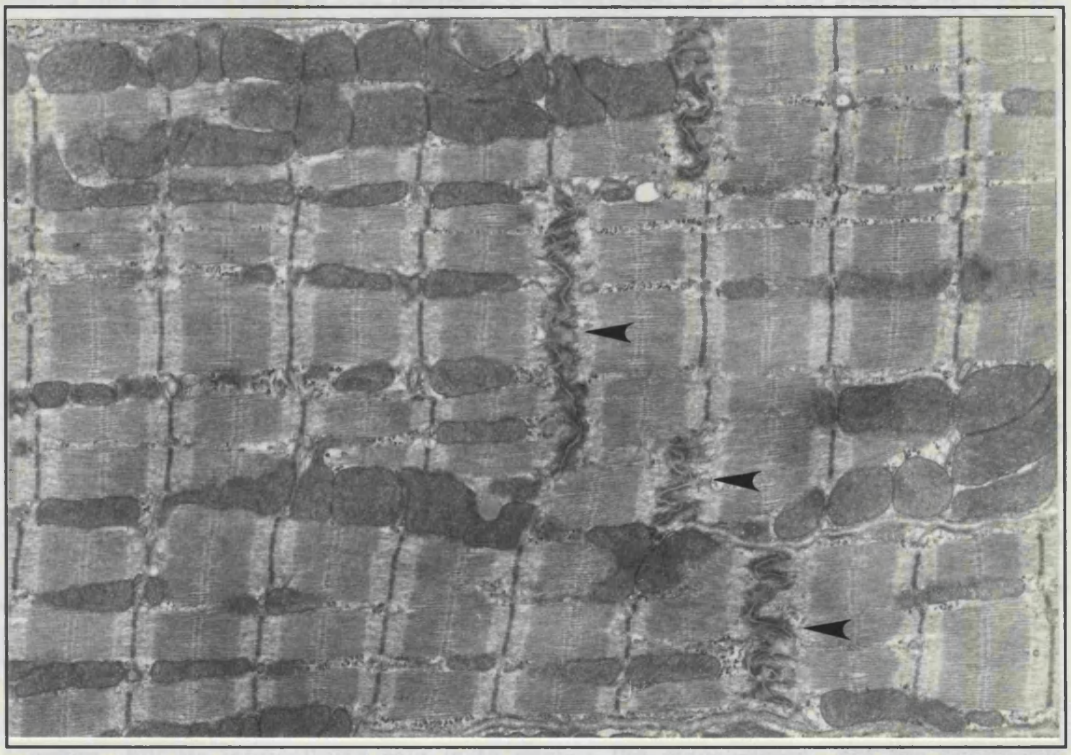

Figure 1.3. Thin section electron micrograph of longitudinally-sectioned normal human ventricular myocardium, showing a portion of a single intercalated disk, segments of which are arrowed. Note how the disk steps back and forth as it traverses between the abutting myocytes, and will not, therefore, lie in a single focal plane if viewed en face. Note also the highly folded and conspicuous transversely-orientated segments (arrowed), and the less conspicuous longitudinal portions. x10,800.

may step in the longitudinal direction by as much as the length of several sarcomeres. The arrangement of the three specialised junction types in the intercalated disk differs between these regions of different orientation (Severs, 1989b). Fasciae adherentes are confined predominantly to the transverse regions, which are highly convoluted, or plicate. Gap junctions are located predominantly in the longitudinal non-plicate regions, although small gap junctions are also present amongst the adhering junctions of the plicate regions (Fig. 1.2). Desmosomes may exist in both regions.

1.2.2b *The anchoring junctions*

The anchoring junctions (fascia adherens and desmosome) establish strong adhesion between the plasma membranes of abutting myocytes. Various forms of anchoring junction occur in a wide range of tissues, but they are particularly abundant in myocardium which is subject to, and requires efficient transmission of, severe mechanical stress.

The fascia adherens is conspicuous for the electron dense "mat" of protein filaments (Maher et al. 1985; Koteliansky et al. 1985; Yamaguchi et al. 1988) on the

cytoplasmic sides of the apposing plasma membranes; some of these proteins specifically anchor the terminal band of thin filaments of the myofibrils. The two plasma membranes comprising the fascia adherens are separated by an intercellular space of about 20nm which contains adhesive molecules termed cadherins, which are a family of structurally and functionally related glycoproteins that participate in Ca^{2+}-dependent intercellular adhesion (Geiger et al. 1985; Volk and Geiger, 1986; Takeichi, 1990). Cadherin-mediated cellular adhesion is likely to play a critical role in the formation and distribution of gap junctions, with which fasciae adherentes are intimately associated in the adult intercalated disk (Severs, 1990). It has been suggested that the mechanical stresses on the fasciae adherentes are a major determinant of cell shape and topology in developing myocardium, and that the establishment of gap junctions is a passive, secondary phenomenon (Richter, 1974). The exact relationship between fascia adherens and gap junctions, its role in cardiac development and when in myocardial maturation these junction types establish their close association, is not fully understood.

Like the fascia adherens, the desmosome also has an intercellular adhesive function, but its intracellular role is to anchor the cytoskeleton, not the contractile apparatus (Granger and Lazarides, 1979; Severs, 1989b). Desmosomes are the point of anchorage of intermediate filaments, which are non-contractile proteins that form webs throughout the cytoplasm, in association with which the internal components of the cell are organised (Granger and Lazarides, 1979; Severs, 1989b).

1.2.3 The gap junction

The gap junction is relatively inconspicuous at thin section electron microscopy because there is little electron dense material on the cytoplasmic side of the membranes, which are separated by a gap of only 2-3 nm (Revel and Karnovsky, 1967). The entire structure comprising the paired plasma membranes (Fig. 1.4) thus spans only about 14 to 19 nm in transverse sectional view (Severs, 1989b). Electron micrographs of thin sectioned tissue reveal a septilaminar structure, composed of the two trilaminar unit membranes separated by the small gap (Fig. 1.4), although often the gap is not visible and only five distinct layers can be seen (Severs, 1989b).

The integral proteins of the gap junction exist in hexameric units called connexons, each of which possesses a 1.5 to 2 nm central pore (Fig 1.5), and makes contact with another connexon in the apposing membrane (Fig 1.4). The pair forms a

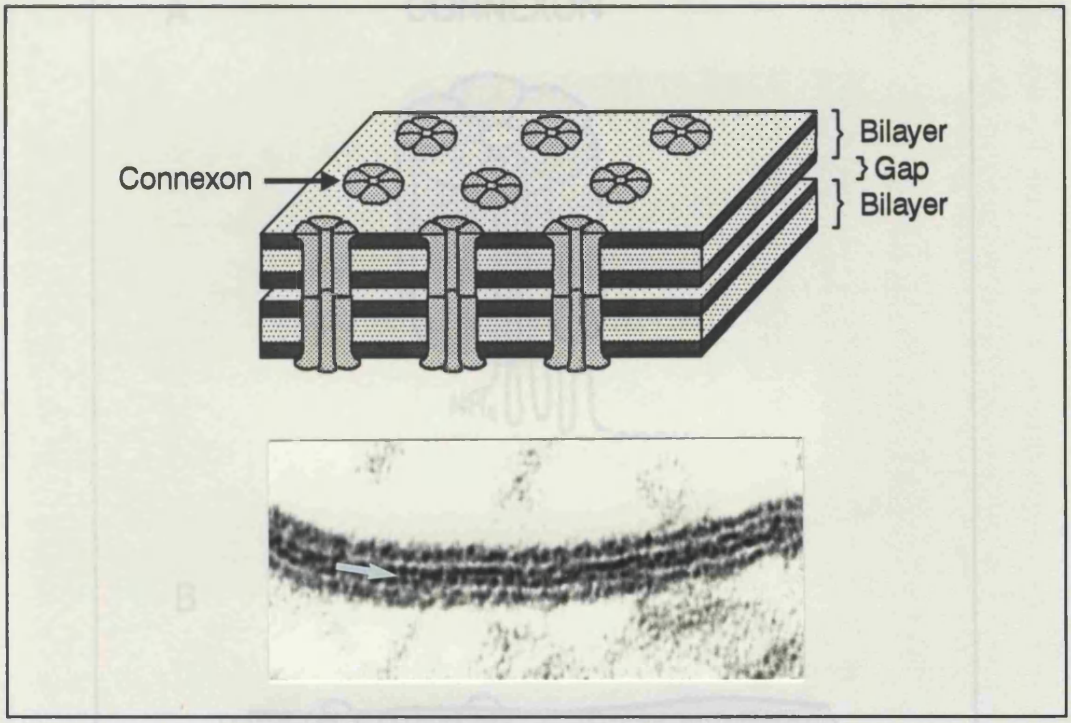

Figure 1.4. A: Diagram of gap junction structure. The closely apposed membrane lipid bilayers (gap ≈ 2 - 3 nm), each contain closely packed connexons consisting of six protein molecules (connexins) around the central pore (diameter ≈ 1.5 - 2 nm).
B: High power thin section electron micrograph of transected gap junction. The septilaminar structure is visible in regions in which the "gap" between the constituent membranes can be resolved (arrow). Micrograph courtesy of Dr N J Severs. x380,000.

complete channel linking the cytoplasmic compartments of the abutting cells, providing a low resistance pathway for the passage of ions and small molecules (up to 1 kDa) (Imanaga, 1974; Imanaga, 1987; Baldwin, 1981), and electrical propagation (Spray and Burt, 1990).

The technique of freeze-fracture (Fig 1.6) enables electron microscopic examination of detail of a platinum/carbon replica of the fractured surface (Rash and Hudson, 1979; Pinto da Silva, 1987). By this technique, therefore, detail of gap junctions can be viewed face on (Pinto da Silva, 1987; Severs, 1989a), in the plane of the membrane (Fig 1.7), with visualisation of the densely packed individual connexons therein (Fig 1.8). The gap-junctional membrane so observed is easily distinguished from the surrounding diffuse, heterogeneous particles representing other integral sarcolemmal proteins (Pinto da Silva, 1987), and from the membranes of mitochondria which characteristically and consistently lie in the sarcoplasm subjacent to gap junctions (Forbes and Sperelakis, 1982).

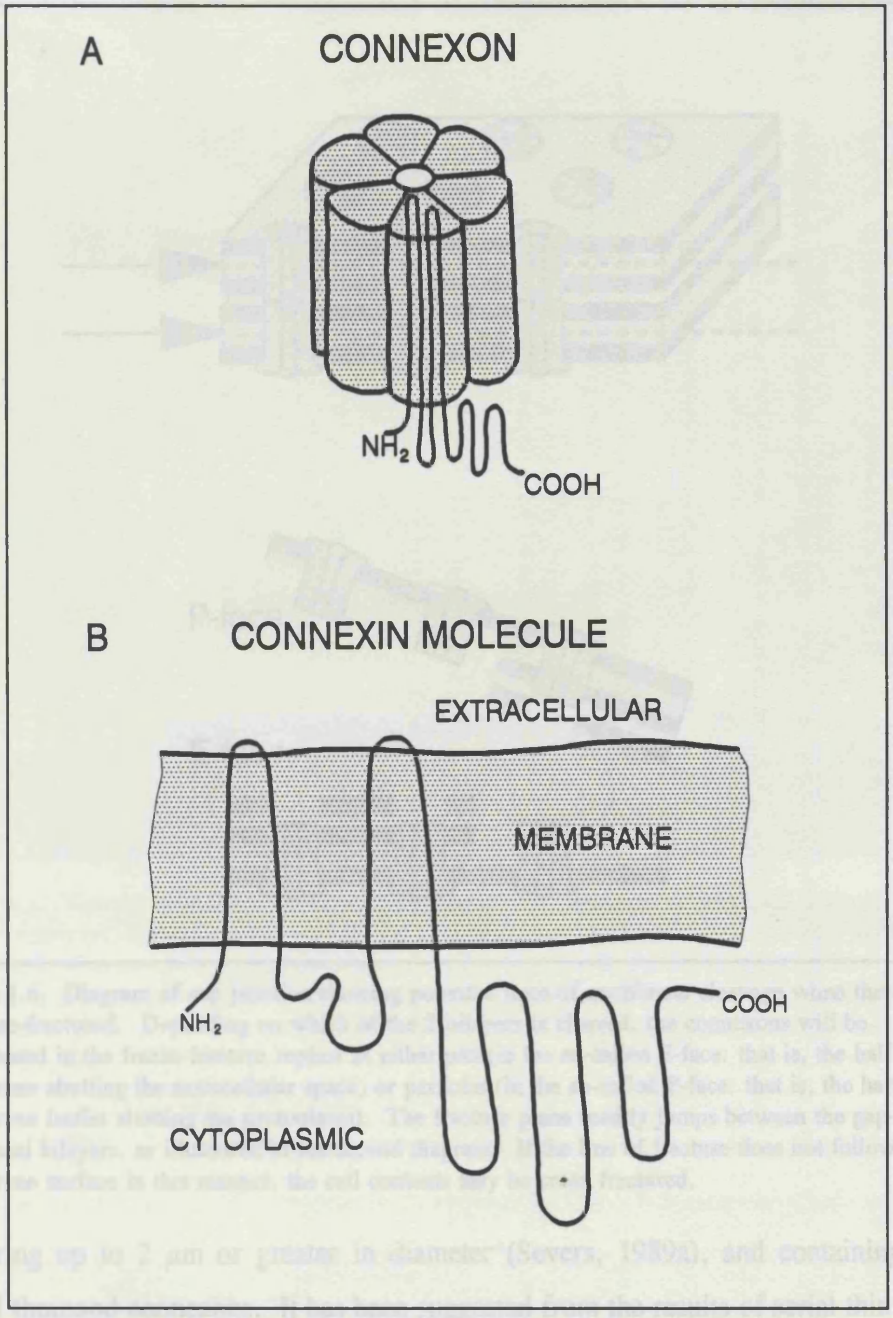

Figure 1.5. A: Diagram of a connexon, which consists of 6 connexin molecules around the central pore. One connexin molecule is shown schematically. B: Diagram of the arrangement of the connexin molecule in the cell membrane. Note the organisation in relation to cytoplasmic and extracellular sides of the membrane. The connexin molecule traverses the membrane four times, with the amino-terminal, cytoplasmic loop and carboxy-terminal on the cytoplasmic side. The third transmembrane segment (counting from the NH_2 end) is thought to line the central pore of the connexon.

1.2.3a *Distribution of gap junctions*

Freeze-fracture and serial thin section electron microscopy have revealed that in mammalian ventricular myocardium, gap junctions are confined almost exclusively to the well-developed intercalated disks, and exist therein as ovoid or irregular plaques,

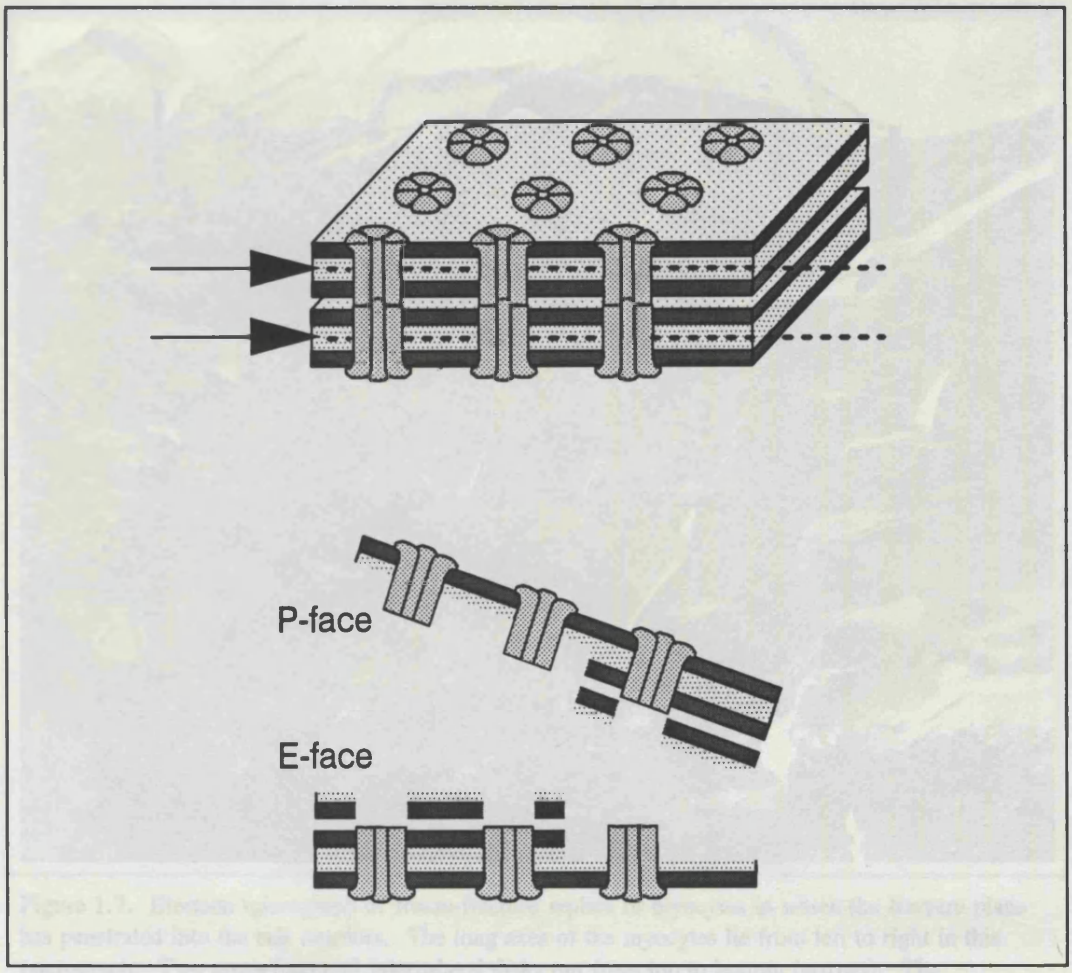

Figure 1.6. Diagram of gap junction showing potential lines of membrane cleavage when the tissue is freeze-fractured. Depending on which of the 2 bilayers is cleaved, the connexons will be represented in the freeze-fracture replica as either pits (in the so-called E-face: that is, the half-membrane abutting the extracellular space) or particles (in the so-called P-face: that is, the half-membrane leaflet abutting the protoplasm). The fracture plane readily jumps between the gap-junctional bilayers, as illustrated in the second diagram. If the line of fracture does not follow a membrane surface in this manner, the cell contents may be cross fractured.

measuring up to 2 μm or greater in diameter (Severs, 1989a), and containing up to several thousand connexons. It has been suggested from the results of serial thin section electron microscopy that the large gap junctions of the interplicate regions of the intercalated disk in canine ventricle are organised as abundant ribbon-like structures with their long axes transverse to that of the cell (Hoyt et al. 1989). Other freeze-fracture studies on mammalian heart have shown no such ribbon-like elongation of junctions, and have shown a variable orientation of the junctions (Severs, 1989a). This apparent contradiction has not been resolved. It has been suggested that electron microscopy of standard thin sections can result in incomplete detection of tangentially sectioned gap junctions (Chen et al. 1989), which may be more abundant in longitudinally sectioned tissue, resulting in an apparent elongation of gap-junctions in the transverse plane

Figure 1.7. Electron micrograph of freeze-fracture replica of myocytes in which the fracture plane has penetrated into the cell interiors. The long axes of the myocytes lie from left to right in this micrograph. Two cross-fractured intercalated disks run from top to bottom (arrows). The meandering plicate regions of the disks are visible, with the plane of fracture running along plicate membrane in parts (p). It is in just such regions that the smaller gap-junctional domains tend to occur. x12,000.

(Severs, 1989b). The possibility of inter-species variation also remains, although a recent comparison of rat and canine myocardium showed little interspecies variation, and failed to substantiate the presence of an abundance of ribbon-like junctions (Dolber et al. 1992).

1.2.3b *Quantitative morphometry of gap junctions*

Until recently serial thin section electron microscopy in conjunction with random sampling was the only feasible approach to quantitative morphometry of gap junctions (Spira, 1971; Matter, 1973; Page, 1978; Stewart and Page, 1978; Manjunath and Page, 1985; Hoyt et al. 1989). Freeze fracture provides invaluable information about the organisation, size and cellular relations of individual gap junctions, but is a difficult technique to use for systematic sampling, and cannot provide information on overall content of gap junctions in a tissue volume. Further, the curvature and convolution of

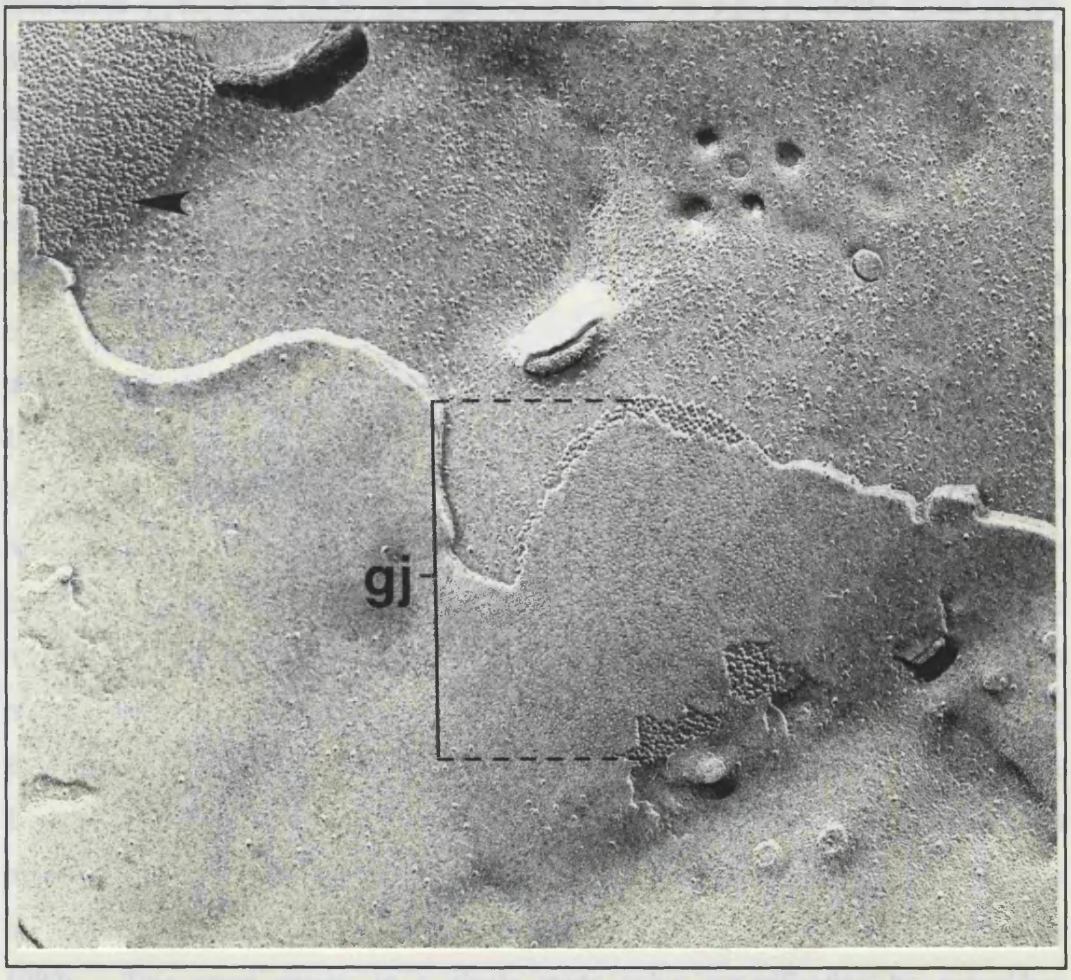

Figure 1.8. Freeze-fracture electron micrograph of an entire gap-junctional domain (gj) in the membrane of a myocyte in left ventricular myocardium from a patient with the Wolff-Parkinson-White syndrome. In this example, most of the junction is seen in E-face view (connexons represented as arrays of small pits), but parts of the border of the gap junction are seen on the adjacent P-face (connexons seen as particles). A second gap junction seen predominantly in P-face view is in the top left corner (arrow). x78,000.

cell membranes, particularly the plicate regions of the intercalated disks, make it less likely that a large area of such membrane will lie in the plane of fracture, and will result in a bias against detection of junctions in these regions (Severs, 1989a).

Morphometry using standard thin section electron microscopy, however, is not without problems, not least of which is the possible failure to detect the full extent of tangentially-sectioned junctional membranes, which may result in a 3.8-fold underestimation of junctional area (Chen et al. 1989). Despite this, thin section electron microscopy has been a valuable and for many years the only available tool for the study of gap junction organisation, and there is a sizeable body of literature reporting results derived by this technique. Among findings from the early 1970s were the following: gap-junctional area of the intercalated disk of the rat ventricular myocyte is 47-94 μm^2, containing a minimum of 6.7×10^5 gap-junctional channels (Matter, 1973); canine atrial

gap junctions constitute 4-6% of the area of an intercalated disk (Spira, 1971); the specialised myocytes of the bundle branches in the calf have gap junctions which occupy 3.3% of the cell border (Arluk and Rhodin, 1974); and gap junctions occupy 4.7% of the total "path length" along intercellular clefts in sheep Purkinje fibres (Hellam and Studt, 1974).

In the late 1970s, in keeping with a variety of emerging morphometric studies on cell membranes, Stewart and Page (1978) established what became the standard units for expressing gap junction quantity in tissue; that is, μm^2 of gap junction area per μm^3 myocardial volume, referred to by some workers as "surface density" (Luke et al. 1989a). Using thin section electron microscopy, studies of the ventricle of the rat, which has been the most extensively studied animal, have since demonstrated the mean area of the gap junction to be 0.018 $\mu m^2/\mu m^3$ cell volume (Chen et al. 1989), with a mean channel density of 12.9 x 10^3 channels per μm^2 gap junction (Page, 1992). Results of other morphometric studies demonstrate considerable consistency across different mammalian species. These include rabbit ventricle (0.017 $\mu m^2/\mu m^3$) (Shibata et al. 1980), rat ventricle (0.0047 and 0.0022-0.0154 $\mu m^2/\mu m^3$) (Page, 1978; Stewart and Page, 1978) and canine ventricle (0.0085 $\mu m^2/\mu m^3$) (Hoyt et al. 1989). Saffitz's group, in a recent thin section electron microscopic study of dog ventricle, concluded that the ratio of gap junction area in interplicate segment compared to plicate is about 3.6 (Hoyt et al. 1989). This same group, in a single study using quantification by peroxidase immunohistochemistry, estimated a gap-junctional area of 0.0052 $\mu m^2/\mu m^3$ in canine ventricular myocardium (Luke et al. 1989a). According to Dr Saffitz, he has not pursued further immunohistochemical quantification owing to technical limitations in the precision of tissue sampling, label detection and image analysis [personal communication].

It has been suggested that a useful consequence of these scant and disparate pieces of quantitative morphometry is the possibility of working out, in an indirect fashion, the area of gap-junctional membrane and the number of intercellular channels in any given weight of ventricular myocardium (Page, 1992). If morphometric data are to have any applicability to tissue function, however, direct quantification of gap junctions, and the ability to relate gap-junctional area to numbers of intercellular contacts and cell size is necessary, since it is the number and area of junctional interfaces per unit distance and volume of myocardium that are the morphometric variables relevant to the function of myocardium as a whole. It was to this end that the morphometric studies in this thesis were undertaken, using advanced immunohistochemical and imaging techniques to overcome the technical limitations encountered by other groups in the field, and to

attempt direct measurement of gap junction content in appropriate volumes of intact tissue.

1.2.3c *Gap junction assembly and turnover*

Freeze-fracture studies of mammalian embryonic hearts have shown that gap-junctional assembly during early development probably starts with the progressive aggregation of individual connexons to form linear, circular and then hexagonal arrays (Gros et al. 1978; Navaratnam et al. 1986) from about 8 to 10 days post-coitus in the mouse, and therefore coincident with the first detectable coordinated cardiac contractions (Fromaget et al. 1992). The early plaques so formed have extensive aisles free of channel particles, which fill progressively (Shibata et al. 1980). Plaque enlargement follows such that gap-junctional area per unit cell volume progressively increases. Particularly striking changes occur after birth; in the rabbit, for example, gap junction quantity increases from an initial value of 0.004 $\mu m^2/\mu m^3$ in the neonate, by about 3-fold in the young animal (until 30 days postpartum), subsequently falling again to 0.004 $\mu m^2/\mu m^3$ in the adult (Shibata et al. 1980).

Once gap junctions have formed, there is constant turnover of gap-junctional channel proteins. This is known to occur rapidly in the liver (Fallon and Goodenough, 1981; Yancey et al. 1981), and although the rate of turnover in myocardium has not been determined with certainty, recent evidence suggests that the half life of connexin43 in cultured neonatal cardiac myocytes is 2 to 3 hours (Page, 1992). There may, however, be differences in connexin43 turnover between cultured neonatal myocytes and myocytes in vivo, especially in the adult, but it is likely that turnover is, none-the-less, rapid in the functioning adult heart. Morphological findings consistent with rapid turnover have been suggested. Multiple small gap junctions < 0.5 μm in diameter, and containing 100 connexons or fewer, are present in both the plicate and interplicate regions of the intercalated disk, and are characteristically present around the periphery of larger junctions (Severs, 1989b). It has been suggested that these small ("satellite") junctions represent stages in assembly or disassembly of the central large junction (Severs, 1989b). Although the half life of cardiac connexin43 may be short, gap junctions as a whole appear to be stable structures representing a steady state of assembly and disassembly under uniform conditions.

When mammalian myocytes undergo experimental enzymatic disaggregation, the closely apposed membranes of gap junctions do not separate from each other, but remain intact at one cell, being torn away from the other (Severs et al. 1989). The gap-

junctional membranes are endocytosed over a few hours to form cytoplasmic vesicles (Mazet et al. 1985; Jacobson and Piper, 1986; Severs et al. 1989), even under hypoxic conditions, but do not appear to undergo rapid degradation (Severs et al. 1989; Decker et al. 1989). When dissociated adult myocytes are brought back into contact, electrophysiological studies have suggested that they may rapidly reestablish gap-junctional communication, although formation of new gap junctions is relatively slow (Jongsma et al. 1987; Weingart and Maurer, 1988; Page, 1992). Reinsertion of the endocytosed junctions has been suggested as one explanation for this apparent discrepancy, but there is little direct evidence to support this theory. Cytoplasmic gap-junctional membrane in the form of apparent vesicles has been reported to occur abundantly in perfusion-fixed mammalian ventricle, particularly during the rapidly increasing phase of neonatal gap-junctional growth (Chen et al. 1989). These appearances may be attributed to invaginated or endocytosed surface junctional membrane, and this may be further indirect evidence of intracellular vesicles having a possible role in the control of the quantity of surface gap junctional membrane. However, one might speculate that, following the same pathway of biogenesis as that of other integral membrane proteins (Severs and Hicks, 1979; Morré et al. 1979), these vesicles are Golgi-derived.

Another possible mechanism of rapidly reversible gap junction disassembly is that of dispersal of connexons in the plane of the membrane, a process detected in other cell types (Lane and Swales, 1980; Braun et al. 1984), but not confirmed in the myocyte (Green and Severs, 1984a).

1.2.3d *Packing of gap-junctional connexons*

Freeze-fracture studies demonstrate clearly the arrangement of connexons within gap-junctional membranes (Fig 1.7) (Ashraf and Halverson, 1978; Peracchia, 1980; Shibata and Page, 1981; Burt et al. 1982). There has been some debate as to whether connexon arrangement reflects the functional status of the junction (Peracchia, 1980), or whether alterations in arrangement are artefactual, resulting from the technique of tissue preparation. The matter was resolved by demonstrating that junctions frozen directly in functioning hearts in the living animal have the arrangement of constituent connexons characteristic of optimally fixed healthy myocardium; multiple small hexagonal arrays separated by lipid aisles (Green and Severs, 1984b). Uncoupling agents failed to alter this arrangement, but postmortem tissue showed alterations in connexon arrangement, of the sort previously thought to reflect changes in functional state (Green and Severs,

1984b). These results suggest that a change of arrangement is possibly an artefactual phenomenon from suboptimal tissue preservation, and does not necessarily reflect a state of uncoupling of the tissue in vivo. However, it remains possible that some, but not all, of these changes are also inducible by in vivo hypoxia (Peracchia, 1980).

1.2.4 Methods of study of the structure of cardiac gap junctions

The structure of cardiac gap junctions can be studied in whole, intact tissue (Luke et al. 1989b; Gourdie et al. 1991), in freshly isolated myocytes (Severs et al. 1989), or from gap-junctional membranes separated from a tissue homogenate by biochemical fractionation (Harfst et al. 1988; Harfst et al. 1990). The first two methods of preparation are appropriate for special light microscopic techniques, such as immunohistochemistry, producing information concerning the distribution of gap junctions throughout cells and the intact tissue as a whole (Gourdie et al. 1991). All of these types of preparation may be examined by electron microscopy of either ultrathin sections or freeze-fracture replicas as appropriate, to derive detail of the ultrastructural composition and relations of gap junctions at the cellular level (Severs, 1989b). Scanning electron microscopy may add further to investigating the surface topology of junctions at the cellular level, but its use has, as yet, been unconvincing (Hoyt et al. 1989). Computer-assisted image processing of electron micrographs (Manjunath and Page, 1985), low dose electron microscopy (Gogol and Unwin, 1988) and X-ray diffraction (Tibbitts et al. 1990) have been used to resolve the structure and arrangement of individual channels in gap-junctional isolates.

Immunohistochemistry was the principal technique employed in the present series of studies, using one of the earliest developed and most efficient antibodies to connexin43 (Harfst et al. 1990), combined with the novel technique of scanning laser confocal microscopy. This powerful combination of tools for immunolocalisation in whole tissue at the light microscopic level was used in conjunction with standard thin section electron microscopy, freeze-fracture electron microscopy, and both immunofluorescence light microscopy (of labelled isolated myocytes) and immunogold electron microscopy. The general principles of these techniques will now be summarised, but the full detail of the methodology is given later (Chapter 2).

Preservation of biological material for morphological analysis requires fixation of the structure before, or as soon as possible after, removal from the body, to minimise degenerative changes. Gap junctions exist within fluid membranes, so rapid fixation and

preservation is particularly important for the ultrastructural (electron microscopic) studies. The specimens in this series of studies were whole tissue and freshly isolated myocytes, mainly from human subjects, and could not, therefore, be fixed by the ideal method of perfusion-fixation in situ. Chemical fixation in preparation for all the microscopic techniques used involves exposure to an aldehyde which cross-links amino acids and, therefore, stabilises the protein content of the tissue. For the light-microscopic immunolabelling techniques the specimen is fixed in a formaldehyde solution and the tissue is embedded in wax for sectioning. The cell membranes are subjected to limited chemical disruption in order that the gap-junctional antibody can gain access to, and label, the appropriate region of the connexin molecule. In preparation for standard thin section electron microscopy, aldehyde (usually glutaraldehyde) fixation is followed by secondary fixation and lipid membrane stabilisation by osmium tetroxide before embedding in resin for sectioning (Severs et al. 1985). For freeze-fracture, glutaraldehyde-fixed tissue is treated with glycerol to prevent ice-crystal damage, rapidly frozen and stored in liquid nitrogen, before being fractured (Severs, 1989a).

Staining or labelling of the specimens in preparation for visualisation of detail is by heavy metals (uranium, lead, platinum, gold) for the electron microscopic techniques, and fluorescein immunolabelling for light and confocal microscopy (Gourdie et al. 1990b).

By combining these microscopic techniques, tissue can be examined to provide information about gap junctions ranging from detail and organisation of the integral protein units (connexons) comprising individual junctions (by freeze-fracture), to the arrangement of junctions in relation to individual cells and their other constituents (mainly by thin section electron microscopy, by which morphologically-distinct gap junctions can be identified), and to the organisation of individual and groups of gap junctions within volumes of whole tissue (by confocal microscopy of immunolabelled tissue).

1.3 **Physiological properties of gap junctions**

The physiological properties of gap junctions have been extensively studied at the cell-pair level, but there is little information available relating the physiological properties of gap junctions to whole myocardial tissue function, either mechanically or electrically. Most of the general principles of gap junction function were established from studies of non-cardiac junctional types (Furshpan and Potter, 1959), but many specific

characteristics of mammalian cardiac gap junctions have subsequently been determined.

1.3.1 Permeability

In general, gap-junctional membrane is several orders of magnitude more permeable than an equal area of non-junctional plasma membrane. This suggests that gap-junctional channels are present in much greater numbers, with a greater proportion and stability in the open state, and that the "pore" through the channel is larger than that of the other specific transmembrane channels of non-junctional plasma membrane (Page, 1992).

Studies using molecular probes to investigate the nature of gap-junctional coupling have demonstrated that the aqueous pore is 1.5 to 2 nm in diameter (Flagg-Newton et al. 1979), may contain fixed negative charges (Brink and Dewey, 1978; Loewenstein, 1981), and although some gap junctions may act as chemical rectifiers (Bennett, 1977), the conductance of most junctions within a given system does not depend on the direction of the electrical field or chemical gradient across them (Loewenstein, 1981).

1.3.1a *Regulation of gap junction permeability*

The permeability of a gap junction (or "junctional conductance") is determined by:-

1. The number of junctional channels (paired connexon units) per unit area of junction,
2. The proportion of channels that are in an open state.
3. The permeability of an open channel (or "unitary conductance").
4. The total surface area of the gap junction.

Changes in gap junction permeability are thought to occur by a number of different mechanisms (Page, 1992). The number of junctional channels present at the cell surface changes during tissue development (Gros et al. 1979; Gourdie et al. 1992). There is recent evidence to suggest that there may also be developmental changes in the expression of distinct connexin isoforms in avian cardiac and other tissues (Beyer et al. 1990b; Gourdie et al. 1993), and possibly in the mammalian heart (Kanter et al. 1992). Evidence is beginning to emerge that the different isoforms may have different unitary conductances. The alterations in gap junction permeability brought about by these structural changes in protein synthesis are thought to occur relatively slowly. Changes in the kinetics of junctional gating, affecting the proportion of channels in the open state, underlie the more rapid alterations of junctional conductance caused by changes of the chemical and electrical environment of the junction (Spray et al. 1985). Until recently,

it has generally been assumed that the unitary conductance of a single channel does not vary, and that the channel functions in an all-or-nothing manner — either open or closed (Rook et al. 1988). Accepting this assumption, the determinants listed above were considered to be related by the following equation:-

$$g_j = N\gamma_j P_o$$

where g_j is the gap junctional conductance, N is the number of channels (units) in the junction, γ_j is the open-state unitary conductance (of a single channel) and P_o is the probability of the open state (Fozzard and Arnsdorf, 1992; Page, 1992). There is, however, recent evidence to suggest that the unitary conductance (γ_j) in gap junctions of some types may not be constant (Prod'hom et al. 1987; Rook et al. 1988; Chen and DeHaan, 1992; Veenstra et al. 1992; Jongsma, 1993), which would make it necessary to modify the equation. This added complication does not, however, change the general principle that developmental and structural changes of myocardium alter the number of channels (and/or the connexin isoform) slowly, and cellular chemical and electrical factors alter the opening probability (and/or the unitary conductance states) rapidly (Page, 1992). Although some of these variables have been investigated in in vitro simulations of physiological disturbances, such as hypoxia (Hoyt et al. 1990), acidosis and increased $[Ca^{2+}]$ (Noma and Tsuboi, 1986), very little is known of the changes, either structural or functional, that may take place in disease.

1.3.2 Direct measurements of cardiac gap-junctional conductance

The physiological properties of cardiac gap junctions have been extensively examined by the dual whole-cell patch-clamp technique (Neyton and Trautmann, 1985; Weingart, 1986; Spray et al. 1993), in which a pair of myocytes coupled by gap junctions each has a suction micropipette attached to its plasma membrane, so that the electrical potential and current flow in each of the cell pair can be measured and controlled by a voltage-clamp circuit (Fig 1.9). The current flowing between the two cells changes in a linear manner with the voltage applied, and this linear current-voltage relationship contrasts with the non-linear relationship for non-junctional plasma membrane (Weingart, 1986; Page, 1992). Furthermore, the magnitude of current flow is independent of the direction of the voltage change, and in which cell of the pair the change is made (Weingart, 1986). These results imply that a gap junction represents a passive low resistance barrier with

no directionality or selectivity, although there is recent evidence of selectivity of diffusion of molecules, depending on their size and, possibly, their charge (Veenstra et al. 1993).

The properties of single gap-junctional channels have also been extensively investigated by a modified whole-cell patch-clamp technique, by studying cell pairs that are coupled by only a few channels (Harris et al. 1983; Neyton and Trautmann, 1985) (Fig 1.9). The junctional conductance of well coupled cells is a steady state achieved by a perpetual opening and closing of the constituent channels, with a constant net proportion open (Burt and Spray, 1988a). If the number of channels capable of opening is reduced, either by altering the chemical environment of the cells or by using cells that have only recently been brought into contact with each other, the opening and closing events of the individual channels can be detected as quantum changes in intercellular current (Burt and Spray, 1988a; Jongsma and Gros, 1991) (Fig 1.9). As stated above, recent studies of this nature suggest that two or more discrete unitary conductance states may exist in some junction types (Chen and DeHaan, 1992; Veenstra et al. 1992), although alternative explanations for the results, such as cooperative recruitment of channels, or variation of channel sizes, have been proposed (Chen and DeHaan, 1992).

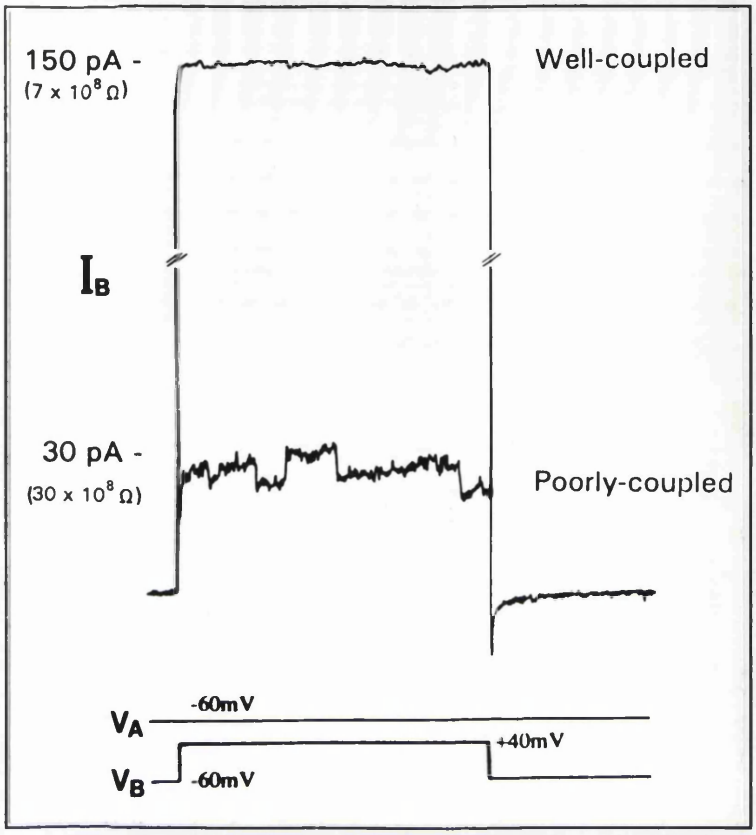

Figure 1.9. Representative traces of whole-cell patch-clamp studies (adapted from Jongsma and Gros, 1991).
With the potential of cell A held constant (V_A), a +100 mV step applied to cell B (V_B) causes current to flow between the cells via gap junctions (I_B). When cells are **well-coupled**, with extensive gap-junctional contact, the resistance to current flow is low (high junctional conductance), and the large numbers of opening and closing channels produce a steady-state tracing of current flow. When **poorly-coupled** by few gap-junctional channels, gap-junctional conductance is low, and discrete steps in the trace result from opening and closing events of individual channels, and demonstrate their unitary conductance.

Cardiac gap-junctional conductance varies with the size of the junction, but is of the order of 600 nS (range 10 to 1000 nS), equivalent to a resistance of the order of 2 Mohm (Noma and Tsuboi, 1986). The conductance of a single connexin43 channel is said to be of the order of 50 pS (Burt and Spray, 1988a; Rook et al. 1988; Weingart and Maurer, 1988), although recent preliminary data suggests that connexin43-gap junctions may exhibit as many as three conductance states under experimental conditions (Jongsma, 1993). The physiological significance of this, however, remains to be elucidated.

1.3.2a *Factors affecting gap-junctional conductance*

By these techniques, some of the factors that change gap-junctional conductance have been determined.

Cytosolic $[Ca^{2+}]$ and pH. Gap-junctional conductance is reduced at high $[Ca^{2+}]$ (Délèze, 1970) and at low pH (Spray et al. 1985; Turin and Warner, 1993), and single-channel studies have shown this to be due to a change in opening probability, the single-channel conductance remaining unchanged (Burt and Spray, 1988a; Veenstra and DeHaan, 1988; Rüdisüli and Weingart, 1989).

Noma and Tsuboi (1986) investigated pH and $[Ca^{2+}]$ in the control of junctional conductance, and demonstrated the interrelationship between these factors. Junctional conductance remained almost constant between pH 7.4 and 6.5, but then diminished sharply as pH was reduced further to 5.4. This relationship was unaffected by changes in $[Ca^{2+}]$. Increasing cytosolic $[Ca^{2+}]$ reduced junctional conductance; the concentration at which 50% of the maximal number of closable channels are closed is about 3×10^{-7} M, and the lower the pH, the greater the $[Ca^{2+}]$ required to reduce junctional conductance to its half-maximal value. These results suggest that although changes of pH within the physiological range may not directly affect junctional coupling, they may modulate the response to changes in $[Ca^{2+}]$ (Noma and Tsuboi, 1986), and pH may become an important direct influence at the low pH associated with hypoxia and ischaemia in diseased myocardium.

Although $[Ca^{2+}]$ within the physiological range may affect junctional conductance, rapid transients exceeding the threshold for channel closure, which accompany myocyte excitation and contraction for example, may be too rapid to have any effect on coupling (Spray et al. 1985; Page, 1992).

Hypoxia. Internal longitudinal resistance through the intracellular pathway in

myocardium increases substantially in myocardium deprived of oxygen (Kléber et al. 1987; Hiramatsu et al. 1988). This phenomenon is mediated predominantly by intracellular pH and calcium concentrations that accompany hypoxia (De Mello, 1985). There is evidence, however, that there may be early ischaemic and hypoxic changes in connexon packing density in gap junctions (Ashraf and Halverson, 1978; Peracchia, 1980; Hoyt et al. 1990), and although there is experimental evidence to suggest that such changes may be artefactual (Severs, 1989b), they may nevertheless represent a stage of altered gap junction function before the irreversible changes heralding the onset of irreversible cell damage.

Cytosolic ATP. Lowering cytosolic ATP reduces junctional conductance (Sugiura et al. 1990), and studies have shown conflicting results with regard to whether this effect is mediated by cyclic AMP-dependent phosphorylation of the channel proteins (Burt and Spray, 1988b; Spray et al. 1993) or not (Sugiura et al. 1990). Phosphorylated forms of connexin43 have recently been detected, and there is evidence that phosphorylation may alter unitary conductance (Jongsma, 1993). In adult cardiac gap-junctional plaques, connexin43 appears normally to be present in the phosphorylated form (Laird et al. 1990). Protein kinase C phosphorylates seryl residues of a C-terminal region of connexin43 (Sáez et al. 1990).

Transjunctional voltage. In large gap junctions containing many cell-to-cell channels, both the instantaneous (immediately after applying an intercellular potential difference) and steady-state current-voltage relationships are linear (White et al. 1985; Noma and Tsuboi, 1986; Weingart, 1986). When only a few open channels are present, although the instantaneous relationship is linear, the steady-state current-voltage relationship progressively falls to near zero (Veenstra, 1990; Veenstra, 1991). This observation reflects so-called voltage dependence of channel gating causing a progressive closure of channels, a phenomenon that is not apparent when measuring the net conductance of larger junctions (Noma and Tsuboi, 1986), and is of unknown physiological significance.

n-Alkanols and volatile anaesthetics. Heptanol (Rüdisüli and Weingart, 1989) and octanol (Burt and Spray, 1988a) both reversibly reduce gap-junctional conductance, and since they do not affect unitary conductance (Burt and Spray, 1988a), this action is thought to be due to a reduction in opening probability, although the mechanism is unknown. These agents are useful for experimental purposes, but may also affect non-junctional

plasmalemmal ion transporters (Na^+/Ca^{2+} exchange and Na^+ channel (Jalife et al. 1989)). The volatile anaesthetic agents halothane and ethrane reversibly reduce junctional conductance (Burt and Spray, 1988a; Burt and Spray, 1989) without affecting unitary conductance.

Fatty acids. Doxyl stearic acids (with a fatty acyl chain), but not stearic acids, rapidly and reversibly reduce junctional conductance to very low levels without affecting the unitary conductance (Burt, 1989; Burt, 1991).

1.4 **Molecular biology of gap junctions**

The cloned sequence of the 382-residue connexin43 molecule (Beyer et al. 1987), in conjunction with x-ray diffraction data (Makowski, 1988) and prediction of the relative hydropathicity of parts of the molecule (Kyte and Doolittle, 1982), enabled determination of the topology of the molecule within the junctional membrane and in relation to its neighbouring connexins (Fig 1.5). As the gene sequences of other members of the connexin family, principally from non cardiac tissues, have been detected (Paul, 1986), the high degree of homology between different connexins has become apparent. As noted earlier, these studies have shown that connexins pass through the plasma membrane four times (Fig 1.5), with the carboxy- and amino-terminals on the cytoplasmic side (Kyte and Doolittle, 1982; Makowski, 1988). The hydrophilic third transmembrane segment is thought to line the channel "pore" itself. The two extracellular loops are highly conserved between connexin sequences predicted from many tissues throughout the animal kingdom (Paul, 1986; Beyer et al. 1987; Ebihara et al. 1989; Kanter et al. 1992).

The mode of interaction between the extracellular loops of abutting connexons to create the cytoplasm-to-cytoplasm channel remains poorly understood. One of the only means of separating the membranes constituting a gap junction is with high concentrations of urea (Manjunath et al. 1984), suggesting that the bonds between abutting connexons are neither covalent nor ionic, but possibly van der Waals or hydrogen bonds (Page, 1992).

Gap junction isolates from cardiac tissue can be produced by use of detergent (Manjunath and Page, 1986) or detergent-free (Manjunath et al. 1987; Gourdie et al. 1988; Gourdie et al. 1990b) methods. By use of the latter method, a 70-kDa protein that cross-reacts with connexin43 antiserum was detected in the hearts of small mammals,

suggesting the presence of another connexin in the cardiac gap junction (Harfst et al. 1990). No glycoproteins or proteolipids, structural molecules commonly associated with non-gap-junctional integral membrane proteins, have been detected in association with gap junctions.

The isolation and characterisation of the principal mammalian cardiac gap-junctional protein, connexin43, and cloning of its gene sequence, have both greatly enhanced understanding of the cardiac gap junction, and provided the "tools" for recent further study. These lines of investigation are at a relatively early stage in their evolution, and include studies of the region of a connexin molecule that confers its functional properties (Yancey et al. 1989), the detection of genomic evidence for other connexin types in myocardium, sequence polymorphism detection (El Aoumari et al. 1990), and studies by which cultured cell lines are transfected with genomic material such that the expression of different connexin isoforms can be controlled in vitro and their functional properties investigated (Moreno et al. 1990; Moreno et al. 1991a; Moreno et al. 1991b; Spray et al. 1992). Further, molecular biological techniques have facilitated structural studies ranging from the detection of other proteins associated with gap junctional membranes, to determination of the patterns of distribution of gap junctions within volumes of intact tissue (Gourdie et al. 1990b; Gourdie et al. 1990a; Gourdie et al. 1991).

It is in relation to this last line of investigation, and the potential of determining gap junction organisation through large enough volumes of tissue to enable correlation of structure and function at the whole-tissue level, that the series of studies comprising this thesis were principally aimed.

1.4.1 Immunolocalisation of connexins

Although a number of studies have used connexin43-mRNA levels as an indicator of connexin43 expression, it is necessary to detect connexin43 directly to confirm that translation into a stable protein occurs, and to determine many of the characteristics of the molecule that are relevant to gap-junctional function and its assembly, disassembly and turnover.

Primary antibodies made against amino acid sequences of connexin43 have been reacted with isolated gap junction vesicles visualised at thin section electron microscopy by labelling with secondary antibodies linked to colloidal gold particles (Beyer et al. 1989; Yancey et al. 1989; El Aoumari et al. 1990). The use of primary antibodies to

different segments of connexin molecules has confirmed the relative lack of homology of the components of connexins exposed on the cytoplasmic side of the membrane (Fig 1.5); that is, the amino-terminal, the loop between the second and third transmembrane regions, and especially the tail at the carboxy-end (Beyer et al. 1987; Beyer et al. 1989; Yancey et al. 1989; Beyer et al. 1990a). Although the extracellular "gap" of the junction is impenetrable to antibodies, the greater homology of the extracellular regions has also been confirmed by cross-reactivity at Western blotting (Page, 1992).

By immunolabelling, connexin43 has been localised in atrial and ventricular myocardium, and a number of studies on the distribution of this connexin in different parts of the developing and adult mammalian heart have been conducted(Yancey et al. 1989; Gourdie et al. 1990b). Connexin43 has been shown to be highly conserved among vertebrate hearts (Dupont et al. 1988), although there may be sequence polymorphism of connexin43 within this group (El Aoumari et al. 1990). Antibodies to the amino- and carboxy-termini have been shown to attenuate dye coupling (Yancey et al. 1989), and information of this sort may give clues to the important regions of the connexin molecule in functional terms.

1.5 Gap junctional coupling and cardiac function

The evidence that gap junctions, by being the low resistance pathways for electrical impulse propagation, facilitate the synchronisation of myocardial contraction is now considerable, and the onset of synchronised beating of the embryonic heart is coincident with the earliest detection of connexin43 (Beyer et al. 1987; Lloyd and Baldwin, 1990; Gourdie et al. 1992; Kanter et al. 1992). Relating gap-junctional coupling to cardiac function, however, has only been studied extensively at the level of isolated cell pairs (Weingart and Maurer, 1987; White et al. 1985) and myocyte culture (Jongsma et al. 1987), with very little information on how coupling relates to myocardial and whole heart function. A recent report, however, demonstrated how coronary infusion of heptanol reduces ventricular myocardial conduction velocity in the intact heart (Callans et al. 1992). Although providing minimal detail of the effects of uncoupling ventricular myocardium, this net reduction is as would be expected from in vitro experimentation on isolated myocardium (Balke et al. 1988; Jalife et al. 1989).

In normally coupled myocyte pairs isolated from adult guinea pig and rat hearts, normal impulse transmission may occur, without delay, at gap-junctional membrane resistances up to 265 Mohm (Weingart and Maurer, 1988). At intercellular resistances

up to 375 Mohms, there is transfer of the action potential with up to a 24msec delay, and at >780 Mohm (equivalent to about 35 open junctional channels), complete block of action potential transfer occurs (Weingart and Maurer, 1988). Importantly, Weingart and Maurer (1988) also demonstrated in this study that for a variable period after being brought into contact with each other, spontaneously contracting myocytes may continue to beat independently, with no demonstrable transfer of action potential between them. This and similar results of other workers (Jongsma et al. 1987) are evidence against ephaptic transmission (Arvanitaki, 1942) and electric field coupling (Sperelakis, 1979) as possible mechanisms of impulse transmission that would not involve gap junctions. However, synchronisation may occur as early as the first beat after being brought into contact, implying that a critical number of junctional channels is already present in the membranes and are able to link up rapidly (Jongsma et al. 1987).

1.5.1 Computer modelling

The interaction between the active membrane ionic properties determining the characteristics of the action potential, and intercellular coupling is complex, and it has not been possible to measure this interaction extensively in whole tissue using an experimental model. Computer modelling of resistively-coupled current sources simulating one dimensional (Quan and Rudy, 1990) and two-dimensional (Lesh et al. 1989) cardiac tissue has elucidated and explained some of the missing elements in experimental data. Computer models have demonstrated that cellular coupling is the predominant variable controlling myocardial conduction velocity (Quan and Rudy, 1990) and, therefore, an important determinant of anisotropic conduction. Reduced coupling will substantially slow conduction (Quan and Rudy, 1990), increase the dispersion of action potential duration (Lesh et al. 1989), and render anisotropic conduction non-uniform. Computer models have also suggested that the active membrane ionic properties are affected by alterations of cellular coupling, and by combining all these factors, a consensus of computer models is that reduced cellular coupling is significantly arrhythmogenic (Joyner, 1982; Lesh et al. 1989; Quan and Rudy, 1990).

1.5.2 Gap junctions and cardiac electromechanical dysfunction

Although the effects of alterations of gap-junctional coupling on myocardial mechanical function and the coordination of contraction have not been extensively investigated either

experimentally or by modelling, the direct gap-junctional intracellular flow of current is thought to synchronise myocardial activation for maximum contractile efficiency. Changes in the degree of cell coupling can significantly alter the characteristics of cardiac conduction and may also influence automaticity (Delmar et al. 1987; Balke et al. 1988). Experimentally, a reduction in cell coupling provides an electrophysiological substrate that increases susceptibility to cardiac arrhythmias and mechanical inefficiency induced principally by altering rates and the anisotropy of conduction (Spear et al. 1983; Ursell et al. 1985; Dillon et al. 1988) (Fig 1.10), and by abnormal impulse generation (Spach et al. 1982a). Although a causative relationship between uncoupling and myocardial

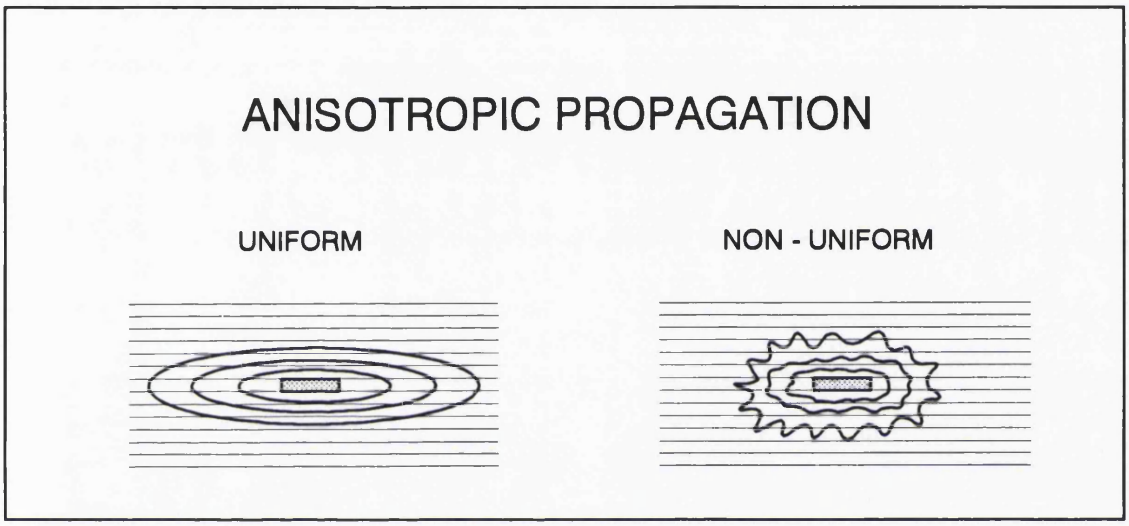

Figure 1.10. Schematic diagrams showing what is meant by uniform and non-uniform anisotropic propagation of the electrical impulse in ventricular myocardium. The horizontal parallel lines represent the long axes of the constituent myocytes, one of which is shown at the centre. Normal uniform anisotropy is characterised by smooth wavefronts of impulse conduction, which is up to 4 times more rapid longitudinally than transverse with respect to the myocardial fibre axis, as illustrated by the concentric lines representing conduction isochrones spreading from the centre. Non-uniform anisotropic propagation is heterogeneously slowed, giving rise to fractionated wavefronts and electrograms.

mechanical disturbances and arrhythmogenesis had not been shown when the series of studies comprising this thesis was undertaken, there was evidence, both from in vitro experiments (Delmar et al. 1987) and from computer modelling (Lesh et al. 1989), that disrupted cell coupling should contribute to the generation and perpetuation of disturbances of cardiac rhythm.

1.5.3 Pathophysiological role of gap junctions

Following the identification of gap junctions, their role in pathophysiology has centred on in vitro studies of the effects of hypoxia and ischaemia. Using the then new

technology of electron microscopy in the late 1960s and early 1970s there were a number of reports of changes of myocardial ultrastructure in general, and intercalated disks in particular, both in experimental ischaemia and hypoxia (Sulkin and Sulkin, 1965; Büchner and Onishi, 1968) and in other pathological conditions such as hypertrophy (Laks et al. 1970; Goldstein et al. 1974) and Coxsackie infection (Sun et al. 1967; Burch and Sohal, 1969). This technique led also to a crop of case reports on changes of the intercalated disk in a disparate variety of biopsied human cardiac diseases (Poche, 1958; Poche and Ohm, 1963; Kawamura et al. 1964; Kawamura et al. 1969). However, all these animal and human studies were reported as showing only the same basic alteration of the intercalated disk; that is, so-called dissociation of the disks, with variable degrees of separation of the component junctions of the disks and the width of the disk space, but an almost universal lack of separation of the component membranes of the gap junctions. This non-specific finding, therefore, provided limited insight into the pathophysiological role of gap junctions with respect to myocardial function, but gave important clues to a possible common step in the mechanism of irreversible cell damage in myocardial diseases. This point is discussed further below.

Myocardial ischaemia and hypertrophy are associated with arrhythmias, which present one of the foremost clinical challenges in ischaemic (Fujimoto et al. 1983) and hypertrophic (Kannel, 1983) heart diseases. There are few references in the literature to alterations of cellular coupling or gap-junctional changes in myocardial hypertrophy, but the physiological effects of acute ischaemia, hypoxia and associated metabolic disturbances on coupling and alterations of anisotropic conduction (Fig 1.10) have been investigated (Spear et al. 1983; Kléber et al. 1987; Hiramatsu et al. 1988; Kieval et al. 1992). Long after Engelmann (1877) first showed that severely injured cardiac myocytes rapidly become electrically isolated from their neighbours, this phenomenon was shown to be the result of a rapid and profound increase in gap-junctional resistance (Weidmann, 1952; Délèze, 1970; De Mello, 1983; De Mello, 1987b; Kieval et al. 1992). In vitro simulation of ischaemic and hypoxic conditions have been investigated in preparations in which it has been possible to measure longitudinal intracellular resistance and conduction velocity (Kléber and Riegger, 1987; Kléber et al. 1987). Both hypoxia and ischaemia have qualitatively similar effects, with a lag time (of about 10 to 15 minutes), after which there is up to a threefold increase in intracellular resistance in the next 5 minutes, suggesting substantial uncoupling of the cells, and associated with a rapid reduction in conduction velocity (Kléber and Riegger, 1987; Kléber et al. 1987; Kieval et al. 1992). There may be associated changes in the action potential that enhance this effect on

conduction velocity (Levine et al. 1987; Lesh et al. 1989; Jalife et al. 1989), and although the relative contributions of the changes in active and passive electrical properties have not been assessed, it is considered that the changes in gap-junctional coupling play a major, if not predominant, role in determining myocardial conduction velocity (Lesh et al. 1989; Wit and Janse, 1992). The mechanism of electrical uncoupling in this setting remains uncertain, but the accumulation of intracellular Ca^{2+} that occurs after 15 minutes ischaemia, and the accompanying intracellular acidosis, are both factors known to increase coupling resistance (De Mello, 1987a; De Mello, 1983; De Mello, 1986).

Cellular uncoupling heralds the onset of irreversible cell damage (Hoyt et al. 1990), in which gap junctions play a further key role. Whether the pathophysiological process leading to cell damage is that of hypoxia (with or without reoxygenation), ischaemia (with or without reperfusion), or depletion followed by restoration of Ca^{2+} (the "calcium paradox"), the common step leading to irreversible cell damage is the resulting contracture of the myocytes (Ganote and Nayler, 1985; Severs et al. 1990; Altschuld et al. 1991). With the adhering junctions (but not the gap junctions) weakened by the preceding insult, the contracture of the myocytes is caused by abutting cells ripping themselves apart at their gap-junctional contacts when contractile competence is restored, resulting in holes and loss of plasma membrane integrity (Severs et al. 1990). Morphological studies have shown that beyond this point there is extensive disruption of myocyte ultrastructure, including focal pathological separation of intercalated disk membranes (Hoyt et al. 1990), but with the majority of gap junctions dissociated entirely from one or other of the abutting cells, leaving a hole in the reciprocal cell membrane (McCallister et al. 1979). After one hour of hypoxia, irreversible cell damage has ensued. This is associated with a reduction in gap-junctional surface density of 45% (Hoyt et al. 1990), possibly in part due to altered connexon packing within gap junctions, but probably by endocytosis similar to that described in relation to the consequences of myocyte isolation techniques (Severs et al. 1989). Although, as previously discussed, there has been disagreement about the nature of possible early changes of connexon packing within individual gap junctions in hypoxic conditions (Peracchia, 1980; Severs and Green, 1983), changes of intercalated disk and whole gap junction morphology and organisation have been shown only in the setting of irreversible cell damage, and therefore, associated with more gross histological cellular disruption and death. Healing of myocardium in which myocytes have been irreversibly damaged is associated with fibrosis which increases effective septation and separation of bundles of myofibrils (Spach

et al. 1982b; Dolber and Spach, 1989; Luke et al. 1989b; Saffitz et al. 1992; Pogwizd et al. 1992). Fibrotic healing is repeatedly said to constitute the arrhythmogenic anatomical substrate late after myocardial infarction, by influencing the degree of mainly side-to-side coupling of myocytes (Spach et al. 1982b; Dolber and Spach, 1989; Luke and Saffitz, 1991; Saffitz et al. 1992; Pogwizd et al. 1992). Uncoupling is generally considered to occur secondarily to the fibrotic process (Dolber and Spach, 1989; Luke and Saffitz, 1991; Saffitz et al. 1992).

1.6 **Clinicopathological basis and hypothesis behind this work**

Myocardial diseases may cause electromechanical dysfunction and have an arrhythmic tendency without having a significant fibrotic component (at least, not in their early stages). Is it possible that there is an anatomical substrate of impaired cellular coupling underlying impaired coordination of myocardial contraction and arrhythmogenesis that does not require a relatively gross histological feature such as fibrosis as the primary morphological disturbance? Could there be primary changes in the organisation of gap junctions in chronic myocardial disease, whether associated with fibrotic scarring, or not? At a time when a number of clinical reports are questioning the conventional wisdom of the understanding and treatment of potential abnormalities of the active ionic membrane systems of the myocytes of the arrhythmic heart, should greater attention be given to investigating possible primary abnormalities of gap-junctional intercellular coupling? All these questions can be linked to a central hypothesis.

1.6.1 CENTRAL HYPOTHESIS

The central hypothesis examined in this thesis is that a primary disturbance of connexin43 gap-junctional organisation underlies electromechanical dysfunction and arrhythmogenesis in human myocardial disease.

To examine this hypothesis, the initial aim of this work was to characterise normal human ventricular myocardium with respect to gap junction organisation, both in the adult and immature hearts, and to investigate the possibility of alterations in gap junction organisation in ischaemic, hypertrophic and congenitally abnormal hearts. This required

quantitative as well as qualitative analysis of volumes of intact myocardial tissue, and the production of data in a form that may be relevant to whole tissue electromechanical function. This work was carried out by combining one of the first and most effective antibodies to be raised to a cardiac gap-junctional protein, with state-of-the-art microscopy employing novel confocal technology, to enable precise detection and localisation of connexin43 gap junctions. A medical background provided knowledge of, and access to, fresh human tissue to study.

CHAPTER 2 - GENERAL METHODOLOGY AND INITIAL STUDIES

The principles and methods of acquiring and processing the myocardial specimens investigated were common to all of this series of studies, and are detailed in this chapter.

2.1 Patient selection

Patients for inclusion were selected from those satisfying the study criteria (specified in the relevant chapters) during the period of tissue collection for each study, on the operating lists of the surgeons who had agreed to take part; Graeme Bennett, John Pepper, Asghar Khagani and Sir Magdi Yacoub for the adult and transplant tissue, and Christopher Lincoln, Daryl Shore and Sir Magdi Yacoub for paediatric tissue. There was no interference with, or modification of, patient preparation for surgery, anaesthesia or operative procedures, which were carried out according to routine surgical practice. When the planned surgical procedure itself required resection or biopsy of tissue appropriate for these studies, this tissue was handed over for processing as soon as it was excised. The specimens from cardiac transplantation hearts fell into this category. Approval of the Ethics Committee of the Royal Brompton National Heart and Lung Hospital was obtained to biopsy patients specifically for the studies undertaken, either by scalpel excision of up to three small ventricular samples, or by use of a needle bioptome (Trucut) to obtain transmural samples. Potentially appropriate patients from this category were seen preoperatively, and the details of the study were explained to them both verbally and in writing. All questions were answered and if patients had any remaining concerns about the work they were advised not to give consent. When consent was obtained, if the operative findings were as expected, and at the surgeon's discretion, tissue for study was resected at the earliest opportunity after establishment of routine cardiopulmonary bypass and hypothermic cardiac arrest.

2.2 Acquisition of tissue

To maximise tissue preservation, all biopsies required immediate fixation on removal, and the specimen was therefore divided as required in the operating theatre, keeping note of tissue orientation to enable matching of areas analysed by the different microscopical techniques used. Perfusion fixation of fresh human specimens is obviously not possible,

and the methods of immersion fixation of whole myocardium used in this series of experiments were based on standard published techniques (Gourdie et al. 1991), some of which had been assessed by other members of the laboratory. Modifications of some of these techniques, particularly for application to very small tissue samples and isolated myocytes, were developed in the course of the series of studies included in this thesis, as were the optimal conditions for preservation of specimens for electron microscopic analysis (see below - section 2.5).

2.3 **Tissue preparation for immunohistochemistry**

Tissue was put in Zamboni's fixative (2% paraformaldehyde, 0.2% picric acid, 0.1M phosphate-buffered saline, pH 7.4) (Toshimori et al. 1987) for 2-6 hours. After fixation, all samples were washed in tap water, dehydrated in alcohol, placed in chloroform and embedded in wax following standard histological procedures (Gourdie et al. 1991).

2.3.1 Antibodies

The primary antiserum used to localise cardiac gap-junctional connexin43 was raised (by N J Severs and C R Green) against a synthetic peptide matching residues 131-142 of the cytoplasmically-exposed segment of the connexin43 molecule (Gourdie et al. 1990b; Harfst et al. 1990). The peptide, supplied by N. B. Gilula (Research Institute of the Scripps Clinic, La Jolla, California) was prepared using the simultaneous multiple peptide synthesis procedure of Houghten (1985), and was coupled using glutaraldehyde to the carrier protein, keyhole limpet haemocyanin, for subcutaneous injection into Sandy half-lop rabbits. A summary of the derivation of this antibody (designated "HJ") is illustrated in Figure 2.1, and full details of the production and characterisation of the polyclonal antiserum are reported by other members of the laboratory (Gourdie et al. 1990b; Harfst et al. 1990; Green et al. 1993; Severs et al. 1993).

2.3.2 Immunolocalisation

Ten-micrometer sections of wax-embedded tissue were de-waxed and rehydrated, and incubated in a trypsin solution (containing 0.1% trypsin (Sigma T-8128), 0.1% $CaCl_2$, 20mM Trizma base, pH 7.4) for 10 minutes at room temperature to re-expose antigenic sites altered by fixation and processing (Harlow and Lane, 1988). The sections were

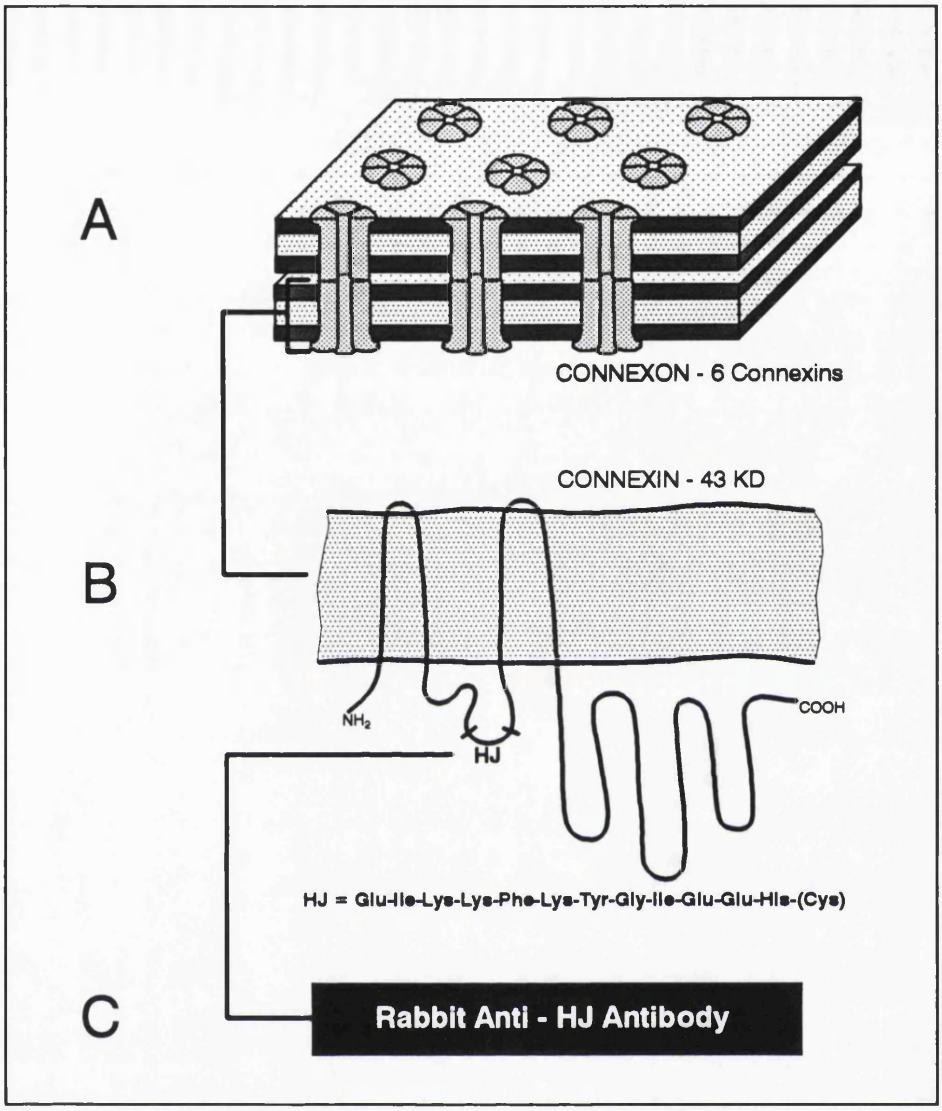

Figure 2.1. Summary of the derivation of the "HJ" antibody used for gap-junctional immunolocalisation. The antibody was raised in rabbits (C) to a 12-residue segment (designated "HJ", with the sequence shown) of the cytoplasmic loop of the connexin43 molecule (B) of the mammalian cardiac gap junction (A).

washed and treated with 0.1 M L-lysine (as blocking agent) in phosphate-buffered saline (PBS) containing 0.1% Triton X-100 (as a wetting agent). Incubation with the primary antiserum (dilution 1:10 in PBS) was carried out for 1 hour at 37°C. After washing, secondary antibody treatment with swine anti-rabbit fluoroscein isothiocyanate (FITC: Dako, 1:20 dilution) was given for 1 hour in the dark at room temperature. After final washing in PBS, the slides were mounted using Citifluor mounting medium (Agar Scientific, Stansted, England). Under the conditions described, the immunolabelling procedure produces even and consistent staining through the depth of the sections. All immunolabelled tissue was stored at 4°C and when used for quantitative analysis, it was examined within 12 hours to avoid complications arising from significant fading of

fluorescence.

Immunolabelled sections were examined by conventional epifluorescence and confocal laser scanning microscopy. Phase contrast microscopy was used to obtain detail of tissue structure, and adjacent sections, stained with haematoxylin and eosin, were routinely examined by standard light microscopy. Control specimens in which the antiserum was substituted by preimmune rabbit serum or buffered saline, or the second antibody by buffered saline, were routinely run in parallel in all experiments in this series of studies. The specificity of the antiserum for the peptide, for isolated cardiac gap-junctional protein and for ultrastructurally-defined gap junctions was demonstrated as part of the characterisation of the antiserum (Harfst et al. 1990; Severs et al. 1993).

2.4 Confocal laser scanning microscopy

For confocal microscopy, immunolabelled sections were examined using a Bio-Rad Lasersharp MRC-500, running on standard Bio-Rad software, with the digitised images stored on optical computer disks.

The principles behind confocal microscopy are illustrated diagrammatically in Figure 2.2. With a small aperture setting, the image acquired has a very narrow depth of field, and can be considered as a single optical slice of data with minimal thickness, at a particular depth with respect to the z-axis. The intensity of scanning laser stimulation of a specimen labelled cleanly with a high affinity antibody is such that optical slices can be acquired through a considerable depth of tissue, without interference from signal or tissue outside the focal plane (Gourdie et al. 1990b). The motor-driven z-axis movement of the specimen stage therefore permits a number of optical slices to be obtained, through a known depth (ie. volume) of tissue, and the Bio-Rad software enables an optical-section series so derived to be processed in a number of ways. These include superimposition to create a single ("projection") image containing data from the entire volume of tissue all in focus, creation of a stereo pair of images, and rotation of the reconstituted volume of data.

For the work conducted in the studies comprising this thesis, the microscope was used with the blue high-sensitivity filter block inserted for optimal excitation of fluoroscein at its absorption peak wavelength of 488 nm and detection of the emission in the peak 520 nm range. A series of objective lenses (x10, x20, x60 oil) were used which, in conjunction with a series of software zoom adjustments, permitted a range of field sizes from 1080 μm x 720 μm (x10, zoom 1) to 45 μm x 30 μm (x60, zoom 4).

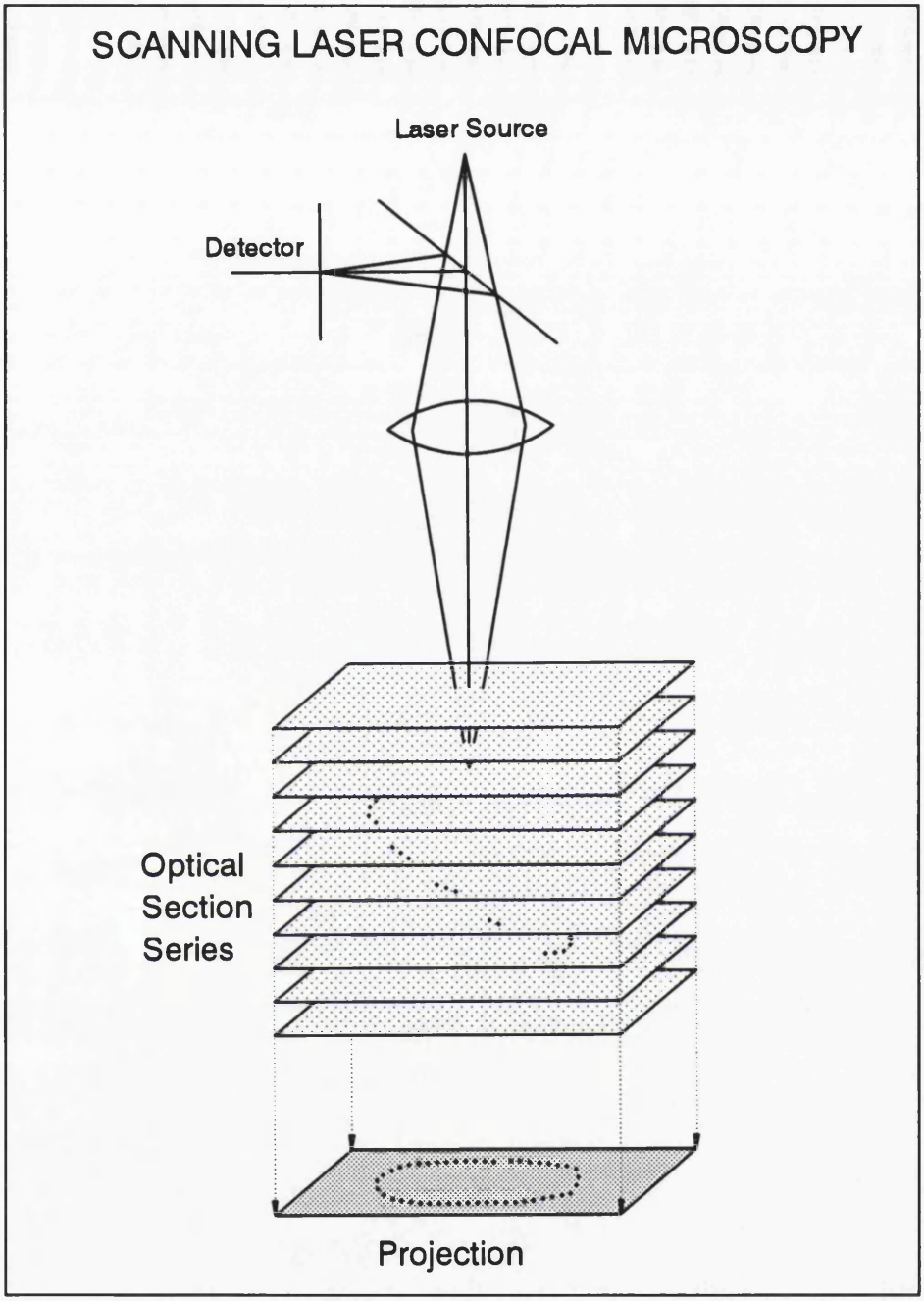

Figure 2.2. The principle of confocal technology. Digital image data are acquired through a very small aperture, thereby eliminating out-of-focus information that does not come from the focal plane. When used for detection of fluorescence stimulated by scanning laser excitation, the intensity of the signal is such that by moving the specimen in the z-axis (vertically in the diagram), optical data can be acquired slice-by-slice through a depth (volume) of tissue. The digitised data can be reconstructed in a number of forms, one of which is by superimposition of a number of optical slices to form a projection image.

The system provided a digitised image displayed on the monitor, composed of 393,216 pixels, each of which had a 255-point scale of black-white intensity (grey-scale), and each image occupying 384,000 bites of computer memory. At the time of image acquisition, the black level (background) and gain levels could be adjusted to optimise use of the full

grey-scale, and neutral density filters could be put in the path of the stimulating laser to reduce fluorescence fading during data collection. When data were being taken for quantitative measurement, however, these settings were standardised for consistency between data sets. Although the software provided for further electronic manipulation of the image data, no adjustments to the grey images were made. However, for some image analysis, the more versatile PC IMAGE software (Foster-Findlay Associates, Newcastle-upon-Tyne, England) was used, with which the grey image could be binarised automatically, such that each pixel was either on or off, as determined by an adjustable threshold on the 255-point grey scale, to eliminate sub-threshold data. The binary image took the form of a coloured overlay of the grey image on the monitor, such that the operator could toggle between the original grey image and the binary overlay so that concordance could be assessed and any editing necessary done, before a variety of different measurements of the binary data (the "on" pixels) could be made automatically.

2.4.1 Quantitative analysis of confocal data

For quantitative assessment of myocardial gap junctions, all aspects of tissue processing, labelling and image acquisition and analysis were strictly standardised.

2.4.1a *Measurements of individual features in the image field*

Measurements of the length or area of an individual feature or region within the image field were made directly from the monitor screen by use of the hand-held mouse and cursor, and the "length" or "area" composite commands in the Bio-Rad software.

2.4.1b *Automated total-field measurements*

Measurements of total area, or simultaneous length and area measurements of all objects in the field with an intensity greater than a preset threshold, were made automatically using the PC IMAGE image analysis software.

2.4.2 Statistical analysis

Unless otherwise indicated, all results throughout this thesis are expressed as mean $\pm$ SD. Group data are compared by two-sample t tests.

2.5 Electron microscopy

To ensure as rapid a fixation as possible, specimens for electron microscopic analysis were cut into pieces of the smallest size (down to $< 1 mm^3$) that was consistent with maintaining a record of tissue orientation.

A Philips EM 301 microscope was used to examine all electron microscopic specimens.

2.5.1 Thin section electron microscopy

Standard methods of tissue preparation for thin section electron microscopy were used (Severs et al. 1985). Samples were fixed in 2.5% glutaraldehyde in 0.1M sodium cacodylate buffer, pH 7.3, for 2 hours, rinsed in cacodylate buffer, and post-fixed in 2% osmium tetroxide (cacodylate-buffered) for 2 hours. They were then dehydrated in an ethanol series with en bloc staining with uranyl acetate at the 50% ethanol stage, before embedding in epoxy resin. Ultrathin sections were stained with uranyl acetate and lead citrate. Semi-thin sections for light microscopy were prepared in parallel, and examined after staining with 1% toluidine blue in a solution of 1% borax/50% ethanol.

2.5.2 Freeze-fracture

Standard procedures were used for freeze-fracture examination of tissue (Severs, 1989a). Following fixation in glutaraldehyde (as above) samples for freeze-fracture analysis were stored at 4°C for up to 24 hrs in 30% glycerol in 0.1M sodium cacodylate buffer before dissection, mounting in standard Balzers gold-nickel holders, freezing in liquid Freon and storage in liquid nitrogen. Fracture was performed by microtome at -120°C and 5×10^{-7} mbar in a BAF 400T apparatus (Balzers High Vacuum Ltd, Berkhamsted, England). Standard platinum-carbon replicas were prepared and cleaned in chromic acid.

All measurements of freeze-fracture material were made from electron micrographs at a final print magnification of x70,000, using an Olivetti M24 computer linked to a digitizer tablet and mouse, and VIDS III software (Analytical Measurement Systems, Cambridge, England).

2.6 Production and immunolabelling of isolated myocytes

Myocytes were isolated either by the modified Langendorff collagenase-perfusion method from guinea pig hearts (Farmer et al. 1983; Harding et al. 1990), or by a modification of this for dissociation of myocardial biopsy specimens, as used in studies previously described by Harding et al (1990). Ventricular myocytes were isolated from human specimens (Chapters 3 and 7) with assistance from Federica del Monte.

The procedure for isolating ventricular myocytes from guinea pigs (Chapters 6 and 10), carried out by Peter O'Gara, was as follows. The heart was perfused by the Langendorff method for five minutes with Krebs-Henseleit solution (composition (mM); NaCl 120, $NaHCO_3$ 25, KCl 4.7, $MgSO_4$ 0.97, KH_2PO_4 1.2, glucose 11 containing 1 mM Ca^{2+}, equilibrated with 95% O_2/5%CO_2 to bring the pH to 7.4). The perfusate was then changed to low calcium solution for five minutes at 37°C (composition (mM); NaCl 120, KCl 5.4, $MgSO_4$ 5, pyruvate 5, glucose 20, taurine 20, HEPES 10 and nitrilotriacetic acid (NTA) 5 bubbled with 100% O_2, with a final free [Ca^{2+}] of 12-14 μM). This same solution, but with the NTA omitted, was then infused with added pronase (4 U/ml, Sigma) for two minutes, followed by added collagenase (0.3 mg/ml, Worthington) and hyaluronidase (0.6 mg/ml, Sigma) for a further 10 minutes. The left ventricles were removed, chopped and shaken in the collagenase mixture for two further periods of 5 minutes. The dispersed cells were then strained through a 300 μm gauze, centrifuged at 40 g for 1 to 2 minutes and washed twice by centrifugation in the Krebs-Henseleit solution. The procedure for isolation of myocytes from human myocardial specimens was similar (Harding et al. 1990), but required cutting the tissue into 1 mm^3-pieces and initial incubation, rather than perfusion, with the appropriate solutions. A pellet of the isolated cells produced by either method was immediately dispersed in Zamboni's solution and processed for gap junction immunolabelling.

Preliminary experiments were carried out to determine the best method for immunolabelling isolated myocytes. Modifications of the whole-tissue protocol (section 2.3.2) were performed in order to develop a procedure that gave good signal with the lowest background, and a high yield of rod-shaped myocytes. The solutions listed in the following description of the technique are modifications of those in section 2.3.2, and only the principal or modified constituent is referred to.

After fixation by suspension in Zamboni's solution for 1 hour, the cells were re-pelleted by centrifugation at 40 g, and washed in phosphate-buffered saline. The resuspended cells were incubated with 0.01% trypsin solution for 90 seconds, treated

with 0.1 M L-lysine, before incubation with connexin43 antiserum for 30 minutes at 37°, and the swine anti-rabbit FITC for 20 minutes. The labelled cells were mounted suspended in Citifluor mounting medium, and examined by standard epifluorescence and confocal microscopy, and by phase contrast microscopy. Standard controls were run in parallel.

2.7 INITIAL STUDY 1 - Comparing gap junction sizes measured by immunohistochemistry and freeze-fracture electron microscopy

2.7.1 Introduction

In addition to the specificity of the antibody, which had already been demonstrated (Gourdie et al. 1990b), it was necessary to show that the immunohistochemical technique enabled valid and meaningful measurements of junctions in order to use this technique for quantifying the gap-junctional content of tissue. At the ultrastructural level, the membranes of intercalated disks have undulating topology and the gap junctions therein have different planes of orientation (Severs, 1989b), so correspondence of immunohistochemical and ultrastructural data cannot be assumed.

In fluorescence mode, the confocal microscope is capable of resolutions of 200 nm in the focal plane (Brakenhoff et al. 1990), but the limit of detection of a smaller structure depends on other factors (Wells et al. 1989), including properties of the fluorophore and the microscope. Although the theoretical understanding of many of these factors has been addressed, there is a lack of conclusive biological data relating quantification of immunofluorescent-labelled cellular structures to corresponding electron microscopic measurements.

To confirm that the measurement of the fluorescent spots by the immunohistochemical technique to be used in this series of studies provided a reliable guide to the true size of gap junctions, fluorescent spot sizes were compared with myocardial gap junctions measured on freeze-fracture electron micrographs. This study was carried out with other members of the laboratory (C R Green, R G Gourdie, N J Severs and S Rothery), as verification of the quantitative and semiquantitative use of connexin43 immunohistochemistry (Green et al. 1993) was important for a number of projects in progress in the laboratory.

2.7.2 Materials and methods

Female Sprague-Dawley rats (250g) were used.

2.7.2a *Freeze-fracture electron microscopy*

The hearts of 4 anaesthetised rats were fixed by retrograde perfusion via the aorta, and samples further fixed by immersion for 2 hours before processing as described in section 2.5.2.

Long axis measurements of a total of 325 junctions, with approximately equal numbers from each animal, were made. In freeze-fracture replicas, the larger the gap junction, the more likely it is that a portion of it will part from the plane of fracture. If measurement is restricted to entire junctions only, there would, therefore, be a potential bias towards smaller junctions. To minimise this bias, when portions of the junction were missing, attempts were made to extrapolate the likely complete shape, and when this could be achieved with reasonable certainty, these junctions were included. This method minimised, as far as was possible, the bias against larger junctions.

2.7.2b *Connexin43 immunohistochemistry*

Zamboni-fixed wax sections were immunolabelled (section 2.3.2) and examined using the x60 Nikon objective lens and the zoom 4 setting of the confocal microscope, resulting in a final magnification of x6000 on the 12 inch colour monitor. The detector black level was set at its mid-point (5) and the gain adjusted such that the pixel intensity spanned the full grey scale (0-255). Optical section series were taken at 1 μm intervals through transversely-sectioned myocardium from each animal, thereby imaging the entire gap-junctional population of a total of 8 entire intercalated disks (Fig 2.3). Measurements of the longest axis of 385 gap junctions were made from the projection image of each disk, by two methods; first, by manual mouse-and-cursor measurement of each individual fluorescent spot (gap junction), and secondly, by using the PC IMAGE software to create a binary image of the labelled gap junctions, the number and long axis lengths of which were measured automatically. Single isolated pixels were rejected as background noise from the binary before analysis.

2.7.2c *Analysis of data*

At the magnification used for this study, a single pixel had a long axis (diagonal) dimension equating to 80 nm, and an object had to be longer than this to impinge on

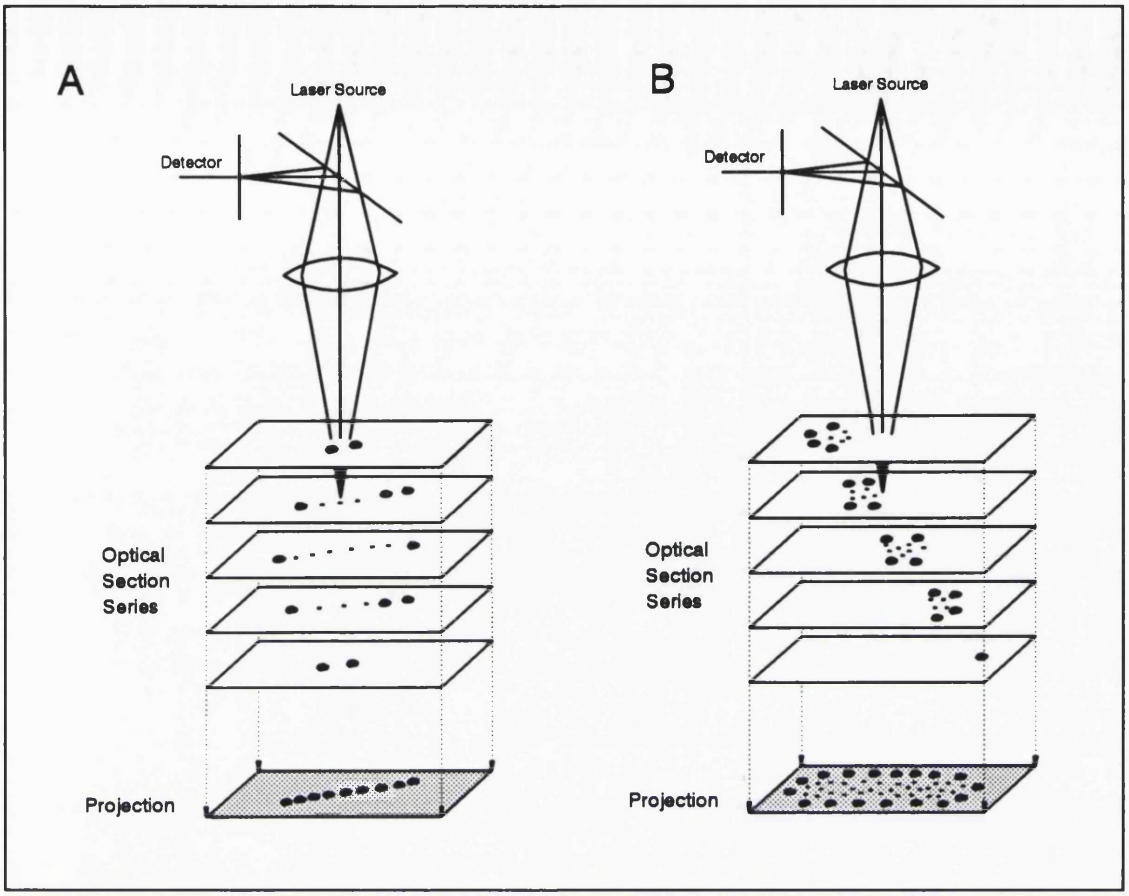

Figure 2.3. Diagrammatic illustration of the potential problem of attempting to quantify data in the projection of an image series acquired in an inappropriate plane of section. On microscopic examination, intercalated disks in longitudinally-sectioned myocardium (A) are viewed edge-on, with extensive overlap and superimposition of gap-junctional labelling in the projection image. This would result in underestimation of total label content and erroneous assessment of gap junction sizes. In (B), a projection image of obliquely-sectioned myocardium is shown through the same intercalated disk. This image contains individually resolved junctions. Measurements of gap-junctional size were therefore made from transversely-sectioned myocardium.

more than one pixel and have a theoretical chance of being detected (and not rejected as noise). To compare the data obtained, therefore, the manually and automatically measured immunohistochemical values were compared not only with the full set of freeze-fracture values, but also with modified freeze-fracture data in which junctions of < 80 nm length were eliminated. All sets of data were expressed as frequency distributions using 0.1 μm size classes, and analysis of variance of the $\log_{10}$-transformed data performed.

2.7.3 Results

The freeze-fracture replicas revealed gap junctions of typical structure (Severs, 1989b), forming clearly defined domains comprising as few as 15 connexons (long axis 25 nm),

with occasional junctions up to 3 μm long (Fig 2.4).

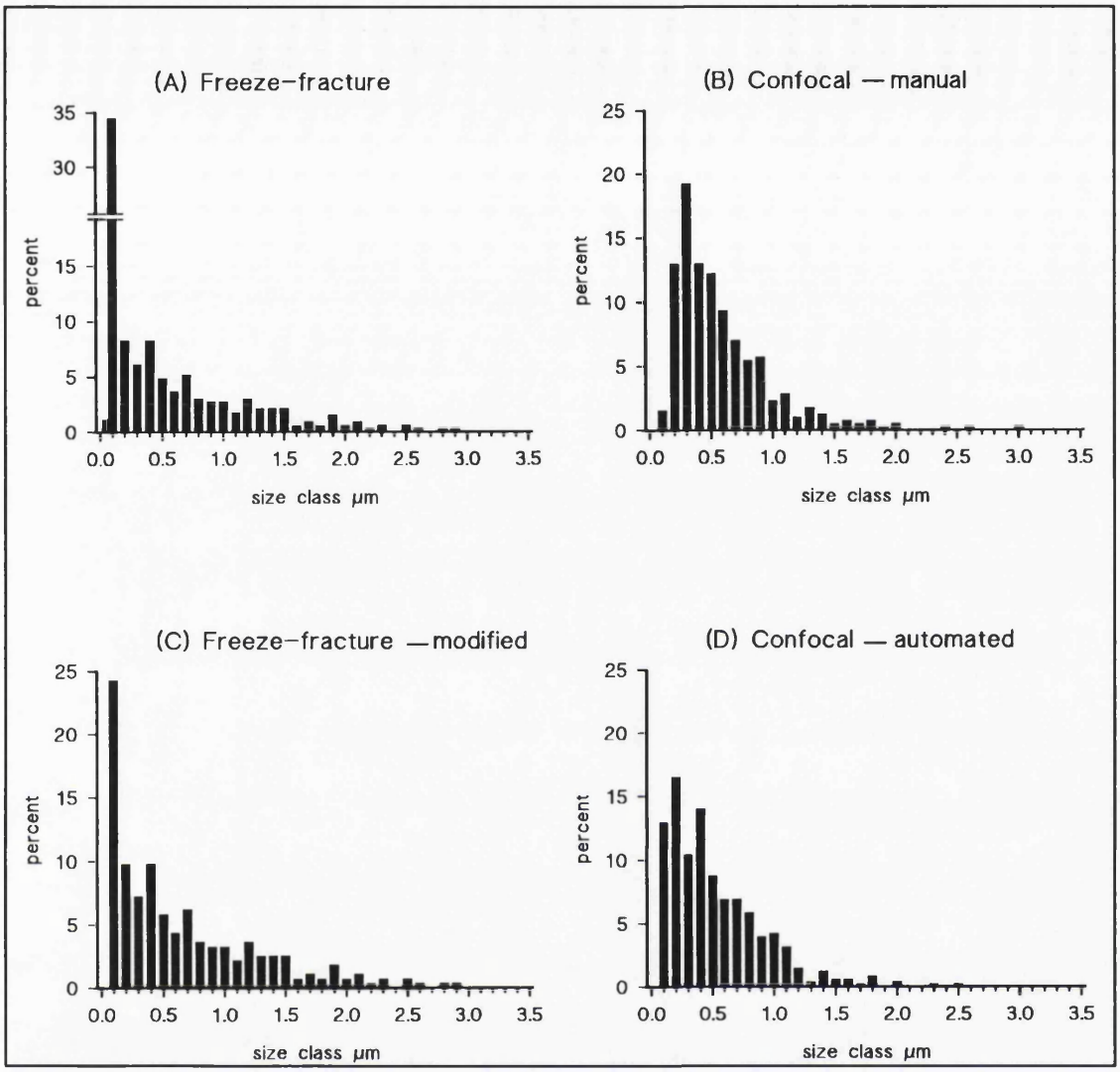

Figure 2.4. Histograms comparing the frequency distributions of long-axis lengths of gap junctions measured in rat ventricle using freeze-fracture and confocal microscopic techniques.
A. Freeze-fracture data in 0.1 μm size classes. As the length measurements are rounded to the nearest 0.1 μm (the midpoints of each size class), junctions below 0.05 μm appear in a half-class at the left of the distribution.
B. Confocal data measured manually by mouse, using the "length" command of the BioRad SOM software.
C. Modified freeze-fracture data after exclusion of junctions <0.08 μm long.
D. Automated confocal measurement of the same images as in B, using PC-Image software.
Analysis of variance of the $\log_{10}$-transformed data demonstrates similarity between the adjusted freeze-fracture (C) and automated confocal (D) data sets only ($p=1.0$).

The most striking difference between the frequency distributions of the immunohistochemical and freeze-fracture data is the large proportion of junctions < 0.1 μm long at freeze-fracture (Fig 2.4). The mean junctional length in the freeze-fracture data (0.56 μm) does not differ substantially from the confocal measurements (mean from manually-acquired data, 0.59 μm; automatically-acquired, 0.53 μm), but the difference in the frequency distributions is reflected in the medians (freeze-fracture, 0.35 μm;

confocal, 0.41 μm). When the junctions of 0.08 μm or less are excluded from the freeze-fracture data set, however, the modified distribution shows a close resemblance with the confocal data, and similar medians (modified freeze-fracture median 0.44 μm). Analysis of variance of the $\log_{10}$-transformed data confirms the similarity of means and distributions of the modified freeze-fracture data (mean -0.39, SD 0.45) compared with the automated confocal data (mean -0.39, SD 0.32; $p=1.0$), but not the manual confocal data ($p=0.006$). Underlying this is a significant difference in the distributions of the manually and automatically acquired confocal data ($\log_{10}$-transformed data; $p<0.001$), due principally to the detection and inclusion of more junctions <0.03 μm in the automated data.

2.7.4 Interpretation and Conclusion

The ability of freeze-fracture to display junctional domains in face-on view, with well-delineated borders, has made it the method of choice for measuring the dimensions of individual gap junctions. However, freeze-fracture data can give very little indication of gap-junctional content or pattern of distribution in relatively large volumes of tissue — volumes that might be appropriate to analyse if functional data relating to the electromechanical properties of the tissue are to be correlated with patterns of tissue coupling. Although the immunohistochemical technique to be used in this series of studies can provide qualitative information from such appropriate volumes of tissue, it may also in theory, permit quantitative analysis (Brakenhoff et al. 1990). Although detection of the smallest gap junctions by an immunohistochemical technique cannot be as sensitive as when using freeze-fracture, which itself has limitations (as discussed in part in section 2.7.2a), the extensive overlap in the size range of detectability of the two microscopical methods used in this study has permitted comparison of the immunohistochemical data with the widely accepted method of choice for sizing gap junctions.

The results show that down to objects of 2-pixel size on the monitor screen (140-170 nm), there is broad agreement between the automated confocal measurement and the freeze-fracture data. This size limitation in the detection of small junctions does not significantly affect quantification of the total gap-junctional content of a volume of myocardium. Despite their abundance (15% of total), exclusion of junctions of less than 80 nm from the freeze-fracture data reduces the total gap-junctional length measured by only 1.8% and junctional area estimation is, accordingly, barely reduced (by <0.04%).

The difference between the automated and manual confocal data resulted from the tendency to miss (or ignore) the smaller junctions when surveying a monitor screen of data for manual measurement.

The practical implications of these results are as follows:-

i. Measurement from confocal images of immunolabelled gap junctions, using standardised techniques throughout, can be used reliably for quantification of the junctions.

ii. Quantification of the data should be automated wherever possible.

iii. Rigorous inclusion of all small junctions must be ensured whenever manual measurements are being made.

These conclusions were therefore incorporated into the methodological approach used in this thesis.

2.8 INITIAL STUDY 2 - The effects of tissue fixation in Zamboni's solution on gap-junctional ultrastructure at thin section electron microscopy

2.8.1 Introduction

Zamboni's solution contains picric acid specifically to cause perforation of the plasma membrane to enable access of the connexin43 antibody to the epitope (Toshimori et al. 1987). This perforation may have the additional benefit of eliminating significant osmotic disruption to the myocytes when chemically treating fixed tissue. However, although Zamboni's solution provides adequate aldehyde fixation of proteins for observation at the light microscopical level, it is inadequate for structural preservation at the electron microscopical level.

For ease of handling of fresh myocardial specimens in the operating theatre, an ideal approach would be to place the tissue directly in Zamboni's solution; this would allow it to be taken back to the laboratory before being subdivided to obtain portions for transfer into glutaraldehyde fixative for electron microscopy. To determine whether this approach would adequately preserve gap junction and intercalated disk ultrastructure, thin section electron microscopic examination was carried out to compare ventricular myocardium prepared in this way with that processed by the standard method of immediate fixation in glutaraldehyde.

2.8.2 Materials and Methods

The heart of a female Sprague-Dawley rat (250 g) was removed immediately post-mortem, and the left ventricular free wall was divided into 1-2 mm^3 pieces for immersion fixation in either glutaraldehyde for 2 hours, or Zamboni's solution for 2 hours before further fixation for 2 hours in glutaraldehyde. Subsequent tissue processing was by the standard procedures detailed in section 2.5.1 of this chapter.

2.8.3 Results

Immediate immersion fixation in glutaraldehyde produced good tissue preservation, with few disrupted mitochondria, no margination of nuclear chromatin, intact cellular membranes and few areas of myofibril contracture with little variation in sarcomere lengths. The samples exposed to Zamboni's solution before fixation in glutaraldehyde showed some disruption of the plasma membranes and mitochondrial membranes, with mild and uniform contraction of the myofibrils, and loss of cytoplasmic detail. The

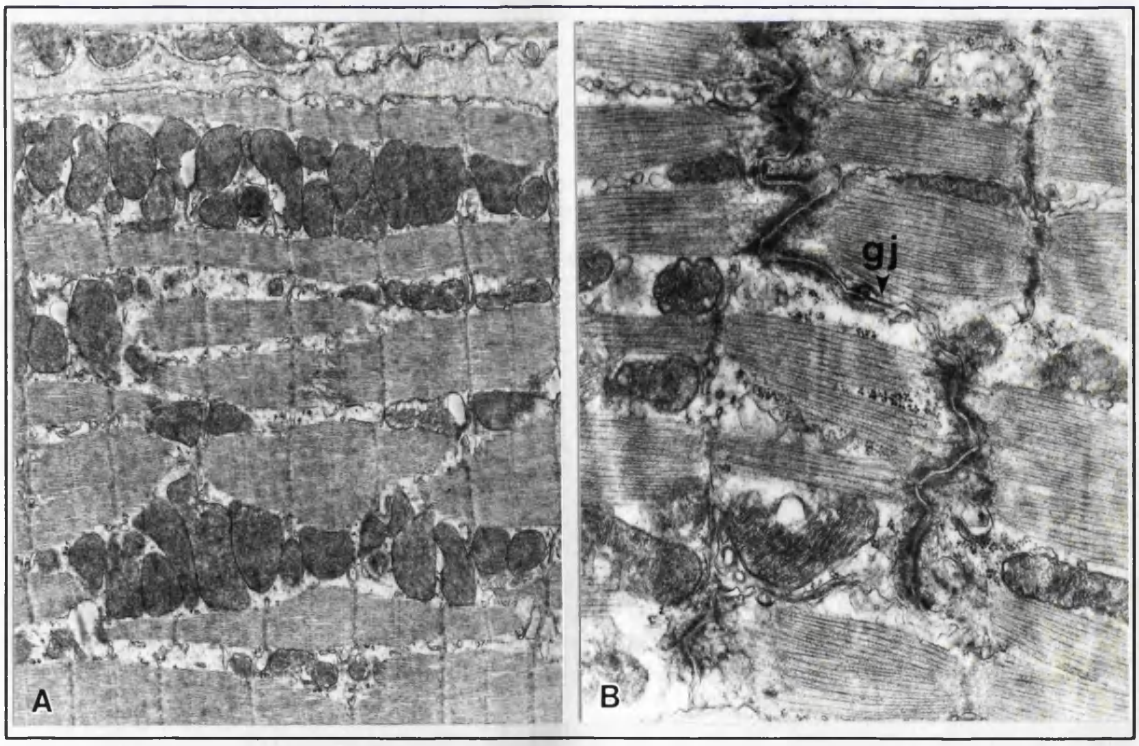

Figure 2.5. Thin section electron micrographs of longitudinally-sectioned rat left ventricle fixed by immersion in Zamboni's solution for two hours before immersion in glutaraldehyde for a further two hours. The cellular ultrastructure shows some disruption of the mitochondrial membranes, mild and uniform contraction of the myofibrils (in A), with intact intercalated disks and gap junctions (gj) in particular (in B). A, x7,300; B, x23,400.

intercalated disks, however, showed little disruption and appeared intact and of normal arrangement (Fig 2.5).

2.8.4 Interpretation and Conclusions

The results of this study demonstrate adequate intercalated disk and, in particular, gap-junctional preservation after Zamboni's fixation. There was no detectable disruption to either the gap junctions, or the gross topology of the intercalated disks at magnifications of up to x70,000. However, although overall tissue architecture was intact, and despite adequate preservation after Zamboni's fixation for the examination of gap-junctional organisation at the light microscopical level, the degree of disruption, particularly of membranous structures, was not ideal for ultrastructural tissue examination.

The practical implications of these results are as follows:-

i. Zamboni's fixation of tissue, as used in the relatively low-magnification immunohistochemical procedure, results in no significant disruption of either the overall ultrastructure or the orientation and topology of the structures being labelled.

ii. Prolonged exposure to Zamboni's solution before fixation in glutaraldehyde results in imperfect ultrastructural preservation. Although the quality of preservation is fair, it is clear that initial handling in Zamboni's solution is not ideal for electron microscopic examination. As a result, tissue obtained for the series of studies comprising this thesis was immediately divided in the operating theatre, and placed directly in either Zamboni's solution or glutaraldehyde, as appropriate.

2.9 **General methodological problems**

2.9.1 Biopsy techniques

Three different biopsy techniques were employed, as appropriate to the particular source of tissue.

i. Scalpel excision was used in cases in which myocardium was being resected as a matter of course during the surgical procedure itself, and in some instances, specifically for the purposes of this study. Myocardium from the removed diseased hearts of patients undergoing cardiac transplantation was obtained by scalpel excision.

ii. Needle (Trucut) biopsy was used by approval of the ethics committee, and by written

informed consent of selected patients from whom appropriate tissue was potentially appropriate for study, pending the surgical findings and at the discretion of the operating surgeon. This technique for ventricular myocardial biopsy has been used safely in previous studies (Pepper et al. 1982).

iii. Cardiac transplant donor hearts are routinely biopsied several times before implantation using a transvenous-type pinch bioptome, and a small quantity of ventricular myocardium was available at the discretion of the surgeon.

All biopsy material showed some disruption of the myocytes to a distance of up to about 5 cells' width from the cut surface (Fig 2.6), with marked contracture banding and associated distortion of the overall plicate and interplicate arrangement of the intercalated disks. The junctions comprising the disks remained intact. For the studies of gap-junctional distribution, however, particularly for those with quantitative aspects, it was essential that the disrupted tissue was avoided. In all cases, the original biopsy surfaces were discarded when sections were prepared for examination. In the case of the pinch biopsies little useful tissue remained but was nevertheless sufficient for study.

Direct comparison of the ultrastructure at thin section electron microscopy of transmural ventricular myocardium removed (from a diseased explanted heart) by scalpel excision, and an adjacent needle biopsy, revealed no detectable differences in the degree of tissue disruption of the deeper tissue within each specimen.

2.9.2 Tissue quantity

Freeze-fracture tissue examination was not required routinely for every specimen, but only to supplement other data where necessary. This was a fortunate feature of the study design, since a result of the obvious limitation of the amount of tissue that could be obtained from any surgical patient, and the requirement for subdividing specimens for the different imaging techniques, was that fragments for freeze-fracture analysis were often not available or inadequate to produce useful data.

2.9.3 Glutaraldehyde contamination

Glutaraldehyde fluoresces intensely under laser stimulation in the confocal microscope, completely masking any labelling. With most samples obtained being hurriedly divided between the appropriate fixative solutions for immunohistochemical and electron

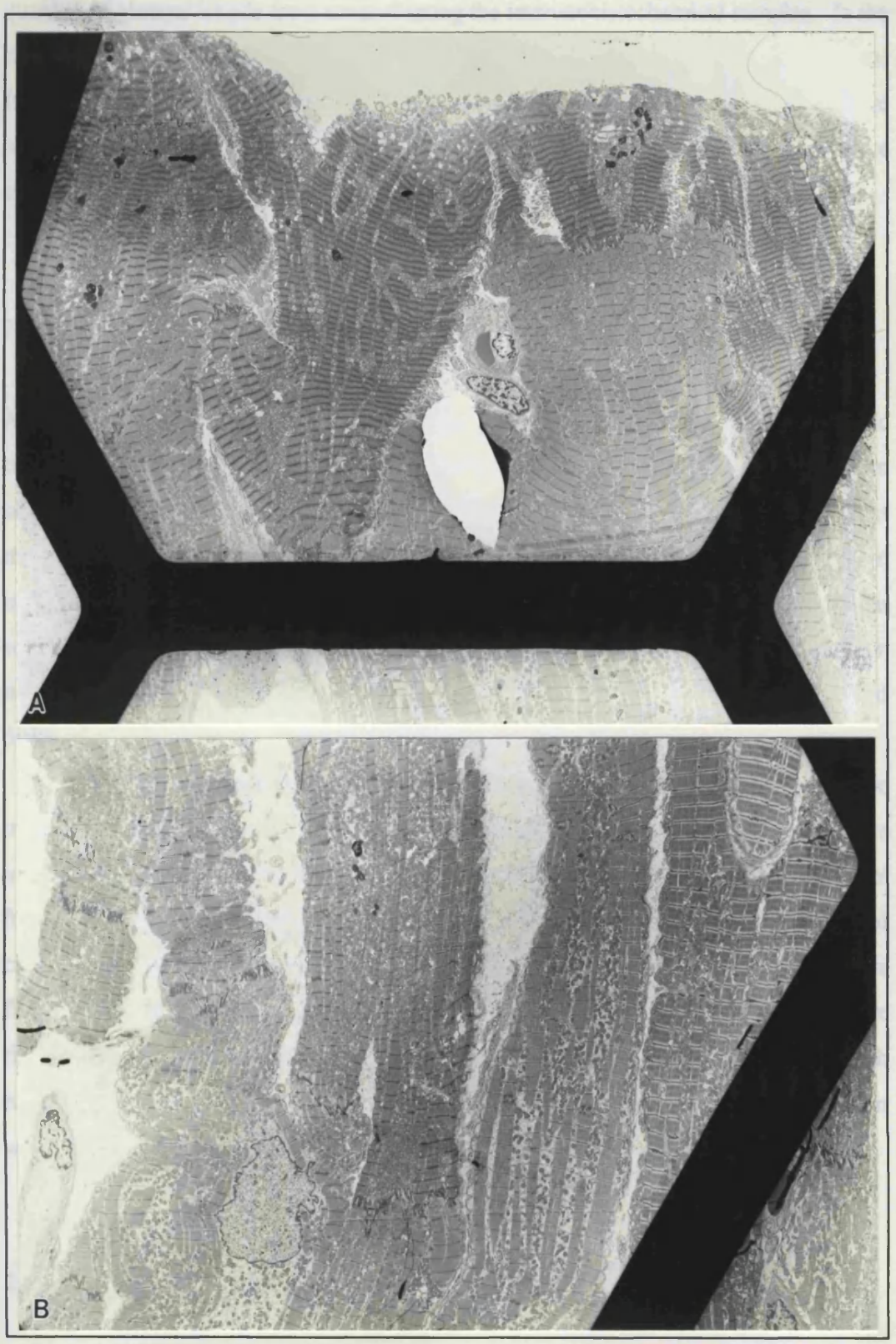

Figure 2.6. Low power thin section electron micrographs of healthy myocardium biopsied by the needle (Trucut) technique. A shows extensive contractures and disruption of the myocytes at and near the cut surface. B is a representative field at a distance of one field-width ($\approx 100\mu m$) from the surface of the same sample of healthy myocardium. Although the myocytes are in a variable state of contraction, there are no contractures. A & B, x1,300.

microscopic analysis, there was a practical problem of preventing even the smallest quantity of glutaraldehyde from contaminating the immunohistochemical samples. In the early studies performed, this occurred, spoiling some immunohistochemical experiments. Initial handling of each biopsy in Zamboni's solution before subdivision would have helped minimise this problem, but as discussed in section 2.7, was found to produce suboptimal tissue preservation.

2.9.4 Cold cardioplegic solutions

All surgical specimens had been exposed for varying lengths of time to hypothermic cardiac arrest, with or without use of cold cardioplegic solution, before being fixed. In some cases, exposure was for only 2 to 3 minutes, but in others the myocardium was maintained for up to 4 hours in cold cardioplegic solution. Reviewing electron micrographs from studies confining themselves to assessing ultrastructural preservation with cold cardioplegia (Mankad et al. 1992), there are no features to suggest disruption of either the cellular topology and gross architecture of the tissue, or of the intercalated disks.

The cases that had been exposed to cardioplegic solution for longest were the transplant donor hearts, which were biopsied at the implanting centre after up to 4 hours in iced cardioplegic solution since explantation from the donor. In an attempt to control further for this, a transmural needle biopsy obtained immediately after establishing cold cardioplegic arrest from one of the surgical human hearts was divided i) for immediate fixation, and ii) for storage in refrigerated cardioplegic solution for 4 hours before fixation. Both specimens were examined by thin section electron microscopy, which revealed that there were no detectable qualitative differences. The quality of preservation was adequate in both cases.

2.9.5 Lipofuscin

This product of degradation of cellular components occurs in collections near the nucleus of adult cardiac myocytes (Cotran et al. 1989). It autofluoresces when stimulated with laser light at the wavelength used, producing an emission that is pink, and which can therefore be readily distinguished from the green fluoroscein emission when viewed

through a standard epifluorescent microscope. The pink lipofuscin deposits also have a characteristic appearance, resembling rounded bunches of grapes, so are easily distinguishable by this feature alone in the confocal microscope by which black and white images are produced. The combination of the pink colouration of standard epifluorescence and the very distinctive shape of collections, therefore permitted easy distinction of lipofuscin from connexin43 label in experimental images. Autofluorescence of vascular smooth muscle was also easily distinguished in confocal images. For an example of an image containing lipofuscin fluorescence, see Fig 3.6 in Chapter 3.

PART II - GAP JUNCTIONS IN NORMAL HUMAN VENTRICULAR MYOCARDIUM

CHAPTER 3 - GAP JUNCTIONS IN ADULT HUMAN VENTRICULAR MYOCARDIUM

3.1 Introduction

The normal pattern of anisotropic conduction in ventricular myocardium, by which conduction parallel to the myocyte long axis is up to four times more rapid than in the transverse direction (Delmar et al. 1987; Dillon et al. 1988), is dependent in part on the low resistivity of the gap-junctional membranes, and on their distribution and abundance. Despite recognition that changes in the passive resistivity encountered by a propagating impulse can reduce conduction velocity and increase heterogeneity of conduction, irrespective of changes in active ionic membrane properties (Fozzard, 1977; Arnsdorf, 1984; Binah and Rosen, 1992; Saffitz et al. 1992), little information is available on the quantity and distribution, or the function, of gap junctions in human myocardium in health or disease. It is known that human ventricular myocardium contains gap junctions with the characteristic overall arrangement common to all mammals (Gourdie et al. 1991), but prior to starting work on the series of studies comprising this thesis, there had been no published studies on human myocardium with respect to gap junction quantification or the potential disturbances of gap junction quantity and organisation in disease.

In order to investigate abnormalities of gap junction organisation that may exist in diseased myocardium, it is essential first to establish some baseline characteristics of the normal heart. The aim in this chapter therefore is to examine the structural organisation of gap junctions in normal human ventricular myocardium using confocal immunohistochemical detection of connexin43 and electron microscopic techniques. A novel technique was developed for determining gap junction content by acquiring data in a form that could not only be used for quantification in the conventional units ($\mu m^2/\mu m^3$) for stereological assessment of this sort (Stewart and Page, 1978), but, importantly, could also permit an estimate of junctional content **per myocyte** to be derived (Chapter 6), thus enabling meaningful comparisons between tissues with different sized constituent cells.

3.2 Materials and Methods

3.2.1 "Normal" ventricular myocardium

Completely normal human myocardium for immediate fixation is not available for experimentation. For the purposes of this study "normal" myocardium was obtained from the following sources:-

i. Cardiac transplant donor hearts from which a single right ventricular biopsy was obtained on arrival at the implanting hospital, following transportation of the heart in cardioplegic solution on ice (for up to 4 hours).

Samples of both ventricles of normal donor hearts, which for technical reasons were not used for transplantation as intended, were also studied.

ii. The left ventricular apical region from patients with the Wolff-Parkinson-White syndrome. This group of patients experienced occasional but symptomatic tachyarrhythmic episodes, but had no other detected cardiac dysfunction on routine preoperative assessment, and underwent surgical division of the accessory pathway. Ventricular myocardium from hearts such as these, with infrequent arrhythmic episodes, has not been shown to have any structural abnormality and is generally considered normal (Wit and Janse, 1992).

By these criteria 5 "normal" left ventricular samples (2 transplant donor hearts and 3 Wolff-Parkinson-White syndrome hearts) were studied and 5 right ventricular samples (transplant donors). The tissue was divided and processed for connexin43 immunohistochemistry, thin section and freeze-fracture electron microscopy, as described in section 2.3.2.

3.2.2 Quantitative connexin43-immunohistochemistry

A low power survey of each specimen was made by standard epifluorescence and confocal microscopy.

3.2.2a *Sizes of connexin43-gap junctions*

Projection images were made of 4 randomly selected en face intercalated disks from each specimen, imaged in their entirety using the x60 objective and zoom 4 setting on the confocal microscope. Measurements of the longest dimension of the fluorescent spots representing gap junctions were made by the automatic and manual techniques detailed

in Initial Study 1 reported in Chapter 2. This study indicated the tendency to ignore or overlook the smallest fluorescent spots, so attention was paid to collecting all data, including that representing the smallest junctions.

3.2.2b *Myocardial gap junction surface area*

To determine the quantity of gap junction present, myocardial sections were cut transverse to the long axis of the constituent myocytes. The confocal microscope was configured with a small aperture (aperture control withdrawn 1.2 mm) so that the confocality of the 10 optical sections taken at 1 μm intervals permitted minimal overlap between consecutive images, ensuring acquisition of all fluorescence present (Fig 3.1). These series of images were collected using the x60 objective lens and the zoom 1 computer setting (field 180x120 μm^2), with neutral density filter 1 to eliminate significant fading of fluorescence. The "black level" was constant (at 4.0) such that the outlines of the individual cross-sectioned cells were visible and the "gain" control was adjusted so that the spectrum of label intensities spanned the full 255-level grey scale.

The image data from the known volume of tissue of 180x120x10 μm^3 were then analysed. First, from the 5th optical slice, the area of the field occupied by myocytes was determined by subtracting from the total sample field all regions that were either completely devoid of signal (interstitial fibrosis) or recognisable as blood vessels. A projection image was constructed for each 10-image series (Fig 3.1), and a binary overlay of the projection was created automatically, with a set threshold of 60 on the 255-point grey scale, to eliminate the background cell outlines. The binary image was then edited by hand to reject all extraneous lipofuscin and blood vessel autofluorescence, which were easily identifiable, and an automatic count made of the total number of pixels in the "on" state. This area represented the total area of labelled gap junction, and analysis of the optical section series by this technique enabled determination of the quantity of gap junction, expressed as $\mu m^2/\mu m^3$ myocyte volume.

3.2.2c *Intercalated disks per myocyte and myocardial cell arrangement*

To determine the number of intercellular abutments in normal ventricular myocardial architecture, counts were made of the number of cell-surface clusters of gap junction label in 100 randomly selected isolated left ventricular myocytes pooled from 3 of the normal hearts. Myocytes were isolated and processed by the methods described in Chapter 2, and epifluorescence microscopy was used to count the number of focal clusters of label, each representing an intercalated disk.

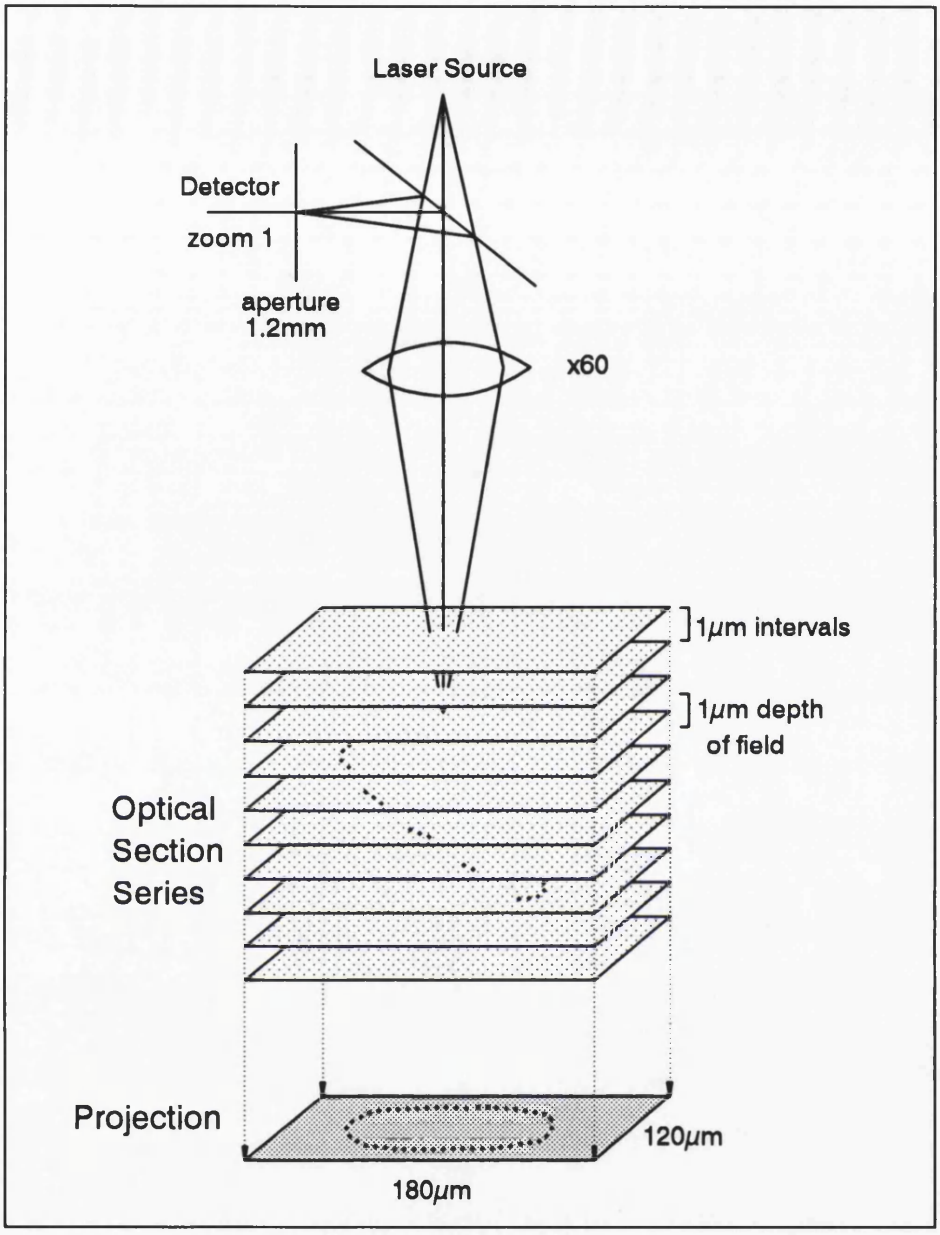

Figure 3.1. To acquire confocal data for quantification, the scanning laser confocal microscope was set up with the x60 objective lens and zoom 1 setting in the SOM software (field size 180x120 μm^2), with the aperture control withdrawn 1.2 mm (depth of field $\approx$ 1 μm), and 1-μm steps between each of the 10-image series.

3.2.3 Connexon packing density

Freeze-fracture electron micrographs were used to measure the connexon surface density within individual gap junction plaques pooled from the patients from which enough tissue was obtained to permit freeze-fracture examination. As the precise packing arrangement of connexons is reported to alter under various conditions, as discussed in section 1.2.3a (Peracchia, 1980; Green and Severs, 1984b), it is important for this study that any variation in connexon density (regardless of the precise arrangement of the packing) is

accounted for in the interpretation of the measured spot sizes obtained by the immunohistochemical technique. If connexon packing density were to vary with gap-junctional size or in different disease states, then for immunohistochemical quantification to be representative of the total number of gap-junctional channels and, therefore, the maximal potential for gap-junctional intercellular coupling, the size distribution of the individual gap junctions would have to be taken into account.

In order to investigate variation in connexon packing density with junctional size, an electron micrograph with a final magnification of 70,000x of each gap junction plaque was used to determine the junctional area, using VIDS III software (Analytical Measuring Systems, England). The connexon packing density was determined by counting the number of connexons within a hole in a mask placed randomly to provide a sample field on the micrograph.

3.3 **Results**

Details of the patients from whom specimens were taken for this study are shown in Table 3.1. The average age of the patients from whom normal left ventricular tissue was obtained was 43.4 $\pm$ 12.6 years, and that of patients from whom normal right ventricular tissue was obtained was 35.4 $\pm$ 10.1 years.

Table 3.1 Details of "normal" ventricular myocardial biopsies

Patient/heart no.	diagnosis	age (yrs)	ventricle sampled	biopsy technique
N1	WPW syndrome	37	left	scalpel
N2	Transplant donor	46	left & right	scalpel & Trucut
N3	WPW syndrome	28	left	scalpel
N4	Transplant donor	44	left & right	scalpel & Trucut
N5	WPW syndrome	62	left	scalpel
N6	Transplant donor	26	right	bioptome
N7	Transplant donor	37	right	bioptome
N8	Transplant donor	24	right	bioptome

3.3.1 Histology and General Ultrastructure

The histological and thin section electron microscopic appearances of ventricular myocardium from the transplant donor and Wolff-Parkinson-White subjects were normal, as illustrated in Figure 3.2.

3.3.2 Immunolabelled Connexin43 Gap Junction Distribution at Confocal Microscopy

Immunolocalisation of connexin43 gave consistent patterns of gap junction labelling, common to left and right ventricle. In both groups, gap junctions were visualised with the normal adult mammalian patterns previously described (Gourdie et al. 1991); bright fluorescent domains marking the positions of intercalated disks between myocytes, appearing as transverse lines of individually-resolved spots in longitudinally-sectioned myofibres (Fig 3.3), and discoid arrays delineated peripherally by large gap junctions in transversely-sectioned myocardium (Fig 3.4 and 3.5). The gap-junctional label was confined almost exclusively to positions of intercalated disks; the only potential exceptions were occasional spots of label that were part of sufficiently small or diffuse a cluster to make it unclear whether they formed part of a disk or not. Otherwise, each fluorescent spot appeared as part of a linear cluster orientated transverse to the long axis of the myocytes. Although immunolocalisation for connexin43 gave a strong signal for myocyte gap junctions, no immunostaining of non-myocyte cell types (i.e. interstitial fibroblasts or vascular smooth muscle cells) was detectable. A high level of autofluorescence was, however, apparent in vascular smooth muscle. Although easily discriminated from the surrounding myocardial signal, this vascular autofluorescence masked any possible arterial smooth muscle signal.
Controls in which antiserum treatment was omitted or substituted with pre-immune serum showed no fluorescent labelling (Fig 3.6g). Grape-like collections of lipofuscin (Fig 3.6g) with characteristic pink autofluorescence (section 2.9.5) were present.

3.3.3 Quantitative Characterisation of Gap Junctions

3.3.3a *Analysis of Connexon Density in Freeze-fractured Gap Junctions*

Small quantities of left ventricular myocardium were processed for freeze-fracture analysis from all 5 patients, such that the number of tissue fragments available for fracturing varied from 2 to 8. As a result of unavoidable technical wastage from the

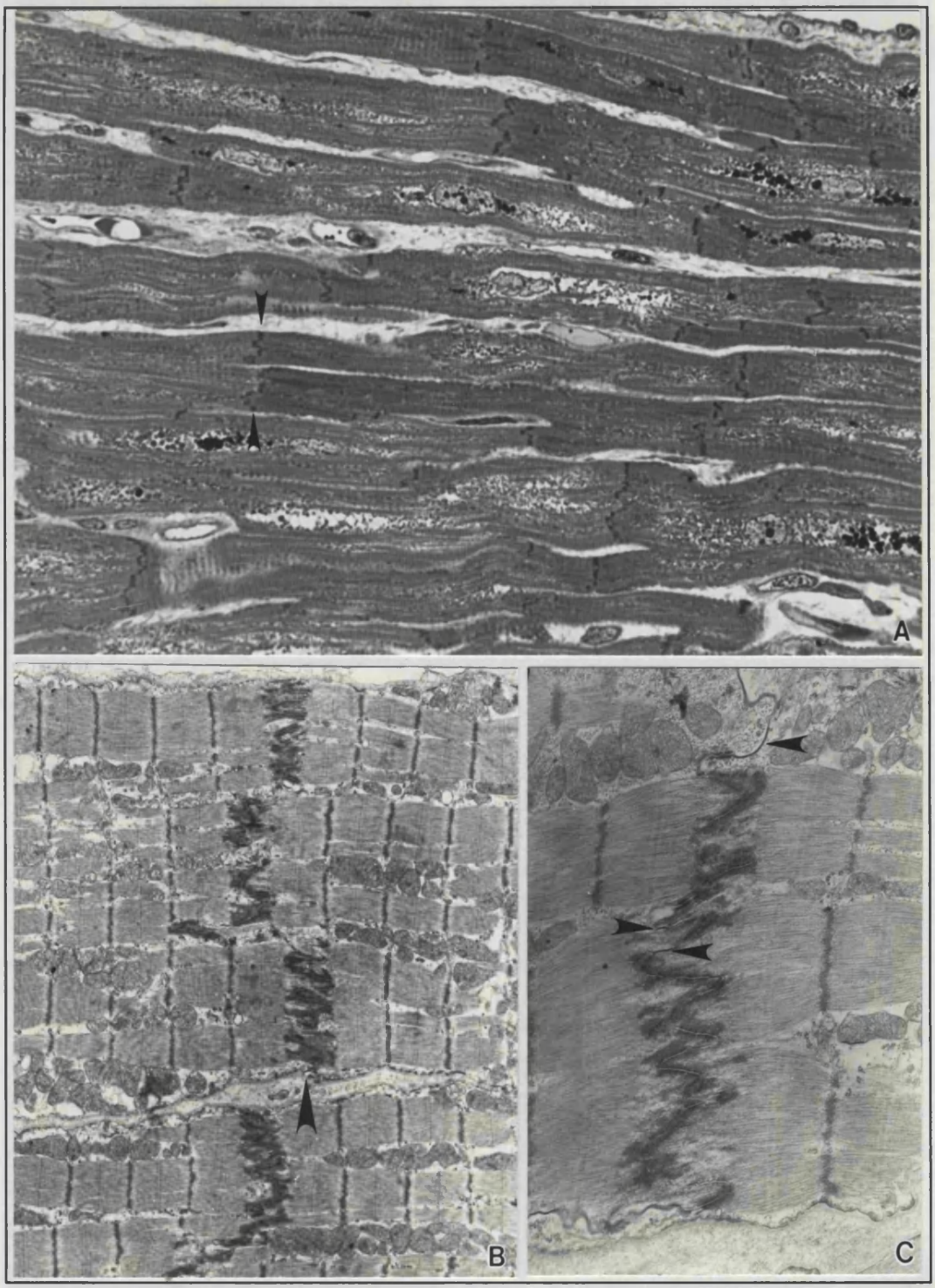

Figure 3.2. Typical microscopic features of normal ventricular myocardium. **A:** Light microscopy of a toluidine blue-stained resin section showing aligned, cross-striated myocytes, and the dark intercalated disks running transversely across between abutting myocytes (arrows). x625. **B:** Low power electron micrograph showing an electron-dense intercalated disk (arrow) traversing between cells. The striations of the sarcomeres are aligned in this healthy tissue. x4,900. **C:** Higher power electron micrograph showing characteristic gap junctions (arrow). x12,700.

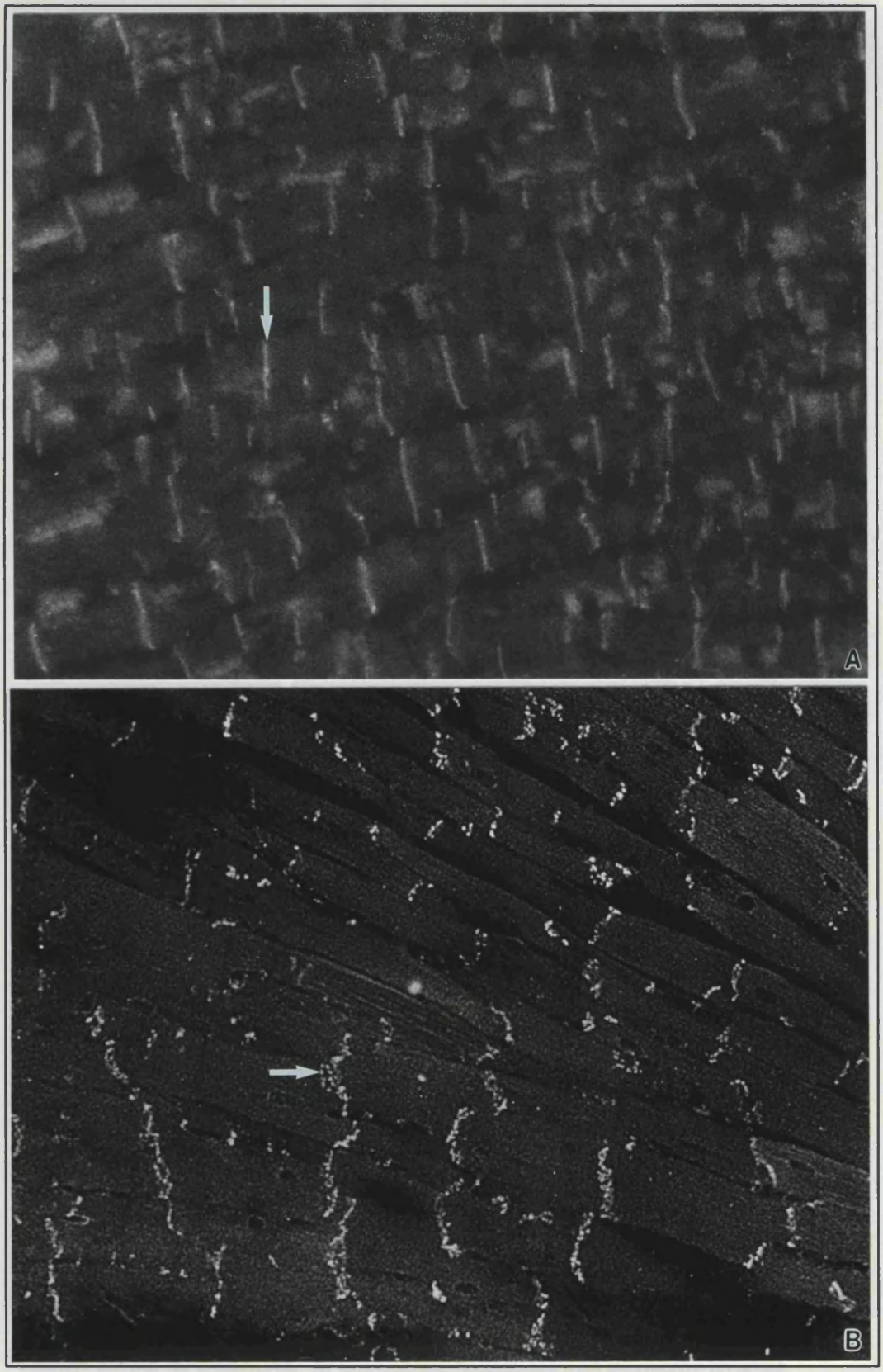

Figure 3.3. Immunolocalisation of gap junctions in longitudinally-sectioned normal human left ventricle labelled for connexin43. **A:** Conventional fluorescence light microscopy reveals labelling of the gap junctions marking the intercalated disks as blurred lines traversing the tissue (arrow). **B:** A single optical section by laser scanning confocal microscopy reveals each individual gap junction domain as a separate spot (arrow), with striking clarity. A & B, x400.

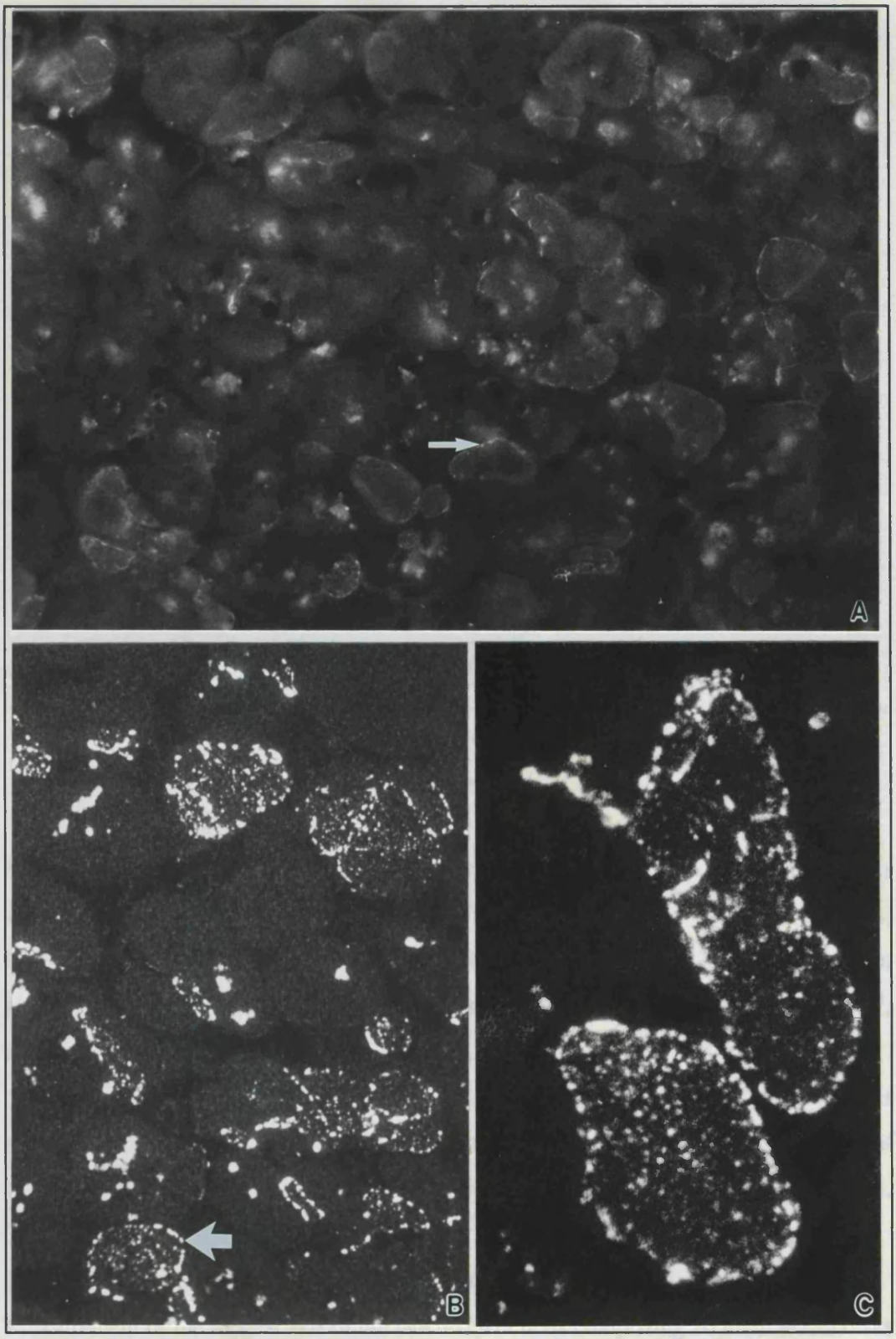

Figure 3.4. Immunolocalisation of gap junctions in transversely-sectioned normal human left ventricle labelled for connexin43. **A:** Conventional fluorescence light microscopy revealing collections of blurred label defining the positions of the intercalated disks (arrow). x400. **B:** A projected optical series showing the characteristic features of a disk viewed en face (arrow), with a peripheral ring of large junctions and smaller central domains. x550. **C:** High power view of en face disks, showing the entire gap junction population of each disk in focus. x2,200.

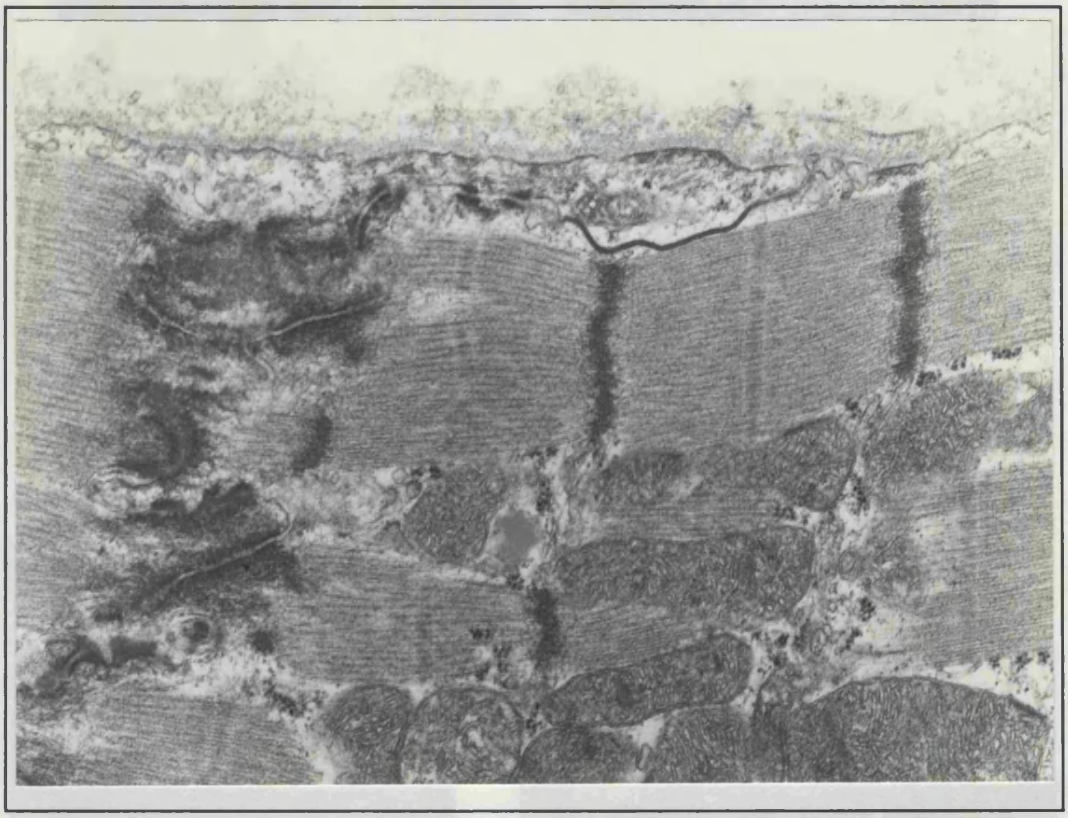

Figure 3.5. Thin section electron micrograph showing the characteristic long run of gap-junctional membrane at the edge of an intercalated disk. This feature is consistent with the immunohistochemical finding of the peripheral ring of larger gap junctions around the edges of en face-viewed disks. x31,000.

fracturing process, replica generation and cleaning procedures, the yield of gap junctions was low. The total of 22 gap junctions (Fig 3.7) pooled from these patients was, however, adequate for this simple analysis, which demonstrated no correlation between gap junction size and the density of the component connexons (99.3 ± 14.4 x10^{-4}nm^{-2}, n=22). These results are plotted in Figure 3.8 (r=0.045, p=0.84).

Measurement of total label present in the immunohistochemical images in this study will therefore be proportional to the number of connexons and the quantity of connexin regardless of any variation in spot size distribution between different samples.

3.3.3b *Size of Immunolabelled Gap Junctions*

Measurement of the longest axis of the labelled junctions comprising 20 intercalated disks selected at random from the 5 normal left ventricular specimens revealed a mean length of 0.52 ± 0.30 μm, with a distribution as shown in Figure 3.9. The larger junctions at the periphery of the disk had a mean length of 0.67 ± 0.32 μm (maximum 2.8 μm); the junctions in the central area of the disk 0.36 ± 0.17 μm (minimum 0.1 μm).

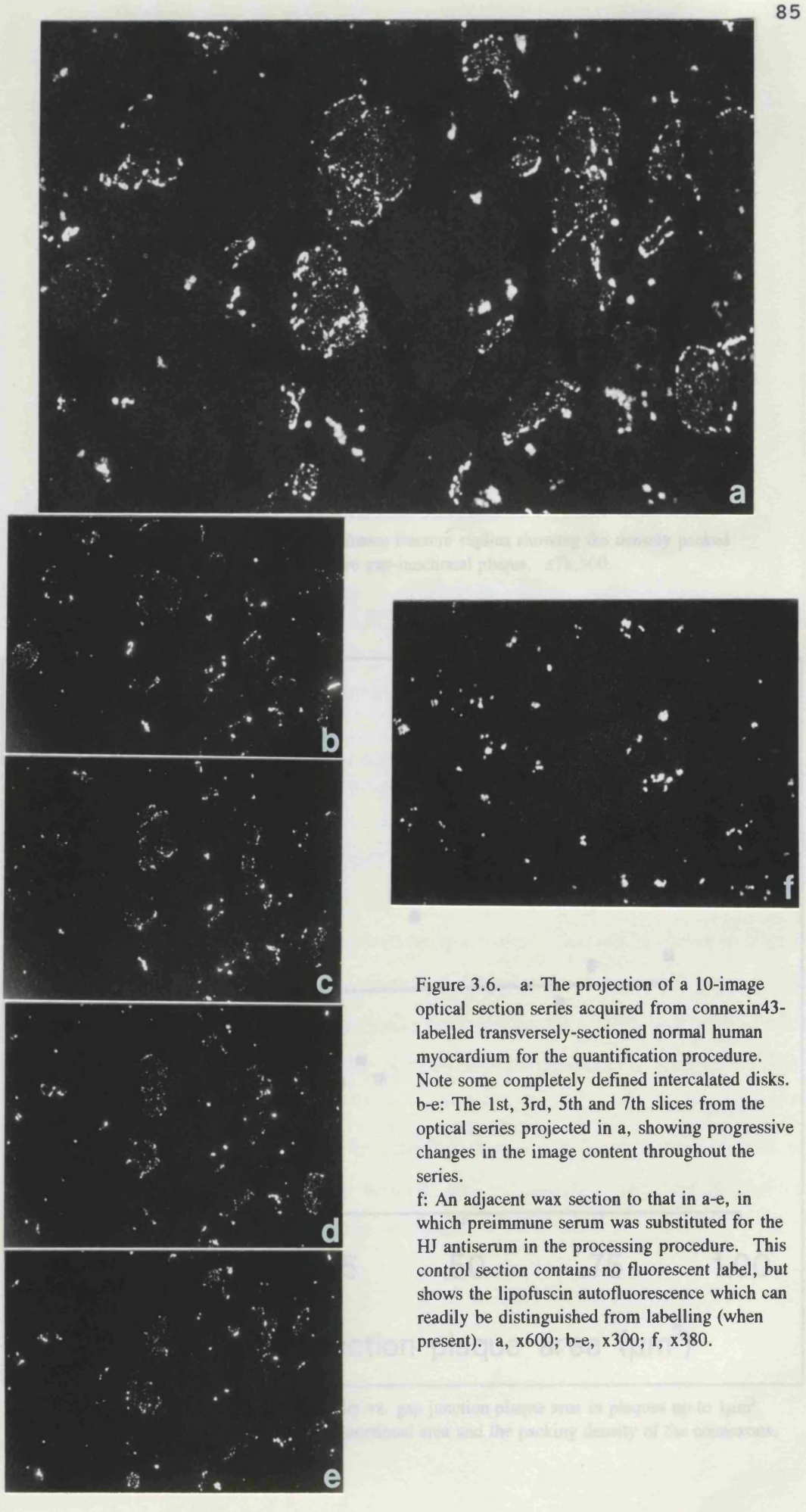

Figure 3.6. a: The projection of a 10-image optical section series acquired from connexin43-labelled transversely-sectioned normal human myocardium for the quantification procedure. Note some completely defined intercalated disks. b-e: The 1st, 3rd, 5th and 7th slices from the optical series projected in a, showing progressive changes in the image content throughout the series.
f: An adjacent wax section to that in a-e, in which preimmune serum was substituted for the HJ antiserum in the processing procedure. This control section contains no fluorescent label, but shows the lipofuscin autofluorescence which can readily be distinguished from labelling (when present). a, x600; b-e, x300; f, x380.

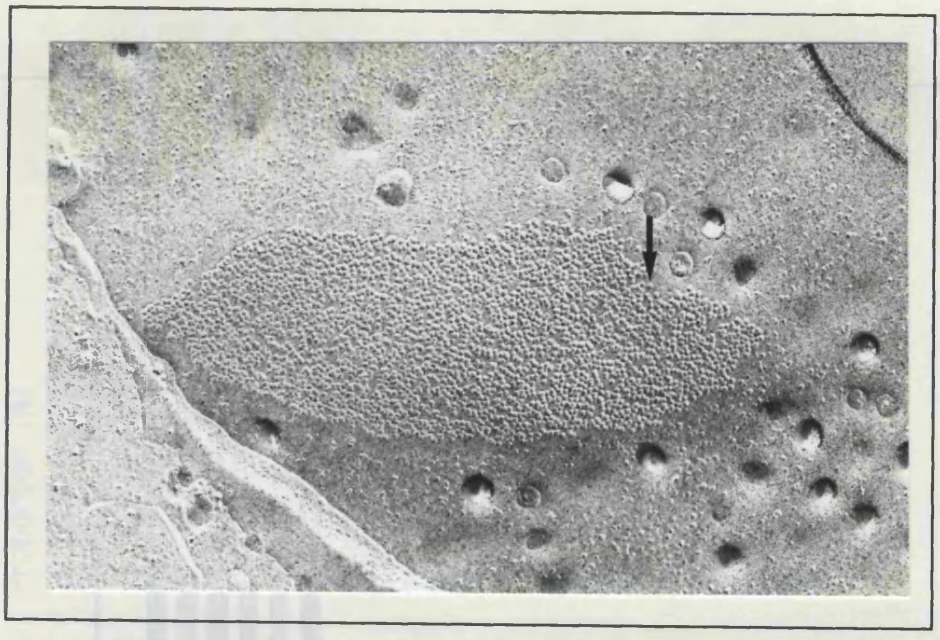

Figure 3.7. Electron micrograph of freeze-fracture replica showing the densely packed connexon particles (arrow) of an entire gap-junctional plaque. x78,500.

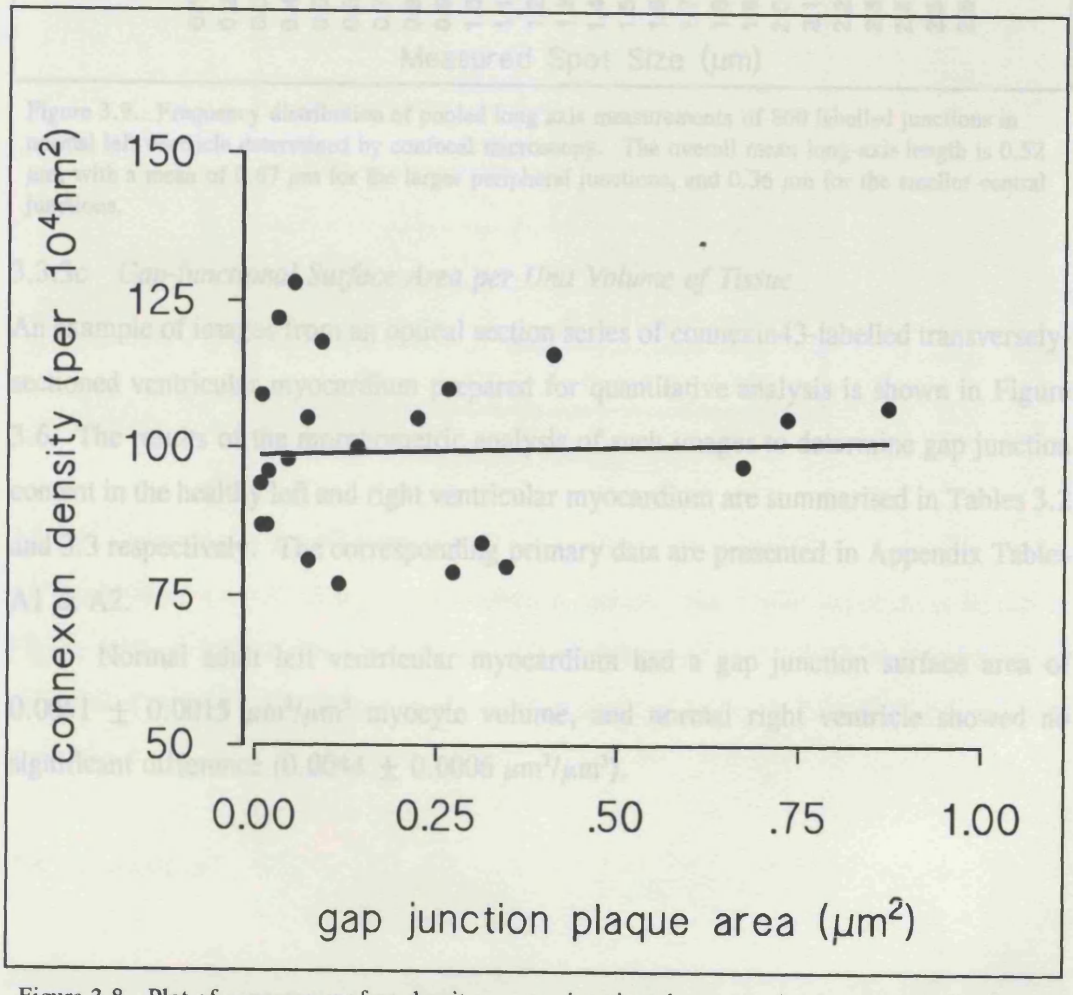

Figure 3.8. Plot of connexon surface density vs. gap junction plaque area in plaques up to 1μm^2. There is no correlation (p=0.84) between junctional area and the packing density of the connexons, and the slope is not significant.

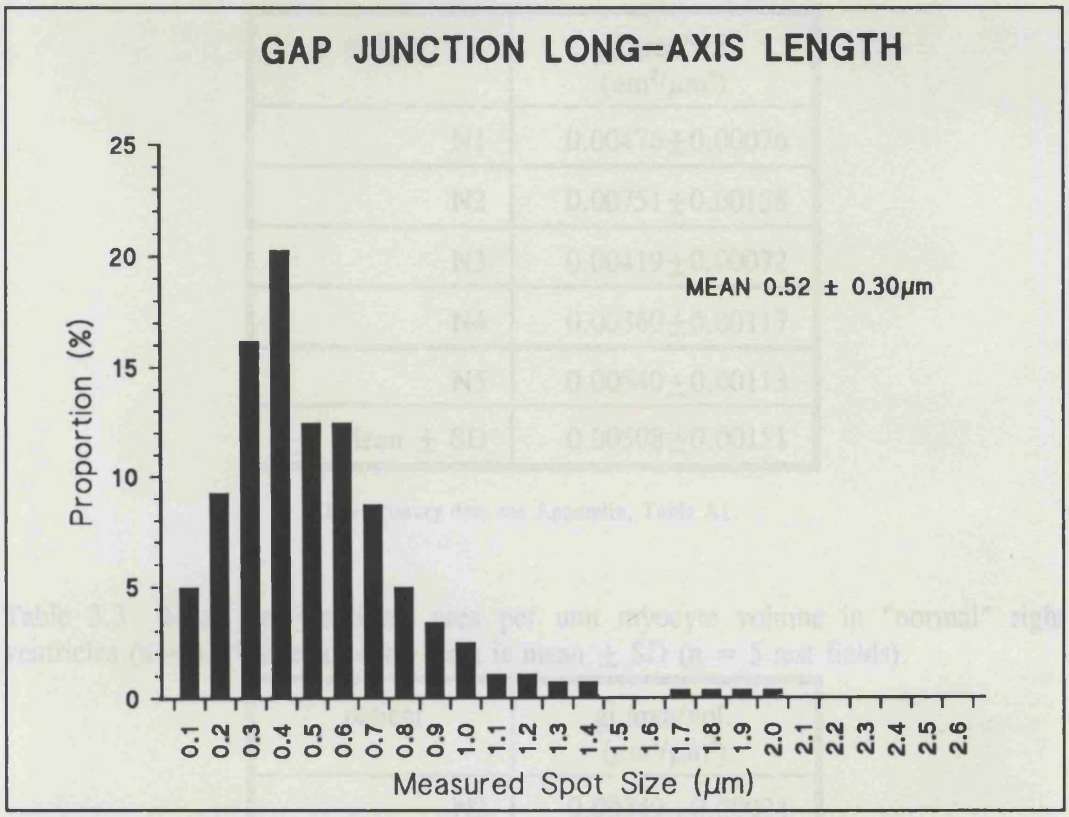

Figure 3.9. Frequency distribution of pooled long axis measurements of 860 labelled junctions in normal left ventricle determined by confocal microscopy. The overall mean long-axis length is 0.52 μm, with a mean of 0.67 μm for the larger peripheral junctions, and 0.36 μm for the smaller central junctions.

3.3.3c *Gap-junctional Surface Area per Unit Volume of Tissue*

An example of images from an optical section series of connexin43-labelled transversely-sectioned ventricular myocardium prepared for quantitative analysis is shown in Figure 3.6. The results of the morphometric analysis of such images to determine gap junction content in the healthy left and right ventricular myocardium are summarised in Tables 3.2 and 3.3 respectively. The corresponding primary data are presented in Appendix Tables A1 & A2.

Normal adult left ventricular myocardium had a gap junction surface area of 0.0051 ± 0.0015 $\mu m^2/\mu m^3$ myocyte volume, and normal right ventricle showed no significant difference (0.0044 ± 0.0006 $\mu m^2/\mu m^3$).

Table 3.2 Mean gap-junctional area per unit myocyte volume in "normal" left ventricles (n=5). Value for each heart is mean ± SD (n = 5 test fields).

patient	gj area/vol ($\mu m^2/\mu m^3$)
N1	0.00476±0.00076
N2	0.00751±0.00158
N3	0.00419±0.00072
N4	0.00360±0.00117
N5	0.00540±0.00113
Mean ± SD	0.00508±0.00151

For primary data see Appendix, Table A1.

Table 3.3 Mean gap-junctional area per unit myocyte volume in "normal" right ventricles (n=5). Value for each heart is mean ± SD (n = 5 test fields).

patient	gj area/vol. ($\mu m^2/\mu m^3$)
N2	0.00349±0.00034
N4	0.00501±0.00106
N6	0.00464±0.00123
N7	0.00402±0.00038
N8	0.00473±0.00050
Mean ± SD	0.00438±0.00061

For primary data see Appendix, Table A2.

3.3.3d *Intercalated Disk Counts*

An example of a confocal image of a labelled isolated ventricular myocyte is shown in Figure 3.10. When used to count the number of clusters of connexin43 label representing the number of intercalated disks in 100 cells, a mean of 11.55 ± 2.20 disks per cell was determined.

3.4 **Discussion**

Previous quantitative studies of gap junctions in mammalian myocardium, most of which used thin section electron microscopy, are confined to species other than man (Page, 1978; Stewart and Page, 1978; Shibata et al. 1980; Hoyt et al. 1989), and no attempts

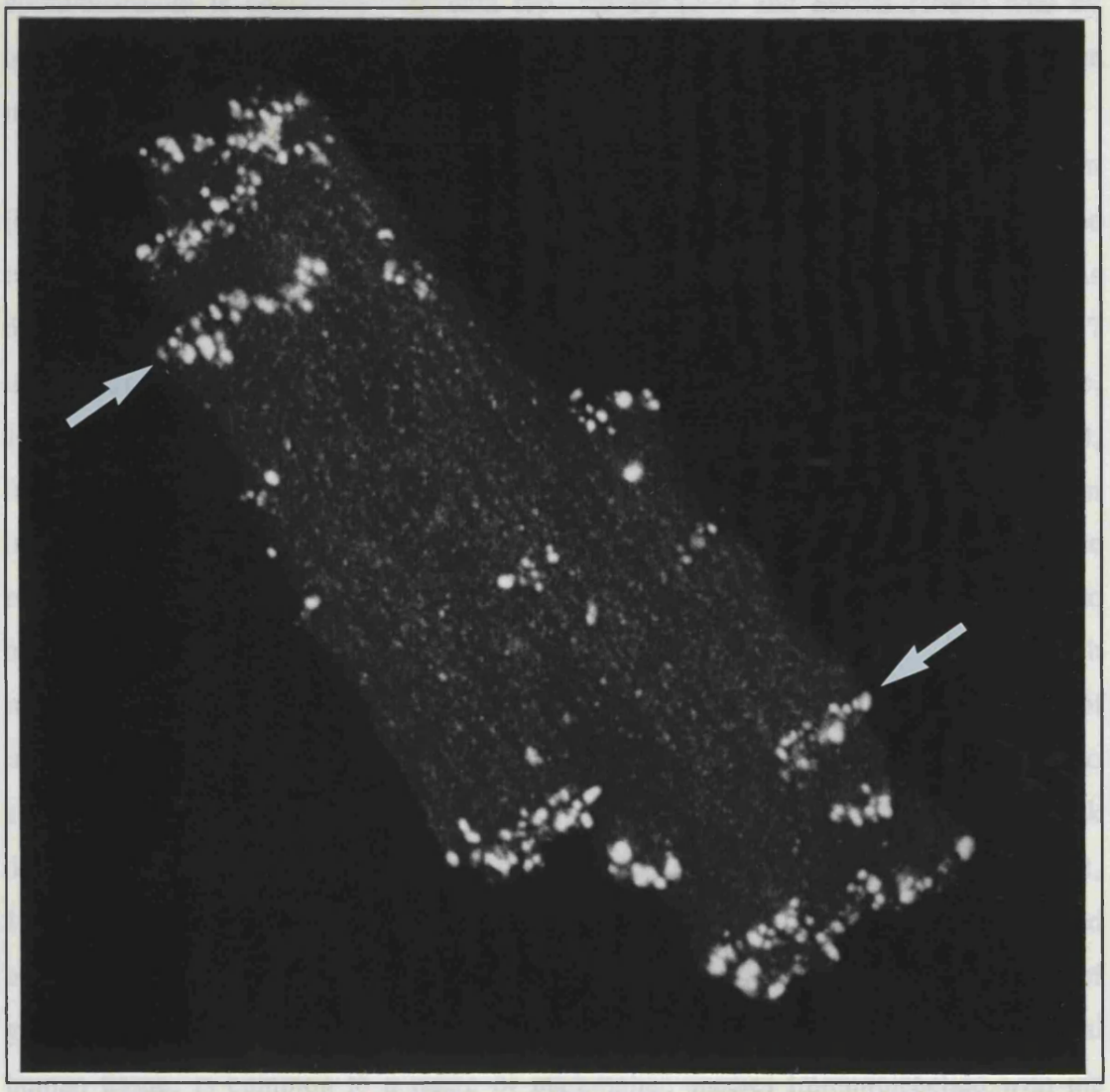

Figure 3.10. Laser scanning confocal micrograph of a projection image of a single isolated myocyte labelled for connexin43, revealing the positions of the intercalated disks as clusters of transversely-orientated labelled gap junctions (examples arrowed). x1960.

have, therefore, been made to characterise fully the changes that take place in human disease states.

The antibody in the present study produced immunolabelling which was apparently specific for cardiac muscle cell gap junctions. The lack of convincing immunolabelling of vascular smooth muscle may be attributable to the small size of the gap junctions, and the high level of autofluorescence in these cells. Although valvular myofibroblasts possess gap junctions, the nature of their component connexins remains to be determined. Fibroblasts, even though capable of forming close associations with myocytes, are not thought to establish gap-junctional communication with them in vivo.

This study has established some of the normal characteristics of gap junctions in adult human ventricular myocardium. The demonstration of a mean of 11.55 $\pm$ 2.2

intercalated disks (i.e. clusters of gap junctions) per myocyte in normal human epimyocardium is consistent with data reported by Luke and Saffitz (1991) who by quantitative light microscopy demonstrated a mean of 11.2 intercalated disk contacts per myocyte in normal canine ventricular myocardium.

The gap-junctional surface area in normal human left ventricular myocardium (0.0051 $\mu m^2/\mu m^3$ myocyte volume), as determined in the present study, falls within the range of values reported in electron microscopic ultrastructural studies in animals. As detailed in section 1.2.3b of Chapter 1, these studies include rabbit ventricle (0.017 $\mu m^2/\mu m^3$) (Shibata et al. 1980), rat ventricle (0.0047 and 0.0022-0.0154 $\mu m^2/\mu m^3$) (Page, 1978; Stewart and Page, 1978) and canine ventricle (0.0085 $\mu m^2/\mu m^3$) (Hoyt et al. 1989), from which Luke et al (1989a) have also estimated a value of 0.0052 $\mu m^2/\mu m^3$ by an immunohistochemical technique using light microscopy. In contrast with all these reports, the technique used in the present study enables the quantity of gap junction to be related directly to entire and completely visualised intercalated disks sampled through relatively large volumes of tissue. The overall patterns in the distribution of immunostained gap junctions observed by confocal microscopy accords with, but also adds to, the classical concepts of gap junction organisation at the cardiac intercalated disk derived from light and electron microscopy (Forbes and Sperelakis, 1985; Severs, 1989b), including a recent immunohistochemical study on non-human material examined by standard light microscopy (Luke et al. 1989a). Prominent ring-like arrangements of gap junctions at the periphery of the disk, as was a characteristic feature in the normal human tissue, is common to a range of mammalian species immunolabelled with the connexin43 antibody when examined with the resolution and clarity obtainable with confocal microscopy (Gourdie et al. 1991). Furthermore, with this tool, the data reported in this chapter provide a starting point for meaningful comparisons of quantity and distribution of gap junctions in diseased and healthy myocardium, as undertaken in subsequent chapters. Ideally, quantitative morphometry of this sort might be used in conjunction with measurements of myocardial electrophysiological and mechanical function, as assessed before tissue fixation, to correlate the organisation of intercellular coupling with myocardial function at the whole-tissue level.

CHAPTER 4 - CHANGING DISTRIBUTION OF INTERCELLULAR JUNCTIONS DURING MYOCARDIAL GROWTH IN HUMAN INFANCY

4.1 Introduction

Many functional differences between neonatal and adult myocardium relate to immaturity of tissue components (Friedman, 1972; Kaufman et al. 1990; Wibo et al. 1991; Quantk et al. 1992), which are responsible in part for the limited ability of the neonatal heart to cope with various acute metabolic and haemodynamic stresses (Colan et al. 1988; Baylen et al. 1986; Van Hare et al. 1990). Although most of these systems rapidly mature in early postnatal life, infant ventricular mechanics remain different from that of the adult (St.John Sutton et al. 1982; Fouron et al. 1988), and more able to adapt appropriately to substantial progressive changes in haemodynamics (Langer et al. 1975; Colan et al. 1988; Belik and Light, 1989) such as those that accompany the physiological circulatory changes and substantial growth in this period.

Coordination of development and growth in order to adapt to changing functional demands of the cardiac chambers is presumed to be due to patterns of flux and gradients of genetically determined tissue growth factors. These factors include morphogenetic signals that diffuse intracellularly via gap junctions (Warner et al. 1984; Guthrie and Gilula, 1989), which have been shown to be essential for normal tissue development (Guthrie and Gilula, 1989) and growth (Mehta et al. 1986).

Little is known of the developmental changes that may occur in the patterns of gap-junctional (and therefore electrical and chemical) coupling between myocytes, or when in human development the characteristic intercalated disk is formed (McNutt, 1970). Moreover, it is unclear whether the close association between gap junctions and adherentes junctions found in the mature intercalated disk exists before this time. In small mammals, developmental changes may occur in myocardial gap junction quantity (with a substantial increase in connexin43 levels briefly postpartum (Shibata et al. 1980; Fromaget et al. 1990; Fishman et al. 1991)), and in junction distribution (Van Kempen et al. 1991; Fromaget et al. 1992; Gourdie et al. 1992), but differences in the maturity at birth of different species prohibits extrapolation of these findings to man. However, that the arrangement of intercellular coupling may alter with postnatal human myocardial development has been suggested in a case report of a single immature heart (Oosthoek

et al. 1993), and is further supported by differences in the rate of electrical propagation through the myocardium; the duration of ventricular depolarisation increases by only about 20% despite a sixteen-fold increase in heart weight in the first few years of life (Zak, 1974). Increasing conduction velocity reported in maturing atrial (Dolber and Spach, 1989) and Purkinje tissue (Rosen et al. 1981), the explanation for which remains unclear, is therefore likely also to occur in ventricular myocardium. As in the atrium (Dolber and Spach, 1989), there may be associated changes in the degree of anisotropy of conduction in maturing ventricular myocardium, and the possibility exists that continuing changes occur in the pattern of distribution of cellular coupling by gap junctions. To investigate this possibility, and to establish some of the characteristics of gap junction organisation in human myocardium in infancy and childhood, confocal immunolocalisation of connexin43 was performed on paediatric surgical ventricular myocardial specimens. The distribution of adherentes junctions was investigated in parallel to establish the temporal and spatial relationships in the expression of both classes of junction in postnatal cardiac development. This knowledge may advance understanding not only of the mechanics of intercalated disk development, but also of the changes of electromechanical function and adaptability of the young human heart.

4.2 **Materials and Methods**

4.2.1 Human myocardial samples

Ventricular myocardial samples were taken at the time and from the site of initial ventriculotomy, within 3 minutes of the establishment of cold cardioplegic cardiac arrest, from the right ventricular free wall of 20 patients (4 weeks to 15 years), undergoing reparative right ventricular surgery for congenital anomalies (tetralogy of Fallot in 15, and double outlet right ventricle in 5).

To determine whether right ventricular myocardium from these abnormal hearts could be considered representative of "normal" myocardium, right ventricular myocardium was also obtained from 3 normal paediatric transplant donor hearts (ages 25, 48 and 68 months) at the time of routine biopsy immediately before implantation, having been maintained in cold cardioplegic solution.

All specimens obtained were immediately divided and placed in the appropriate fixative for the imaging techniques used. Immunohistochemical examination was carried out to determine the organisation of connexin43 throughout the whole tissue, and electron microscopic examination with and without immunogold labelling (detailed below) was

carried out to identify morphologically-recognisable gap junctions and foci of immunolabelling at the ultrastructural level.

In addition immunohistochemical and immunogold labelling of cadherins was performed on tissue sections adjacent to those labelled for connexin43, in selected specimens spanning the age range of the entire series.

4.2.2 Immunolocalisation of gap junctions and fasciae adherentes

4.2.2a *Antibodies*

Gap junctions - Connexin43. The connexin43 antibody was used in both immunohistochemical and immunogold labelling procedures detailed below.

Fasciae adherentes - Cadherin. The antibody used to detect fascia adherens was raised in rabbits against a 24 residue segment of the C-terminus of N-cadherin (the major calcium-dependent cell-cell adhesive molecule of the fascia adherens), and was kindly supplied by Dr Benjamin Geiger of The Weizmann Institute, Israel (Geiger et al. 1990). This antibody has been shown to give specific labelling of the fascia adherens of the cardiac intercalated disk in a range of mammalian species (Geiger et al. 1990).

4.2.2b *Immunohistochemical labelling of tissue*

The standard tissue preparation and labelling procedures detailed in section 2.3.2 of Chapter 2 were used for both connexin43 and cadherin immunohistochemistry, using the appropriate primary antiserum in each case.

4.2.2c *Microscopy of immunolabelled tissue*

Series of confocal optical slices, with a depth of field of less than 1 μm, were taken at steps of 1 μm through the depth of the tissue sections. Phase contrast microscopy of the immunolabelled sections was used to obtain detail of tissue structure, and adjacent tissue sections were stained with haematoxylin and eosin to assess orientation, hypertrophy and adequacy of preservation.

4.2.2d *Analysis of the Immunohistochemical data*

For each specimen, a single confocal optical slice (depth of field < 1 μm) from each of 3 randomly selected fields (size 180x120 μm using x60 objective lens) of longitudinally-sectioned myocardium was analysed to express the proportion of the total label present that was organised into collections characteristic of the adult intercalated disk (i.e. at the intercellular abutments lying transverse to the long axis of the myocytes). The total label

area present in each field was defined as the total number of pixels of signal intensity greater than 100 on the 255-point grey scale, determined automatically by binarising the image with this threshold using PC IMAGE image analysis software. When ventricular myocardium is sectioned longitudinally, the transected cell membranes of the elongated, blunt-ended abutting myocytes (and the gap-junctional label therein) are aligned either approximately parallel or perpendicular to the fibre axis. Labelled junctions organised into clusters of 4 or more aligned transversely at points of intercellular abutment, were then edited from the total binary data. The remaining area of longitudinally-orientated label in the binary image was automatically counted. From these data, which were acquired whilst blinded to the ages of the patients, the proportion of the total label present that was distributed in longitudinal or transverse arrays with respect to myocyte long axis was determined.

4.2.3 Electron microscopy

4.2.3a *Standard thin section electron microscopy*

When more detailed ultrastructural examination was needed to clarify the confocal findings, thin section electron microscopy was carried out on selected specimens of tissue from regions adjacent to those processed for immunohistochemical analysis.

4.2.3b *Electron microscopy of immunocytochemically labelled thin sections*

To determine whether the fluorescence detected at immunohistochemistry was specifically labelling intact and morphologically distinct gap junctions and fasciae adherentes, immunogold labelling of connexin43 and cadherin was carried out at the ultrastructural level.

Immunogold labelling was performed on myocardial specimens embedded at low temperature in Lowicryl K4M (Agar Scientific Ltd, Stansted, UK) (Carlemalm et al. 1981). Samples were fixed for 1 hour with 4% paraformaldehyde in phosphate-buffered saline, pH7.4, and dehydrated in an ethanol series under progressive cooling to -35°C in absolute ethanol. Infiltration was carried out with Lowicryl K4M:ethanol mixtures and then pure Lowicryl which was polymerised with UV light initially at -35°C, and then at room temperature. Ultrathin sections were incubated with the primary antiserum (to connexin43 or cadherin), followed by 10nm-gold/goat anti-rabbit complexes (BioCell, Cardiff, UK) following standard procedures (Slot and Geuze, 1984).

4.3 Results

The details of the 20 patients undergoing surgery for congenital cardiac anomalies, and the 3 paediatric cardiac transplant donor patients, are shown in Table 4.1.

Table 4.1 Details of myocardial specimens from infant and child hearts, with the proportion of the total Cx43 label arrayed transversely in each.

patient/heart no.	age	diagnosis	mean proportion of label in transverse arrays
1	4 weeks	TOF	0.53
2	9 weeks	DORV	0.47
3	6.5 months	TOF	0.49
4	8.5 months	TOF	0.58
5	9 months	TOF	0.53
6	12 months	TOF	0.76
7	14 months	TOF	0.58
8	15 months	TOF	0.59
9	20 months	TOF	0.59
10	24 months	TOF	0.61
11	25 months	TP	0.68
12	28 months	TOF	0.77
13	31 months	DORV	0.71
14	38 months	TOF	0.78
15	41 months	DORV	0.88
16	48 months	TOF	0.70
17	48 months	TP	0.80
18	57 months	DORV	0.71
19	64 months	DORV	0.94
20	68 months	TP	0.88
21	70 months	TOF	0.91
22	86 months	TOF	0.97
23	180 months	TOF	0.94

TOF = tetralogy of Fallot
DORV = double outlet right ventricle
TP = cardiac transplant donor

Immunohistochemical connexin43 labelling was carried out on right ventricular myocardium from all patients, and cadherin labelling was carried out on patients 1, 12, 17, 22.

4.3.1 Neonate

4.3.1a *Gap junctions*

A typical single confocal optical slice through longitudinally-sectioned connexin43-immunolabelled right ventricular myocardium from the 4 week infant is shown in Figure 4.1. This image is an example of those used for determining the longitudinal/transverse

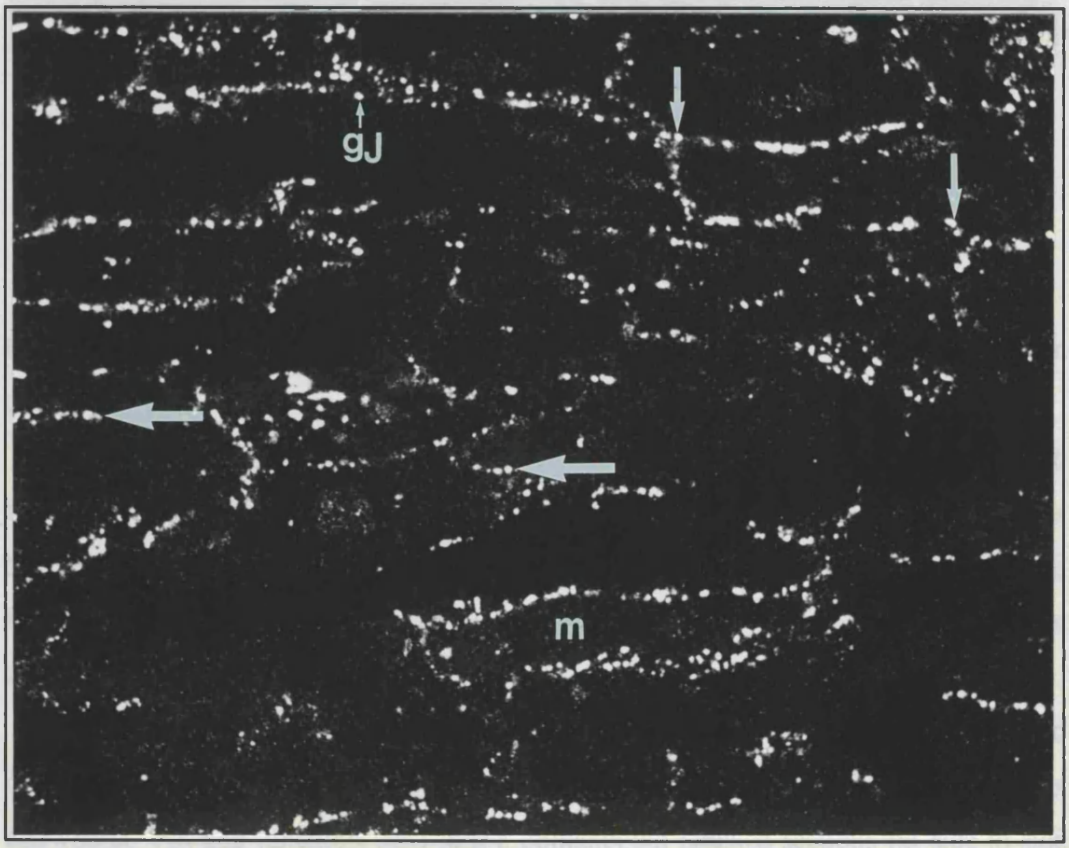

Figure 4.1. A single confocal optical slice of longitudinally-sectioned connexin43-immunolabelled right ventricular myocardium from a 4 week infant. The long axes of the constituent myocytes are approximately horizontal in this micrograph. Gap junctions (gj) are distributed over the entire surface of the myocytes. The outlines of some myocytes (m) are completely delineated by profuse label. The proportion of label present in longitudinal (large arrows) and transverse (small arrows) arrays was quantified. x1,300.

ratio of label distribution. At this early stage, the punctate immunolabelling is distributed over the entire surface of the myocytes. This feature is demonstrated with even greater clarity when a number of adjacent optical slices through the same tissue field are superimposed to produce a single image consisting of data acquired through a 7 μm depth of myocardium (Fig 4.2A). When sectioned transversely, this same specimen has label distributed around the edges of the cross-sectioned myocytes (Fig 4.2B), consistent with

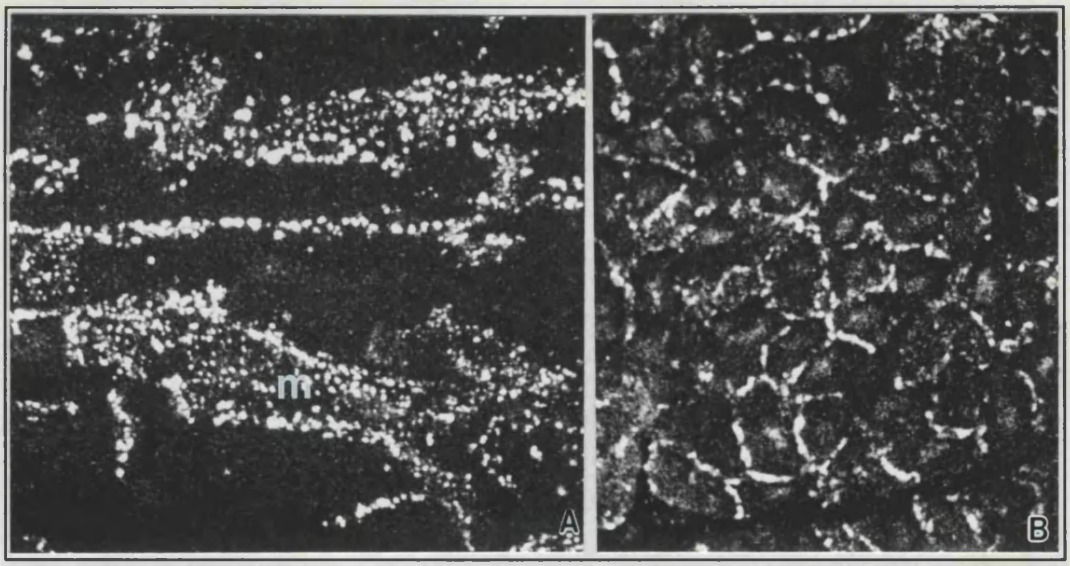

Figure 4.2. Confocal images of connexin43-immunolabelled right ventricular myocardium from a 4 week infant.
A: A projection image of confocal optical slices of longitudinally-sectioned tissue taken at 1μm intervals through a depth of 7μm. Profuse label can be seen to envelope entire myocytes (m).
B: Projection image of confocal optical slices through a depth of 7μm of transversely-sectioned myocardium. The label forms a reticular pattern, delineating the abutting surfaces of the transected myocytes. A & B, x1,300.

the longitudinal appearances. There was no detectable difference in gap junction organisation from endocardium to epicardium across the ventricular free wall.

That this label represented intact gap junction was supported by the electron microscopic findings of frequent gap junctional contacts between the lateral interfaces between myocytes (Fig 4.3). Annular profiles of gap-junctional membrane were frequently observed, associated with the convoluted lateral plasma membrane, and did not appear necessarily to be a point of intercellular contact (Fig 4.4).

Connexin43 immunogold labelling revealed gold particles specifically concentrated on morphologically-defined gap-junctional membrane (Fig 4.5), with no localised clusters elsewhere. All gap junctions seen in the immunogold-labelled sections (at side-to-side and end-to-end cellular abutments, and the annular forms) had associated gold particles, suggesting that connexin43 is present in every gap junction visualised.

4.3.1b *Fasciae adherentes*

The distribution of immunolabelled cadherin at confocal microscopy was indistinguishable from that of connexin43 on adjacent tissue sections (Fig 4.6). At electron microscopy, however, although there was a general tendency to there being an association between gap junctions, fasciae adherentes and desmosomes, with small combinations of these junction types lying adjacent to one another, characteristic gap junctions were frequently distant from other junction types, as illustrated by the examples in Figures 4.3 and 4.4.

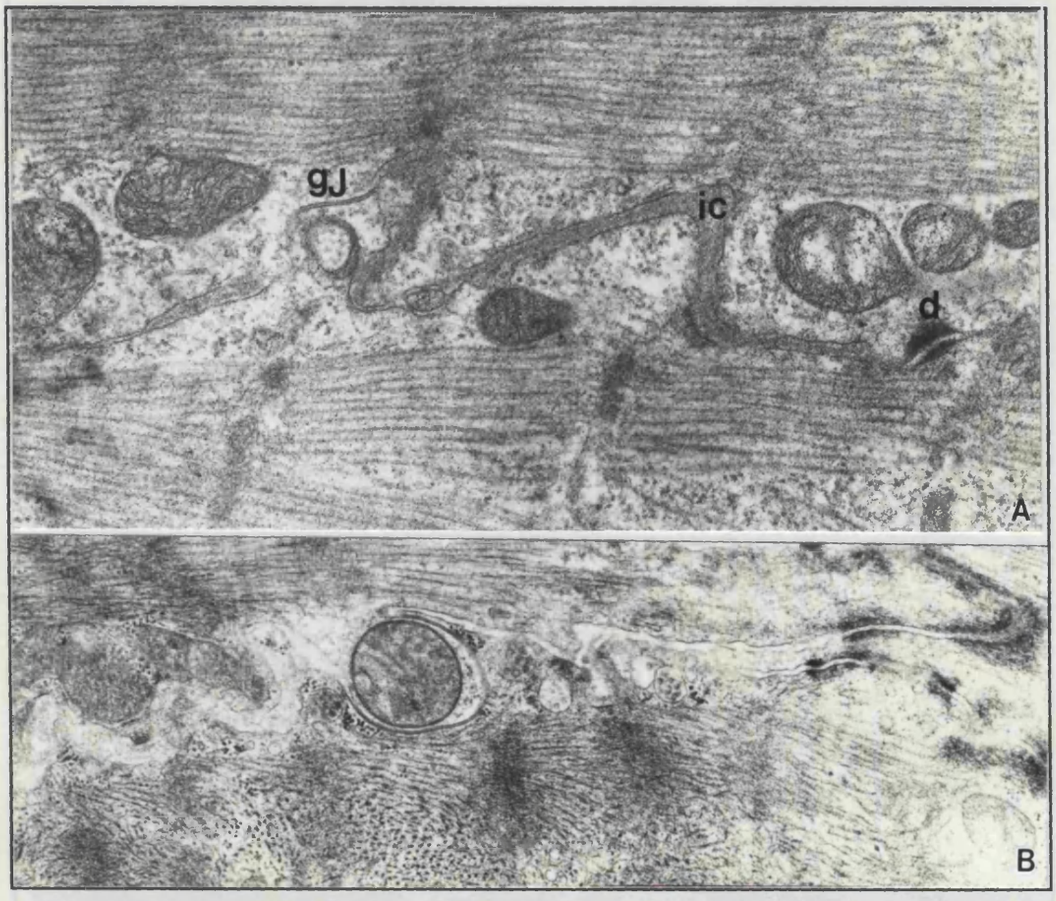

Fig 4.3. Standard thin section electron micrographs showing interfaces between longitudinal surfaces of adjacent ventricular myocytes.
A: The intercellular space (ic) is interrupted by close approximation of the plasma membranes to form a gap junction (gj) in apparent isolation from other junction types. An isolated desmosome (d) is also visible. x36,400.
B: Gap-junctional membrane close to, but not apparently part of the adjacent intercalated disk structures in either this or adjacent sections. x27,000.

4.3.2 Age 7 years

Confocal microscopy revealed that by 7 years of age, connexin43 labelling was, as in the adult (Fig 3.3), confined to the cell terminals as lines of punctate immunofluorescence, lying transverse to the long axes of the myocytes (Fig 4.7). The immunolabelled cadherin in adjacent tissue sections viewed by confocal microscopy was also confined to the positions of the mature intercalated disks, but showed a greater intensity of labelling (Fig 4.8), with a more confluent appearance than the connexin43 label, consistent with the greater content of fascia adherens than gap junction in the mature disk. The preponderance of fascia adherens junctions is illustrated in Figure 4.9, which demonstrates, by immunogold electron microscopy, that the cadherin immunolabelling

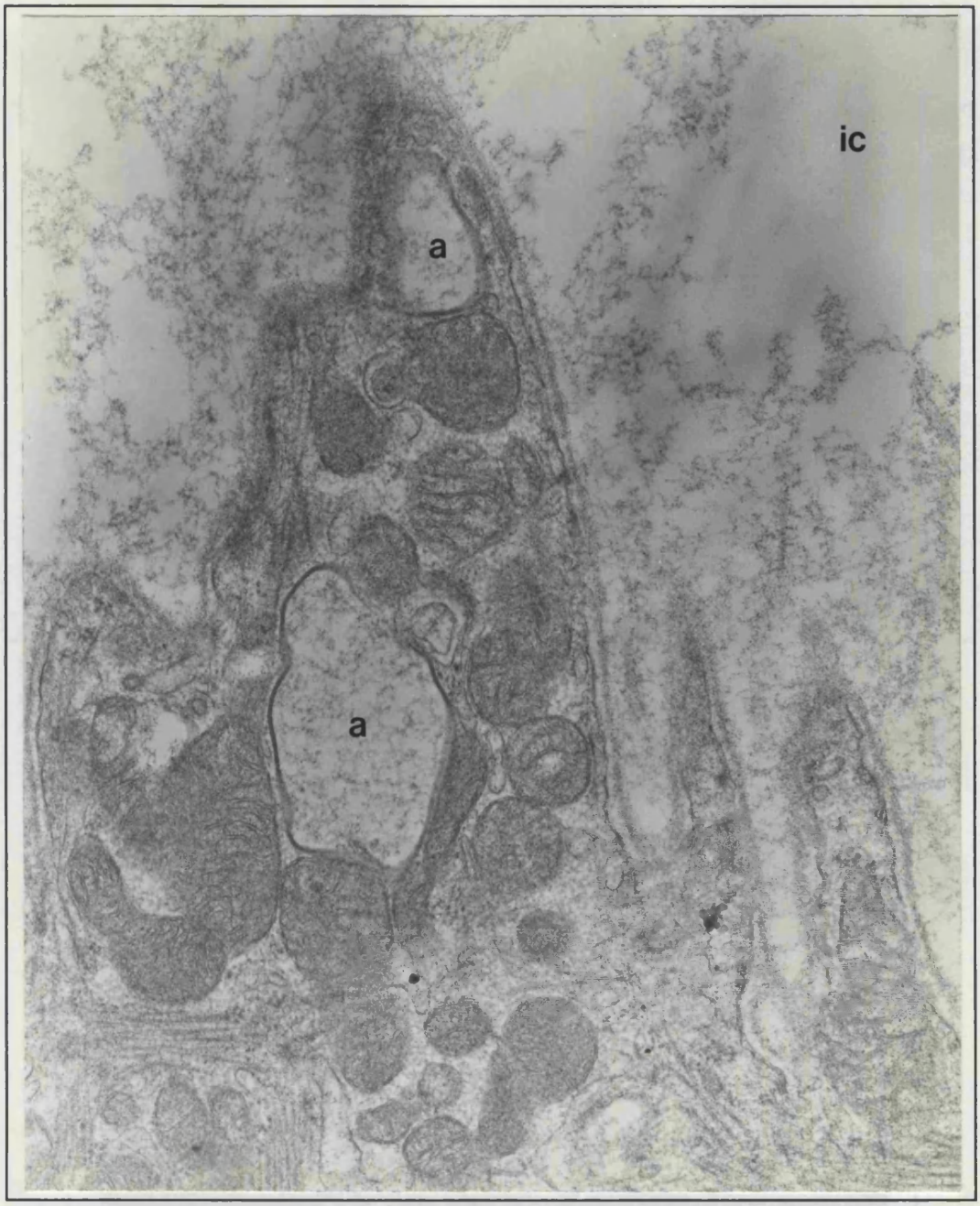

Fig 4.4. Portion of convoluted plasma membrane from the longitudinal surface of a ventricular myocyte. Two annular profiles composed of gap-junctional membrane are present (a). Both contain within them material similar in appearance to that in the intercellular space (ic), and may represent discrete cytoplasmic vesicles of gap-junctional membrane. x41,000.

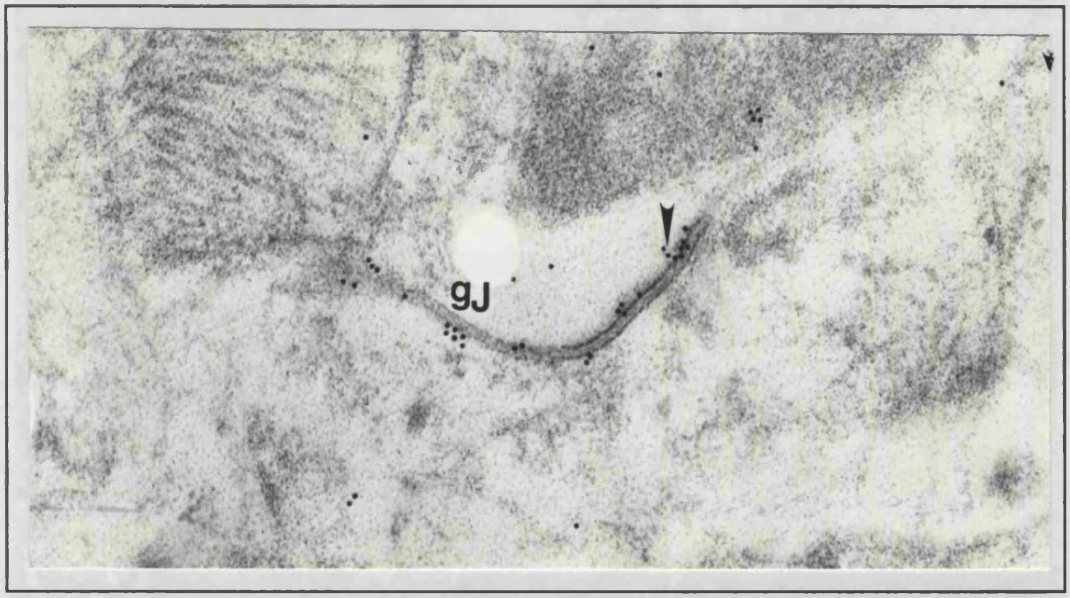

Fig 4.5. Thin section electron micrograph of connexin43 immunogold labelled ventricular myocardium from a 9-week infant, showing gold particles (arrowed) concentrated specifically on a morphologically-defined gap junction (gj). x87,000.

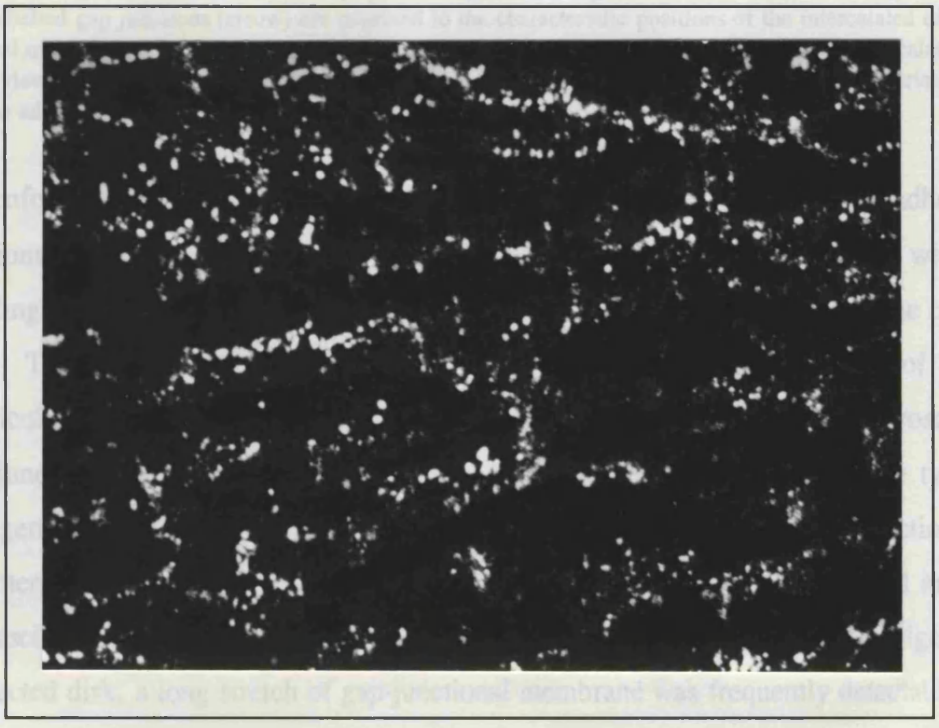

Figure 4.6. Confocal micrograph of longitudinally-sectioned ventricular myocardium from a four-week infant immunolabelled for cadherin. At this age, the punctate pattern of distribution of cadherin (fasciae adherentes) over the entire myocyte surfaces is indistinguishable from that of connexin43 (gap junctions - see Fig 4.1). x1,300.

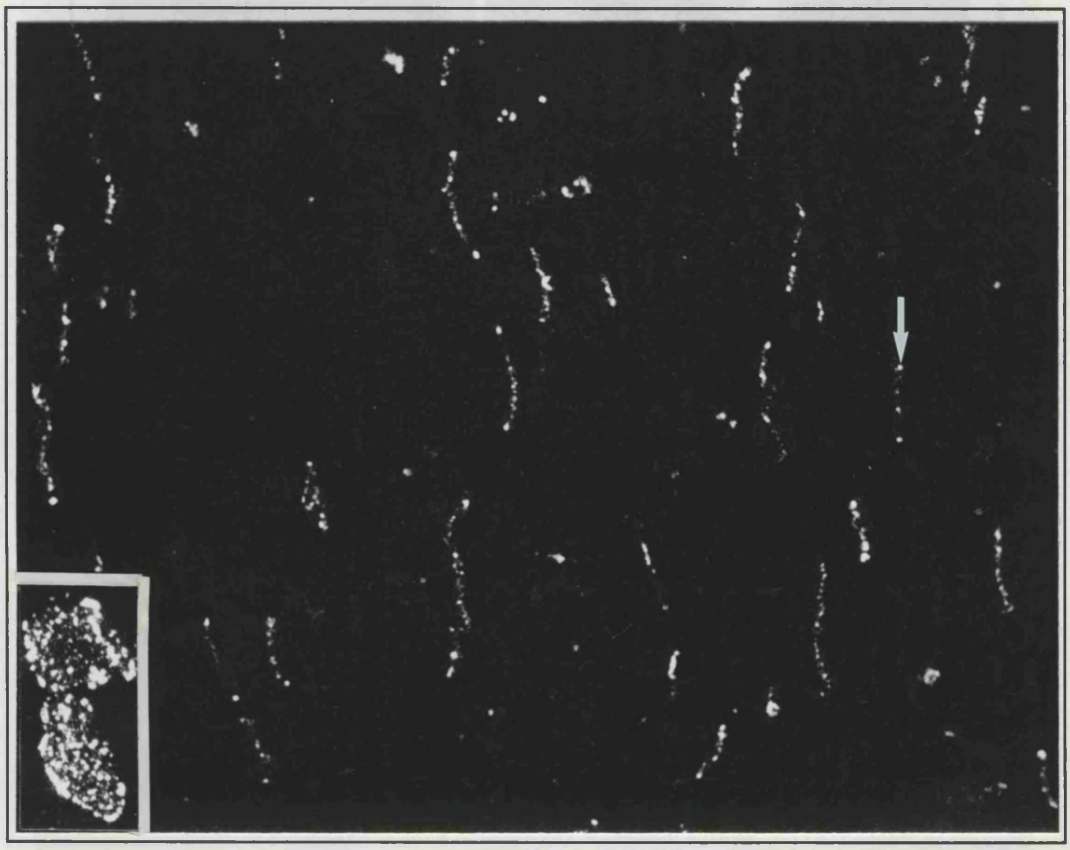

Figure 4.7. A single confocal optical slice of longitudinally-sectioned connexin43-immunolabelled right ventricular myocardium from a 7 year old child. The long axes of the constituent myocytes are approximately horizontal in this micrograph. Compare with Figure 4.1. The transverse arrays of the labelled gap junctions (arrow) are confined to the characteristic positions of the intercalated disks typical of adult ventricular myocardium. Inset: a cluster of gap junctions delineating an intercalated disk viewed en face in the same specimen sectioned transversely. This appearance is characteristic of the adult pattern. Compare with Figs 3.3 & 3.4. x1,000.

at confocal microscopy was specific for morphologically distinct fascia adherens junctions. The fascia adherens junctions are heavily labelled with gold particles, with no labelling of the gap junctions, desmosomes or any other distinct focus within the cells.

That the junctions were confined to intercalated disks characteristic of adult ventricular myocardium was confirmed by standard thin section electron microscopy. The junction types were found to be organised within disks that showed the typical arrangement, with fasciae adherentes in the plicate regions, the larger gap junctions in the interplicate regions, and smaller gap junctions and desmosomes interspersed among the fasciae adherentes in the plicate regions (Severs, 1990). At the extreme edge of a transected disk, a long stretch of gap-junctional membrane was frequently detectable, as seen in adult tissue (Fig 3.5 in Chapter 3), a feature consistent with the peripheral ring of larger gap junctions apparent when intercalated disks are viewed en face in confocal reconstructions of adult ventricular myocardium (Severs et al. 1993). Immunogold

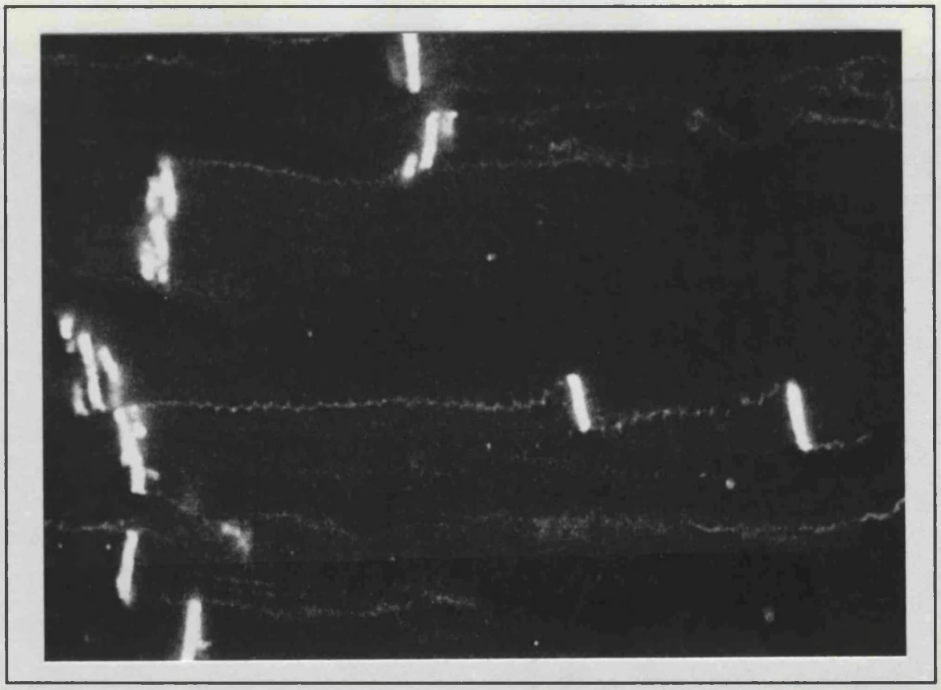

Figure 4.8. Confocal micrograph of longitudinally-sectioned ventricular myocardium from a seven-year old child immunolabelled for cadherin. Cadherin, like connexin43, shows the mature pattern, confined to the intercalated disks. However, the disks have a greater density of labelling in this optical slice, with a more confluent appearance than connexin43 label (see Fig 4.7), consistent with the greater disk content of fascia adherens than gap junction seen at thin section electron microscopy. x800.

labelling of connexin43 at the electron microscopical level again revealed gold particles specifically associated with morphologically recognisable gap junctions.

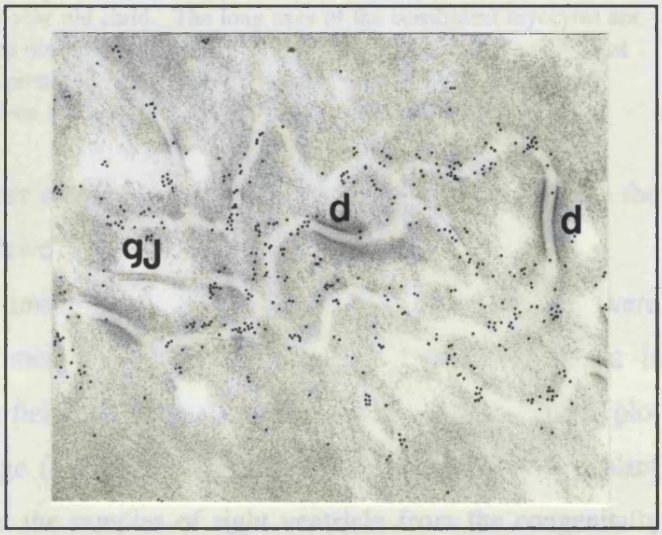

Fig 4.9. Thin section electron micrograph of cadherin immunogold labelled ventricular myocardium showing gold particles concentrated specifically on the convoluted fascia adherens regions (with pale appearance) of this obliquely-sectioned intercalated disk, with sparing of gap junctions (gj) and desmosomes (d). x46,000.

4.3.3 Intermediate ages

Between the neonate and 7 years of age, intermediate patterns of connexin43 gap junction distribution were observed (Fig 4.10). The pattern of immunolabelling appeared to change progressively from being dispersed over the entire cell surface as in the neonate, to the polarised adult pattern. Thin section electron microscopy of specimens from these infants up to seven years of age confirmed changes suggestive of

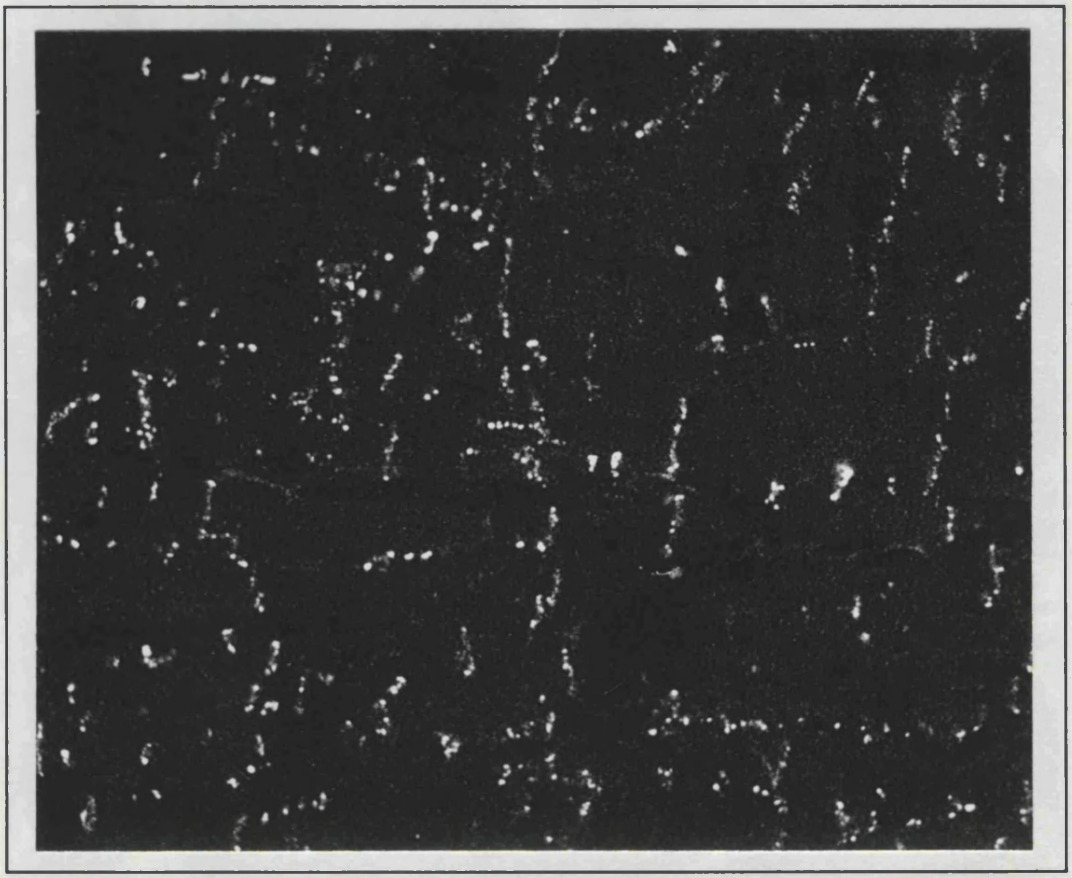

Figure 4.10. A single confocal optical slice of longitudinally-sectioned connexin43-immunolabelled right ventricular myocardium from a 4 year old child. The long axes of the constituent myocytes are approximately horizontal. Note that the distribution pattern of the label is intermediate between that of Figures 4.1 and 4.7, with junctions present over the lateral surfaces of the myocytes, but also more prominently at the transverse end-on abutments. x1,000.

intercalated disk formation; greater association than in the neonatal heart between the adhering and gap junctions, and fewer gap junctions seen in isolation (Fig 4.11).

When the serial confocal image data of the entire age range of patients were analysed and expressed as the mean proportion of the total label present that is transversely-arrayed in the 3 test fields from each heart (Table 4.2), the resulting plot revealed a linear increase with age (Fig 4.12). The data points from the 3 transplant hearts fit this line, indicating that the samples of right ventricle from the congenitally anomalous hearts are not associated with abnormal connexin43 gap junction distribution, and verifying use of these anomalous hearts to establish the changes in ventricular myocardial junctions with maturation.

As in the seven-year heart, the cadherin immunolabelling at confocal microscopy was more intense than connexin43 in each of the two intermediate cases examined (one of which was a transplant patient) but the pattern of its distribution was otherwise indistinguishable.

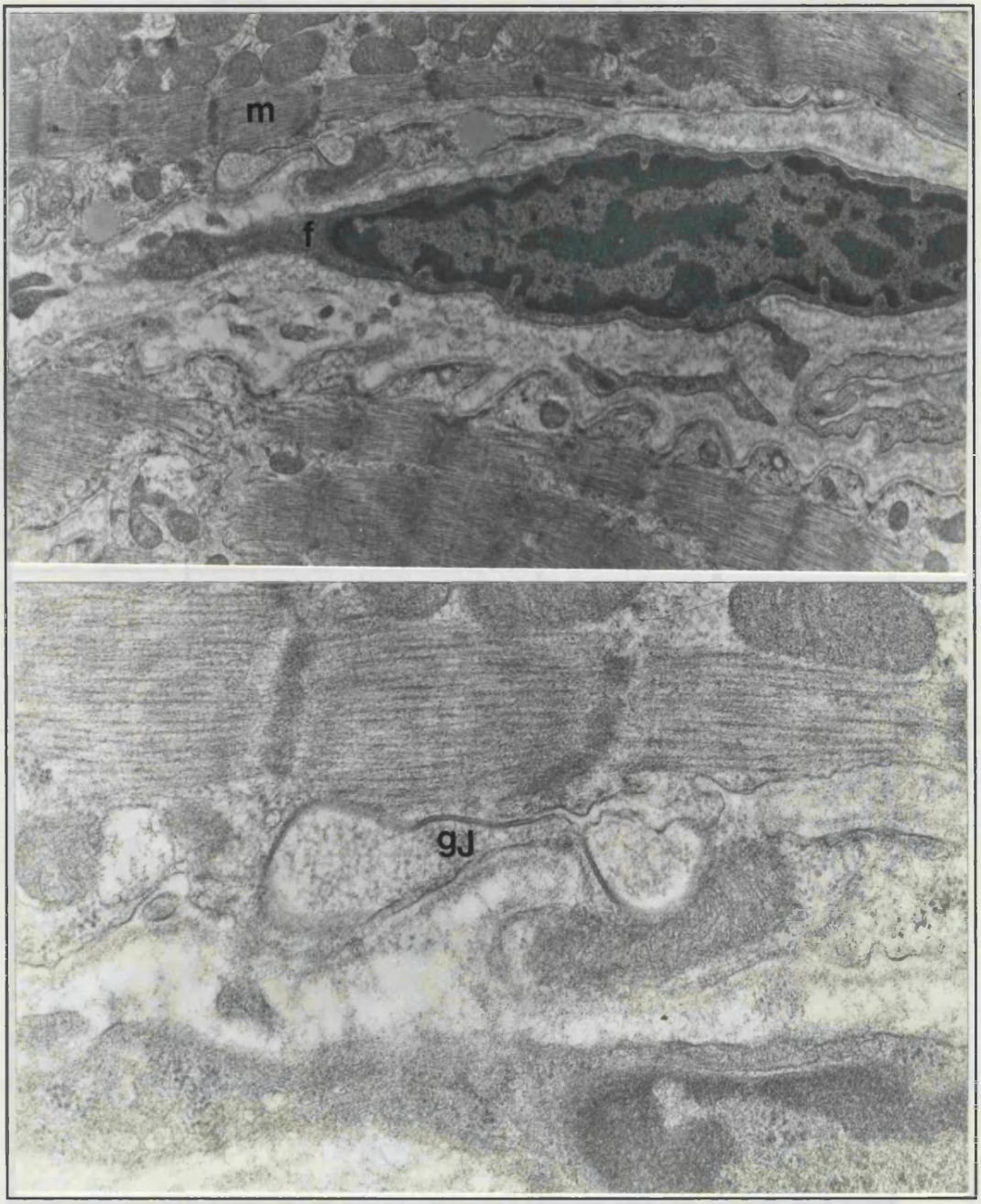

Figure 4.11. Low and high power thin section electron micrographs of ventricular myocardium from a 2 year old, showing a gap junction (gj) apparently along the lateral border of a myocyte (m), with ordinary plasma membrane and no other junction types around it. There is an adjacent fibroblast (f). Upper, x15,000; lower, x53,000.

Table 4.2 The proportion of the total connexin43 label arrayed transversely in 3 random myocardial fields and the mean for each heart.

heart no.	field 1	field 2	field 3	mean
1	0.512	0.463	0.612	0.529
2	0.431	0.492	0.494	0.472
3	0.572	0.541	0.345	0.486
4	0.668	0.482	0.599	0.583
5	0.600	0.423	0.563	0.529
6	0.653	0.823	0.798	0.758
7	0.691	0.499	0.555	0.582
8	0.599	0.631	0.511	0.585
9	0.581	0.572	0.612	0.589
10	0.498	0.667	0.653	0.606
11	0.796	0.741	0.497	0.678
12	0.856	0.617	0.823	0.765
13	0.654	0.697	0.783	0.711
14	0.711	0.840	0.797	0.783
15	0.896	0.949	0.798	0.881
16	0.702	0.587	0.811	0.700
17	0.842	0.766	0.801	0.803
18	0.747	0.634	0.758	0.713
19	0.956	0.966	0.895	0.939
20	0.934	0.877	0.841	0.884
21	0.816	0.954	0.956	0.909
22	0.978	0.98	0.963	0.974
23	0.889	0.978	0.959	0.942

4.4 Discussion

4.4.1 Changing distribution of gap junctions in postnatal myocardium

The results of this study suggest that throughout infancy in man, progressive and substantial changes occur in the distribution pattern of connexin43 gap junctions in

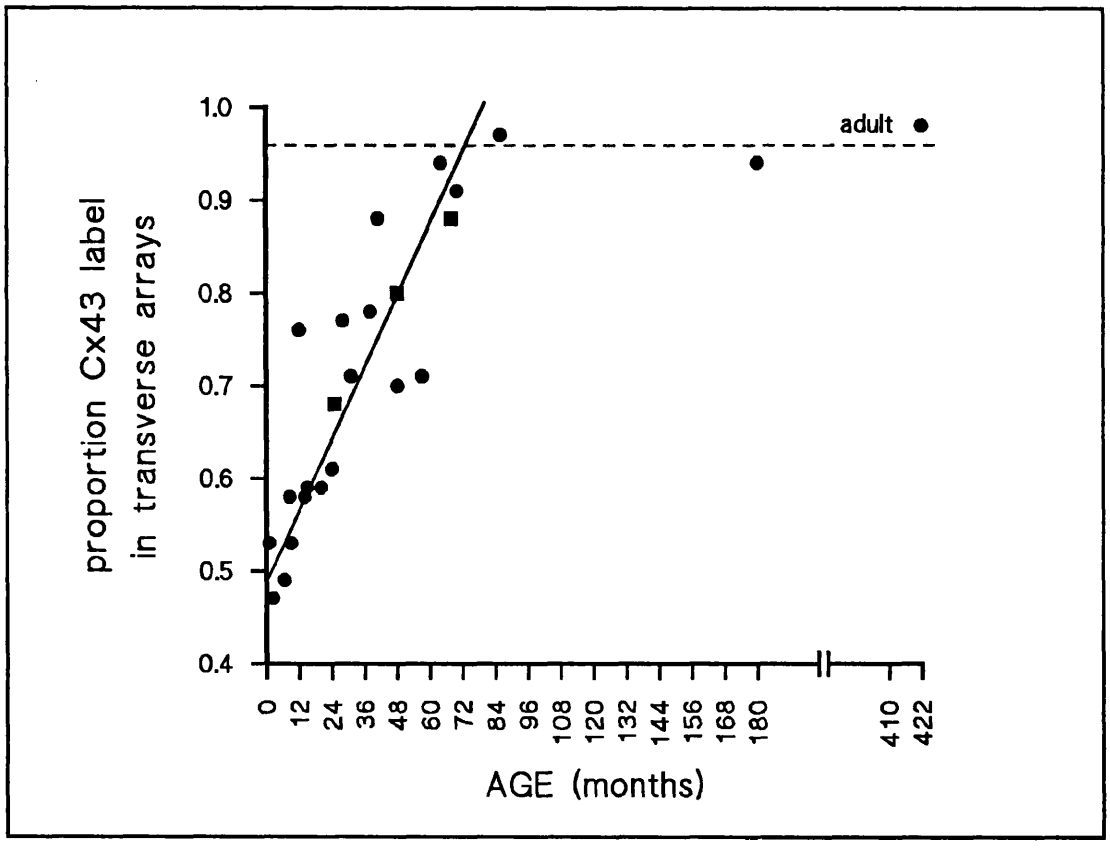

Fig 4.12. Graph showing the change with age of the proportion of connexin43 gap junction that is distributed at the intercellular abutments lying transverse to the long axis of the myocytes. The values derived from the transplant hearts are marked by the squares. The plot has a correlation coefficient of 0.88 ($p<0.01$), and the straight (continuous) line of best fit is shown. This line intercepts with the dashed line of the constant adult proportion at 72 months of age.

ventricular myocardium. From neonatal ventricle, in which the gap junctions of the myocytes are spread over the entire cell surface, there is a progressive redistribution toward the adult pattern in which junctions are confined to the transversely-orientated terminals of the myocytes, within the complex structure of the intercalated disk (Severs, 1990). Analysis of the immunohistochemical data in the present study has shown this change in distribution to be complete by about 6 years of age.

Although connexin43 is the principal mammalian cardiac gap-junctional protein, other cardiac connexins have recently been identified (Kanter et al. 1992). However, the finding in the present study that all morphologically-identifiable gap junctions were immunolabelled with gold particles when connexin43 antibody was used suggests that in working ventricular myocardium, connexin43 antibody alone localises all gap junctions present. Importantly, this finding also suggests that if other gap-junctional connexins are present in right ventricular working myocardium of the human infant, it is likely that they coexist with connexin43 in the same junctions.

In their study of structure and electrophysiology in canine atrium, Dolber and

Spach (1989) showed a significant increase in conduction velocity longitudinally (parallel to the myofibre long axis), but no change in transverse velocity, from the juvenile to adult myocardium, and demonstrated that the immature myocardium is consequently less anisotropic electrically. Enlargement of the myocytes did not provide adequate explanation for these alterations, which were attributed to the changing pattern and extent of separation by connective tissue of the side-to-side interfaces between individual myocytes and groups of cells that occurs in maturing atrial (Dolber and Spach, 1989) and ventricular (Borg and Caulfield, 1981) myocardium. But fine connective tissue septae, per se, will not significantly alter intercellular coupling or conduction velocity through the tissue unless they divide points of potential gap-junctional intercellular contact. Gap junctions occupy a very small proportion of the cell surface (Severs, 1990), so even a substantial increase in septation may have little effect on electrical coupling. Gap junctions and the associated adhering junctions incorporate very close and tightly bound apposition of the cell membranes of abutting myocytes (Severs, 1990), and are unlikely to be separated passively by spreading connective tissue. One might speculate that a primary phenomenon which may alter the rate and anisotropy of conduction is the redistribution of gap junctions predominantly to the end terminals of the cells, as demonstrated in the present study. This would imply that connective tissue changes are secondary, and electrophysiologically incidental.

4.4.2 Relationship between gap junctions and fascia adherentes

The pattern of immunolabelling for cadherins, as seen at the level of confocal microscopy, was qualitatively similar to that of connexin43 in each of the specimens examined, showing the same progression to the adult distribution. It is important to note, however, that thin section electron microscopy showed that neonatal ventricular myocytes contain many isolated gap junctional contacts in the absence of adjacent adherens junctions. Furthermore, although most of the gap junctions seen were demonstrably between abutting myocytes, there were numerous examples of annular gap-junctional membranes that appeared to lie beneath convoluted lateral plasma membrane, and that did not appear to link adjacent cells. Although some of these annular profiles may arise from the plane of section through undulating membrane, the frequency of these appearances suggests that at least some discrete cytoplasmic vesicles of gap-junctional membrane may exist within the myocytes of neonatal ventricular myocardium, as previously described in developing mammalian hearts (Chen et al. 1989). In their recent

study of intercellular junctions in mice, Fromaget et al (1992) concluded that similarity in the patterns of immunohistochemical labelling of two subcellular components would "suggest a close interaction between" them. As illustrated by the present study, complementary ultrastructural examination of the tissue may reveal a more complex situation, and is required to verify such conclusions.

In contrast with rat and mouse hearts, human neonatal myocardium revealed no differences in gap junction organisation between the endocardial side and the epicardial side (Fromaget et al. 1992; Gourdie et al. 1992). This difference may be due to the less mature state of the smaller mammals at birth.

That the distribution of gap junctions in the transplant donor hearts followed the line of best fit for the plot of distribution with age obtained from the hearts with congenital cardiac anomalies suggests that the latter were not associated with a gross disturbance of right ventricular myocardial connexin43 gap junction distribution. Although an intact gap-junctional communication system has been shown to be essential for normal development, tissue differentiation and growth (Mehta et al. 1986; Guthrie and Gilula, 1989), a disturbance of connexin43 gap-junctional expression and organisation lasting into postnatal stages of development does not appear to play a role in the formation of these anomalies.

4.4.3 Development of the intercalated disk

Early electron microscopic studies shed considerable light on the development of the intercalated disk in small mammals (McNutt, 1970), demonstrating that in fetal life the fasciae adherentes, into which the myofilaments insert, are initially independent of the gap junctions. What was not evident, however, was the overall distribution of these junction types over the surface of individual cells or throughout intact myocardium, and the changing postnatal distribution that the present study has revealed. It was postulated that the mechanical tension of the increasing number of myofilaments inserting into the fasciae adherentes explains the predominantly transverse orientation of these junctions within the mature intercalated disk, which was considered to be present from birth in man. If, as shown in the present study, coalescence of the specialised intercellular junction types into the mature intercalated disk does not occur until about 6 years of age, and, therefore, long after establishment of postnatal haemodynamics and mechanical loading and after most of the cardiac growth has taken place, it seems unlikely that the stimulus to fascia adherens reorientation is simply mechanical. This alteration may serve

a functional role, and it is tempting to suggest that the immature junctional distribution may optimise mechanical, electrical and chemical intercellular communication during the periods of adaptation to postnatal haemodynamics and rapid myocardial growth, and that the determinants of the progressive change in distribution are more complex.

4.4.4 Ventricular growth

The diameter of cardiac myocytes increases postnatally by a factor of about 2.4, with greater than 90% of human myocardial growth resulting from such cellular enlargement (Zak, 1974). However, cardiac myocytes retain the capacity for mitotic division for about the first 6 months of postnatal life in man (Zak, 1974; Yasui et al. 1989), during which time hyperplasia accounts for a significant proportion of the ventricular growth. The cellular basis of myocardial growth, therefore, depends on age (Zak, 1974), but a longstanding and hitherto unanswered question is how the heart can maintain its overall geometry and pumping function, whilst growing rapidly.

Richter (1974) referred to the heart as a "topological manifold" in which changes in the surface area and configuration of any cardiac myocyte must affect the cell surface configurations of its neighbours. At that time, he made the largely correct assumption that the adaptive processes of myocardial growth are governed by intercellular information transfer via gap junctions, also essential for electrical propagation. Richter postulated that although considerable configurational changes occurred between individual myocytes, there were "invariants in the surface topology" of the specialised intercellular junctions, which would maintain the same position with respect to each other, the cell surface and the surfaces of adjacent cells, throughout growth. Thus, he postulated that gap junctions not only played an important part in intercellular communication governing patterns of growth, but, with this growth, they were the invarying points of contact and coupling between cells. By demonstrating that the positions of the junctions change markedly with postnatal development, the present study also demonstrates that this postulate is incorrect. In terms of the "topological manifold", however, the infantile junctional pattern may be the means by which the massively growing heart, undergoing hyperplastic as well as hypertrophic enlargement, can maintain the required communicating and adhering contacts between the component myocytes despite the configurational changes. This junctional pattern will influence the mechanical and electrical properties of the immature myocardium.

Animal studies have shown that despite being less compliant than adult

myocardium (Van Hare et al. 1990), significant changes in neonatal ventricular form and mass can occur within 2-3 days of the onset of haemodynamic changes (Belik and Light, 1989). The ability of myocardium to adapt and remodel appropriately to the physiological changes of infancy, whilst maintaining electrical and mechanical coupling, may depend on an appropriate pattern of intercellular adhesion and communication in the early period of rapid growth, with subsequent change to the mature adult pattern. The junctional distribution of early infancy demonstrated in the present study may, at least in part, be responsible for permitting the substantial and rapid changes in myocardial architecture during this period.

4.4.5 Potential implications for the timing of surgery in children

The pattern of intercellular coupling and adhesion demonstrated in this study is likely to be associated with alterations in the functional anisotropy of the tissue, including the directional ease and rates of intercellular diffusion of the small molecules regulating growth, tissue differentiation and maturation (Warner et al. 1984; Green, 1988). The arrangement of communicating and adherens intercellular junctions that exists at birth may best fulfil the requirements of the growing and adapting ventricular myocardium. Progressive change toward the arrangement in the adult ventricle throughout early childhood may not only meet the more stable requirements of the older ventricle, but may also render the myocardium less able to adapt appropriately to altered haemodynamics, and may be of relevance to the timing of cardiac surgery. Despite the increased complications of cardiopulmonary bypass and operative ischaemia in younger infants, corrective surgery for a variety of congenital cardiac anomalies, when performed early in infant or even neonatal life, may improve long term cardiac performance, both mechanical (Kirklin et al. 1986; Gustafson et al. 1988; Colan et al. 1988; Norwood et al. 1988; Losay et al. 1992) and electrical (Walsh et al. 1988). Although the reason for the benefit from early reparative surgery may, in part, be due to reducing the duration of exposure of the myocardium to the adverse haemodynamics before correction, it is likely that other factors are important. Even when early preparative surgery is performed to improve the haemodynamic loading of cardiac chambers before a delayed definitive repair, thereby reducing, but not eliminating, the requirement for later myocardial adaptive remodelling, the longterm results from such two-stage repairs may not be as good as early immediate correction (Danford et al. 1985; Colan et al. 1988; Yasui et al. 1989). One might speculate that the distribution of intercellular junctions of early infancy

may not only facilitate myocardial adaptation to the changing loads and stresses accompanying the physiological circulatory alterations early in life, but may also confer greater adaptive potential after surgery.

PART III — ALTERATIONS OF GAP JUNCTION ORGANISATION IN DISEASE

CHAPTER 5 - CONNEXIN43 GAP JUNCTION DISTRIBUTION IN SURVIVING MYOCARDIUM BORDERING HEALED INFARCTS.

5.1 Introduction

Abnormalities of electrical impulse conduction and propagation are frequently associated with myocardial ischaemia and infarction (Fujimoto et al. 1983), and arrhythmias so arising, either acutely at the onset of severe ischaemia or infarction, or late in the natural history of the disease, are thought to be responsible for more than half the deaths due to ischaemic heart disease (Adgey, 1982). Electrophysiological studies have shown that a major cause of chronic ventricular arrhythmias in this context is circulating excitation forming reentrant circuits in the vicinity of a healed infarct (Kleber, 1987; Hoffman and Dangman, 1987). The precise nature of the structural abnormalities that may lead to arrhythmogenesis in ischaemia and infarction is unclear. Reentry requires an electrophysiological substrate that includes the presence of a region of slow conduction and a region that may block propagation, usually in one direction, around the circuit (Spear et al. 1983; Ursell et al. 1985; Dillon et al. 1988; Wit and Janse, 1992). There is evidence to suggest that surviving myocytes in the chronic phase after myocardial infarction have normal, or near normal, action potential characteristics (Boyden et al. 1982), and cellular electrophysiology therefore does not provide complete insight into the arrhythmogenic substrate in this context. Although fibrotic scarring is a feature of infarct healing and forms anatomical barriers to impulse conduction (Spear et al. 1983; Luke and Saffitz, 1991), fibrosis per se does not provide a full explanation of the anatomical substrate for reentrant arrhythmias. In fact, studies mapping epicardial electrical activity in 4-day old canine infarcts have shown that in the early period after infarction, and before a fibrotic response, reentrant arrhythmias can readily and reproducibly be induced without the presence of an apparent anatomical obstacle for the circuit to circulate around (Dillon et al. 1988). The explanation proposed by those working with this model is that anisotropic conduction in ventricular myocardium, which becomes disturbed in association with infarction, in conjunction with a diminishing degree of dysfunction of the active membrane properties of the myocytes in this period, is the substrate that can support stable reentrant initiation and propagation. That is, changes in the nature and uniformity of anisotropic impulse conduction velocities and refractory periods in the

surviving epicardium result in reentry around functional barriers that are not otherwise (when paced or in sinus rhythm) sites of anatomical or electrical discontinuity (Dillon et al. 1988). Although anatomical barriers are not, therefore, necessary for reentry, fibrosis is a prominent feature in the chronic phase after infarction, and the site of origin of most chronic clinical ventricular tachycardias can be localised to a region of interface between infarct scar and surviving myocardium (Pogwizd et al. 1992; Wit and Janse, 1992; Josephson, 1992). The basis for localised disturbances of conduction velocity in this context remain poorly understood. Electron microscopic studies of the infarct border zone have reported alteration in the number of contacts that each myocyte makes to other myocytes (Luke and Saffitz, 1991), but techniques for investigating gap-junctional organisation throughout larger volumes of tissue have only recently become available. The present study, a collaborative effort involving other members of the laboratory (Smith et al. 1991), set out to investigate gap junction organisation and distribution at the borders of healed human myocardial infarcts. In the course of this work, an abnormal distribution of connexin43 gap junctions was discovered by confocal microscopy, and reported (Smith et al. 1991). This finding provided the impetus for further investigation, both in the completion and extension of this particular study by enlarging the series and doing the complementary electron microscopy to further understanding of the ultrastructural basis of this change (Smith et al. 1991), and by continuing to study more widely, myocardial gap junction organisation in health and disease. Particular aspects focused on in this study were the extent to which the detected abnormalities were to be found in association with myocardial infarction, and the way in which partial-thickness infarction may differ from transmural infarction.

5.2 Materials and Methods

Ventricular specimens for study were obtained from:-

1. Ten explanted hearts from recipients during cardiac transplantation. Patients had 3-vessel coronary disease, documented myocardial infarction at least three months previously, and severe left ventricular dysfunction. A block of tissue of about $8mm^3$ was excised from the edge of a healed left ventricular infarct scar as soon as possible after explantation, ensuring that the heart remained in cold cardioplegic solution if any brief delay occurred.

2. Five patients undergoing coronary artery bypass surgery, with a history of myocardial infarction at least three months previously. Of these patients, three had anterior Q-waves on their preoperative ECGs, and two had ECG evidence of non-Q-wave anterior infarction. Within 3 minutes of establishing cold cardioplegic arrest, left ventricular biopsies were obtained from the anteroapical region, at the apparent interface between pale scar, and viable myocardium, either by scalpel excision of deep epimyocardium about the size of a grain of rice, or by use of a needle (Trucut) bioptome (diameter 1.5mm) to obtain a transmural specimen.

In each case, the specimen was immediately divided for immunohistochemistry and thin section electron microscopy and placed in the appropriate fixatives (Chapter 2). If the biopsy was of adequate size, a small number of fragments were prepared for freeze-fracture electron microscopy. When dividing each specimen, attempts were made to include a region of interface between pale scar tissue and viable myocardium in each fragment. Each specimen was sketched when sub-divided in order to keep track of tissue orientation and relationships between the fragments processed by different techniques. Tissue was prepared for general histological examination (toluidine blue and/or haematoxylin and eosin).

5.2.1 Data collection from Connexin43-immunolabelled tissue

All labelled sections were initially surveyed at low magnifications with both standard epifluorescence, phase contrast and confocal microscopy, in order to assess the overall pattern of distribution of connexin43 with respect to the general tissue structure, cell orientation and preservation, and proximity to regions of infarct scarring. By the same technique used in section 3.2.2a of Chapter 3, projection images obtained from the transplant-recipient ventricles were used to measure the longest dimension of the fluorescent spots representing gap junctions in myocardium most closely related to the borders of scarred regions (so called "infarct border zone" myocytes, which did not have orderly gap junctions grouped into disks; see Results). Similar measurements were made from well-preserved myocardium distant from infarct scar in these, the most severely impaired ventricles.

5.3 Results

Table 5.1 Details of ventricular myocardial biopsies from ischaemic hearts

Patient/heart no.	Age (yrs)	Anterior Q-waves	LV function	Surgery	Biopsy technique
I1	52	yes	LVEF<20%	transplant recipient	scalpel
I2	64	yes	LVEF<20%	transplant recipient	scalpel
I3	62	yes	LVEF<20%	transplant recipient	scalpel & Trucut
I4	48	yes	LVEF<20%	transplant recipient	scalpel
I5	53	yes	LVEF<20%	transplant recipient	scalpel
I6	59	yes	LVEF<20%	transplant recipient	scalpel & Trucut
I7	55	yes	LVEF<20%	transplant recipient	scalpel
I8	53	yes	LVEF<20%	transplant recipient	scalpel
I9	44	yes	LVEF<20%	transplant recipient	scalpel
I10	47	yes	LVEF<20%	transplant recipient	scalpel
I11	54	no	≈ normal	coronary grafts	scalpel
I12	47	yes	mod. impaired	coronary grafts	scalpel
I13	46	yes	mod. impaired	coronary grafts	scalpel & Trucut
I14	48	yes	mod. impaired	coronary grafts	scalpel
I15	53	no	≈ normal	coronary grafts	Trucut

Details of the 15 patients, aged 52.3 ± 5.9 years, are summarised in Table 5.1. The explanted hearts with severe ischaemic heart disease (hearts I1 to I10 in Table 5.1) all had markedly impaired left ventricular dysfunction, and ejection fraction at preoperative radionucleide scanning of <20%. The patients with transmural anterior myocardial

infarction, and absent R-waves in their anterior ECG leads (hearts I12 to I14), had moderately impaired left ventricular function at preoperative ventriculography and those with partial thickness anterior myocardial infarction and retained R-waves (hearts I11 and I15) had minimally impaired left ventricular function.

5.3.1 Histology and General Ultrastructure.

Light microscopic findings in the ischaemic hearts included densely fibrotic areas of healed infarction and areas of more generalised fibrosis (Fig 5.1). Evidence of

Figure 5.1. Light micrograph of toluidine-stained interface between partial-thickness infarct scar and surviving epimyocardium, showing distortion of the normal myocardial architecture and interdigitation of fibrous tissue and myocytes. Extensive interdigitation of scar and the surviving epimyocardial border zone was a characteristic feature particularly of partial-thickness infarcts. The myocytes show marked contracture banding. x315.

degenerative change was common in patches of myocytes immediately adjacent to or projecting into healed infarcts. There were frequent smaller discrete infarcts ($<500\ \mu m$ diameter) throughout the myocardial specimens in each case. These were particularly abundant in the specimens from hearts with partial thickness infarction, in which the borders of the infarct scar were less well defined and had the appearance of confluent small infarcts with extensive interdigitation of scar and myocardium (Fig 5.1).

Many areas of myocardium distant from healed infarcts, however, revealed an orderly arrangement of fibres and an overall cellular structure resembling that of normal myocardium. Myocytes in these "well-preserved" regions appeared to be connected to one another by intercalated disks of normal structure, although features of varying degrees of hypertrophy were present in some samples.

Evidence of degenerative change was, however, common in patches of myocytes immediately adjacent to or projecting into healed infarcts. The principal changes detectable by light microscopy of these cells were disarray of myocyte orientation, reduction of myofibrillar content with clearing of cytoplasm, alteration of cell shape to rounded or attenuated forms, and, in occasional cells, enlarged or multiple nuclei (Fig 5.1). Thin section electron microscopy revealed that myofibrillar disorganisation was widespread, with the individual myofilaments of some altered cells arranged in a parallel zig-zag or undulating fashion (Fig 5.2A). Elsewhere, evidence for disintegration of the myofibrils and their component myofilaments, associated with the appearance of granular (myofibril-free) peripheral patches of cytoplasm (Fig 5.2B), was frequently encountered. The extent of these changes varied considerably in different cells. Although the overall extent of myocardial damage and infarct scarring may have been greater in the explanted group of hearts at the microscopical level, the regions of well-preserved myocardium in these hearts showed no differences in appearances from the less severely impaired surgical group, and were essentially normal.

5.3.2 Immunohistochemistry of connexin43 gap junctions

By low power inspection, healed infarcts were readily identified in the sections immunolabelled for connexin43. Scar tissue showed no immunostaining of gap junctions, but often contained the easily distinguishable pink autofluorescence of lipofuscin. The distribution of gap junctions in the structurally well preserved areas of left ventricular myocardium from the ischaemic hearts appeared normal, and in this respect there was no apparent difference between the well-preserved regions of the specimens, regardless of the degree of ventricular impairment at preoperative assessment. Label in these regions was confined to the transversely-orientated positions of the intercalated disks, in which there was the characteristic peripheral ring of larger junctions (see Chapter 2). Controls in which the primary antiserum treatment was omitted or substituted with pre-immune serum showed no fluorescent labelling.

In keeping with the results of the infarcted hearts already immunolabelled before

I started this series of studies, the infarct border zones of all hearts showed fluorescent staining that was no longer confined to the well-defined foci representing normal intercalated disks, but showed varying degrees of dispersion over the cell surface (Fig 5.3A). Where this was minimal, it was still possible to identify the approximate position of the intercalated disk by the presence of aggregates of labelled junctions. In many instances, however, a recognisable intercalated disk could no longer be seen, and label was distributed over the entire length of the cell (Figs 5.3A & B). Serial optical sectioning revealed that such junctions were situated at (or close to) the surfaces of abutting myocytes (Fig 5.4), but labelling was seldom present along the surfaces of the myocytes apposing the healed infarct. Overall, the disordered patterns of gap junction immunostaining tended to become more pronounced as the size of the infarct and the histological abnormality of its surrounding myocytes increased. The extent of the zone of disordered labelling was variable and the borders sometimes difficult to define

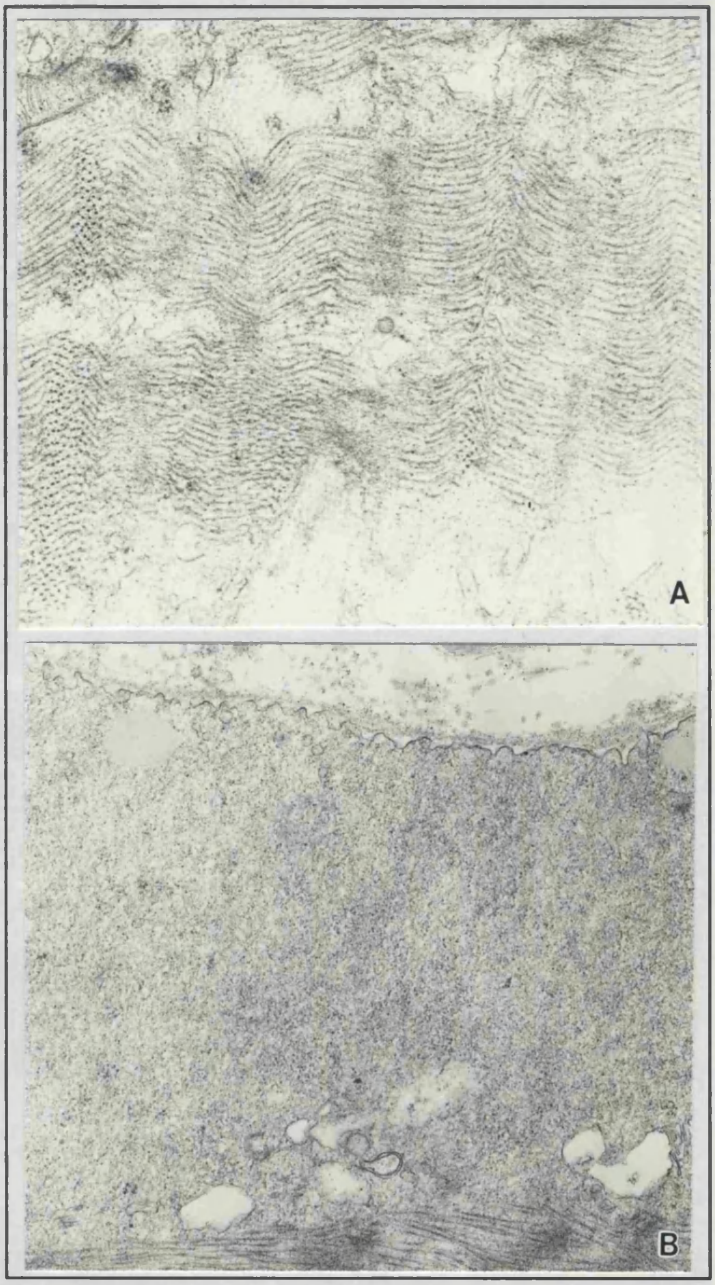

Figure 5.2. Thin section electron micrographs showing abnormalities of the contractile apparatus in the myocytes bordering healed myocardial infarcts.
A. The myofibrils appear intact but show abrupt changes of orientation in a zig-zag fashion.
B. An area of amorphous cytoplasm due to degeneration of the contractile apparatus. This appearance occurred in the periphery of the most severely degenerated myocytes. A & B, x25,000.

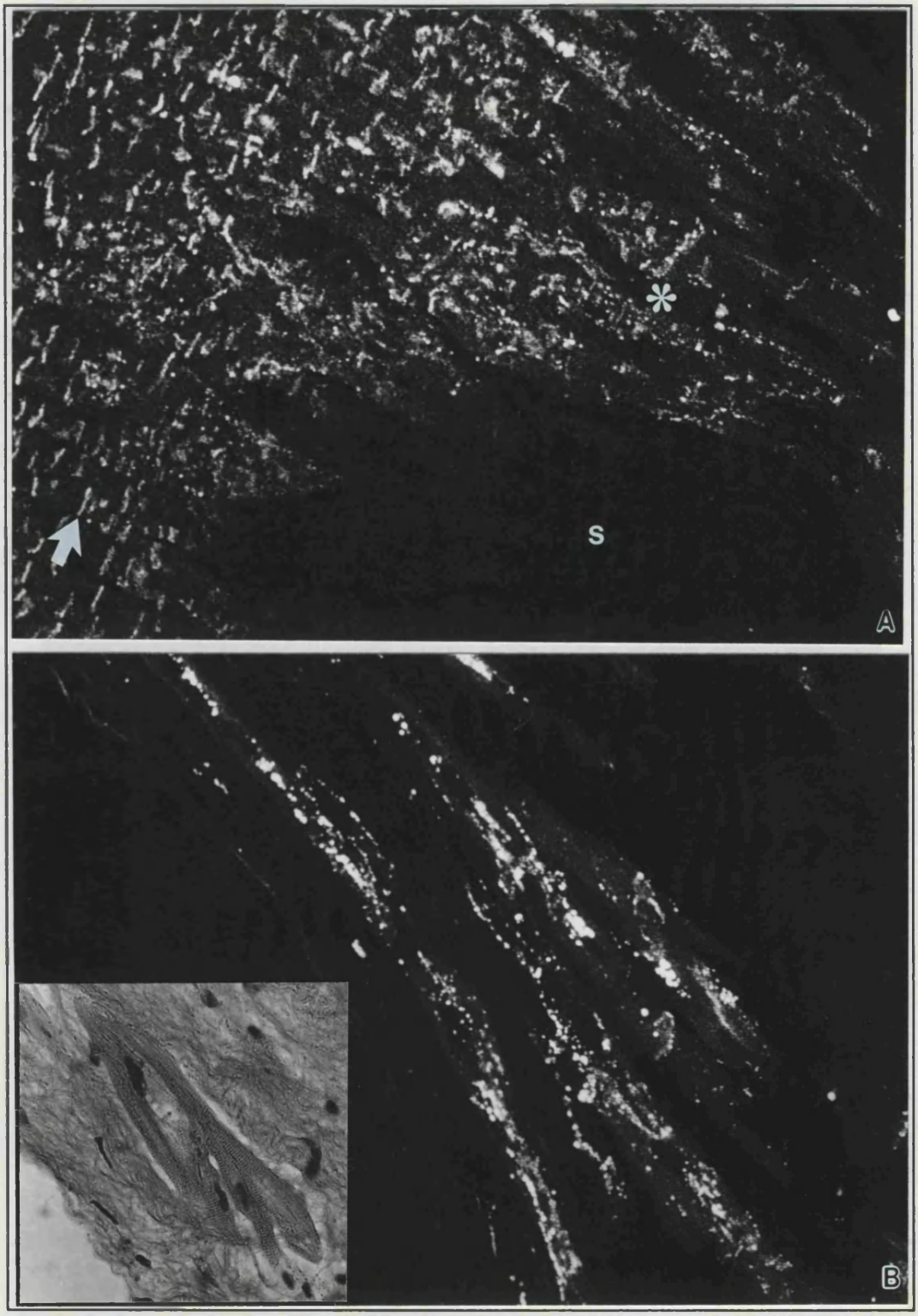

Figure 5.3. Gap junction distribution in myocytes bordering healed myocardial infarcts, as seen by laser scanning confocal microscopy of immunolabelled tissue. A: A low-power image showing progressive disruption of gap junction distribution on nearing the infarct scar (s). Relatively normal distribution, as transverse lines of label, can be seen toward the left side of the image (arrows). The myocytes bordering and projecting into the scar (*) have profuse junctional labelling along the entire length of the cells, and no discernible transverse intercalated disks. B: A higher power projection of an optical section series, with standard light microscopy of an adjacent wax section for comparison (inset). The degenerating myocytes traversing densely fibrotic scar tissue show the profuse abnormally distributed label along their lengths. A, x180; B, x700 (inset x280)

as the disruption was often progressive on nearing the infarct (Fig 5.3A). Pooled measurements from the infarcts examined showed the width of the infarct border zone, as defined by the extent of total label disruption with complete absence of identifiable intercalated disks, to be 122.8 $\pm$ 57.4 μm (n=100) from the edge of the scar, and this value showed no association with the degree of left ventricular dysfunction at preoperative assessment.

It is important to note that this is not simply a phenomenon associated with connective tissue per se. Normal perivascular connective tissue is not associated with a

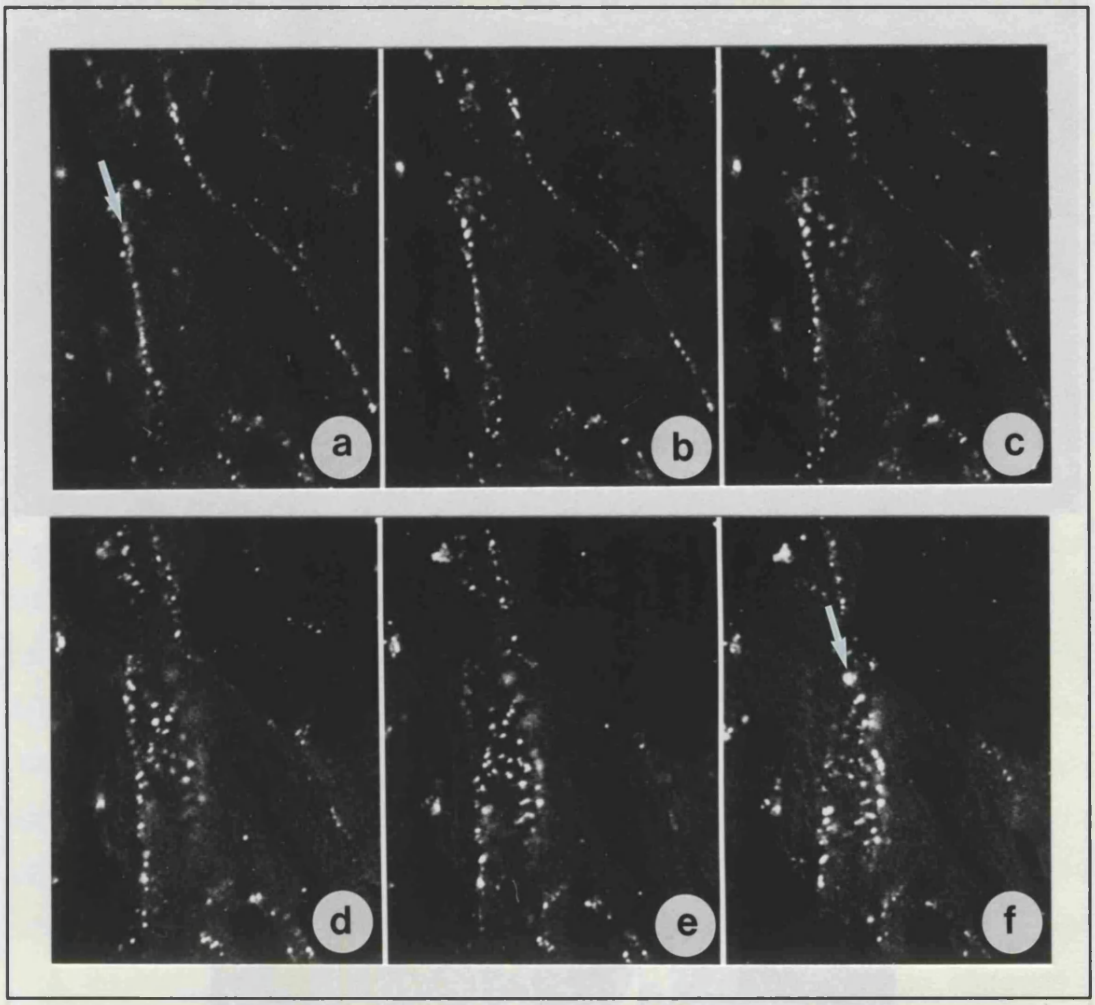

Figure 5.4. A demonstration of the apparent surface positioning of the abnormal junction distribution at the infarct border zone. **a-f:** An optical section series at 2μm intervals through longitudinally-sectioned myocardium showing how the line of label (**a:** arrow), representing the edge of a myocyte, evolves progressively through the series, to describe the surface of the myocyte, and then the opposite edge (**f:** arrow). x900.

disruption of label in the adjacent myocardium (Fig 5.5), and the small areas of fibrosis (less than about 500 μm diameter) in diseased hearts occasionally showed no discernible disruption of gap junction arrangement.

A striking feature of the infarct border zones was the continued presence of

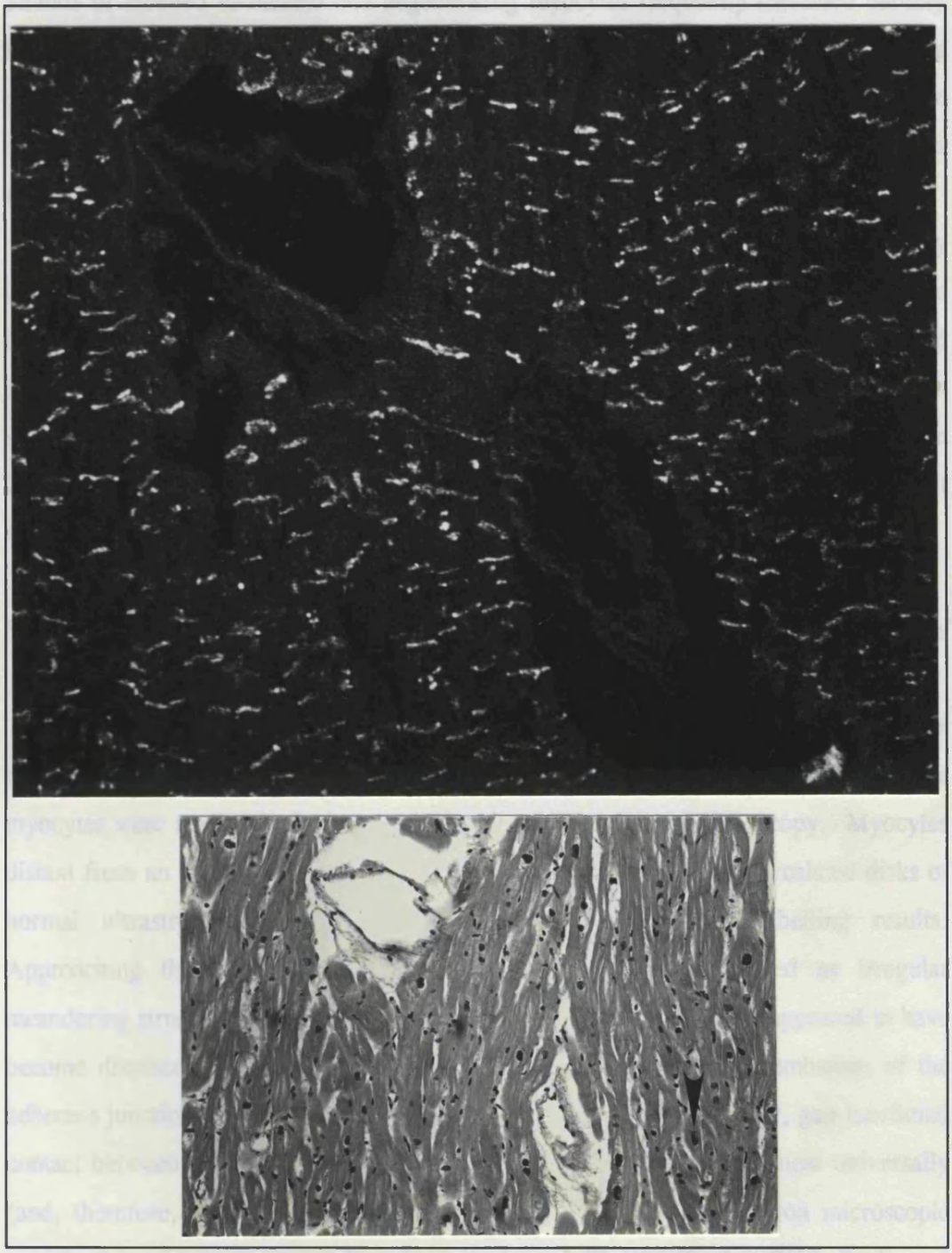

Figure 5.5. Low power projection image of longitudinally-sectioned connexin43-immunolabelled myocardium distant from an infarct, containing a transected artery and vein. Unlike the pathological fibrosis of healed infarction, the normal perivascular connective tissue is not associated with the disruption of gap junction distribution in the adjacent myocytes. Below is a light micrograph (stained with haematoxylin & eosin) of the adjacent wax section, showing the transected vessels. Note that some myocyte nuclei are enlarged, and have a "rectangular" form (arrow), consistent with the compensatory hypertrophy characteristic in myocardium of the infarcted ventricle. Upper, x200; lower, x120.

profuse label where cell degeneration was maximal. There were occasional collections of gap-junctional label at the edges of the healed infarct scar, with an absence of any

associated myocyte structures on standard epifluorescent or phase-contrast microscopy. Strands of labelled attenuated and degenerating myocytes frequently traversed densely fibrotic scar (Fig 5.3B) linking blocks of healthy myocardium, potentially maintaining coupling, and therefore electrical continuity, between them. The myocytes in these bridges predominantly had laterally disposed gap junctions, but discrete intercalated disks were also identifiable, especially as the bridges approached healthy myocardium.

In myocardium from the transplant-recipient, and therefore the most severely impaired ventricles the labelled junction size distribution pooled from randomly-selected infarct border zone regions is shown in Figure 5.6A. For comparison, the labelled junction size distributions from intercalated disks of well-preserved regions distant from infarction in these same hearts, and from normal left ventricle (Fig 3.9) are also shown in Figure 5.6. Analysis of variance of the $\log_{10}$-transformed data shows no significant difference between these distributions.

5.3.3 Ultrastructural Correlates of Altered Immunolabelled Gap Junction Distribution

To investigate the ultrastructural basis for the observed alterations in distribution pattern of immunostained gap junctions, the intercalated disks and junctions of border zone myocytes were studied in further detail by thin section electron microscopy. Myocytes distant from an infarct, showing no degenerative change, revealed intercalated disks of normal ultrastructural appearance, consistent with the immunolabelling results. Approaching the infarct border zone the disks frequently appeared as irregular meandering structures between the cells, and some groups of junctions appeared to have become displaced from one another (Fig 5.7). Separation of the membranes of the adherens junctions was found between some cells, although interestingly, gap-junctional contact between such cells was maintained (Fig 5.8), as described almost universally (and, therefore, non-specifically) in the earliest case reports of electron microscopic examination of human myocardium in a number of diseases (Poche, 1958; Poche and Ohm, 1963; Kawamura et al. 1964; Kawamura et al. 1969).

Where cell shape and overall myocardial architecture was distorted by degeneration and scarring, gap-junctional membrane was frequently displaced from its usual location so that it was no longer found exclusively in association with adherens junctions. Examples of such gap junctions, which characteristically have highly convoluted profiles, are illustrated between cells with abnormally oriented myofilaments in Figure 5.9. Figure 5.9A shows a series of gap junctions, establishing contact in a

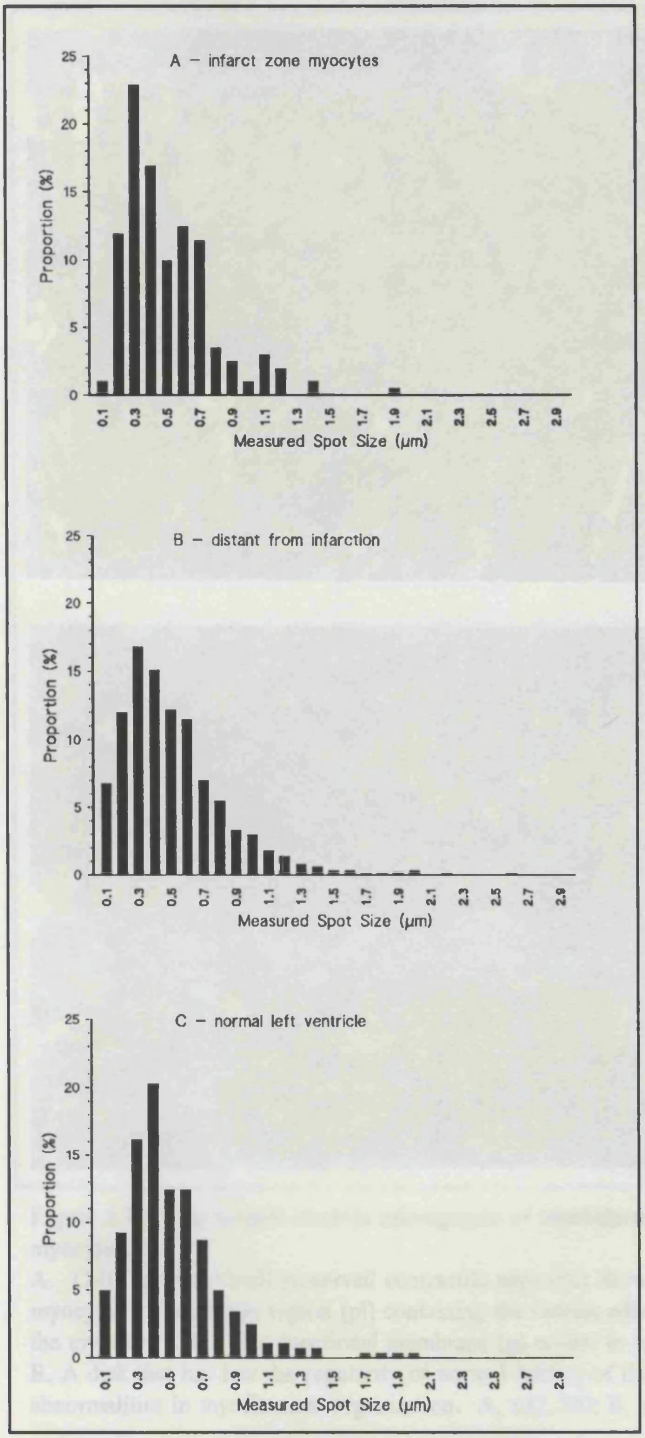

Figure 5.6. Frequency distribution of immunolabelled junction long-axis lengths pooled from infarct border zone myocytes with disrupted gap-junctional organisation (A) and from well-preserved myocardium distant from infarction (B). For (A) and (B), measurements of >400 junctions were made manually using the SOM software "length" command. The distribution for normal left ventricle (Fig 3.9 from Chapter 3) is shown for comparison (C). Analysis of variance of the $\log_{10}$-transformed data demonstrates no significant difference between these distributions ($p=0.12$).

region between two degenerating myocytes that is no longer recognisable as an intercalated disk. The surfaces of such cells are often irregular with cell processes that may form gap-junctional contacts at some distance from the main cell body (Fig 5.9B), and in the absence of other components of an intercalated disk. In some section planes these junctions had the appearance of having been internalised, and annular profiles of gap-junctional membrane are more abundant in infarct zone myocytes than in normal myocytes (Fig 5.9 C & D). The increased convolution of the junctional membranes in degenerating cells appears to be the main explanation for this phenomenon. However, in some instances (e.g. where isolated cytoplasmic adherentes junctions are also observed), these structures may represent cytoplasmic vesicles of internalised gap-junctional membrane (Fig 5.9D). Occasional gap junctions attached to membrane blebs at the cell surface suggest disrupted junctional contacts that may be the precursors to such

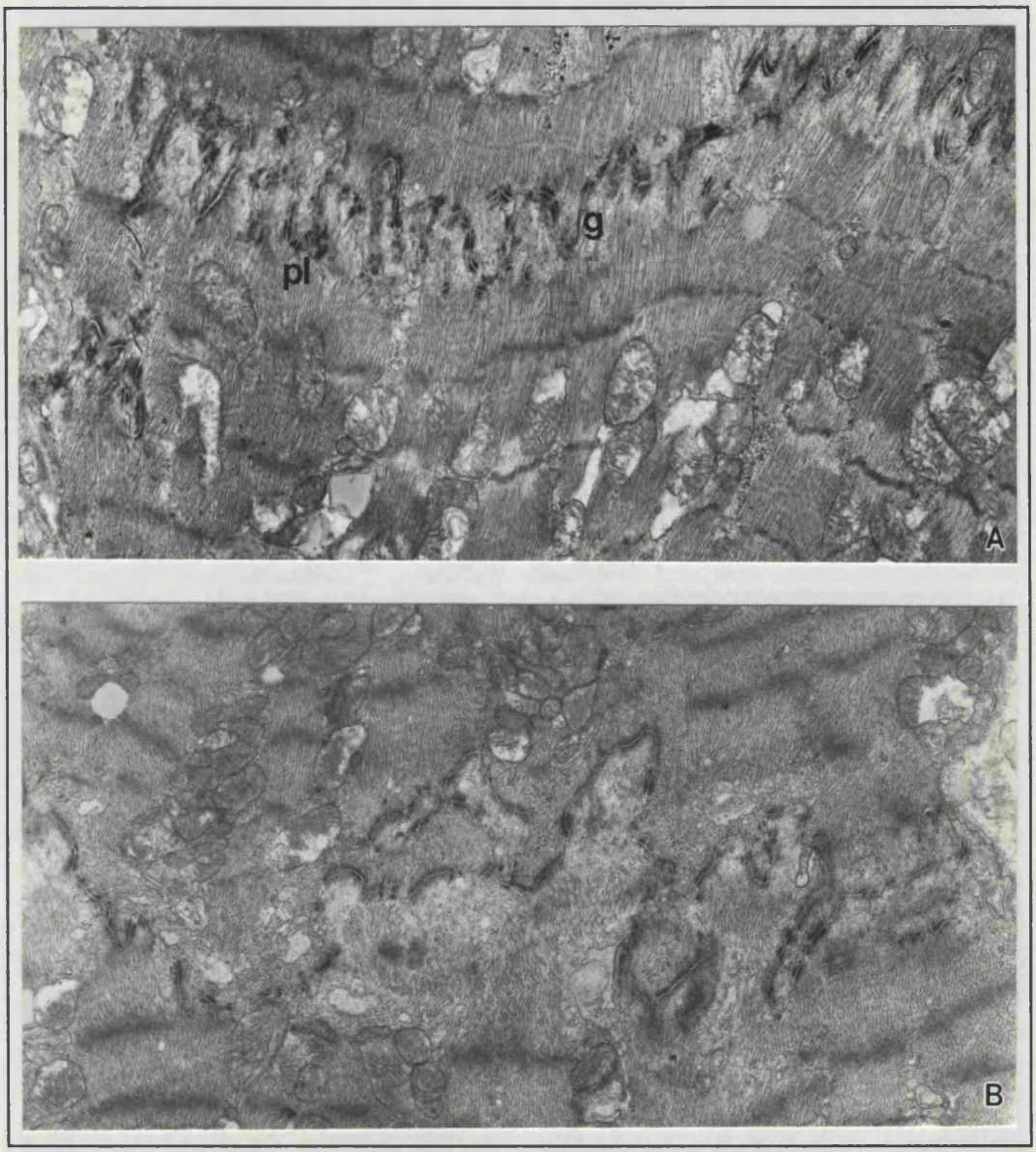

Figure 5.7. Thin section electron micrographs of intercalated disk abnormalities in infarct zone myocytes.
A. Cells that have well preserved contractile apparatus show disk features similar to those of normal myocytes. The plicate region (pl) containing the fasciae adherentes is evenly folded, and traverses the myofibre axis. Gap-junctional membrane (g) occurs in longitudinally orientated segments.
B. A disk that has lost the regularity of normal folding of the plicate region, between cells showing abnormalities in myofilament organisation. A, x12,200; B, x13,600.

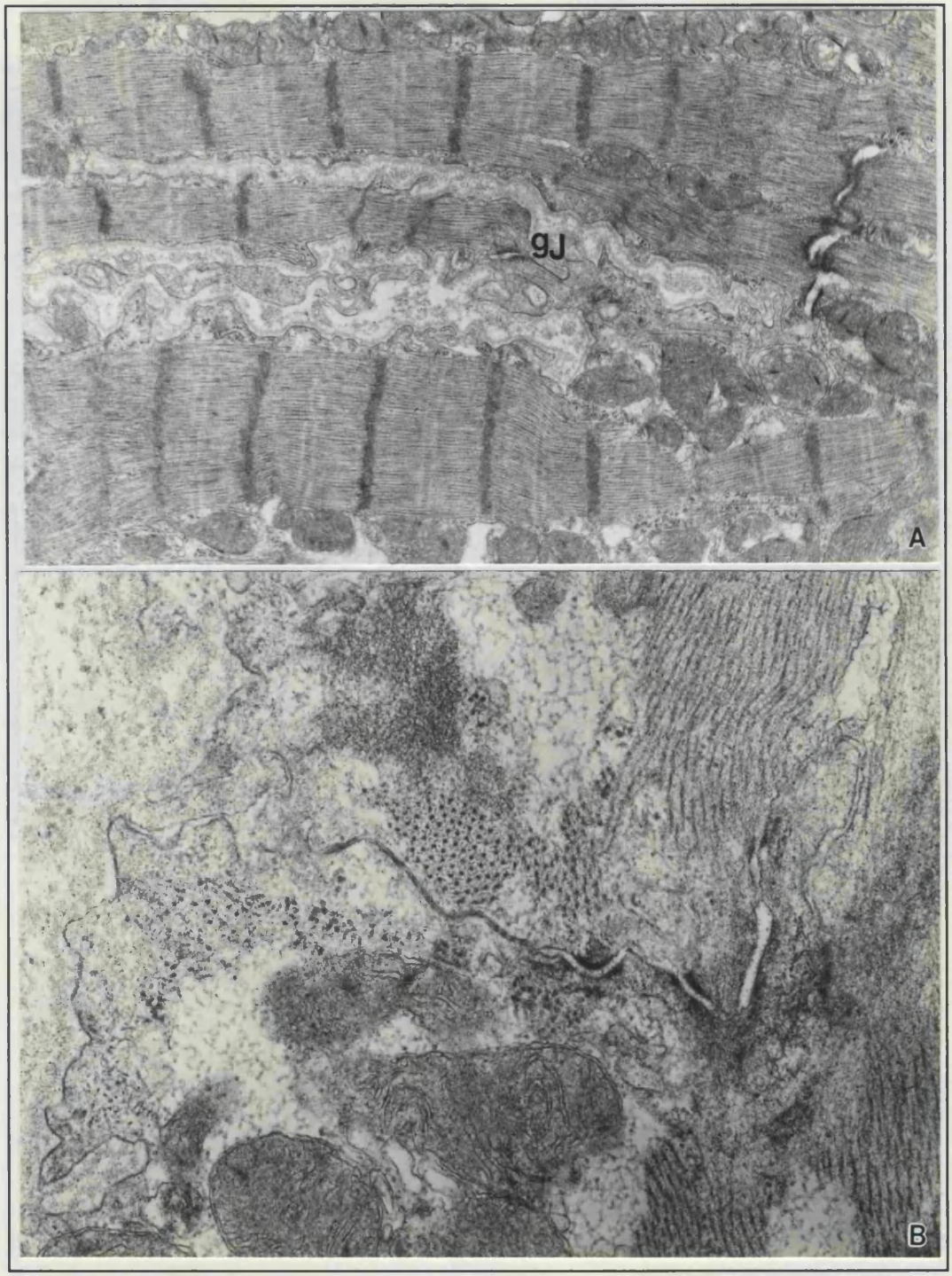

Figure 5.8. Dissociation of the adhering junctions in intercalated disks of degenerated border zone myocytes. Separation of the component membranes of the adhering junctions was a frequent observation.
A. Clear dissociation of a disk, with no apparent loss of contact at a distant gap junction (gj).
B. Higher power electron micrograph showing less pronounced separation of fascia adherens and desmosome membranes, with intact adjacent gap junction. A, x16,200; B, x52,000.

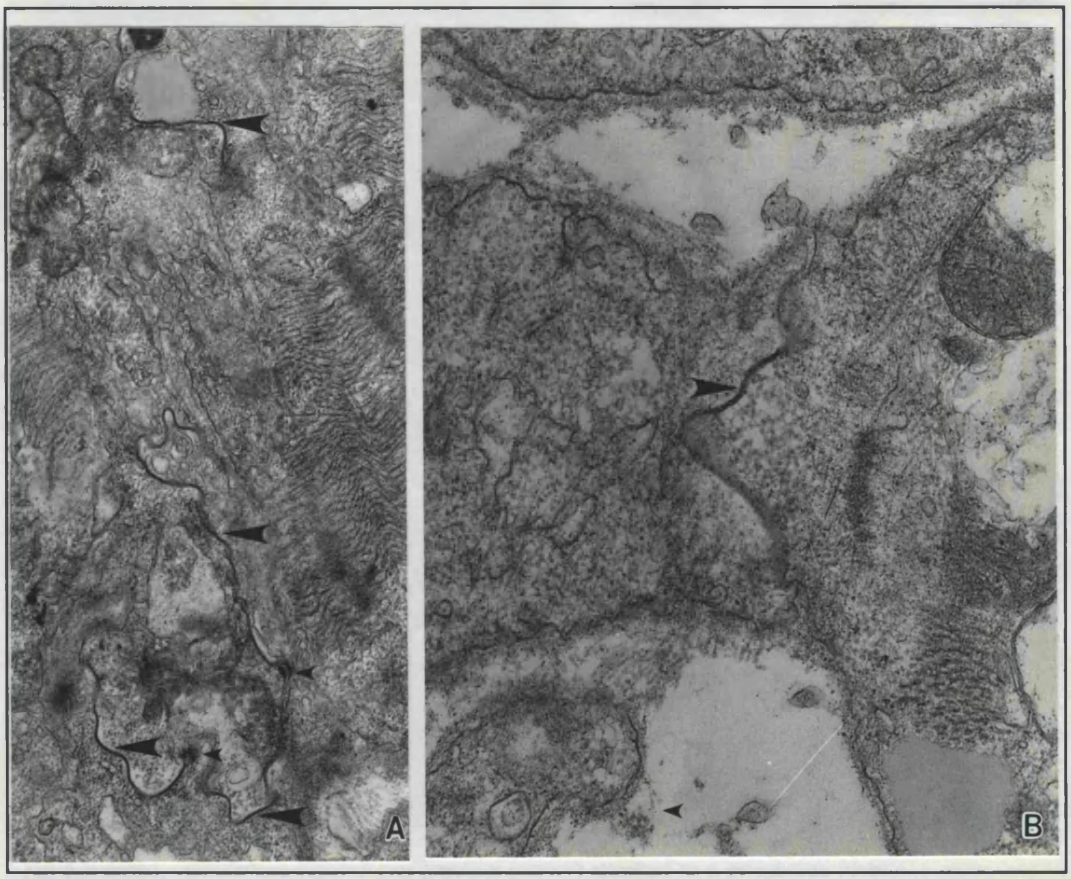

Figure 5.9. Thin section electron micrographs showing abnormal gap-junctional contacts between infarct border zone myocytes. In each example there is an absence of recognisable intercalated disks.
A. A series of gap junctions (large arrows), with two small desmosomes (small arrows) but no other adherens junctions, between two degenerating myocytes that have convoluted surface contacts and abnormal undulating myofilaments.
B. A gap junction (arrow) occupying an entire contact between two cell processes between highly degenerated cells. A, x26,000; B x52,000.
C and D - on next page:-

internalised vesicles (Fig 5.9C).

In summary, these diverse alterations of myocyte, intercalated disk and gap-junctional architecture would be consistent with the highly abnormal label distribution on immunohistochemical analysis.

5.3.4 Freeze-fracture of infarct border zone tissue

When portions of the border zone interface between white (fibrotic) and pink (myocardial) tissue were carefully dissected for examination by freeze-fracture, the replicas contained sparse small areas of membrane fracture, with large regions of fractured collagen (Fig 5.10). The myocyte-containing tissue was generally cross-fractured, but occasional small and incomplete gap junctions were seen (Fig 5.11). That

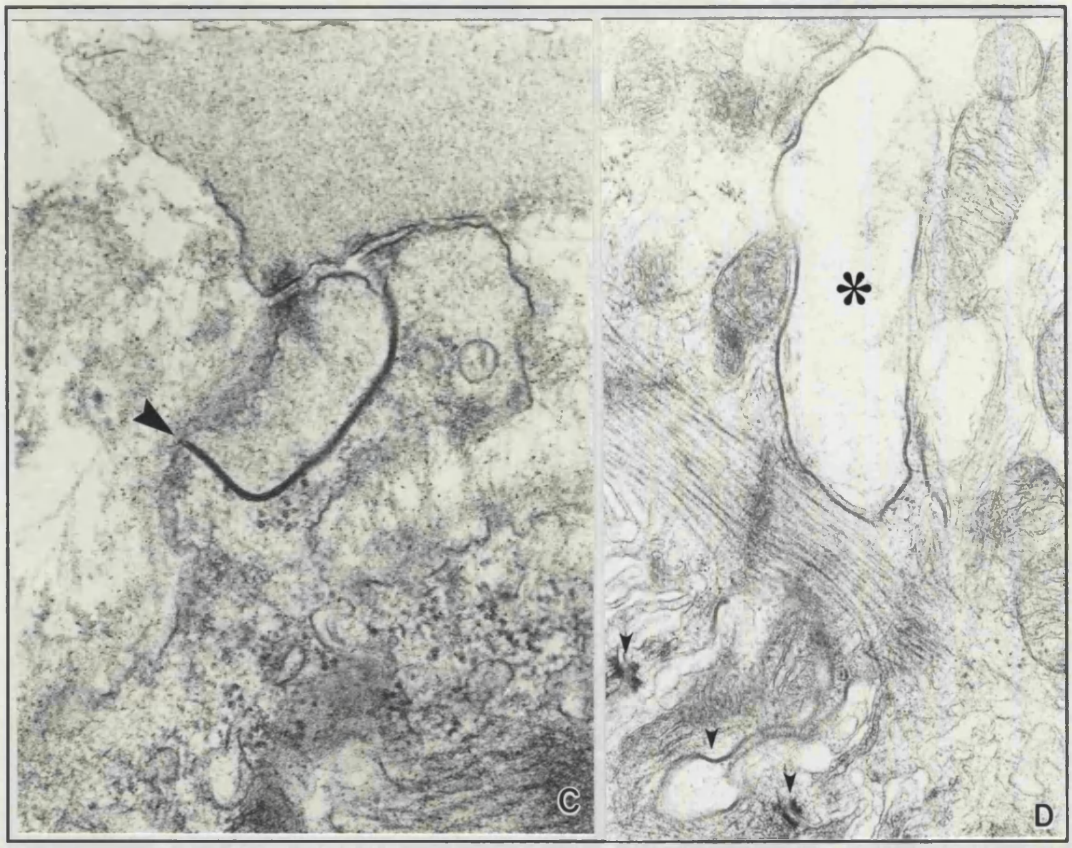

Fig 5.9 contd. C. Surface-located gap junction (arrow) attached to a membrane bleb.
D. A large annular gap junction (*) with other abnormally positioned junction types (arrows), all of which may be part of a convoluted intercalated disk. C, x75,000; D, x47,000.

larger junctions were not seen in their entirety was likely to have been a result of fracturing relatively hard and heterogeneously distorted fibrotic tissue. Although no gap-junctional area estimations could, therefore, be made from these very incomplete domains, the mean connexon packing density from those that were large enough to measure was $102.95 \pm 12.76 \times 10^{-4} nm^{-2}$ (n=20).

5.4 Discussion

The results presented here demonstrate that gap junction distribution is characteristically and universally altered in myocytes at the border zones of healed myocardial infarcts. Comparatively few labelled gap junctions are organised into discrete intercalated disks, and many are spread laterally over the cell. Bridges of degenerated and attenuated myocytes extend across densely fibrotic scar, apparently linking the myocardial masses at their ends. This latter feature was most evident in partial-thickness myocardial infarction, in which the demarcation between scar and myocardium was less discrete, with greater interdigitation of these tissues. Although "peninsulas" and bridges across

Figure 5.10. Freeze-fracture electron micrograph of an infarct border zone region. An expanse of myocyte plasma membrane fracture (m) is surrounded by cross-fractured collagen (with spiky appearance). No gap junctions are visible, but note how the caveolae are in clusters (c), which was observed frequently in fractured border zone tissue. x10,000.

infarcted regions have been previously reported in histological studies (Factor et al. 1978), an important finding in the present study was that these incarcerated and degenerated strands of myocardium retained profuse gap-junctional labelling at confocal microscopy. Electron microscopic examination confirmed intercellular gap-junctional contact, and, therefore, the potential for coupling and electrical continuity between the component myocytes and the muscle masses that are linked by them.

This study revealed some basic morphological characteristics of myocardial gap junctions and intercalated disks in patients suffering from ischaemic heart disease, enabling comparison with the normal findings noted in Chapter 3. The finding that the labelled junction long-axis length distribution showed no significant difference between

Figure 5.11. Higher power freeze-fracture electron micrograph at a site of abutment between myocytes in an infarct border zone region (Note the collagen at the top). The plane of fracture passes from the plasma membrane (pm) of one cell, to the interior of its neighbour (i). Along the line of abutment, possibly representing a degenerating intercalated disk similar to that in Figure 5.7, two small gap junctions are visible (gj). x38,000.

the infarct border zone and the distant left ventricle is of particular note. This finding suggests that the disruption of the gap junction distribution in the infarct-related tissue is possibly due to a redistribution of the preexisting population of junctions, rather than the cells producing an entirely new, modified population. In this context it is worthy of note that although the rate of turnover of connexin43, and probably connexons may have a half life of a few hours (Page, 1992), it is likely that overall, gap-junctional plaques are relatively stable, with little change in their total channel content. The similarity in the labelled junction size distributions in the present study would be consistent with this notion. The finding that the labelled junction long-axis length distribution in the left

ventricular myocardium outside the infarct border zone in the most severely impaired hearts is not significantly different from that in the normal myocardium suggests that not only is the pattern of distribution of gap junctions in the non-infarct related ischaemic ventricle normal, but the population of junction sizes is also normal. The question as to whether the total gap-junctional content of this apparently well preserved myocardium distant from infarction is quantitatively normal, however, is not addressed by these data; this topic is explored in Chapter 7. What can be concluded from the present results is that in ischaemic heart disease, myocardium that is not immediately associated with infarct scar, and of essentially-normal appearance histologically, does not have widespread derangement in gap junction organisation, and there is, therefore, no generalised derangement underlying functional impairment in the severely diseased and failing ischaemic ventricle.

Arrhythmias, and in particular reentrant arrhythmias, are a prominent feature of ischaemic heart disease (Wit and Janse, 1992). In experimentally-induced infarction, electrophysiological studies have identified the border zone of myocardial infarcts as sites in which slow conduction, responsible for sustained re-entry, arises (Spear et al. 1983; Ursell et al. 1985; Dillon et al. 1988; Pogwizd et al. 1992). Slow conduction, attributable to intercellular uncoupling, and areas of complete conduction block, persist at the sites of experimentally-induced infarction after healing, thereby contributing to chronic arrythmogenesis (Spear et al. 1983; Ursell et al. 1985; Dillon et al. 1988). Ultrastructurally, examination of the intercalated disks in border zone-myocytes after experimental infarction reveals attenuation of "contact zones" between them (Ursell et al. 1985). In the present study, the ability to demonstrate gap junction distribution throughout intact volumes of myocardium, as afforded by the immunohistochemical technique, has shown that the most prominent and consistent feature of border zone myocytes in human ischaemic heart disease is a disorderly pattern of labelled gap junctions. Since normal uniform anisotropic conduction is mediated at least in large part by the pattern of gap junction arrangement (Janse, 1992), it is tempting to suggest that such a derangement of gap junctions might contribute to reentrant arrhythmias by altering the normal uniform anisotropic conduction within the network of myocytes adjacent to, and interdigitating with, the interface with the infarct scar. The possibility thus exists that injury-induced disruption of the normal gap arrangement could play a direct role in slowed and non-uniform conduction, and may therefore be the morphological basis of the electrophysiological substrate for arrhythmogenesis. That such networks of myocytes coupled in an apparently disorganised manner were found to exist adjacent to regions of

scar as small as about 500 μm diameter suggests that the total burden of abnormally coupled myocytes is likely to be even greater in partial-thickness infarction, in which multiple small partially-confluent areas of fibrosis exist, presenting a large area of interface with surviving myocardium.

It should again be noted that the presence of label should be interpreted strictly as the presence of the polypeptide to which the "HJ" antibody reacts, and is not necessarily a marker for the fully functional gap junction. However, thus far in the series of studies presented in this thesis, there have been a number of lines of experimental evidence to suggest that the distribution of label can generally be considered to represent morphologically-distinct gap junction. These lines of evidence are: i) the immunolabelling patterns correlate with gap junction distribution at the electron microscopic level, ii) the confocal data on normal human myocardium (Chapter 3) accord with the values obtained from mammalian myocardium by standard electron microscopic morphometry (Page, 1978; Stewart and Page, 1978; Shibata et al. 1980; Hoyt et al. 1989), and iii) immunogold labelling (Chapter 4) confirms specific binding of the antibodies to gap junctions (Severs et al. 1993).

Disassembly of gap junctions, at least in some systems, may involve separation of the once-abutting connexons of adjacent membranes, and their lateral dispersion in the plasma membrane (Lane and Swales, 1980; Braun et al. 1984), or internalisation of gap-junctional membrane (Larsen and Risinger, 1985) into vesicles which may persist just below the cell surface for substantial periods (Severs et al. 1989). Although serial optical sections revealed that some of the dispersed patches of immunostaining were located in the vicinity of cell-to-cell appositions, the technique does not have the resolution required to determine whether these structures lie on or just below the cell surface. That the lateral labelling found in border zone myocytes may at least in part be due to gap junction disassembly cannot, therefore, be excluded.

Thin section electron microscopy provided further insight into these issues by revealing multiple and variable alterations to the intercalated disk and gap junctions of border zone myocytes. Myocytes in the vicinity of healed infarcts undergo diverse alterations in morphology, associated with a remodelling of their intercellular interactions. Individual junctions and groups of junctions, though often maintaining intercellular contact, appear to be displaced by this remodelling process, so that discrete intercalated disk zones are, overall, less clearly defined. Some junctional contacts are entirely disrupted by these changes, leaving junctional membrane associated with blebs at the cell surface, or internalised just below the surface as intracytoplasmic structures. Both gap

junctions and adherentes junctions are affected by these processes. It is noteworthy that intracytoplasmic junctions (mainly adherentes junctions but also gap junctions) have previously been reported as a feature of degenerating myocytes associated with areas of fibrosis in a variety of cardiac pathological conditions (Buja et al. 1974). Both displaced gap junctions that maintain contact between cells, and internalised, non-functional, gap-junctional membrane, are likely to contribute to the dispersed immunostaining pattern observed by confocal microscopy. However, while electron microscopy can reveal the fine detail of the ultrastructural location of individual segments of junctional membrane, it is only by confocal microscopy of immunostained preparations that the full extent of the reorganisation in the distribution of gap-junctional membrane in the tissue as a whole becomes apparent.

In conclusion, the disturbed pattern of gap junction distribution at the borders of a healed myocardial infarct is likely to permit intercellular coupling in a similarly disorganised manner, significantly disrupting the normal pattern of anisotropic conduction. The resulting heterogeneity of propagation in tissue composed of disrupted and degenerated myocytes, may, under the right conditions, provide the substrate for the ventricular arrhythmias associated with healed myocardial infarction. Although this disturbance of gap junction distribution is a universal finding at the border zone of healed infarcts, the bulk of ventricular myocardium in the ischaemic heart has a well preserved pattern of gap junction distribution. What has not been addressed in the present study, however, is the question of whether there are quantitative changes in gap-junctional content of the apparently well-preserved myocardium distant from infarction in the ischaemic ventricle. This question will be addressed in Chapter 7.

CHAPTER 6 - DETERMINATION OF GAP-JUNCTIONAL CONTENT PER MYOCYTE IN INTACT VENTRICULAR MYOCARDIUM

6.1 Introduction

In Chapter 3, gap-junctional content of healthy adult human ventricular myocardium was expressed in the standard units used conventionally for quantifying cell surface membrane structures, $\mu m^2/\mu m^3$ tissue volume (Luke et al. 1989a). These units of measurement may be particularly useful for comparing tissues under conditions in which there may be alterations of expression of the membrane structure, but are of more limited value if there are concomitant changes in the size of the cells comprising the tissue. Human myocardial disease, whether of ischaemic, inflammatory, degenerative or hypertrophic pathophysiology, is associated with changes in myocyte size. Under these circumstances, gap-junctional surface area per unit volume of tissue, which takes no account of cell volume, provides no indication of the gap-junctional membrane expression and potential for intercellular coupling per myocyte. A separate and potentially more meaningful way of expressing gap-junctional content for comparative purposes would be to normalise the value with respect to cell volume, producing a measure of gap junction area **per cell.** Previous stereological studies of myocardium have not attempted to determine this factor, largely for technical reasons which are indeed difficult to overcome. In the case of human myocardial disease there are the added difficulties of differences in the state of contraction of different samples, the heterogeneity in the extent of disease involvement, and the variation in cell size and state of contraction between adjacent regions of the same sample. For this reason, in order to express gap junction quantity per myocyte, it was important to derive a measure of the volume of the myocytes comprising the actual fields from which gap-junctional content was quantified. Although randomly selected microscopical volumes of transversely-sectioned ventricular myocardium will contain a large proportion of incomplete cells, thereby preventing precise or absolute cell volume determination, a method for deriving an index of constituent cell volume for comparative purposes was sought. By applying this cell volume index to the gap junction quantity determined per unit volume of myocyte, a further index of gap-junctional area per cell permits more meaningful comparisons between normal and diseased myocardium.

This chapter explains the method developed for deriving the cell-volume index of the tissue field from which the gap-junctional area was measured, with experimental work

to verify its use.

6.2 Theoretical basis of deriving a cell volume index

There is considerable variation in the dimensions of adult ventricular myocytes but there are some common morphological characteristics. The elongated form of the myocytes is derived mainly from the constituent parallel bundles of myofibrils, which vary in length, and, as described in section 1.2.2a of Chapter 1, result in multiple step-like transversely-orientated cell terminals (Severs, 1989b). These are the sites of the intercalated disks (see Figs 1.1 & 3.10). In a simplified model, whole ventricular myocardium can, therefore, be considered to consist of irregular bundles of columns of abutting cylinders (myocytes), with transversely-orientated faces (intercalated disks) situated not only at their two ends, but also at intervals along their lengths (Fig 6.1).

The primary data from which the volume index was derived consisted of images of transversely-sectioned myocardium, in which, by this model, transected myocytes have circular profiles, with intercalated disks lying in the plane of section (Fig 6.1; see also Fig 3.6). The ratio of the number of cross-sectioned cells to the number of complete disks lying within the known depth of the sample field gives an indirect measure of cell length. For a given field, this value multiplied by the average cross-sectional area of the constituent myocytes can thus be used to derive the index of cell volume. If myocytes had the form of simple cylinders, with an intercalated disk at each end only, the method of derivation of cell length described would give an absolute value, which, when multiplied by the average cross-sectional area of the cells, would provide a precise measure of average cell volume. That is, for example, if the tissue section was 10 μm in depth, and of 120 transected myocytes (cylinders) of mean sectional area 300 μm^2, 12 intercalated disks fell within this depth, the cylinders comprising that tissue would have an average length of 120/12 x 10 = 100 μm, and an average volume of 100 x 300 = 30,000 μm^3. In reality, however, myocytes are not simple cylinders; they possess multiple intercalated disks. The disks, however, all lie in the plane approximately transverse to the long axis of the cell (Fig 6.1). Providing this basic structural arrangement is present in all tissues to be compared, with equivalent numbers of intercalated disks per myocyte, the result of the cell volume determination will provide a relative measure of cell volume suitable for comparative purposes.

This theoretical derivation of a means of determining the relative volumes of myocytes comprising specific volumes of intact ventricular myocardium was tested

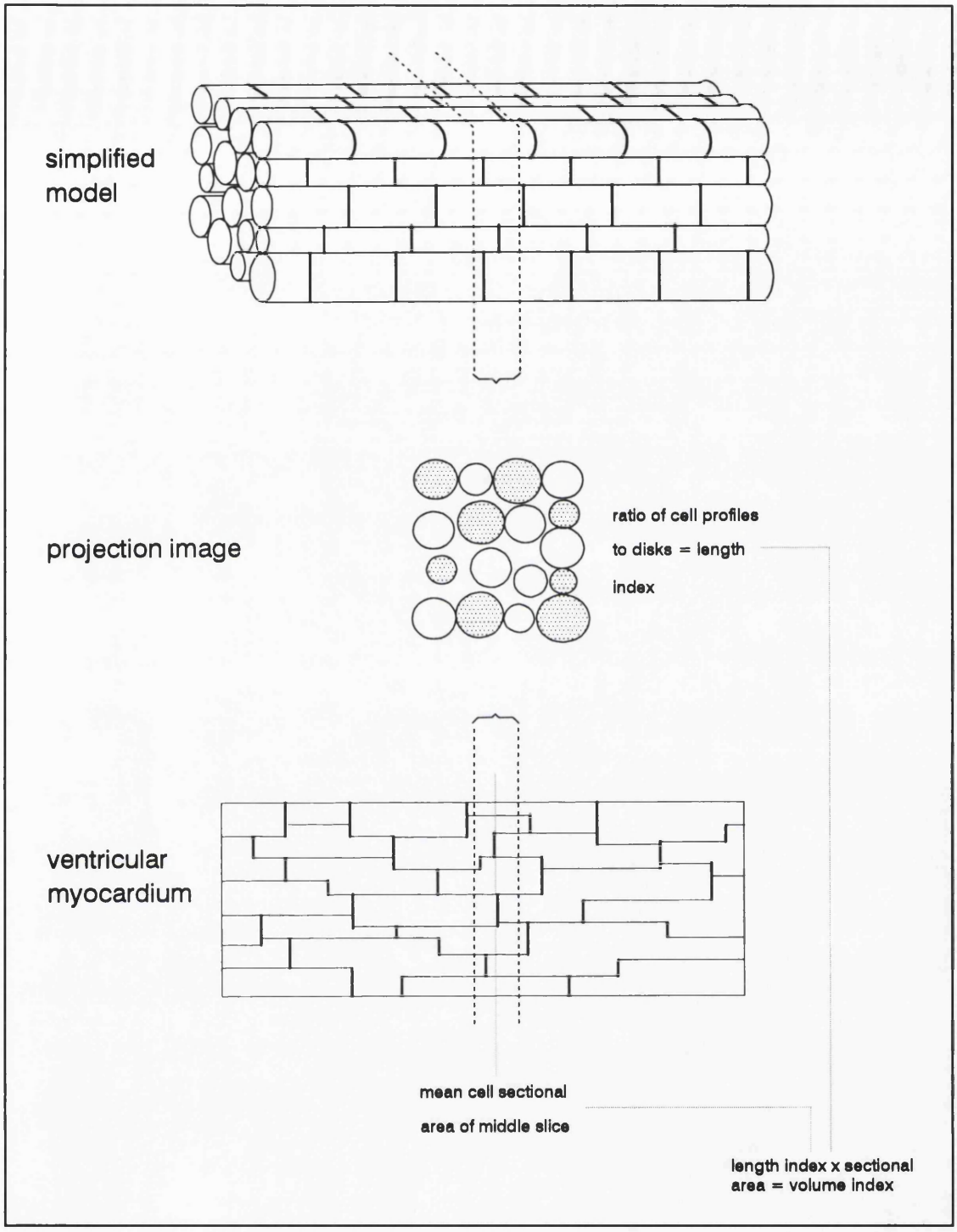

Figure 6.1. Derivation of the cell volume index. The **simplified model** consists of continuous uniform columns of cylinders. When transversely-sectioned, the **projection image** of an optical section series of known depth would have disks in a proportion of the transected columns, from which the average cell length of the composite cylinders can be determined. The projection image of the more complex structure of **ventricular myocardium** cannot be used to derive absolute values, but indices of cell length and, therefore, of volume, can be derived by the same principle.

experimentally by comparing the results of confocal data of whole myocardium analysed in this way, with the cell volumes of myocytes isolated from the same ventricular myocardium. By applying confocal technology to isolated myocytes, cell volume can be determined simply and precisely by planimetry, using optical section series through each myocyte.

6.3 **Materials and methods**

Fresh hearts from 11 male Dunkin-Hartley guinea-pigs were used for this study. A portion of the left ventricular myocardium was divided into a whole-tissue sample which was immediately fixed for connexin43 immunohistochemistry, and the remainder was used for immediate myocyte isolation. Processing and immunolabelling of the tissue and isolated cells was as detailed in Chapter 2.

6.3.1 Cell volume index from whole tissue

For each heart, three randomly-selected fields in which the tissue was transversely sectioned were analysed from the left ventricular whole tissue sample. An optical section series of 10 images at 1 μm intervals using the x60 objective lens and the zoom 1 setting was obtained from each field (sample volume 180x120x10 μm^3). Data were, therefore, acquired using an identical procedure to that described for data acquisition from normal (Chapter 3) and diseased (Chapters 5 and 7) human tissues. As with the studies on humans, preliminary investigation was used to determine the black level and gain settings to be used consistently throughout the experiment, in order that the cross-sectional myocyte profiles were just visible, and the label intensity extended to maximum on the grey scale (See Fig 3.6).

The image data were analysed as follows: the 5th optical slice was used to count the number of transected myocytes, and to determine their mean cross-sectional area by measuring and subtracting from the total field, the non-myocyte areas using a mouse and cursor. A projection image of the entire 10-image series (spanning 10 μm) was then constructed (see Fig 3.6), and the number of complete or near-complete (>75% circumference intact) collections of gap junctions representing intercalated disks was counted. The cell volume index was determined using the following equation:-

Cell volume index = 10 x sectional myocyte area x myocyte number/disk number

6.3.2 Cell volume measurement from isolated myocytes

For each heart, 6 myocytes that had retained a rod-like shape after the isolation and labelling procedure, were randomly selected from the field and analysed to determine the absolute cell volume by planimetry. This was done by serial optical sectioning at 1.5 μm intervals through the entire myocyte, with the aperture control withdrawn 1.5 mm, and the x60 objective and the zoom 1 setting. Preliminary studies were used to determine the black level and gain settings that would distinguish clearly the cell outline of each optical slice. The sectional area of each slice was determined automatically using PC IMAGE software by binarising the image with a threshold of 60 on the 255-point grey scale.

A low threshold binary image of this sort contains many inhomogeneities resulting from there being pixel-to-pixel variation in the intensity of the original grey image. The result is that there are small deficiencies (holes) in the binary image of the sectioned cell, and spurious pixels in the on-state in the surrounding background. To eliminate both of these inaccuracies, the binary image was automatically adjusted by a series of steps in which all edges of each binary object in the field had a layer of single pixels either added ("closing" - which will tend to fill deficiencies), or removed ("opening" - which will remove spurious small clusters of pixels). Preliminary studies showed that optimal processing of the raw binary image was achieved by "closing" twice, followed by "opening" three times. This produced a clean image without inhomogeneities of either the cell section (on-pixels) or the background (off-pixels), with a cell section outline that was indistinguishable from that in the native grey image when toggling between the two on the computer monitor. A macro-programme was written and used to create the binary image, process it to remove inhomogeneities by the procedure detailed above, and then measure the total on-pixel area automatically. Before each automatic result of myocyte cross-sectional area was accepted, the final binary image was always compared with the native grey image to ensure consistency.

For each myocyte examined, the sum of the cell sectional areas (in μm^2) so determined, multiplied by the interval between optical slices (1.5 μm), produces an accurate, absolute value (in μm^3) of myocyte volume.

For each of the 11 hearts, the whole-tissue mean cell volume index, derived from three random fields, was plotted against the mean myocyte volume determined from isolated cells. The correlation coefficient and slope of this plot was used to test the reliability of the technique for deriving the volume index from whole ventricular myocardium.

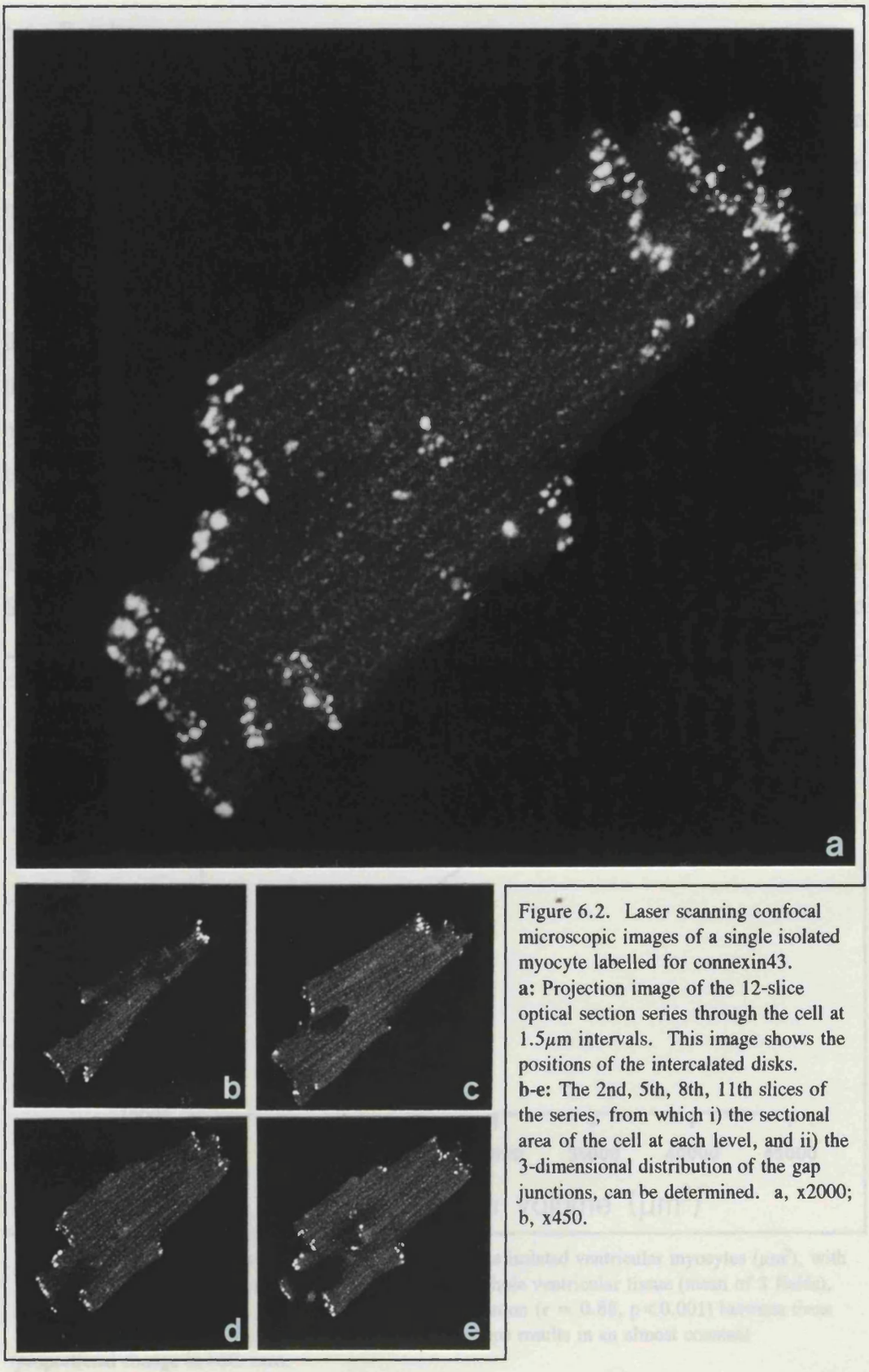

Figure 6.2. Laser scanning confocal microscopic images of a single isolated myocyte labelled for connexin43.
a: Projection image of the 12-slice optical section series through the cell at 1.5μm intervals. This image shows the positions of the intercalated disks.
b-e: The 2nd, 5th, 8th, 11th slices of the series, from which i) the sectional area of the cell at each level, and ii) the 3-dimensional distribution of the gap junctions, can be determined. a, x2000; b, x450.

6.4 Results

The hearts used in this study were 11 of the 12 hearts used for the investigation in Chapter 10. For the present technical study, however, confined simply to comparing two methods of measurement, details of the animals are omitted, but can be found in section 10.3 (animal nos. 22 to 33, not including no. 29).

An example of image data from optical section series of the sort used for deriving the whole-tissue cell volume index is shown in Chapter 3 (Fig 3.6), and an example of the image data of a labelled isolated ventricular myocyte is shown in Figure 6.2. The mean volume measurements derived by the two methods (whole-tissue volume index and isolated-cell volumes) for each animal, are summarised in Table 6.1. The corresponding primary data from which these means were derived are given in Appendix Table A3. The mean volume estimations by the two methods are plotted against eachother in Figure 6.3. The correlation coefficient of this plot is 0.88 ($p<0.001$), with a slope resulting in

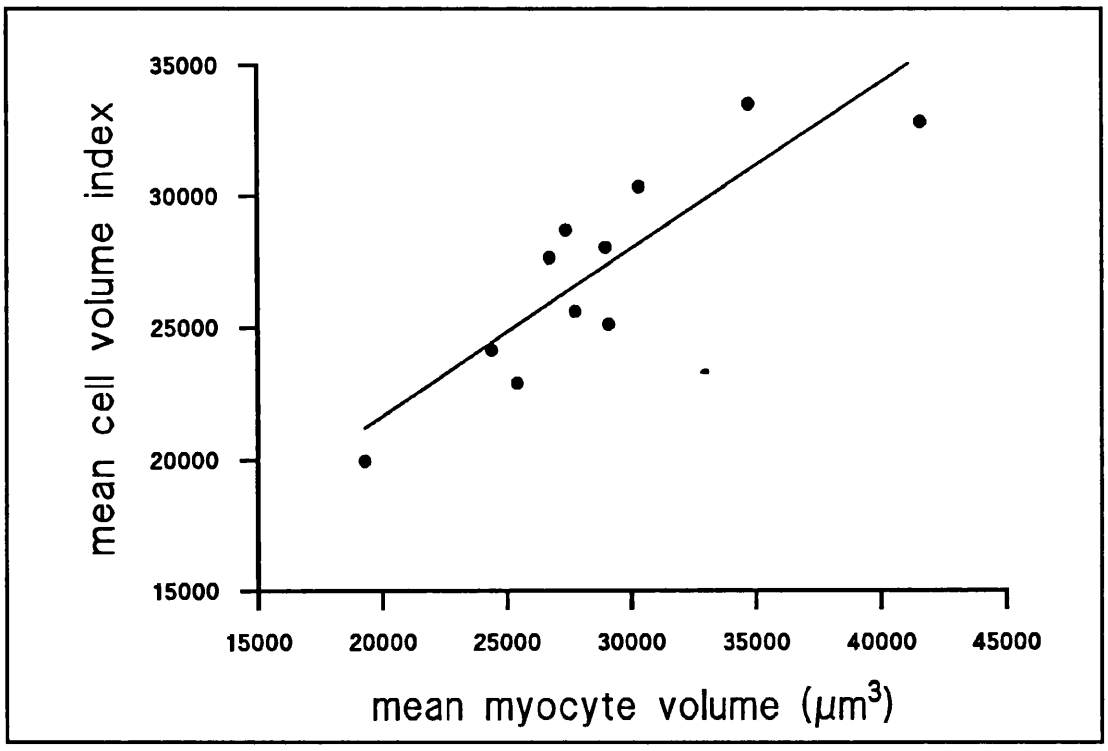

Figure 6.3. Graph comparing mean cell volumes of single isolated ventricular myocytes (μm^3), with the cell volume index (arbitrary units) derived from the whole ventricular tissue (mean of 3 fields), for each guinea pig ($n=11$). There is a significant correlation ($r = 0.88$, $p<0.001$) between these two methods of mean cell volume determination. The slope results in an almost constant proportional change in both axes.

an almost constant proportional change in both axes.

Table 6.1 Mean myocyte volume measurements from 6 isolated cells and 3 whole-tissue fields from each guinea pig (n=11).

animal	mean isolated cell vol. (μm^3)	mean tissue index of cell vol.
22	27766.48	25601.1
23	19279.58	19966.6
24	26742.65	27642.57
25	25425.15	22919.73
26	34717.22	33474.57
27	28981.61	28029.2
28	41589.48	32784.03
30	30321.42	30323.7
31	24391.56	24155.6
32	27395.65	28689.2
33	29104.92	25114.57

6.5 Interpretation and Conclusions

The results demonstrate that the method for deriving an index of cell volume from whole ventricular myocardium produces a valid indicator of cell volume. By applying this method of estimating average constituent cell volume to the quantity of gap junction determined from the same tissue field, a valid estimate of gap junction content per myocyte can be derived. The successful development of this approach made it possible to proceed with meaningful comparisons of gap junction content in health and disease, as reported in the next chapter.

CHAPTER 7 - CONNEXIN43 GAP JUNCTION QUANTIFICATION IN WELL-PRESERVED VENTRICULAR MYOCARDIUM FROM ISCHAEMIC AND HYPERTROPHIED HUMAN HEARTS

7.1 Introduction

In Chapter 5, a marked disturbance of gap-junctional distribution was demonstrated in a rim of surviving myocardium at the interface with the scar of healed infarction, the usual site of origin of the most commonly encountered clinical ventricular tachycardia. However, important though this phenomenon may be, clinical evidence suggests that abnormal intercellular coupling may be a more widespread phenomenon in heart disease, and may extend beyond this narrow rim of tissue, contributing further to disturbances of electromechanical function in the ischaemic heart. Partial or frequently recurrent ischaemia of a region of ventricular myocardium without infarction can result in localised loss of coordination of contraction manifest as hypokinesia, dyskinesia or even akinesia (so-called hibernating myocardium) despite normal or only mildly disturbed action potential and metabolic characteristics (Wit and Janse, 1992) that do not adequately explain the loss of coordinated function. Ventricular arrhythmias in the setting of chronic recurrent ischaemia may be abolished if intervention to reperfuse the ischaemic region of myocardium is successful (Wit and Janse, 1992). Further, in experimental reentrant ventricular tachycardia in infarcted dogs, stable functional reentrant circuits can extend outside the immediate region of infarction, indicating that slowed anistropic conduction may exist beyond the immediate interface with the infarct (Dillon et al. 1988). There are many factors contributing to these ischaemic phenomena, but a potential role for cellular uncoupling in myocardium that is exposed to a chronic or recurrent ischaemic insult was an unexplored possibility that stimulated the investigation reported in this chapter.

A number of lines of evidence point to the possibility that cellular coupling may be reduced in ischaemia. In the acute phase of experimental ischaemia and hypoxia, cellular uncoupling occurs (Kléber et al. 1987), and with ischaemia persisting to the point of irreversible damage and destruction of the cells, there may be a consequent reduction in gap-junctional surface area (Hoyt et al. 1990). But this stage is, by definition, not reached in the patient with recurrent or persistent ischaemia without infarction. Nevertheless, in this setting, and also in the case of the chronically hypertrophied

ventricle, there are abnormalities of ventricular wall motion and coordination of contraction that remain poorly understood, and which may relate to the lowered arrhythmic thresholds of these hearts by the common factor of slowed conduction. Do alterations of myocardial gap-junctional coupling exist in myocardial diseases known to be associated with chronic ventricular electromechanical dysfunction and arrhythmic tendency, but without associated evidence of irreversible cellular damage and scarring? As reported earlier (Chapter 5), the myocardium distant from infarcted areas showed a normal pattern of gap junction distribution, and this remained the case even where the myocytes showed features to suggest significant hypertrophy. But, might there be quantitative changes in gap-junctional coupling in this myocardium? In an attempt to answer this important question, myocardium lacking evidence of irreversible cell damage from chronically ischaemic and chronically hypertrophied hearts was investigated for quantitative alterations of connexin43 gap-junctional content, using the methods developed in the previous chapter. The results provide new insights into a possible anatomical factor in the pathogenesis of electromechanical dysfunction and arrhythmias.

7.2 Methods

7.2.1 Myocardial samples

Ventricular specimens were obtained from patients fulfilling the study criteria (defined below), selected at random from those undergoing cardiac surgery who had given prior written consent, and from transplant donor hearts. The biopsies were taken from the left ventricular apex by either excision of a 3mm ellipse of epimyocardium, or using a transmural needle bioptome (diameter 1.5mm) from which the epimyocardial end was used for study. All biopsies obtained at routine surgery were taken immediately after arresting the heart on cardiopulmonary bypass.

7.2.1a *Myocardium from Ischaemic Ventricle*

Left ventricular myocardium was obtained from 5 patients with 3-vessel coronary artery disease undergoing coronary artery bypass grafting for symptomatic relief from angina. Myocardium from these patients was included in the study of the infarct border zone region (Chapter 5), and their details are given in Table 5.1 (patients 11 to 15). To summarise, all patients had had documented anterior myocardial infarction (with or without Q waves on ECG) at least 3 months previously. In addition to these details, they

were all normotensive, and had had preoperative thallium-201 perfusion scintigraphy which had demonstrated symptomatic exercise-induced reversible ischaemia in the remainder of the anteroapical territory, from which the biopsies of viable epimyocardium used in this study were obtained. Myocardium immediately abutting scar from past infarction, was not included for analysis in the present study. For the same reason subendocardial myocardium, which may contain widespread small scars in patients with chronic coronary disease (Cotran et al. 1989), which would tend to disrupt gap-junctional distribution and distort tissue architecture, was also avoided. This strategy enabled sampling of viable myocardium associated with a region of recurrent reversible ischaemia, but distant from detectable histological abnormalities, to establish whether alterations of gap junction organisation, in the absence of more gross histological disruption, affect these regions. A detectable reversible thallium perfusion defect with associated angina pectoris is suggestive of ischaemia affecting the full myocardial thickness (Wackers et al. 1976; Mueller et al. 1976; Heller et al. 1991; Sutton and Topol, 1991; Nishimura et al. 1991), but direct demonstration that the epimyocardial samples taken had themselves been subjected to ischaemia was not feasible.

7.2.1b *Hypertrophied left ventricle*

Left ventricular apical biopsies were taken during replacement of stenosed aortic valves in 5 patients with electrocardiographic and echocardiographic evidence of left ventricular hypertrophy.

7.2.2 Tissue processing

Specimens were immediately divided for thin section electron microscopy, connexin43 immunohistochemistry, and when there was adequate tissue, freeze-fracture. The specimens were processed as detailed in Chapter 2.

7.2.2a *Connexin43 gap junction quantification*

For quantitative assessment of myocardial gap junctions, all aspects of tissue processing, labelling and image acquisition and analysis were strictly standardised to produce as near identical conditions to those used for processing and labelling the normal myocardial specimens in Chapter 3. In reality, immunolabelling and image acquisition of the normal, ischaemic and hypertrophied ventricular tissue were performed in parallel. In each labelling run one of each of these tissues, plus a control specimen, was included to

minimise any biases caused by variability between runs.

For each specimen from the ischaemic hearts, the same variables as those investigated in normal myocardium in Chapter 3 were measured; immunolabelled gap junction long-axis length distribution, intercalated disk count per myocyte, connexon packing density (freeze-fracture) and total gap junction surface area ($\mu m^2/\mu m^3$). Gap junction surface area per unit volume of myocyte was also measured for each of the hypertrophied specimens. By deriving the cell volume index of each of the fields from which gap junction surface area was quantified in ischaemic, hypertrophied, as well as the normal (Chapter 3) myocardium, the gap junction content of these tissues can be expressed per cell, and therefore in a form that makes comparisons between the tissues more meaningful.

All the data from normal myocardium in Chapter 3 were compared with corresponding data for the diseased myocardium in this series of specimens.

7.2.2b *Statistical analysis*

Group data are compared by two sample t-tests of mean values for each heart.

7.3 **Results**

Details of the 5 ischaemic hearts are summarised in Table 5.1 (patients 11 to 15) in Chapter 5, and the 5 hypertrophic hearts in Table 7.1. The 5 patients with ischaemic heart disease were 49.6 $\pm$ 3.7 years of age. The patients with aortic stenosis were 59.6 $\pm$ 4.6 years.

Table 7.1 Details of hypertrophied LV myocardial specimens obtained from patients with aortic stenosis.

Patient/ heart no.	age (yrs)	aortic valve gradient(mmHg)	evidence of LV hypertrophy	biopsy technique
H1	60	77	ECG and echo	scalpel
H2	56	50	ECG and echo	scalpel
H3	54	110	ECG and echo	scalpel
H4	63	80	ECG and echo	scalpel
H5	65	60	ECG and echo	scalpel

7.3.1 Histology and General Ultrastructure

The myocardium in the regions selected for study in both the ischaemic and hypertrophic groups had an orderly arrangement of fibres, with no tissue distortion and no apparent fibrosis. Varying degrees of hypertrophy were present in the ischaemic hearts (illustrated in Fig 5.5), but thin section electron microscopic appearances were otherwise normal. The myocardium from patients with aortic stenosis had the classical features of hypertrophy, with myocyte enlargement and hyperchromatic rectangular nuclei, the extent of which varied from cell to cell.

7.3.2 Distribution of Immunolabelled Connexin43-Gap Junctions at Confocal Microscopy

Immunolocalisation of connexin43 gave consistent normal patterns of gap junction labelling in myocardium from hearts with aortic stenosis and ischaemic disease: bright fluorescent domains marking the positions of intercalated disks between myocytes, appearing as transverse lines of individually-resolved spots in longitudinally-sectioned myofibres, and discoid arrays delineated peripherally by large gap junctions, in transversely-sectioned myocardium (Figs 3.3 & 3.4).

Controls in which antiserum treatment was omitted or substituted with pre-immune serum showed no fluorescent labelling, but autofluorescent lipofuscin collections were present to a greater extent in diseased than in normal myocardium.

7.3.3 Quantitative Characterisation of Gap Junctions

7.3.3a *Analysis of Connexon Density in Freeze-fractured Gap Junctions*

Analysis of data from 50 freeze-fractured gap junctions pooled from the ischaemic hearts (Fig 7.1) shows that there is no correlation ($r=-0.22$, $p=0.13$) between gap junction size and the density of its component connexons ($101.1 \pm 16.8 \times 10^{-4} nm^{-2}$, $n=50$). Figure 7.2 shows the plot of these variables for gap junction plaques from the ischaemic hearts of less than 1 μm^2 surface area. There was no difference in density distribution between myocardium from the normal (Chapter 3, Fig 3.8) and ischaemic hearts.

7.3.3b *Intercalated Disk Counts*

Intercalated disk number per myocyte in ischaemic hearts (11.87 ± 2.49, $n=100$) did not differ significantly from that in normal hearts (11.55 ± 2.20; $p=0.33$).

Figure 7.1. Electron micrograph of a freeze-fracture replica showing an entire gap-junctional domain of normal appearance in a small portion of membrane fracture at the tip of a cross-fractured plicate fold of an intercalated disk from an ischaemic heart. x78,000.

7.3.3c *Size of Immunolabelled Gap Junctions*

The distribution of the long axis measurements of labelled junctions (Fig 7.3) pooled from ventricular myocardium associated with recurrent ischaemia (mean 0.54 $\pm$ 0.42 μm) showed no significant difference from those of normal ventricles when analysis of variance of the $\log_{10}$-transformed data was performed ($p=0.32$).

7.3.3d *Gap-junctional Surface Area per Unit Volume of Tissue*

Left ventricular myocardium from recurrently ischaemic hearts had a significantly reduced gap junction surface area of 0.0027 $\pm$ 0.0009 $\mu m^2/\mu m^3$ (Table 7.2) compared with the normal value (0.0051 $\pm$ 0.0015 $\mu m^2/\mu m^3$: $p=0.024$) presented in Chapter 3.

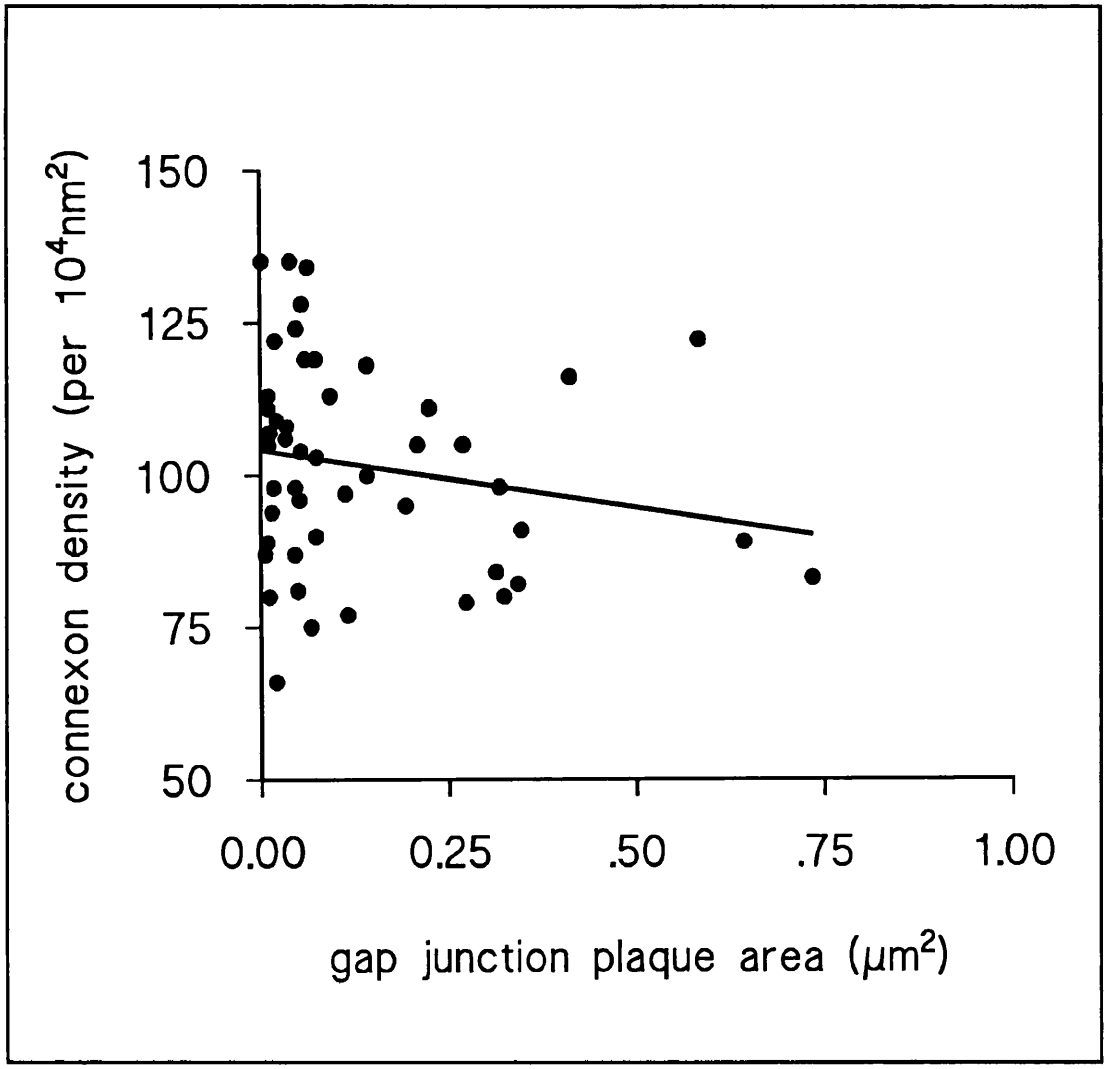

Figure 7.2. Plot of connexon surface density vs. gap junction plaque area in plaques up to 1μm^2 in ventricular myocardium from ischaemic hearts.
There is no correlation (p=0.18) and the slope is not significant. The distribution is no different from that of normal myocardium

Table 7.2 Mean gap-junctional area per unit myocyte volume in ischaemic left ventricles (n=5). Value for each heart is mean ± SD (n = 5 test fields).

patient	gj area/vol (μm^2/μm^3)
I11	0.00230±0.00098
I12	0.00199±0.00038
I13	0.00192±0.00046
I14	0.00351±0.00162
I15	0.00388±0.00099
Mean ± SD	0.00272±0.00091

For primary data see Appendix, Table A4.

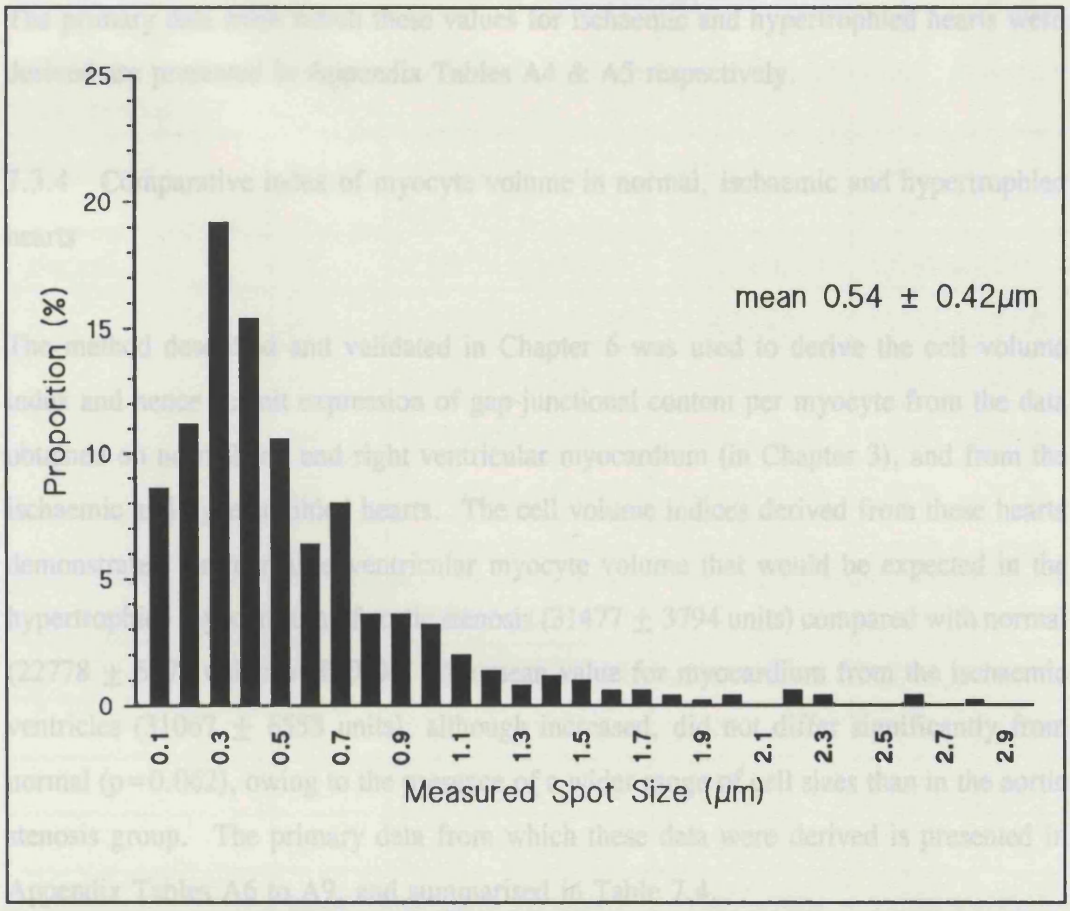

Figure 7.3. Frequency distribution of immunolabelled junction long-axis lengths pooled from ischaemic ventricular myocardium distant from infarction. Measurements of 700 junctions were made manually using the SOM software "length" command. Mean junction length 0.54 μm. (Compare with the distribution in normal ventricle in Chapter 3, Fig 3.9).

Hypertrophied left ventricle from patients with aortic stenosis (Table 7.3) also had a reduced gap junction surface area (0.0031 $\pm$ 0.0005 $\mu m^2/\mu m^3$) when compared with normal ($p = 0.048$), and did not differ significantly from ischaemic ventricle.

Table 7.3 Mean gap-junctional area per unit myocyte volume in hypertrophied left ventricles (n=5). Value for each heart is mean $\pm$ SD (n = 5 test fields).

patient/heart	gj area/vol. ($\mu m^2/\mu m^3$)
H1	0.00352±0.00029
H2	0.00265±0.00033
H3	0.00333±0.00021
H4	0.00253±0.00080
H5	0.00359±0.00118
Mean ± SD	0.00313±0.00050

For primary data see Appendix, Table A5.

The primary data from which these values for ischaemic and hypertrophied hearts were derived are presented in Appendix Tables A4 & A5 respectively.

7.3.4 Comparative index of myocyte volume in normal, ischaemic and hypertrophied hearts

The method described and validated in Chapter 6 was used to derive the cell volume index and hence permit expression of gap-junctional content per myocyte from the data obtained on normal left and right ventricular myocardium (in Chapter 3), and from the ischaemic and hypertrophied hearts. The cell volume indices derived from these hearts demonstrated the increased ventricular myocyte volume that would be expected in the hypertrophied myocardium of aortic stenosis (31477 $\pm$ 3794 units) compared with normal (22778 $\pm$ 5174 units: $p=0.019$). The mean value for myocardium from the ischaemic ventricles (31067 $\pm$ 6553 units), although increased, did not differ significantly from normal ($p=0.062$), owing to the presence of a wider range of cell sizes than in the aortic stenosis group. The primary data from which these data were derived is presented in Appendix Tables A6 to A9, and summarised in Table 7.4.

7.3.5 Comparative index of gap-junctional surface area per myocyte

As the cell volume indices were derived from the same tissue fields as the gap-junctional surface density values, these data may enable approximation of gap junction area per myocyte for each myocardial sample, from the product of the surface density and the volume index (Appendix Tables A6 to A9). This value is reduced in myocardium from the ischaemic hearts (10325 $\pm$ 1585 units: $p=0.019$) compared with normal (14726 $\pm$ 2046 units). Hypertrophied myocardium, by comparison, has a value of 12652 $\pm$ 1527 units ($p=0.11$).

Table 7.4 presents a complete summary of the quantitative morphometric analyses of normal, ischaemic and hypertrophied ventricular myocardium.

Table 7.4 Results of quantitative confocal morphometric analysis of normal, ischaemic and hypertrophied myocardium.

Heart type	patient	gj area/vol ($\mu m^2/\mu m^3$)	cell vol. index	index of gj area/cell
Normal LV	N1	0.00476±0.00076	29436±5377	18232.0±1958.3
	N2	0.00751±0.00158	15347±859	15153.2±2192.6
	N3	0.00419±0.00072	23516±5534	12915.9±2576.3
	N4	0.00360±0.00117	24668±6998	12456.3±6200.0
	N5	0.00540±0.00113	20925±1170	14870.3±2129.0
	Mean	0.00508±0.00151	22778±5174	14725.6±2045.7
Normal RV	N2	0.00349±0.00034	22582±3136	10413.0±1164.0
	N4	0.00501±0.00106	22799±3512	14773.5±1379.4
	N6	0.00464±0.00123	26901±8047	15579.4±1861.4
	N7	0.00402±0.00038	22577±3146	11965.2±1341.0
	N8	0.00473±0.00050	22639±3424	14114.2±1581.4
	Mean	0.00438±0.00061	23499±1904	13369.1±1903.8
Ischaemic LV	I11	0.00230±0.00098	39067±9993	11077.0±2218.8
	I12	0.00199±0.00038	36756±9360	9394.8±1404.3
	I13	0.00193±0.00046	29346±6100	7752.3±3226.8
	I14	0.00351±0.00162	25723±6528	11097.4±2618.8
	I15	0.00388±0.00099	24443±3072	12302.8±1903.9
	Mean	0.00272±0.00091*	31067±6553	10324.9±1584.8*
Hypertroph. LV	H1	0.00352±0.00029	29070±3853	13635.0±2243.4
	H2	0.00265±0.00033	32804±4312	11423.4±942.2
	H3	0.00333±0.00021	34204±4156	15179.9±2371.8
	H4	0.00253±0.00080	35104±9979	11194.3±3052.7
	H5	0.00359±0.00118	26052±6612	11831.0±2705.2
	Mean	0.00313±0.00050*	31447±3794*	12652.8±1527.4

* = $p < 0.05$ compared with the value for normal left ventricle

7.4 Discussion

Both ischaemic heart disease and left ventricular hypertrophy are associated with reduced efficiency of ventricular mechanics, ventricular arrhythmias and sudden cardiac death (Kannel, 1983; Fujimoto et al. 1983). The development of treatment strategies for cardiac arrhythmias requires a detailed and complete knowledge of the mechanisms by which these arrhythmias are generated, and the findings of the present study add new insights into a possible anatomical basis for electromechanical dysfunction and arrhythmogenesis.

One of the many adverse effects of cardiac ischaemia is a decrease in conduction velocity (Jongsma and Gros, 1991; Fozzard and Arnsdorf, 1992), a factor increasing the likelihood of arrhythmias. Although gap junctions are established as the organelle determining intercellular and whole tissue conductance and conduction velocity (Jongsma and Gros, 1991; Page, 1992; Fozzard and Arnsdorf, 1992), and an absence of gap junctions results in electrical isolation (Spray and Burt, 1990), the relationship between the relative abundance of gap junctions, intercellular conductance and conduction velocity is poorly understood. Evidence suggests that regions of the heart with slow conduction and relatively low intercellular conductance (such as the atrioventricular node) contain fewer gap junctions than regions of more rapid conduction (Jongsma and Gros, 1991). The possibility exists, therefore, that a reduction in gap junction surface area per unit volume of about 40% in ventricular myocytes from ischaemic and hypertrophied ventricles, as demonstrated in the present study, may significantly alter patterns and rates of impulse propagation.

The group of ischaemic patients in this study tended to be older (49.6 $\pm$ 3.7 yrs) than the group of patients investigated in Chapter 3, from whom data on "normal" ventricular myocardium was obtained (43.4 $\pm$ 12.6 yrs). This difference is difficult to overcome given the reasons for which these groups undergo surgery, but is not statistically significant ($p=0.35$), and there were no trends to suggest age-related changes in any parameters within any of the study groups examined.

The greater myocyte volume that characterises hypertrophied myocardium associated with chronic aortic stenosis was evident in the present study. Compensatory hypertrophy that might be expected in the myocytes of the myocardium around a healed infarct (Anversa et al. 1985; Cotran et al. 1989) was not statistically apparent, however, owing to the large standard deviation.

The normal intercalated disk counts in myocardium from the ischaemic hearts in the present study, despite changes in cell size distribution, suggest that the basic architecture of intercellular abutments was not significantly altered. Although Luke and Saffitz (1991) showed a reduced number (6.5) of such intercellular contacts in canine myocardium associated with infarction, these authors had specifically selected regions with marked fibrotic scarring. That the distribution of labelled junction lengths also showed no difference from the data on normal hearts presented in Chapter 3 suggests that the reduction in gap-junctional content occurs as a result of reduction in the numbers of all sizes of junction per intercalated disk. Electron microscopic examination of the canine infarct border region reported by Luke and Saffitz (1991) suggested a preferential reduction of the larger junctions, but the context of fibrotic scarring may, again, have accounted for this difference.

7.4.1 The substrate for abnormal impulse propagation

It has long been suggested that fibrosis plays a part in the anatomy explaining both impaired ventricular mechanics and arrhythmogenesis (Mehra et al. 1983), but the results of the present study suggest a mechanism by which intercellular coupling, and therefore electromechanical function, may be impaired in the diseased heart without invoking fibrosis as the explanation.

As previously described, the underlying mechanism of many clinical cardiac arrhythmias is a myocardial reentrant electrical circuit (Mines, 1914), perpetuation of which requires areas of slowed conduction within the circuit, so that the advancing wave front encounters excitable tissue (Mines, 1914; Cranfield and Dodge, 1992), and initiation of which is enhanced by a local dispersion of recovery of excitability of the constituent myocytes (Allesi et al. 1958; Han, 1971; Kuo et al. 1983). These factors are thought to provide the substrate for clinical reentrant arrhythmias (Fozzard and Arnsdorf, 1992). Increased passive resistivity encountered by a propagating impulse can reduce conduction velocity and increase heterogeneity of conduction, irrespective of changes in active membrane properties (Fozzard, 1977; Arnsdorf, 1984; Binah and Rosen, 1992; Saffitz et al. 1992). Experimentally reducing gap-junctional conductance using the uncoupling agent, heptanol, not only produces the expected slowing of ventricular myocardial conduction, but also alters the degree of anisotropy and can induce conduction block in the direction transverse to the fibre axis while longitudinal conduction continues (Callans et al. 1992). Alterations of the degree of gap-junctional coupling in myocardium may, therefore,

influence three major pathophysiological factors in arrhythmogenesis; conduction velocity, the dispersion of action potential duration and the degree of anisotropy. Although a reduction in gap junction surface area of about 40% as demonstrated in ischaemic and hypertrophied ventricular myocardium in the present study may not, per se, induce and sustain ventricular arrhythmias, a reduction of this order may impair coordination of contraction and may lower the arrhythmic threshold.

7.4.2 Functional significance: correlating morphology with electrophysiology

Although electrophysiological studies of arrhythmogenic cardiac disease have documented significant abnormalities of active membrane properties (Cranfield and Dodge, 1992), many have failed to do so (Boyden et al. 1982; Spach and Dolber, 1986). Indeed there are reports of normal membrane potential characteristics in myocytes from myocardium with markedly abnormal electrophysiologic properties and manifest arrhythmias (Boyden et al. 1982; Spach and Dolber, 1986; Kieval et al. 1992). Boyden et al (1982) concluded that altered "morphologic features" of the myocardium were responsible for the electrophysiological disturbances in chronically hypertrophied canine atria. Kieval et al (1992) demonstrated normal action potential characteristics, but abnormal gap-junctional intercellular conductance, in postischaemic myocyte pairs. Lower junctional conductance in cultured myocytes infected with *Trypanosoma cruzi*, the cause of Chagas cardiomyopathy, is associated with a qualitative reduction in connexin43 expression (Campos De Carvalho et al. 1992). A reduction in gap-junctional coupling between myocytes may, therefore, be an important morphologic feature that could interact with altered active membrane properties in diseased myocardium of a variety of aetiologies. It is likely that arrhythmogenic states result from a combination of changes of both membrane properties and coupling characteristics of the myocardium, and it has been suggested that abnormal cellular coupling may be the predominant electrophysiological derangement at the border of a healed myocardial infarct (Lesh et al. 1989).

It has not been possible to study the interaction between the action potential and myocardial resistivity during programmed stimulation (Tsuboi et al. 1985; Spach et al. 1988; Delmar et al. 1989; Lesh et al. 1989). A number of computer models simulating this interaction have been developed; Joyner (1986) showed that as coupling resistance increases, the "intrinsic" cellular differences of action potential duration become increasingly manifest, and Lesh et al (1989) showed a coincident increase in axial resistivity, leading to slowed conduction. A combined summary of these findings is

represented in Figure 7.4. The combination of dispersion of action potential duration and

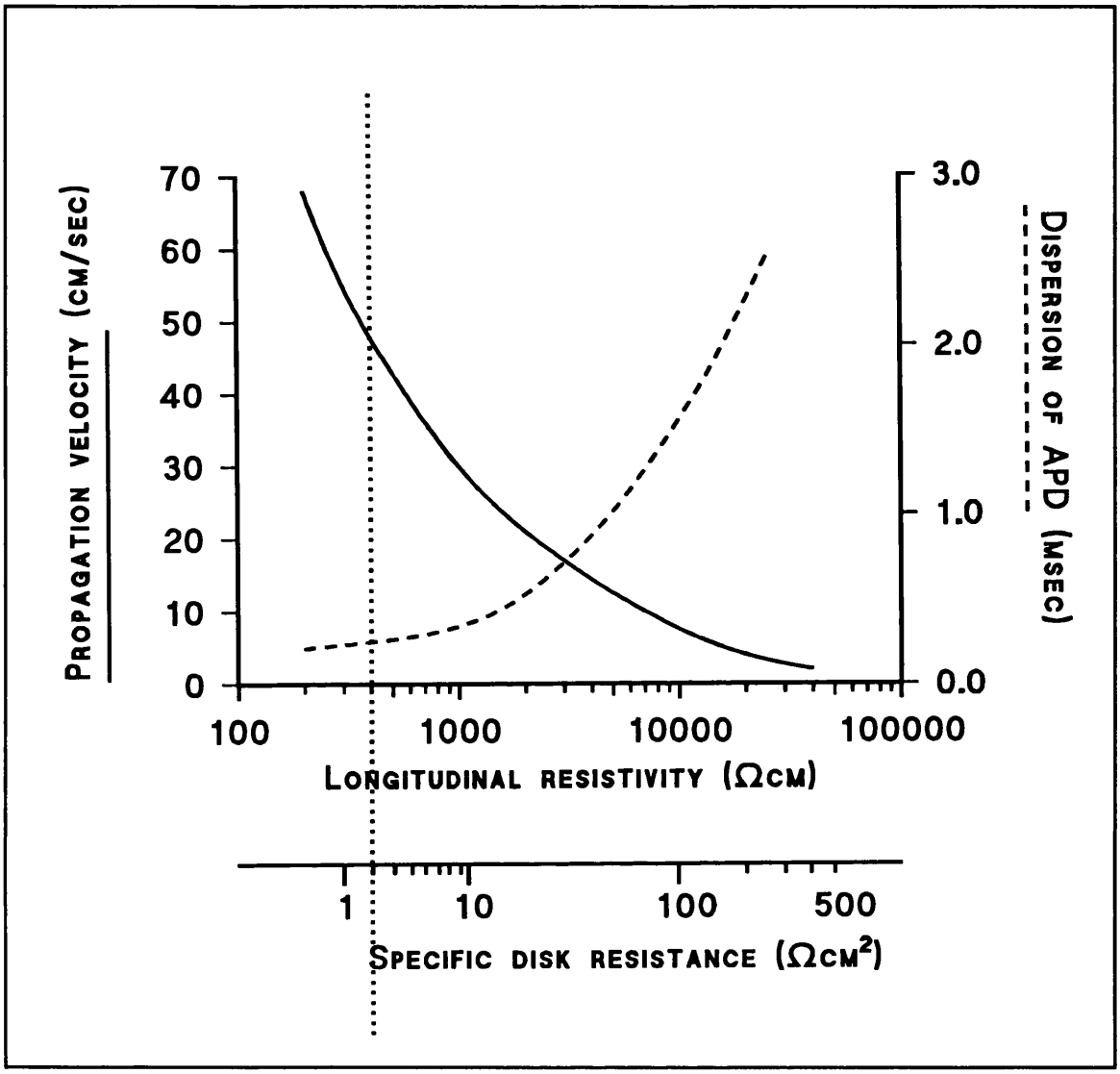

Figure 7.4. Representation of data produced by groups studying computer models of myocardial electrophysiology (Joyner, 1986; Lesh et al. 1989). An increase in specific disk resistance and the subsequent increase in longitudinal myocardial resistivity (typical values for which are shown by the dotted line), result in a reduction in propagation velocity and an increase in dispersion of action potential duration. These changes will promote arrhythmogenesis.

slow conduction promotes reentrant tachycardia initiation and perpetuation (Fozzard and Arnsdorf, 1992), and the model of Quan and Rudy (1990) suggests that cellular uncoupling is arrhythmogenic by just these mechanisms.

Importantly, the change in conduction velocity will also alter the synchrony of force development of the individual cells of the myocardial syncytium, contributing to the reduced mechanical efficiency of these hearts, and with increased coupling resistance the normal anisotropic propagation pattern in the ventricle will fragment (Jalife et al. 1989), as predicted by the computer models (Joyner, 1986; Lesh et al. 1989). The process of uncoupling adds further to this heterogeneity by actually inducing changes in action

potential characteristics (Hoffman and Rosen, 1982; Lesh et al. 1989) and recovery of excitability (Lesh et al. 1989).

7.4.3 Implications of results

The findings of the present investigation, when set in the context of these studies, may be of importance for a number of reasons. That the gap junction content per myocyte in hypertrophied ventricular myocardium (from patients with aortic stenosis) was not significantly reduced, suggests that the reduction in gap junction content per cell in ischaemic myocardium may be a feature of the ischaemia, and not simply the hypertrophy in the ischaemic heart. The freeze-fracture study demonstrated that label quantity is proportional to the number of connexons present, and therefore the number of gap-junctional channels available. Each junctional channel has a unitary conductance and contributes to lowering the intercellular component of resistance to electrical propagation. A reduction in gap junction coupling may, therefore, change conduction velocity and "unmask" intrinsic differences in action potential characteristics, manifest at the clinical level by non-specific changes in the QRS complex on the ECG, changes in the coordination of contraction and the mechanical efficiency of the heart, and a possible lowering of arrhythmic threshold. These clinical phenomena are well recognised, but not fully understood, in the ischaemic and hypertrophied hearts. There is, however, growing evidence of the role of abnormal intercellular coupling as a major factor in myocardial electromechanical dysfunction (Spach et al. 1982b; Hoffman and Rosen, 1982; Dillon et al. 1988; Lesh et al. 1989; Jalife et al. 1989; Kieval et al. 1992; Wit and Janse, 1992; Fozzard and Arnsdorf, 1992). The results of the present study suggest that changes in resistivity, as evidenced by altered gap junction quantity in the diseased human ventricle, may indeed occur.

These results have implications for the understanding of arrhythmias and their treatment. The classification of antiarrhythmic agents depends on their action with respect to the active membrane ionic properties, but very little is known about their action on cellular coupling and anisotropy. Kadish et al (1986) have shown that procainamide, for example, in addition to its effects on the fast sodium current, reduces the degree of anisotropy in canine ventricular myocardium. This action may be mediated by changes in cellular coupling which, in the context of the arrhythmogenic, ischaemic myocardium, with its reduced gap-junctional content, may cause a normalising increase in intercellular coupling and a re-masking of the intrinsic differences in action potential.

Further, pharmacological uncoupling agents have differential effects on longitudinal and transverse conduction (Delmar et al. 1987; Callans et al. 1992) thereby altering the pattern of propagation. One such agent, heptanol, has been shown to render regions of infarct-related myocardium, with severely disturbed intercellular coupling, electrically inactive (Delmar et al. 1987; Balke et al. 1988), thereby isolating a potentially arrhythmogenic region.

The resistivity of myocardium, a potentially important factor in clinical arrhythmias, has been ignored in many electrophysiological studies that have been confined to relating active membrane properties to the behaviour of the tissue and the heart as a whole. In the present study the demonstrated abnormalities of gap junction content would be consistent with the clinically apparent disturbances of electromechanical function in ischaemic and hypertrophied hearts, the explanation of which has not previously been fully elucidated. At a time when a number of clinical trials are questioning the conventional wisdom of pharmacological arrhythmia treatment (Akiyama et al. 1991), a broader approach to understanding and treating cardiac electromechanical dysfunction in general may require greater attention to gap junction intercellular coupling.

CHAPTER 8 - GAP JUNCTION ORGANISATION AND CELLULAR ULTRASTRUCTURE OF THE ACCESSORY ATRIOVENTRICULAR PATHWAY IN THE WOLFF-PARKINSON-WHITE SYNDROME.

8.1 Introduction

The variation in electrophysiological properties of the accessory atrioventricular pathways in the Wolff-Parkinson-White syndrome, both in the natural history of individual cases and between different cases, is poorly understood. The precise anatomy of the accessory atrioventricular pathway in the Wolff-Parkinson-White syndrome has long been sought, giving rise to considerable speculation and controversy. Kent (1893; 1913) made the erroneous claim that there were multiple muscular atrioventricular connections in the normal heart (Anderson and Becker, 1981). Subsequently, it was often stated that the accessory pathway passed through holes in the atrioventricular connective tissue (Verduyn Lunel, 1972) and that, with maturation of the connective tissue, the muscular connections were later "pinched off" and interrupted. It is now known that the accessory atrioventricular pathway in the Wolff-Parkinson-White syndrome is a congenital anomaly, and although variations may occur in its behaviour and clinical expression throughout life, this is thought to be due predominantly to physiological changes, the anatomical substrate being a persistent, but not necessarily invariable, feature (Anderson and Ho, 1991). The precise cellular structure and interconnections of the accessory atrioventricular pathway, however, remain unknown.

The first accessory atrioventricular pathway to be reported in the literature was a right-sided structure (Wood et al. 1943), but most morphological knowledge comes from light microscopic studies of left-sided pathways identified in postmortem specimens (Öhnell, 1944; Becker et al. 1978; Klein et al. 1980). These studies have demonstrated that the connections skirt the intact fibrous atrioventricular annulus, running around its epicardial aspect on the left side. Right-sided connections have been less frequently studied, but usually follow a subendocardial course, through deficiencies in the less well developed right-sided annulus (Becker et al. 1978). Although the majority of connections have been reported to consist of "normal working myocardium" at standard histological examination, cells said to resemble the normal atrioventricular node have also been reported (Becker et al. 1978; Guiraudon et al. 1988).

The presence of specialised cells within accessory atrioventricular pathways would be expected to affect the electrophysiological properties of the connection. Despite recognition that the pathway tissue may not all be "normal working myocardium", this description has been perpetuated in the literature for half a century, with no more detailed an analysis of the morphology than is possible with light microscopy. Thus, precise information is lacking regarding the ultrastructural phenotype of the myocytes involved, the structure of the intercalated disks and, in particular, the presence and organisation of gap junctions. As accessory atrioventricular pathways could theoretically take origin from a number of myocyte subtypes (which could vary with anatomical location), the characteristics of the gap junctions in the pathways are not only relevant to the variability of accessory atrioventricular pathway conduction properties, but will also provide important clues to the nature of the cells of origin. Connexin43 is abundant with different distinct patterns of distribution in ordinary atrial and ventricular myocytes, is present at low levels with no distinct pattern in the atrioventricular nodal cells, and is immunologically undetectable in other parts of the central conducting axis (Oosthoek et al. 1990; Van Kempen et al. 1991; Gourdie et al. 1992). Immunolocalisation of this connexin can contribute to distinguishing between these myocyte subtypes, and the pattern of immunolabelling in accessory atrioventricular pathways may, therefore, shed light on their tissue of origin.

8.2 Materials and Methods

Informed, written consent was obtained from 8 patients with the Wolff-Parkinson-White syndrome who were due to undergo surgical resection of an accessory atrioventricular pathway. In each case, during routine endocardial dissection through the connective tissue of the atrioventricular junction, a careful search was made for a discrete strand of tissue traversing from atrium to ventricle at the site determined as the position of the pathway by intraoperative electrical mapping. As this study was in part designed to investigate the overall ultrastructural morphology of the myocytes comprising the pathways, it was important to control for abnormalities resulting from imperfect tissue preservation and a period of ischaemic arrest at 28°C with St Thomas' cardioplegia before resection of the "pathway". Myocardial biopsies were, therefore, also taken from the right atrium and the left ventricular apex of each patient. All specimens obtained were immediately divided and placed in the appropriate fixative for subsequent analysis by standard thin section electron microscopy and immunohistochemical labelling of gap

junctions. By minimising trauma to the tissue and transferring it to fixative solution within 30 seconds of excision, deterioration of the tissue would be expected to be limited. The specimens (atrium, ventricle and pathway) from each patient were processed in parallel and compared, so that any abnormal ultrastructural features arising from imperfect preservation would be common to all three and, therefore, identifiable as being artefactual.

8.3 **Results**

A strand of tissue traversing the atrioventricular annulus identified by the surgeon as being the possible accessory pathway was found in 5 of the 8 patients during routine dissection, and was carefully excised. In 2 cases, histology showed the resected tissue to be a blood vessel, with no discernible myocardium. In the 3 remaining cases, light microscopy enabled identification of a bundle of myocytes along the length of the specimen, completely enveloped in connective tissue that extended to the resected margins (Fig 8.1A). These structures were therefore taken to be the accessory pathways. The case histories of these 3 patients were as follows:-

Case 1. A 17-year-old male symptomatic of atrioventricular reentrant tachycardia for 3 years had a left lateral accessory pathway. Radiofrequency catheter ablation produced transient loss of preexcitation only, and at surgery an incision was made around the annulus of the mitral valve from the left fibrous trigone to the interventricular septum. Endocardial thickening from the previous transvenous ablation attempt was observed, but was situated 5mm medial to the structure later shown to contain a strand of myocardium. Dissection to clear the posterior ventricular wall extended inferiorly to the epicardial reflection. There was no evidence of preexcitation at postoperative electrophysiologic study, nor thereafter.

Case 2. A 37-year-old male symptomatic of recurrent atrioventricular reentrant tachycardia for 18 months had intermittent preexcitation on electrocardiogram. An orthodromic reentrant tachycardia involving a left posterolateral pathway was induced at electrophysiologic study. At surgery, the incision and dissection were as described for Case 1. Following surgery, electrophysiologic studies showed normal conduction and no inducible tachycardia. Despite transient postoperative paroxysmal atrial fibrillation, atrioventricular conduction has been normal.

Case 3. A 27-year-old male with a history of intermittent palpitations and one syncopal episode since the age of 13 years was found at electrophysiologic study to have a right

paraseptal accessory pathway. The earliest activation during tachycardia was just outside the mouth of the coronary sinus. The right paraseptal location was confirmed on intraoperative epicardial and endocardial mapping, and dissection was carried out through an incision around the insertion of the mural (inferior) leaflet of the tricuspid valve, extending to the right atrial free wall. Posteroseptal dissection extended to the epicardial reflection. Following surgery, there has been no recurrence of preexcitation.

8.3.1 Connexin43 immunohistochemistry and cellular morphology of accessory atrioventricular pathways

8.3.1a *Left-sided*

The myocytes of the left-sided pathways were morphologically indistinguishable from "normal working myocardium" on electron microscopic examination (Fig 8.1B). The myofibrils had normal sarcomeric banding patterns and distribution within the cells. Intercalated disks, located at end-on abutments between myocytes, had the usual arrangement of conspicuous adherens junctions, and gap junctions. Immunohistochemical detection of connexin43 gap junctions by scanning laser confocal microscopy revealed label confined to the myocyte terminals lying transverse to the long axis of the cells and to the pathway as a whole (Fig 8.2B).

8.3.1b *Right-sided*

The right-sided accessory pathway, in contrast, was composed of myocytes with some highly abnormal features. At the level of light microscopy, these cells were of widely varying size but had clearly discernible Z-bands and intercalated disks, with no obvious abnormalities (Fig 8.1A). Examination by thin section electron microscopy, however, revealed marked ultrastructural abnormalities (Fig 8.1C). The electron-dense Z-bands were indeed clear and adjacent I-bands were identifiable, but A-bands were absent (Fig 8.3A). Some electron-dense material, possibly of A-band origin, was strewn along the borders of the I-bands, but the remainder of the A-band region contained interconnected condensed material of intermediate electron density scattered over a pale matrix. In many though not all instances the Z-bands remained approximately in register despite the apparent absence of adjacent components of the myofibril (Fig 8.3B). Another striking abnormal feature was a lack of mitochondria of normal structure. Instead, abundant structures akin to mitochondria were observed, consisting of clusters of electron-dense bodies, 50-100 nm in diameter, connected by filamentous remnants of membranes (Fig 8.3A). Some of these structures appeared sufficiently similar to mitochondria for the

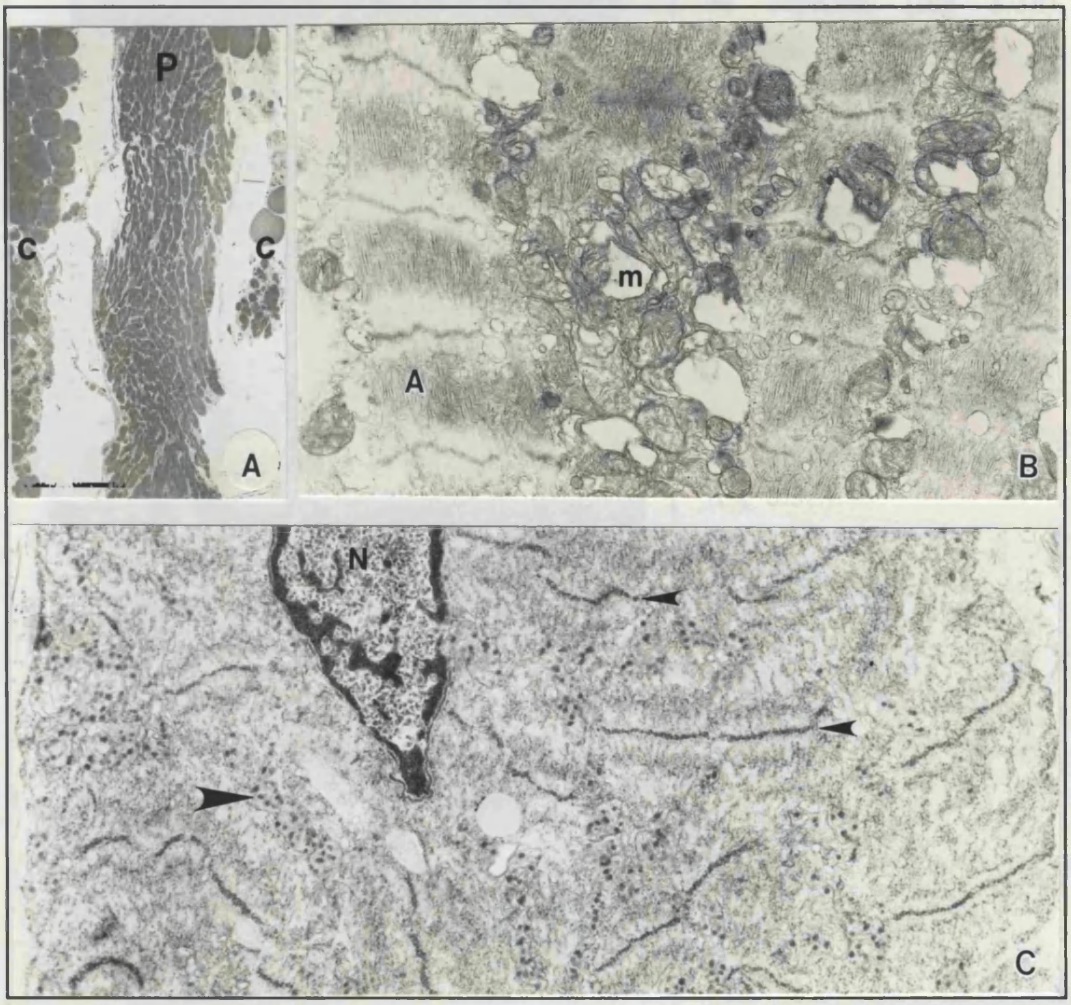

Figure 8.1. A. Light micrograph illustrating the typical low power appearances of all of the resected pathways and surrounding connective tissue. This is the right paraseptal accessory AV pathway from Case 3, sectioned longitudinally and stained with toluidine blue. The pathway (p) has the appearance of "normal working myocardium" and is embedded in connective tissue (c), which has separated from the pathway during preparation. x62.5.
B. Thin-section electron micrographs of longitudinally-sectioned left posterolateral pathway from Case 2. There is mild ischaemic damage to the tissue, but the ultrastructure, and in particular the organisation of the sarcomeres, with obvious A-band (A) myofilaments, resembles that of normal working myocardium. Mitochondria (m) show vacuolation and some loss of cristae, consistent with ischaemic damage. x13,000.
C. Thin-section electron micrograph of longitudinally-sectioned right paraseptal accessory pathway from Case 3. The abnormal structure of the myocytes is immediately apparent, with clear Z-bands (small arrows), and instead of A-band material, which is almost completely absent, collections of electron-dense particles (representing mitochondrial-equivalent structures - large arrows). The nucleus (N) shows peripheral aggregation of chromatin. x16,500.

identification to be made with confidence, though many were altered to a degree that identification of their origin would otherwise have been impossible. The arrangement of the cellular contents was also altered, with absence of the normal pattern of longitudinally-arranged myofibrils interspersed by rows of mitochondria. Instead, the Z-bands often appeared to traverse the entire cell without interruption, and the abnormal mitochondria were disposed in transverse arrays, occupying the position in which the

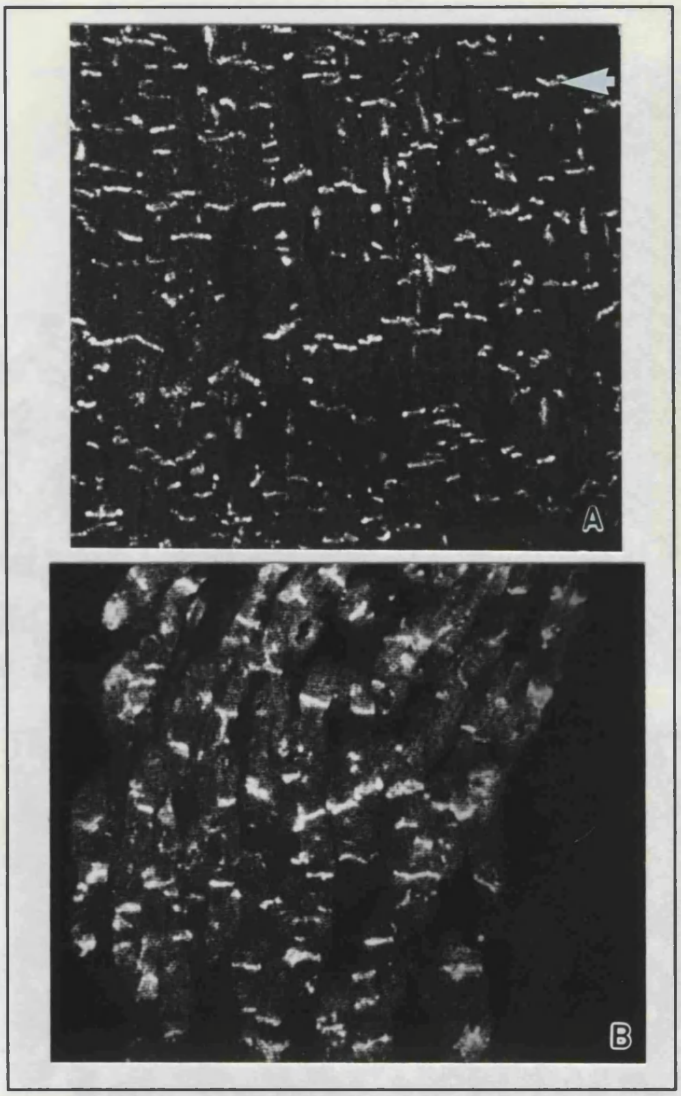

Figure 8.2. Low-power scanning laser confocal micrographs of longitudinally-sectioned myocardium, immunolabelled for connexin43.
A. Left ventricular myocardium of Case 3, shows the distribution of label confined to the positions of the transversely-orientated intercalated disks (arrow), normal for ventricular myocardium. x200.
B. The right paraseptal accessory pathway from Case 3. The label distribution is indistinguishable from that in ventricular myocardium or the left-sided pathways. x250.

absent A-band material would be expected (Fig 8.3B). Intercalated disks tended to show some deviation from the classical geometry, with no clear distinction between the orientations of the adherens junctions and the gap junctions (Page, 1992), but otherwise appeared normal (Fig 8.3C).

Immunohistochemistry gave unambiguous positive labelling of the gap junctions in a distribution indistinguishable from that in the left-sided pathways (i.e. confined to the myocyte terminals lying transverse to the long axis of the cells and to the pathway as a whole. Fig 8.2). Both the left and right-sided pathways examined, therefore, had a connexin43 gap junction distribution similar to that of ventricular myocardium, and not atrial myocardium, atrioventricular nodal or conducting tissue, in which the connexin43 is not confined to transversely-orientated intercalated disks (Severs, 1989b; Jongsma and Gros, 1991; Gourdie et al. 1991).

8.3.2 Ventricular and atrial myocardium

Examination of myocardium taken from the left ventricular apex and right atrium of each of the hearts, subjected to identical preparation procedures, revealed well preserved

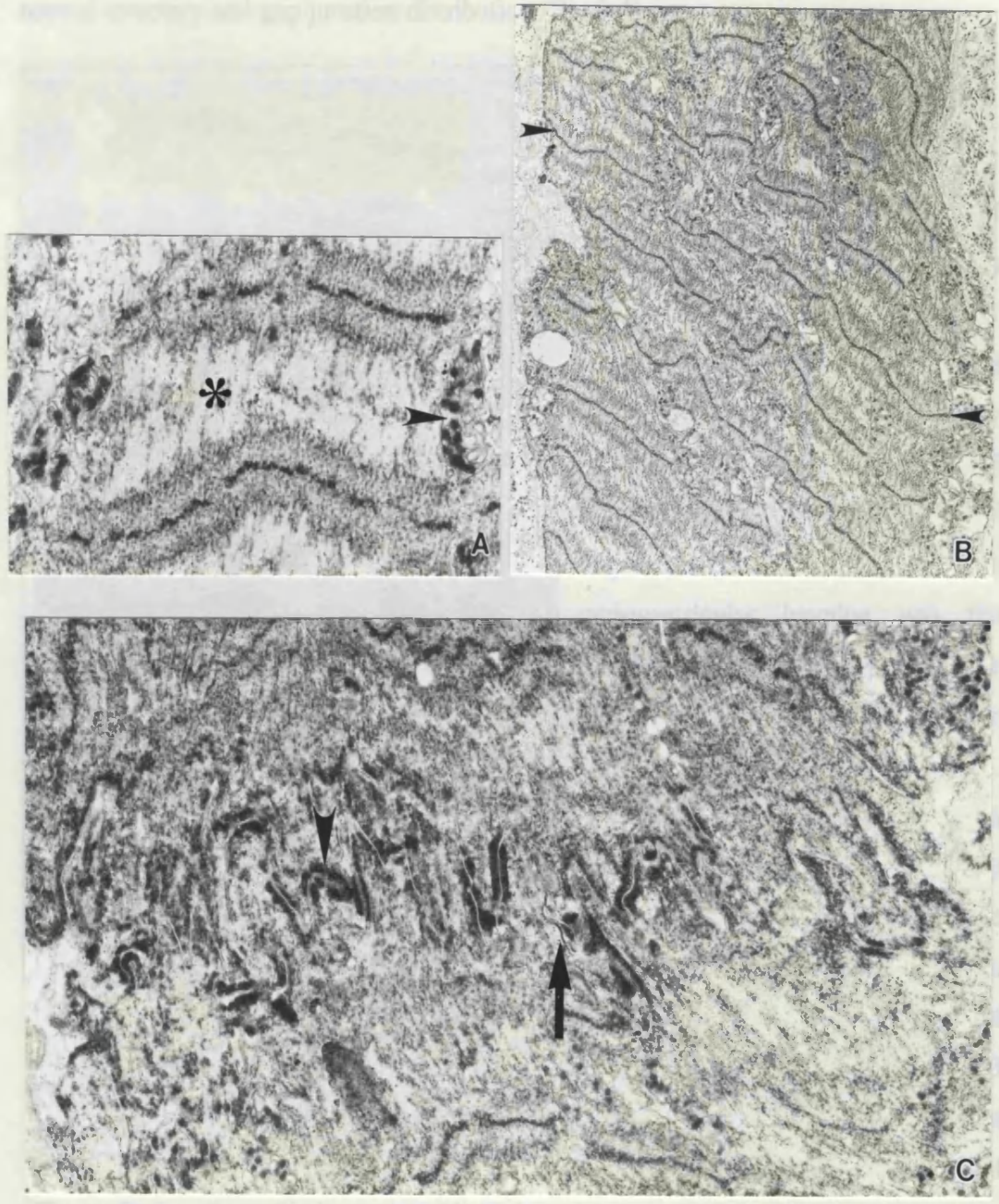

Figure 8.3. Thin-section electron micrographs of longitudinally-sectioned right paraseptal accessory pathway from Case 3.
A. Detail of the abnormal sarcomeric structure, with a lack of A-band material (*), and detail of the mitochondrial-equivalent electron-dense clusters of particles within a membranous structure (arrow).
B. The Z-bands traverse the entire width of a myocyte (arrows) without interruption.
C. An intercalated disk showing mild distortion, fasciae adherentes junctions (arrow-head), and the less conspicuous electron-dense membranes characteristic of gap junctions (arrow). A, x18,000; B, x6,200; C, x19,200.

myofibrils and mitochondria with some features of ischaemic damage, but otherwise normal structure and gap junction distribution (Fig 8.4).

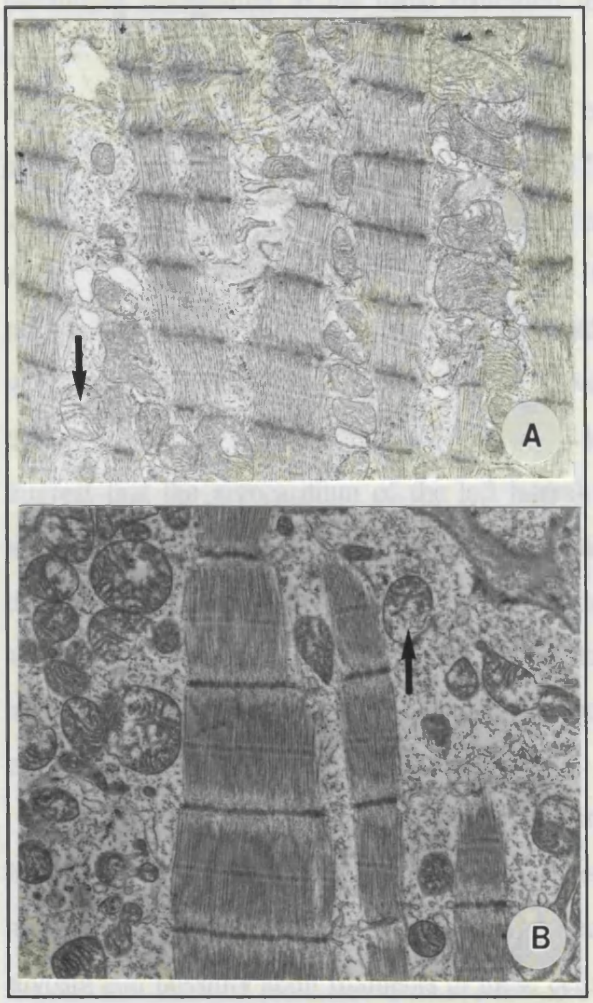

Figure 8.4. Thin section electron micrographs of longitudinally-sectioned myocardium from left ventricle (A) and right atrium (B) from Case 3. There is a mild degree of injury to the tissue, with some loss of mitochondrial cristae (arrows), but no amorphous matrix densities. There is good overall preservation, and normal myocardial appearance. The myofibrils in the ventricular specimen (A) are in a contracted state. A, x9,000; B, x12,000.

8.4 Discussion

The subcellular ultrastructure of accessory atrioventricular pathways has not previously been described. These structures are difficult to locate and identify in life, and our study yielded just 3 pathways from 8 patients entered. That the strand of myocardium traversing the atrioventricular junction was the tissue responsible for the ventricular preexcitation in each case can never be proven with absolute certainty. However, there is no feasible method for locating more precisely a pathway in man than the intraoperative epicardial mapping undertaken in this study, and only one suspect strand of tissue was seen in each of the 3 cases. Furthermore, previous post mortem studies have demonstrated small strands of myocardium related to the atrioventricular connective tissue in the manner found in this study in cases known to have had preexcitation (Becker et al. 1978), and such strands have not been found in hearts without preexcitation. The body of evidence, therefore, suggests that the tissue examined was the structure responsible for ventricular preexcitation in each case.

The nature of the surgical procedure dictated the degree of compromise of tissue preservation. Mitochondrial ultrastructure is one of the most sensitive morphological indicators of early ischaemic damage (Schaper et al. 1979; DeBoer et al. 1983; Lochner et al. 1986; Reimer and Jennings, 1991), and all specimens obtained showed features

compatible with some ischaemic injury (Figs 8.1B, 8.4). Despite these features, the membrane components of the myocytes showed a satisfactory degree of preservation, permitting recognition of the usual structural features, and thus identification of true abnormalities in the right-sided pathway.

Previous light microscopic studies have concluded that the component myocytes of atrioventricular pathways are recognisable as "normal working" myocytes, with a few studies of right-sided pathways reporting cells resembling those of the atrioventricular node (Becker et al. 1978; Guiraudon et al. 1988). In the present study, electron microscopic examination confirmed that left-sided pathways are indeed composed of cells with the morphology of normal working ventricular myocytes, and we further demonstrated a distribution of connexin43 gap junctions typical of such cells. It is of interest that the myocardium of the left lateral accessory pathway (Case 1) had these normal ventricular appearances, and showed no apparent ultrastructural abnormality despite an obvious adjacent endocardial scar from the previous radiofrequency ablation attempt which had transiently abolished preexcitation. As the myocytes of this pathway appeared normal, it is highly unlikely that the previous ablation attempt had any lasting effect on pathway morphology.

Despite "normal" light microscopic appearances, however, the right-sided pathway had far from normal subcellular features. The peculiar myofibril banding implies a gross abnormality of myofilament organisation; the lack of an A-band suggests an absence of myosin and possibly actin filaments in these cells. These features could be attributed to poor structural preservation, but the control ventricular and atrial tissue processed in parallel did not reveal similar changes. The possibility that the peculiar ultrastructural features reflect an abnormal cellular morphology of this pathway, even if some deterioration of structure (eg. due to ischaemia) is superimposed, cannot be excluded. The morphology observed differs from any previously reported myocytes in health or disease, including those of the conduction system. Although equipped with rudimentary contractile apparatus, the cells would appear unlikely to be functionally competent as contractile cells. They remain mechanically coupled, however, and, significantly, electrically coupled by connexin43 gap junctions, which have the usual structural features at thin section electron microscopy.

It is now known that there is a variety of myocardial connexin types (Kanter et al. 1992) which may confer different electrophysiological properties on different parts of the heart (Page, 1992; Gourdie et al. 1993). The cell type from which accessory atrioventricular pathways originate, and whether this factor is consistent or variable

between cases, is relevant to understanding their diverse behaviour. Use of the specific connexin43 antibody in the present study demonstrated the same gap-junctional protein abundant in all of the accessory atrioventricular pathways, with a distribution resembling that in normal ventricular myocardium, and different from both atrial myocardium (Gourdie et al. 1991) and atrioventricular nodal tissues (Jongsma and Gros, 1991). This result does not, however, exclude the possibility of varying proportions of coexisting connexins in the gap junctions of pathways, contributing to their electrophysiological diversity.

In summary, although accessory atrioventricular pathways may consist of normal myocytes, evidence is presented that abnormal myocytes with an apparent absence of normal contractile apparatus are present in some pathways. However, all of the pathways were composed of myocytes coupled by an abundance of connexin43 gap junctions with a distribution and ultrastructural appearance indistinguishable from ventricular myocardium. Taken together, these lines of evidence are consistent with the view that the myocytes comprising the accessory atrioventricular pathways in the Wolff-Parkinson-White syndrome may be of ventricular type, and some of these cells show ultrastructural modification.

PART IV - ANIMAL STUDIES

The initial design and main thrust of the series of studies comprising this thesis was the investigation of gap junction organisation in the human heart in health and disease. However, these studies have raised many questions which were not possible to investigate in man. The work was therefore extended to animal models to address the following questions:-

i) Is the disturbance in the pattern of gap junction distribution at the borders of healed myocardial infarcts (Chapter 5) causally related to the fibrotic scarring and distortion of the healing process, or is it an early primary cellular response of the surviving myocytes, due possibly to critical ischaemia or triggered by infarction of their neighbours?

ii) Are there early, and possibly transient changes in connexin43-gap junction expression by myocytes undergoing active hypertrophy, that may subsequently subside in the chronic phase to restore the gap junction content per myocyte to a level that shows no significant difference from normal (Chapter 7)? At a later stage, when myocardial failure occurs, are there associated changes in gap junction organisation?

These questions will be addressed in the final two chapters of this thesis.

CHAPTER 9 - GAP JUNCTION DISTRIBUTION IN SURVIVING MYOCYTES BORDERING CANINE FOUR-DAY OLD MYOCARDIAL INFARCTS.

9.1 Introduction

In order to investigate whether the disturbance in the pattern of gap junction distribution at the borders of healed myocardial infarcts (Chapter 5) is an early cellular response of the surviving myocytes, or results from interaction with the related fibrotic scarring and distortion from the infarct healing process, a canine model of acute myocardial infarction was used to examine gap junction organisation before fibrotic healing has occurred.

9.2 Materials and Methods

Three mongrel dogs (weighing 28 to 32 kg) underwent two-stage ligation of the left anterior descending coronary artery, 5 - 10 mm from its origin, under sodium pentobarbital anaesthesia (15 to 30 mg/kg iv), performed under sterile conditions by Issy Sanchez. The dogs were allowed to recover and feed ad libitum, for four days, when they were reanaesthetised and a median sternotomy performed in order that epicardial electrophysiological studies could be carried out on the thin layer of subepicardial myocardium known to survive over the infarct in this model (Ursell et al. 1985; Dillon et al. 1988). These studies did not damage the functioning heart, and after their completion, the heart was fibrillated by injection of 20 ml of cold Zamboni's solution into the left anterior descending coronary artery, distal to the occlusion. The heart was removed, and specimens of left ventricular myocardium (~ 1 cm^3) were taken from the centre and the edge of the infarct and from the normal posterior left ventricular wall, and fixed by immersion in Zamboni's solution for two hours. The specimens were processed for connexin43 immunohistochemical examination by the standard procedures described in section 2.3.2 of Chapter 2. The specimens were divided such that transmural and tangential sub-epimyocardial sections of each region could be obtained for examination by connexin43 immunohistochemistry. For this study a Lasersharp 600 confocal microscope was used to examine the immunolabelled sections, and, although easier to use, this updated microscope produced images similar to the 500 model used in all other studies in this thesis. Adjacent wax sections were stained with Mason's trichrome stain to help distinguish infarcted from surviving myocytes.

9.3 **Results**

Myocardium from the left ventricular posterior wall showed normal histological features, and a connexin43-gap junction distribution pattern (Fig 9.1) typical of mammalian ventricular myocardium (Gourdie et al. 1991), as described in man (Chapter 3). In both transmural and tangential subepimyocardial sections, Masson's trichrome stain readily distinguished infarcted myocytes, which, around the edges of infarct and particularly within the surviving subepicardial layer, were present as islands with varying degrees of confluence within "healthy" myocardium (Fig 9.2). Connexin43 immunohistochemistry demonstrated a background level of fluorescence in the infarcted regions, with no focal labelling (Figs 9.2c and 9.3). The apparently viable myocytes, with intact cross-striation and no pathological contractures, that abutted infarcted cells showed varying degrees of disruption of gap junction distribution, although there were occasional interfaces between necrotic and viable cells that showed no disruption (Fig 9.3). Where it was present, the disturbance of the gap-junctional pattern was similar to that described in healed human infarcts (Chapter 5); that is, junctions strewn along the lateral interfaces

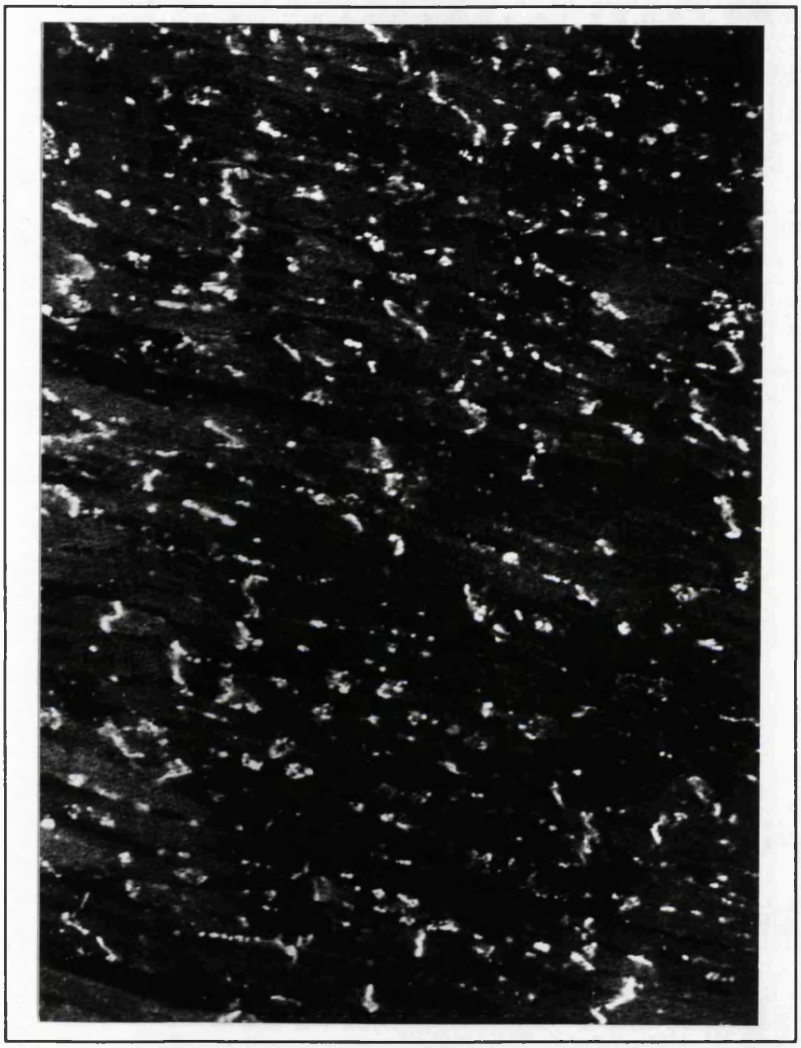

Figure 9.1. Low power confocal micrograph of longitudinally-sectioned connexin43-labelled canine ventricular myocardium from the posterior wall of the left ventricle. The long axis of the constituent myocytes is horizontal in this micrograph. Note the transverse or slightly oblique clusters of label characteristic of normal mammalian ventricular myocardium. x500.

Figure 9.2. Subepicardial myocardium sectioned parallel with the epicardium in the region of four-day old infarction.
A: Low power view of section stained with Mason's trichrome. The pink myocytes interdigitate in a complex manner with the necrotic tissue (lower left) containing inflammatory cells, but very little collagen (stains blue-green) at this stage. x500.
B & C: over the page:-

between myocytes, in longitudinally-orientated arrays (Fig 5.3). This abnormality extended in some regions to about 6 cells' width from the necrotic border, and there was usually a complete absence of gap-junctional labelling along the face of the myocyte that abutted directly onto a necrotic cell (Fig 9.3).

9.4 **Discussion**

Four days after myocardial infarction in dogs, the early phase of premature ventricular depolarisations and acute ventricular arrhythmias from ectopic foci subsides, and a period of inducible ventricular tachycardia due to reentrant circuits ensues (Wit and Janse, 1992). Fibrotic healing is not yet evident at this stage, and the histological features consist principally of surviving muscle fibres interspersed with necrotic cells, with some tissue oedema and inflammatory cells (Ursell et al. 1985). In the canine model of infarction used in the present study, reentrant circuits are frequently localised to the overlying and, by simple light microscopy, apparently healthy myocardium that exists in a thin subepicardial layer. The thinner this layer of surviving myocardium, the more likely it is that a reentrant circuit will exist (Ursell et al. 1985; Wit and Janse, 1992). This implies that the substrate for reentrant circuits in this context is dependent, at least in part, on properties of overall tissue structure and interaction between the surviving cells, rather than due to abnormalities of individual cell behaviour, since the latter would be largely independent

B: Higher power view of myocytes at the interface with a focus of necrotic cells.
C: Confocal image of myocytes at the same interface with the focus of necrotic cells as shown in B, in an adjacent section labelled for connexin43. Note the label strewn along the lateral borders of the surviving myocytes that interdigitate with the necrotic tissue devoid of label. In this example, the next layer of surviving cells has a label distribution of normal appearance. C & D, x500.

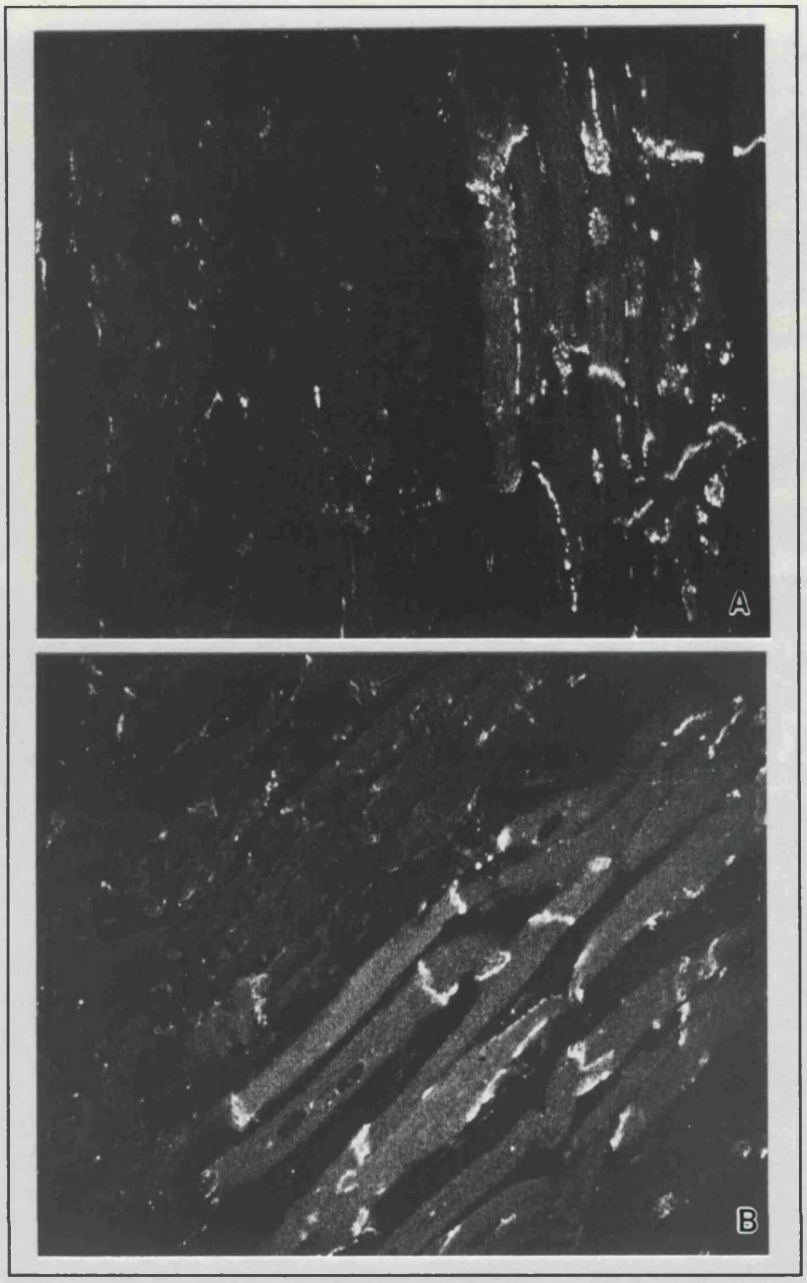

Figure 9.3. Confocal micrographs of infarct border zone. The surviving myocardium is to the right side in both micrographs. In (A), there is an abnormal label distribution, but with an absence of label along the border of the myocytes immediately abutting the infarct (in which the necrotic tissue has no focal labelling). In B, there is minimal disturbance of the label distribution, as was observed occasionally. A & B, x500.

of the thickness of the cell layer. The possibility exists that reentry in this model is due to an abnormality of interaction of the myocytes adjacent to the infarct, which becomes more important when constituting a greater proportion of a thinner surviving cell layer (Fig 9.4). The results of the present study have demonstrated that as early as four days after myocardial infarction there is a disturbance of gap junction distribution in the surviving myocytes of the border zone, similar to that described in association with fibrotic scarring in the healed phase (Chapter 5). This result is strongly suggestive that

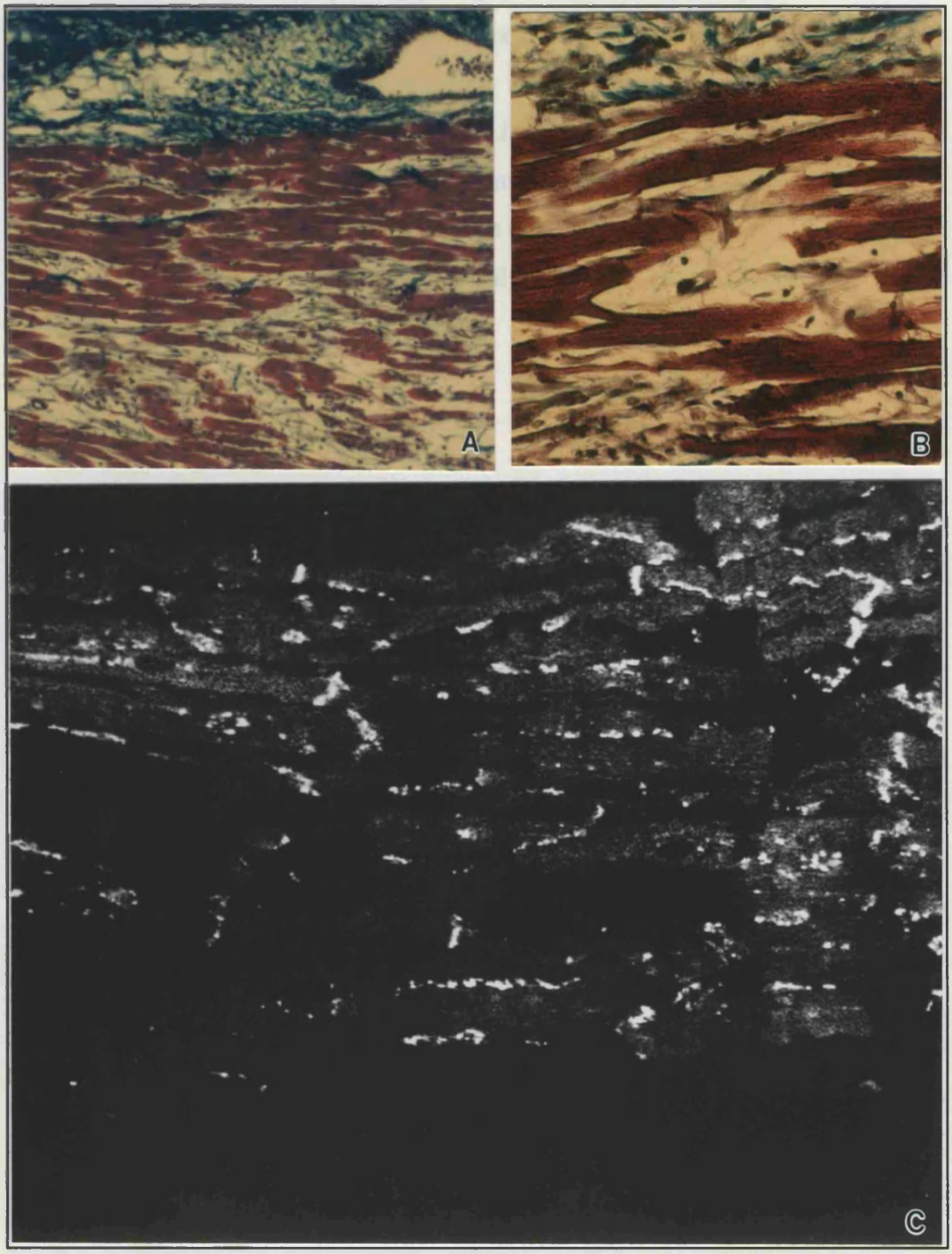

Figure 9.4. Sections perpendicular to the epicardium, showing longitudinally-sectioned subepicardial myocardium in the region of infarction. The epicardium is at the top, and the infarct at the bottom in all 3 plates.
A: Low power Mason's trichrome section, showing a 15 to 20 cell layer of surviving subepicardial myocytes overlying the infarct. Note the heavy blue-green staining of the epicardial collagen.
B: Higher power Mason's trichrome section of a surviving subepicardial layer of < 10 cells.
C: The adjacent wax section to that in B, labelled for connexin43. Note the few orderly arrays of label suggestive of intercalated disks in the uppermost layers of subepicardial cells, but that most of this thin layer of surviving tissue has a haphazard gap-junctional distribution. A, x150; B, x500; C, x500.

this disturbance results from a primary pathophysiological abnormality of these cells, and not solely a result of physical disruption by extrinsic fibrotic scarring and distortion in the healing phase. Reentry, as discussed earlier, is facilitated when anisotropic propagation is rendered non-uniform (Wit and Janse, 1992), and although much has been written on the role of fibrosis and increased connective tissue septation in promoting non-uniformity of propagation, an abnormal pattern of gap junction distribution in the absence of fibrotic scarring, as demonstrated in this study, could provide the substrate for reentry.

CHAPTER 10 - LEFT VENTRICULAR MYOCYTE GAP-JUNCTIONAL CONTENT IN RESPONSE TO ACUTE RENOVASCULAR HYPERTENSION IN GUINEA PIGS.

10.1 Introduction

Ventricular hypertrophy is associated with alterations in myocardial electrophysiology and mechanical function that cannot be explained entirely by changes in the action potential or histology of the myocardium. Despite the abundant literature concerning the importance of ventricular arrhythmias in patients with cardiac hypertrophy and failure, there is a lack of consensus as to the nature and relevance of the basic electrophysiology underlying these pathological conditions. A number of studies over the last 20 years have reported a variety of discrepant cellular electrophysiological measurements made on hypertrophied myocytes and whole tissue, and although reduction of the upstroke velocity and prolongation of the plateau phase of the action potential are now generally accepted alterations in hypertrophy (Bassett and Gelband, 1973; Tritthart et al. 1975; Kowey et al. 1991; Pye and Cobbe, 1992), there is no direct evidence linking these changes to altered myocardial function or arrhythmogenesis, particularly in the early stages of the hypertrophic response (Bassett and Gelband, 1973; Tritthart et al. 1975; Kowey et al. 1991; Pye and Cobbe, 1992). Cardiac failure and hypertrophy are associated with abnormalities of ventricular wall motion, and studies of the underlying contractile disturbance have also yielded conflicting results (Gülch, 1980; TenEick et al. 1989; Harding et al. 1991). Although the use of different models of hypertrophy and a lack of standardisation, particularly of the loading conditions of the tissue, are partly to blame for inconsistent results (TenEick et al. 1989; Kowey et al. 1991), it is now known that there are rapid changes in the physiology of cardiac myocytes in early hypertrophy (Bassett and Gelband, 1973; Tritthart et al. 1975; Swynghedauw, 1991), which may make the timing of study critical. One factor that is relevant to both the coordination of contraction and the arrhythmic tendency of myocardium is conduction velocity, of which gap-junctional cellular coupling is, as discussed earlier, the major determinant. However, few studies have investigated either conduction velocity or cellular coupling in hypertrophied or failing hearts. With the alterations of myocardial architecture and the consequent changes in cellular contacts that must occur with myocyte enlargement and

either elongation or so-called slippage of myocytes in the failing heart (Gerdes et al. 1992), changes in cellular coupling would be expected to occur, even in the absence of interstitial fibrosis that may contribute further to alterations of myocyte interaction in longstanding hypertrophy. Although myocardial conduction velocity has been reported as slowing in hypertrophy, which would be consistent with, but not necessarily entirely attributable to, the changes in the myocyte action potential, conduction velocity in whole myocardium that has these action potential changes has been reported as being paradoxically increased during the active phase of hypertrophy (Tritthart et al. 1975). This increase in conduction velocity, which may only occur transiently in the hypertrophic process, cannot be accounted for by the increasing myocyte diameter alone (Tritthart et al. 1975), and indicates that alterations in cellular coupling may indeed occur, and may be variable, in early hypertrophy.

The purpose of this study was to investigate alterations of gap-junctional organisation in left ventricular myocardium in response to renovascular hypertension. The guinea pig was considered an appropriate model to investigate this since the active membrane-channel properties in guinea pigs are more similar to those in man than are those of other laboratory small mammals, with similar alterations of the action potential under pathophysiological conditions. The cellular coupling of guinea pig ventricular tissue, known to have the typical mammalian gap-junctional distribution (Gourdie et al. 1991), might also be expected to parallel alterations in man in response to induced hypertension.

10.2 **Materials and Methods**

10.2.1 Renal artery clipping

Hypertension was induced by a modified Goldblatt 1-clip 2-kidney model (Smith et al. 1988). Male Dunkin-Hartley guinea pigs weighing between 200 and 300g were anaesthetised using 6.5mg/kg intraperitoneal Hypnovel (midazolam, Roche) and 2.4mg/kg intramuscular Hypnorm (Janssen). Under sterile conditions, Dr K T MacLeod performed surgery in which the left renal artery was located via a dorsal incision, and a clip shaped from 0.1mm thick silver foil was placed around it and tightened to constrict, but not occlude, the lumen. The animal was allowed to recover and kept for a period of 3 weeks, feeding ad libitum, before sacrifice for study. Weight-matched guinea pigs had

sham surgery, with exposure of the renal artery but no clip placement.

10.2.2 Blood pressure measurement

Immediately before sacrifice, the animal was anaesthetised as above, and the arterial blood pressure measured by carotid artery cannulation.

10.2.3 Myocyte isolation and immunolabelling

Immediately after sacrifice, the heart was removed and a small deep subepicardial left ventricular wall sample was put in Zamboni's solution. The heart was then mounted and perfused as detailed in Chapter 2, by the Langendorff method, and treated to isolate the myocytes of the remaining left ventricle.

After fixation in Zamboni's solution, the left ventricular whole-tissue specimens, and the isolated myocyte suspensions were processed for connexin43-immunolabelling using the standard procedures detailed in Chapter 2, and the labelled whole tissue was examined in the confocal microscope to determine the pattern of connexin43 gap-junctional distribution.

10.2.4 Quantitative analysis of the isolated myocytes

Immunolabelled cells were examined by conventional epifluorescence and confocal laser scanning microscopy. Phase contrast microscopy was used to confirm intact, regular sarcomeric striation of the myocytes.

From each preparation, 6 myocytes that had retained a rod-like shape were randomly selected from under the confocal microscope for quantitative analysis. Planimetric measurement of the volume of the myocyte and the total surface area of connexin43 gap-junctional present were determined by the following method. An optical section series was taken at 1.5 μm intervals in the vertical (z) axis through the entire volume of the myocyte, by the same method as detailed in section 6.3.2 of Chapter 6. The aperture control on the microscope was withdrawn by 1.5 mm, producing a degree of confocality that provided minimal overlap between adjacent sections. A "black level" of 4 and a gain level was set so that the cell cross sectional outline was just visible and the image data spanned the 255-point grey scale. Each image of each series was binarised, processed and analysed by the same PC IMAGE program as described in

Chapter 6 to determine the total cross-sectional area of the cell. An additional analysis was performed on each image, using a higher binary threshold (100), to determine the area of fluorescent label in each slice. As in Chapter 6, the cell volume was derived from the product of the sum of the myocyte cross-sectional areas and the interval between them (1.5 μm). The total gap-junctional area per myocyte was the sum of the fluorescence content of its individual slices.

10.3 **Results**

The 12 guinea pigs were sacrificed at between 18 and 21 days after renal artery clipping (mean 20.7 $\pm$ 0.9 days, with no significant difference between groups), and details at the time of sacrifice are shown in Table 10.1.

Table 10.1 Details of guinea pigs at sacrifice

animal		body weight (g)	heart/body weight ratio	blood pressure (mmHg)
Control	23	466	0.51	120/74
	25	386	0.49	93/61
	27	481	0.46	107/62
	29	538	0.45	103/58
	31	504	0.48	104/65
	33	504	0.38	122/76
	Mean$\pm$SD	480$\pm$52	0.46$\pm$0.05	108$\pm$11/66$\pm$7
Hypertensive	22	340	0.54	135/106
	24	390	0.55	155/99
	26	415	0.47	128/92
	28	492	0.41	132/86
	30	490	0.52	143/82
	32	619	0.46	157/87
	Mean$\pm$SD	458$\pm$98	0.49$\pm$0.05	142$\pm$12/92$\pm$9

The six guinea pigs with renal artery clips were hypertensive, with significantly higher blood pressures (142±12/92±9 mmHg) than the normotensive controls (108±11/66±7 mmHg: $p<0.001$). There were no significant differences in the mean total body weight or the ratio of heart to body weights between the control and hypertensive groups.

10.3.1 Confocal analysis of gap junctions

Table 10.2 Mean confocal measurements made from 6 isolated myocytes from each guinea pig.

animal		myocyte volume (μm^3)	area gj/cell (μm^2)	gj area/myocyte volume ($\mu m^2/\mu m^3$)
Control	23	19280±5685	66.3±22.6	0.00341±0.00047
	25	25425±7670	109.2±38.9	0.00480±0.00237
	27	28982±4561	79.3±38.5	0.00269±0.00120
	29	27405±5569	94.7±26.8	0.00346±0.00067
	31	24391±7354	113.3±38.6	0.00475±0.00110
	33	29105±8018	86.0±36.6	0.00289±0.00089
	Mean±SD	25765±3695	91.5±17.8	0.00366±0.00091
Hypertensive	22	27767±3719	159.9±70.1	0.00587±0.00267
	24	26743±5218	129.4±29.7	0.00492±0.00105
	26	34717±8915	137.0±44.3	0.00442±0.00231
	28	41589±5391	146.7±21.7	0.00358±0.00066
	30	30321±10091	153.5±82.9	0.00547±0.00241
	32	27396±6332	150.4±68.5	0.00541±0.00143
	Mean±SD	31422±5778	146.1±11.2#	0.00495±0.00083*

* = $p<0.05$
compared with control value
= $p<0.001$

The whole-tissue specimen from the left ventricular apex in all 12 animals revealed the normal adult pattern of gap junction distribution, in the transverse arrays confined to the

positions of the intercalated disks. The isolated myocytes also showed clear punctate labelling in clusters characteristic of intercalated disks (see Fig 6.2). The mean values for myocyte volume, total gap-junctional area per cell and gap-junctional area per myocyte volume for each animal are summarised in Table 10.2. There was a trend towards a higher mean myocyte volume in the hypertensive than the control animals but, in keeping with the normal heart-to-body weight ratios, there was no significant difference ($p=0.08$). Gap-junctional area per myocyte, however, was significantly greater in the hypertensive animals (146 ± 11.2 μm^2) than controls (91.5 ± 17.8 μm^2: $p<0.001$). When the tendency to a larger cell volume of the hypertensive group was taken into account, the gap-junctional area per volume of myocyte remained significantly greater in the hypertensive animals (0.0050 ± 0.0008 $\mu m^2/\mu m^3$) than controls (0.0037 ± 0.0009 $\mu m^2/\mu m^3$: $p=0.03$).

The values for myocyte volume, total gap-junctional area per cell and gap-junctional area per myocyte volume for each cell are summarised in Appendix Tables A10 & A11.

10.4 **Discussion**

Physiological adaptation of ventricular myocardium to pressure overload is characterised by a reduced maximum unloaded shortening velocity and an increased duration of the action potential, allowing the heart to achieve a lower rate of normal maximum tension development. Although the result is that the myocardium may produce a normal tension at a lower cost to its constituent myocytes, this change may be progressively detrimental at the level of the whole organ, which must function incessantly.

The cellular and intercellular alterations producing these physiological changes are not fully understood, but several growth factors for which protooncogenes have been detected, and which promote widespread DNA replication and transcription, are at least transiently abundant early in various models of myocardial hypertrophy (Swynghedauw, 1991). There are associated changes in gene expression, with alterations in the contractile elements and in the membrane ionic channels, resulting in changes in ion handling (Swynghedauw, 1991). Other plasma membrane components altered include the expression of neurohormone receptors, and there are changes in elements of the cytoskeleton of ventricular myocytes in the initial stages of pressure loading (Swynghedauw, 1991). The results of this study suggest that there is also a substantial change in connexin43 gap junction expression in the early myocardial response to

pressure loading in renovascular hypertension.

One might speculate that this increase in the surface density of the membrane structure that determines intercellular conductance and tissue conduction velocity has a physiological role. To optimise overall myocardial performance in the face of the energy-saving reduction in the rate of maximum tension development of the individual myocytes undergoing hypertrophy, and to minimise the detrimental electromechanical effects of the changes in the action potential, a normalisation (or even increase) in myocardial conduction velocity in early hypertrophy, for which there is experimental evidence (Tritthart et al. 1975), may be facilitated by increased intercellular gap-junctional coupling.

The results of this study are applicable to the early stages of the hypertrophic response, but further studies need to be performed in order to determine whether in the guinea pig gap-junctional expression changes in later stages of hypertrophy and subsequent heart failure. These studies have yet to be performed, but the results of the study of chronic pressure-overload hypertrophy in man (Chapter 7), albeit in a different species and with a different model of hypertrophy, would suggest that, in keeping with other factors in myocardial hypertrophy, there is a degree of "normalisation" of gap-junctional area per myocyte after the initial hypertrophic response.

11.1 FINAL DISCUSSION AND CONCLUSION

Throughout this series of studies, immunohistochemical detection of connexin43, using the combination of a high affinity antibody and a powerful microscopical technique, and supplemented by electron microscopy, has provided new insights into gap junction organisation in relatively large volumes of tissue. Although the amino acid sequence of connexin43 was established in 1987 (Beyer et al. 1987), antibodies that enabled immunohistochemical investigation of connexin43 were not produced until 1989 (Luke et al. 1989a; Beyer et al. 1989; Gourdie et al. 1990b), and the connexin43 antibody used in the present series of investigations is probably the most effective available. The earliest biological applications of scanning laser confocal microscopy were in the mid-1980s (White et al. 1987), with the first commercially available microscopes produced in 1987 (Inoue, 1989). The combination of these recently developed tools to perform detailed immunolocalisation of connexin43, with clarity and resolution that permits quantification, makes the work in this thesis state-of-the-art. Furthermore, this series of studies is at the forefront in taking investigation of a fundamental aspect of cell biology and relating it to cardiac disease, breaking new ground at the interface with current clinical challenges. The potential importance of this is that unlike the results of ultrastructural tissue studies, precise localisation and quantification of gap junction distribution through intact myocardium might, for the first time, permit meaningful correlation of whole-tissue functional assessments, both mechanical and electrical, with this morphometric data. But is knowledge of gap junction organisation itself of any importance? It is becoming increasingly apparent that the answer to this question is that gap junctional coupling, a hitherto largely ignored factor, is central to the coordination of electrical and mechanical myocardial function.

This series of studies has not only established the morphological characteristics of gap junctions in adult ventricular myocardium, and the postnatal sequence of changes in its development, but has also demonstrated detail of normal and abnormal organisation of whole-tissue coupling that are relevant to such clinical issues as wall motion disturbances in ischaemic and hypertrophic heart diseases, anisotropy of conduction, the arrhythmogenic substrate, the diversity of behaviour of accessory atrioventricular pathways, and the changing electromechanical properties of infant myocardium. The extent to which the realisation that understanding gap junction coupling may be fundamental to these clinical challenges, and the gap in the literature reflecting the

difficulties hitherto in producing clinically-relevant experimental data, has led to speculation from major contributors in the field of myocardial electromechanical function. Wit (1989) has suggested that the selective modulation of intercellular coupling in the heart might be an appropriate target for a new class of antiarrhythmic agent, and Saffitz (1993), in a very recent "Point of View" in the journal *Circulation*, has made some highly speculative statements, given the level of published knowledge, in answering the question posed in his title: "Arrhythmogenesis and ventricular dysfunction after myocardial infarction - is anomalous cellular coupling the elusive link?" Speculative though this article is, the results of the work presented in this thesis (Smith et al. 1991; Peters et al. 1993) go a long way to closing the gap linking subcellular structure with clinical challenges, and strongly suggest that the answer to the question posed may indeed be "yes".

APPENDIX

Table A1 Confocal data from "normal" LV myocardium

patient	field	total cell sectional area (μm^2)	gj area (μm^2)	gj area/vol ($\mu m^2/\mu m^3$)
N1	a	20079	1190.685	0.00593
	b	27324	1092.96	0.00402
	c	28837.8	1320.771	0.00458
	d	20200.8	854.4938	0.00423
	e	24824	1256.094	0.00506
	Mean±SD			0.00476±0.00076
N2	a	21417	2034.615	0.0095
	b	21249.2	1515.068	0.00713
	c	12043.2	1011.629	0.0084
	d	17166.6	1242.862	0.00724
	e	13296.8	699.4117	0.00526
	Mean±SD			0.00751±0.00158
N3	a	23051.6	1244.786	0.0054
	b	27733.5	1095.473	0.00395
	c	26573	922.0831	0.00347
	d	25309.9	1030.113	0.00407
	e	22720.6	920.1843	0.00405
	Mean±SD			0.00419±0.00072
N4	a	28712	1352.335	0.00471
	b	27483.6	849.2432	0.00309
	c	19961.6	992.0915	0.00497
	d	20612.7	603.9521	0.00293
	e	20029.2	458.6687	0.00229
	Mean±SD			0.00360±0.00117
N5	a	27253.8	1855.984	0.00681
	b	22764.5	1170.095	0.00514
	c	20525	1241.763	0.00605
	d	23405.8	1221.783	0.00522
	e	18128.8	687.0815	0.00379
	Mean±SD			0.00540±0.00113

Table A2 Confocal data from "normal" RV myocardium

patient	field	total cell sectional area (μm^2)	gj area (μm^2)	gj area/vol. ($\mu m^2/\mu m^3$)
N2	a	21250.4	754.3892	0.00355
	b	23707.2	853.4592	0.0036
	c	26048	875.2128	0.00336
	d	25414.4	767.5149	0.00302
	e	23416.9	922.6259	0.00394
	Mean±SD			0.00349±0.00034
N4	a	20764.8	1158.676	0.00558
	b	26011.2	1339.577	0.00515
	c	27054	1717.929	0.00635
	d	25760.9	1094.838	0.00425
	e	25012.8	917.9698	0.00367
	Mean±SD			0.00501±0.00106
N6	a	22411.2	1299.85	0.0058
	b	26847.2	1006.77	0.00375
	c	28239.2	883.887	0.00313
	d	24948	1152.598	0.00462
	e	21918	1295.354	0.00591
	Mean±SD			0.00464±0.00123
N7	a	23906.7	975.3934	0.00408
	b	27999.4	1159.175	0.00414
	c	26071.1	1006.344	0.00386
	d	23100	801.57	0.00347
	e	21580.8	977.6102	0.00453
	Mean±SD			0.00402±0.00038
N8	a	29113.7	1406.192	0.00483
	b	22775.5	1156.995	0.00508
	c	22852.8	971.244	0.00425
	d	24823.7	1040.113	0.00419
	e	18065	961.058	0.00532
	Mean±SD			0.00473±0.00050

Table A3 Myocyte volume measurements from 6 isolated cells (a-f) and 3 whole-tissue fields (a-c) from each guinea pig.

animal	field/cell	isolated cell vol. (μm^3)	tissue index of cell vol.
22	a	26113.43	27346.2
	b	32180.73	29403.4
	c	31793.52	20053.7
	d	27939.3	
	e	21099.14	
	f	27472.78	
	Mean	27766.48	25601.1
23	a	24631.54	23124.7
	b	22168.87	18226.4
	c	10697.35	18548.7
	d	25190.37	
	e	20544.84	
	f	12444.48	
	Mean	19279.58	19966.6
24	a	25922.05	29957.9
	b	35438.33	27734.2
	c	19053.81	25235.6
	d	24055.42	
	e	30962.36	
	f	25023.94	
	Mean	26742.65	27642.57
25	a	24389.76	17294.8
	b	19931.25	28465
	c	19398.53	22999.4
	d	19994.99	
	e	27556.37	
	f	41280	
	Mean	25425.15	22919.73
26	a	24585.02	36577.6
	b	34780.11	27394.1
	c	37995.47	36452
	d	22861.35	
	e	39090.64	
	f	48990.76	
	Mean	34717.22	33474.57
27	a	33121.83	21385.6
	b	30801.86	30892.6
	c	28784.54	31809.4
	d	20625.38	

	e	26333.14	
	f	34222.93	
	Mean	28981.61	28029.2
28	a	38162.97	38761.2
	b	41975.44	30629.6
	c	31840.63	28961.3
	d	47901.51	
	e	46645.26	
	f	43011.08	
	Mean	41589.48	32784.03
30	a	45115.86	30029.2
	b	28686.05	31292.4
	c	33502.62	29649.5
	d	14306.09	
	e	22323.93	
	f	37993.98	
	Mean	30321.42	30323.7
31	a	26862.98	18272.6
	b	24278.18	27344.2
	c	25377.22	26850
	d	36698.87	
	e	11905.01	
	f	21227.11	
	Mean	24391.56	24155.6
32	a	27128.23	30599.7
	b	29601.12	25473.4
	c	20657.25	29994.5
	d	38806.45	
	e	28460	
	f	19720.85	
	Mean	27395.65	28689.2
33	a	25197.04	26986.7
	b	23430.39	16002.3
	c	45642.57	32354.7
	d	31776.23	
	e	21920.58	
	f	26662.71	
	Mean	29104.92	25114.57

Table A4 Confocal data from ischaemic LV myocardium

patient	field	total cell sectional area (μm^2)	gj area (μm^2)	gj area/vol ($\mu m^2/\mu m^3$)
I11	a	28142.4	509.3774	0.00181
	b	26659.2	381.2266	0.00143
	c	29260.8	596.9203	0.00204
	d	22525	891.99	0.00396
	e	26659.8	607.8434	0.00228
	Mean±SD			0.00230±0.00098
I12	a	26981.9	585.5072	0.00217
	b	26187.6	515.8957	0.00197
	c	27396.6	408.2093	0.00149
	d	28557.2	514.0296	0.0018
	e	17490	438.999	0.00251
	Mean±SD			0.00199±0.00038
I13	a	23110.4	418.2982	0.00181
	b	27220.2	734.9454	0.0027
	c	21899	389.8022	0.00178
	d	19510.4	275.0966	0.00141
	e	29386	564.2112	0.00192
	Mean±SD			0.00192±0.00046
I14	a	20962.9	484.243	0.00231
	b	26353.6	859.1274	0.00326
	c	15955.5	336.6611	0.00211
	d	13784	847.716	0.00615
	e	23403.2	875.2797	0.00374
	Mean±SD			0.00351±0.00162
I15	a	29351	1449.939	0.00494
	b	29144	673.2264	0.00231
	c	20713.5	903.1086	0.00436
	d	22865.4	951.2006	0.00416
	e	23684	864.466	0.00365
	Mean±SD			0.00388±0.00099

Table A5 Data from confocal section series of hypertrophied LV myocardium.

patient	field	total cell sectional area (μm^2)	gj area (μm^2)	gj area/vol. ($\mu m^2/\mu m^3$)
H1	a	28260.8	1042.824	0.00369
	b	28036.8	899.9813	0.00321
	c	29008.1	1064.597	0.00367
	d	17605.8	672.5416	0.00382
	e	23054.4	740.0462	0.00321
	Mean±SD			0.00352±0.00029
H2	a	26128.9	681.9643	0.00261
	b	26928.8	689.3773	0.00256
	c	20501.6	649.9007	0.00317
	d	27080.8	612.0261	0.00226
	e	20131.2	533.4768	0.00265
	Mean±SD			0.00265±0.00033
H3	a	27485.1	915.2538	0.00333
	b	24999.1	804.971	0.00322
	c	27536	949.992	0.00345
	d	24081.6	734.4888	0.00305
	e	28172.2	1011.382	0.00359
	Mean±SD			0.00333±0.00021
H4	a	28285.6	478.0266	0.00169
	b	28919.8	795.2945	0.00275
	c	25821.5	457.0406	0.00177
	d	27542.4	991.5264	0.0036
	e	28383	811.7538	0.00286
	Mean±SD			0.00253±0.00080
H5	a	28185.6	1389.55	0.00493
	b	27451.6	1021.2	0.00372
	c	26365.5	474.579	0.0018
	d	25504.6	1086.496	0.00426
	e	28164	915.33	0.00325
	Mean±SD			0.00359±0.00118

Table A6 Confocal data used to derive gj area/cell in normal LV.

pt	field	no. cells	no. disks	10x cells/disks	mean cell sectional area(μm^2)	index of cell vol.	gj area/vol ($\mu m^2/\mu m^3$)	index of gj/cell
N1	a	48	10	48	418.3125	20079	0.00593	15806.76
	b	54	9	60	506	30360	0.004	16121.59
	c	52	9	57.77	554.5731	32042	0.00458	19481.9
	d	37	6	61.66	545.9676	33668	0.00423	18906.18
	e	44	8	55	564.1818	31030	0.00506	20843.87
	Mean					29435.8	0.00476	18232.06
N2	a	45	15	30	475.9333	14278	0.0095	18006.82
	b	51	14	36.42	416.651	15178	0.00713	14366.47
	c	32	8	40	376.35	15054	0.0084	16787.16
	d	39	11	35.45	440.1692	15606	0.00724	14999.48
	e	36	8	45	369.3556	16621	0.00526	11606.17
	Mean					15347.4	0.007506	15153.22
N3	a	49	11	44.54	470.4408	20956	0.0054	15022.71
	b	44	9	48.88	630.3068	30815	0.00395	16158.66
	c	50	10	50	531.46	26573	0.00347	12240.98
	d	48	11	43.63	527.2896	23009	0.00407	12431.92
	e	55	14	39.28	413.1018	16229	0.00405	8725.552
	Mean					23516.4	0.004188	12915.97
N4	a	47	8	58.75	610.8936	35890	0.00471	22440.91
	b	42	12	35	654.3714	22903	0.00309	9395.004
	c	35	8	43.75	570.3314	24952	0.00497	16462.96
	d	41	9	45.55	502.7488	22903	0.00293	8908.532
	e	42	12	35	476.8857	16691	0.00229	5074.158
	Mean					24667.8	0.003598	12456.31
N5	a	50	14	35.71	545.076	19467	0.00681	17599.17
	b	51	11	46.36	446.3627	20695	0.00514	14121.3
	c	40	10	40	513.125	20525	0.00605	16484.84
	d	45	11	40.90	520.1289	21278	0.00522	14745.09
	e	51	8	63.75	355.4667	22661	0.00379	11401.56
	Mean					20925.2	0.005402	14870.39

Table A7 Confocal data used to derive gj area/cell in normal RV.

pt	field	no. cells	no. disks	10x cells/disks	mean cell sectional area(μm^2)	index of cell vol.	gj area/vol ($\mu m^2/\mu m^3$)	index of gj/cell
N2	a	52	8	65	408.6615	26563	0.00355	12518.48
	b	50	11	45.45	474.144	21552	0.0036	10299.98
	c	50	11	45.45	520.96	23680	0.00336	10562.51
	d	54	11	49.09	470.637	23104	0.00302	9262.756
	e	49	13	37.69	477.8959	18013	0.00394	9421.681
	Mean					22582.4	0.003494	10413.08
N4	a	45	9	50	461.44	23072	0.00558	17090.93
	b	52	12	43.33	500.2154	21676	0.00515	14819.46
	c	53	15	35.33	510.4528	18036	0.00635	15204.08
	d	46	11	41.81	560.0196	23419	0.00425	13213.06
	e	38	9	42.22	658.2316	27792	0.00367	13540.42
	Mean					22799	0.005	14773.59
N6	a	55	14	39.28	407.4764	16008	0.0058	12325.69
	b	41	8	51.25	654.8098	33559	0.00375	16706.54
	c	51	8	63.75	553.7098	35299	0.00313	14667.39
	d	45	9	50	554.4	27720	0.00462	17001.27
	e	53	10	53	413.5472	21918	0.00591	17196.28
	Mean					26900.8	0.004642	15579.43
N7	a	46	9	51.11	519.7109	26563	0.00408	14387.44
	b	48	13	36.92	583.3208	21538	0.00414	11837.28
	c	48	11	43.63	543.1479	23701	0.00386	12145.07
	d	44	10	44	525	23100	0.00347	10641.13
	e	49	12	40.83	440.4245	17984	0.00453	10815.1
	Mean					22577.2	0.004016	11965.2
N8	a	50	11	45.45	582.274	26467	0.00483	16970.63
	b	50	11	45.45	455.51	20705	0.00508	13963.2
	c	56	9	62.22	408.0857	25392	0.00425	14326.23
	d	48	11	43.63	517.1604	22567	0.00419	12552.61
	e	51	10	51	354.2157	18065	0.00532	12758.39
	Mean					22639.2	0.004734	14114.21

Table A8 Confocal data used to derive gj area/cell in ischaemic LV.

pt	field	no. cells	no. disks	10x cells/disks	mean cell sectional area(μm^2)	index of cell vol.	gj area/vol ($\mu m^2/\mu m^3$)	index of gj/cell
I11	a	43	8	53.75	654.4744	35178	0.00181	8452.70
	b	36	6	60	740.5333	44432	0.00143	8434.86
	c	51	6	85	573.7412	48768	0.00204	13207.2
	d	40	10	40	563.125	22525	0.00396	11841.4
	e	40	6	66.66	666.495	44433	0.00228	13448.9
	Mean					39067.2	0.002304	11077.0
I12	a	48	11	43.63	562.1229	24529	0.00217	7066.19
	b	48	6	80	545.575	43646	0.00197	11414.5
	c	31	6	51.66	883.7613	45661	0.00149	9031.87
	d	38	7	54.28	751.5053	40796	0.0018	9748.46
	e	33	6	55	530	29150	0.00251	9713.11
	Mean					36756.4	0.001988	9394.82
I13	a	45	8	56.25	513.5644	28888	0.00181	6941.32
	b	40	7	57.14	680.505	38886	0.0027	13938.0
	c	49	10	49	446.9184	21899	0.00178	5174.76
	d	46	7	65.71	424.1391	27872	0.00141	5217.15
	e	48	10	48	612.2083	29386	0.00192	7490.10
	Mean					29386.2	0.001924	7752.28
I14	a	38	7	54.28	551.6553	29947	0.00231	9183.56
	b	52	13	40	506.8	20272	0.00326	8773.24
	c	32	5	64	498.6094	31911	0.00211	8938.59
	d	38	8	47.5	362.7368	17230	0.00615	14067.1
	e	44	8	55	531.8909	29254	0.00374	14524.5
	Mean					25722.8	0.003514	11097.4
I15	a	49	14	35	599	20965	0.00494	13748.9
	b	50	10	50	582.88	29144	0.00231	8937.31
	c	46	9	51.11	450.2935	23015	0.00436	13321.2
	d	45	9	50	508.12	25406	0.00416	14030.5
	e	50	10	50	473.68	23684	0.00365	11476.0
	Mean					24442.8	0.003884	12302.8

Table A9 Confocal data used to derive an index of gj area/cell from hypertrophied LV.

pt	field	no. cells	no. disks	10x cells/disks	mean cell sectional area(μm^2)	index of cell vol.	gj area/vol ($\mu m^2/\mu m^3$)	index of gj/cell
H1	a	50	8	62.5	565.216	35326	0.00369	17304.8
	b	48	11	43.63	584.1	25488	0.00321	10861.4
	c	51	11	46.36	568.7863	26371	0.00367	12848.1
	d	30	6	50	586.86	29343	0.00382	14880.3
	e	42	8	52.5	548.9143	28818	0.00321	12280.4
	Mean					29069.2	0.00352	13635.0
H2	a	45	7	64.28	580.6422	37327	0.00261	12933.3
	b	51	8	63.75	528.0157	33661	0.00256	11439.6
	c	30	8	37.5	683.3867	25627	0.00317	10784.5
	d	39	8	48.75	694.3795	33851	0.00226	10156.0
	e	32	6	53.33	629.1	33552	0.00265	11803.4
	Mean					32803.6	0.00265	11423.4
H3	a	50	9	55.55	549.702	30539	0.00333	13500.3
	b	39	7	55.71	641.0026	35713	0.00322	15266.1
	c	51	8	63.75	539.9216	34420	0.00345	15764.3
	d	44	8	55	547.3091	30102	0.00305	12188.2
	e	52	7	74.28	541.7731	40246	0.00359	19180.6
	Mean					34204	0.003328	15179.9
H4	a	41	7	58.57	689.8927	40408	0.00169	9065.67
	b	40	14	28.57	722.995	20657	0.00275	7541.29
	c	32	5	64	806.9219	51643	0.00177	12134.7
	d	42	8	52.5	655.7714	34428	0.0036	16453.5
	e	36	10	36	788.4167	28383	0.00286	10776.3
	Mean					35103.8	0.002534	11194.3
H5	a	47	16	29.37	599.6936	17616	0.00493	11529.2
	b	49	11	44.54	560.2367	24956	0.00372	12324.3
	c	46	9	51.11	573.163	29295	0.0018	7000.22
	d	45	11	40.90	566.7689	23186	0.00426	13112.3
	e	51	8	63.75	552.2353	35205	0.00325	15189.1
	Mean					26051.6	0.003592	11831.0

Table A10 Control guinea pigs. Cell volume and gap-junctional area measured by confocal planimetry of 6 cells (a-f) from each animal.

animal	cell	cell volume		gj area		gj area/volume
		(pixels)	(μm^3)	(pixels)	(μm^2)	($\mu m^2/\mu m^3$)
23	a	299108	24631.54	1704	93.5496	0.003798
	b	269203	22168.87	1479	81.1971	0.003663
	c	129901	10697.35	586	32.1714	0.003007
	d	305894	25190.37	1225	67.2525	0.00267
	e	249482	20544.84	1511	82.9539	0.004038
	f	151117	12444.48	744	40.8456	0.003282
25	a	296172	24389.76	2240	122.976	0.005042
	b	242031	19931.25	3383	185.7267	0.009318
	c	235562	19398.53	1944	106.7256	0.005502
	d	242805	19994.99	1356	74.4444	0.003723
	e	334625	27556.37	1777	97.5573	0.003540
	f	501275	41280.02	1233	67.6917	0.001640
27	a	402208	33121.83	1977	108.5373	0.003277
	b	374036	30801.86	1020	55.998	0.001818
	c	349539	28784.54	2645	145.2105	0.005045
	d	250460	20625.38	722	39.6378	0.001922
	e	319771	26333.14	730	40.077	0.001522
	f	415579	34222.93	1579	86.6871	0.002533
29	a	431934	35569.76	2146	117.8154	0.003312
	b	347332	28602.79	2394	131.4306	0.004595
	c	347245	28595.63	1215	66.7035	0.002333
	d	232762	19167.95	1241	68.1309	0.003554
	e	377016	31047.27	2070	113.643	0.00366
	f	260459	21448.80	1284	70.4916	0.003287
31	a	326205	26862.98	2962	162.6138	0.006053
	b	294817	24278.18	1312	72.0288	0.002967
	c	308163	25377.22	2503	137.4147	0.005415
	d	445645	36698.87	2778	152.5122	0.004156
	e	144566	11905.01	1266	69.5034	0.005838
	f	257767	21227.11	1564	85.8636	0.004045
33	a	305975	25197.04	1108	60.8292	0.002414
	b	284522	23430.39	1586	87.0714	0.003716
	c	554251	45642.57	2654	145.7046	0.003192
	d	385868	31776.23	1710	93.879	0.002954
	e	266188	21920.58	485	26.6265	0.001215
	f	323773	26662.71	1861	102.1689	0.003832

Table A11 Hypertensive guinea pigs. Myocyte volume and gap-junctional area measured by confocal planimetry of 6 cells (a-f) from each animal.

animal	cell	cell volume		gj area		gj area/volume
		(pixels)	(μm^3)	(pixels)	(μm^2)	($\mu m^2/\mu m^3$)
22	a	317103	26113.43	1558	85.5342	0.003275
	b	390780	32180.73	2472	135.7128	0.004217
	c	386078	31793.52	1502	82.4598	0.002594
	d	339275	27939.3	4323	237.3327	0.008495
	e	256213	21099.14	2665	146.3085	0.006934
	f	333610	27472.78	4842	265.8258	0.009676
24	a	314779	25922.05	2864	157.2336	0.006066
	b	430338	35438.33	3094	169.8606	0.004793
	c	231376	19053.81	2065	113.3685	0.00595
	d	292112	24055.42	1485	81.5265	0.003389
	e	375985	30962.36	2090	114.741	0.003706
	f	303873	25023.94	2546	139.7754	0.005586
26	a	298543	24585.02	3908	214.5492	0.008727
	b	422345	34780.11	2153	118.1997	0.003398
	c	461390	37995.47	1315	72.1935	0.001901
	d	277612	22861.35	2415	132.5835	0.005799
	e	474689	39090.64	3027	166.1823	0.004251
	f	594909	48990.76	2156	118.3644	0.002416
28	a	463424	38162.97	1619	88.8831	0.002329
	b	509720	41975.44	1831	100.5219	0.002395
	c	386650	31840.63	2583	141.8067	0.004454
	d	581682	47901.51	2946	161.7354	0.003376
	e	566427	46645.26	2931	160.9119	0.00345
	f	522296	43011.08	2824	155.0376	0.003605
30	a	547855	45115.86	1548	84.9852	0.001884
	b	348343	28686.05	2045	112.2705	0.003914
	c	406832	33502.62	2322	127.4778	0.003805
	d	173723	14306.09	1897	104.1453	0.00728
	e	271086	22323.93	2924	160.5276	0.007191
	f	461372	37993.98	6038	331.4862	0.008725
32	a	329426	27128.23	2498	137.1402	0.005055
	b	359455	29601.12	2448	134.3952	0.00454
	c	250847	20657.25	2223	122.0427	0.005908
	d	471238	38806.45	5455	299.4795	0.007717
	e	345598	28460	1616	88.7184	0.003117
	f	239476	19720.85	2196	120.5604	0.006113

REFERENCES

Adgey, A.A.J. (1982) *Acute phase of ischemic heart disease and myocardial infarction.* Martinus Nijhoff, Boston.

Akiyama, T., Pawitan, Y., Greenberg, H., Kuo, C.-S., Reynolds-Haertle, R.A., CAST Investigators, (1991) Increased risk of death and cardiac arrest from encainide and flecainide in patients after non-Q-wave acute myocardial infarction in the Cardiac Arrhythmia Suppression Trial. *Am. J. Cardiol.* **68**, 1551-1555.

Allesi, R., Nusinowitz, M., Abildskov, J.A., Moe, G.K. (1958) Nonuniform distribution of vagal effects on the atrial refractory period. *Am. J. Physiol.* **194**, 406-410.

Altschuld, R.A., Ganote, C.E., Naylor, W.G., Piper, H.M. (1991) What constitutes the calcium paradox? *J. Mol. Cell. Cardiol.* **23**, 765-767.

Anderson, R.H., Becker, A.E. (1981) Stanley Kent and accessory atrioventricular connections. *J. Thorac. Cardiovasc. Surg.* **81**, 649-658.

Anderson, R.H., Ho, S.Y. (1991) The morphologic substrates for pediatric arrhythmias. *Cardiol. Young* **1**, 159-176.

Anversa, P., Beghi, C., Kikkawa, Y., Olivetti, G. (1985) Myocardial response to infarction in the rat. Morphometric measurement of infarct size and myocyte cellular hypertrophy. *Am. J. Pathol.* **484**, 492.

Arluk, D.J., Rhodin, D.J. (1974) The ultrastructure of calf heart conducting fibres with special reference to nexuses and their distribution. *J. Ultrastruct. Res.* **49**, 11-23.

Arnsdorf, M.F. (1984) Cable properties and conduction of the action potential. In: *Physiology and pathophysiology of the heart.* Ed: N. Sperelakis, pp. 109-140. Martinus Nijhoff, Boston.

Arvanitaki, A. (1942) Effects evoked in an axon by the activity of a contiguous one. *J. Neurophysiol* **5**, 89-108.

Ashraf, M., Halverson, C. (1978) Ultrastructural modifications of nexuses (gap junctions) during early myocardial ischaemia. *J. Mol. Cell. Cardiol.* **10**, 263-269.

Baldwin, K. (1981) Cell-to-cell tracer movement in cardiac muscle. Ruthenium red vs lanthanum. *Cell Tissue Res.* **221**, 279-294.

Balke, C.W., Lesh, M.D., Spear, J.F., Kadish, A., Levine, J.H., Moore, E.N. (1988) Effects of cellular uncoupling on conduction in anisotropic canine ventricular myocardium. *Circ. Res.* **63**, 879-892.

Barr, L., Dewey, M.M., Berger, W. (1965) Propagation of action potentials and the structure of the nexus in cardiac muscle. *J. Gen. Physiol.* **48**, 797-823.

Bassett, A.L., Gelband, H. (1973) Chronic partial occlusion of the pulmonary artery in cats. Change in ventricular action potential configuration during early hypertrophy. *Circ. Res.* **32**, 15-26.

Baylen, B, Ogata, H., Ikegami, M., Jacobs, H., Jobe, A., Emmanoulides, G (1986) Left ventricular performance and contractility before and after volume infusion: a comparative study of preterm and newborn lambs. *Circulation* **73**, 1042-1049.

Becker, A.E., Anderson, R.H., Durrer, D., Wellens, H.J.J. (1978) The anatomical substrates of Wolff-Parkinson-White Syndrome: a clinicopathologic correlation in seven patients. *Circulation* **57**, 870-879.

Belik, J., Light, R.B. (1989) Effect of increased afterload on right ventricular function in newborn pigs. *J. Appl. Physiol.* **66**, 863-869.

Bennett, M.V.L. (1977) Electrical transmission: A functional analysis and comparison to chemical transmission. In: *Handbook of Physiology. vol.1 sect.1.* Ed: E.R. Kandel, pp. 357-416. Williams and Wilkins, Baltimore, Maryland.

Beyer, E.C., Paul, D.L., Goodenough, D.A. (1987) Connexin43: a protein from rat heart homologous to a gap junction protein from liver. *J. Cell Biol.* **105**, 2621-2629.

Beyer, E.C., Kistler, J., Paul, D.L., Goodenough, D.A. (1989) Antisera directed against connexin43 peptides react with a 43-kd protein localized to gap junctions in myocardium and other tissues. *J. Cell Biol.* **108**, 595-605.

Beyer, E.C., Paul, D.L., Goodenough, D.A. (1990a) Connexin family of gap junction proteins. *J. Membr. Biol.* **116**, 187-194.

Beyer, E.C., Wetsphale, E.M., Wang, H-Z., Veenstra, R.D. (1990b) Molecular and biophysical characterization of gap junctions from the chick embryo heart. *J. Cell Biol.* **111**, 276a.(Abstract)

Binah, O., Rosen, M.R. (1992) Mechanisms of ventricular arrhythmias. *Circulation* **85 Suppl. I**, I25-I31.

Bode, H.R., Fraser, S.E., Green, C.R., Bode, P.M., Gilula, N.B. (1987) Gap junctions are involved in a patterning process in hydra. In: *Genetic regulation and development.* Ed: W.F. Loomis, pp. 245-261. Alan R.Liss Inc., New York.

Borg, T.K., Caulfield, J.B. (1981) The collagen matrix of the heart. *Fed. Proc.* **40**, 2037-2041.

Boyden, P.A., Tilley, L.P., Pham, T.D., Liu, S-K., Fenoglio, J.J., Wit, A.L. (1982) Effects of left atrial enlargement on atrial transmembrane potentials and structure in dogs with mitral valve fibrosis. *Am. J. Cardiol.* **49**, 1896-1907.

Brakenhoff, G.J., Van der Voort, H.T.M., Oud, J.L., Man, S.A. (1990) Potentialities and limitations of confocal microscopy for the study of three-dimensional biological structures. In: *Optical Microscopy for Biology.* Eds: B. Herman & K. Jacobson, pp. 19. Wiley Liss, New York.

Braun, J., Abney, J.R., Owicki, J.C. (1984) How a gap junction maintains its structure. *Nature* **310**, 316-318.

Brink, P.R., Dewey, M.M. (1978) Nexal membrane permeability to anions. *J. Gen. Physiol.* **72**, 67-86.

Buja, L.M., Ferrans, V.J., Maron, B.J. (1974) Intracytoplasmic junctions in cardiac muscle cells. *Am. J. Pathol.* **74**, 613-648.

Burch, G.E., Sohal, R.S. (1969) Morphologic and pathologic aspects of the intercalated disc of the heart. *Am. Heart J.* **78**, 358-368.

Burt, J.M., Frank, J.S., Berns, M.W. (1982) Permeability and structural studies of heart cell gap junctions under normal and altered ionic conditions. *J. Membr. Biol.* **68**, 227-238.

Burt, J.M. (1989) Uncoupling of cardiac cells by doxyl stearic acids: specificity and mechanism of action. *Am. J. Physiol. (Cell Physiol.)* **256**, C913-C924.

Burt, J.M. (1991) Modulation of cardiac gap junctional channel activity by the membrane lipid enviroment. In: *Biophysics of Gap Junction Channels*. Ed: C. Peracchia, pp. 75-93. CRC Press, Boca Raton, Florida.

Burt, J.M., Spray, D.C. (1988a) Single-channel events and gating behaviour of the cardiac gap junction channel. *Proc. Natl. Acad. Sci. U. S. A.* **85**, 3431-3434.

Burt, J.M., Spray, D.C. (1988b) Inotropic agents modulate gap junctional conductance between cardiac myocytes. *Am. J. Physiol. (Heart Circ. Physiol)* **254**, H1206-H1210.

Burt, J.M., Spray, D.C. (1989) Volatile anaesthetics block intercellular communication between neonatal rat myocardial cells. *Circ. Res.* **65**, 829-837.

Büchner, F., Onishi, S. (1968) *Der Herzmuskel bei akuter Koronarinsuffizienz im elektronenmikroskopischen Bild*. pp. 60-65. Urban and Schwarzenberg, München, Berlin.

Callans, D.J., Kieval, R.S., Hook, B.G., Moore, E.N., Spear, J.F. (1992) Effect of coronary perfusion of heptanol or potassium on conduction and ventricular arrhythmias. *Am. J. Physiol. (Heart Circ. Physiol)* **263**, H1382-H1389.

Campos De Carvalho, A.C., Tanowitz, H.B., Wittner, M., Dermietzel, R., Roy, C., Hertzberg, E.L., Spray, D.C. (1992) Gap junction distribution is altered between cardiac myocytes infected with *Trypanosoma cruzi*. *Circ. Res.* **70**, 733-742.

Carlemalm, E., Garavito, R.M., Villiger, W. (1981) Resin development for electron microscopy and an analysis of embedding at low temperature. *J. Microsc.* **126**, 123-129.

Chen, L., Goings, G.E., Upshaw-Earley, J., Page, E. (1989) Cardiac gap junction-associated vesicles: ultrastructural comparison of in situ negative staining with conventional positive staining. *Circ. Res.* **64**, 501-514.

Chen, Y., DeHaan, R.L. (1992) Multiple-channel conductance states and voltage regulation of embryonic chick cardiac gap junctions. *J. Membr. Biol.* **127**, 95-111.

Colan, S.D., Trowitzsch, E., Wenovsky, G., Sholler, G.F., Sanders, S.P., Castaneda, A.R. (1988) Myocardial performance after arterial switch operation for transposition of the great arteries with intact ventricular septum. *Circulation* **78**, 132-141.

Cotran, R.S., Kumar, V., Robbins, S.L. (1989) The Heart. In: *Pathologic Basis of Disease*. pp. 597-656. W B Saunders, Philadelphia.

Cranfield, P.F., Dodge, F.A. (1992) Slow conduction in the heart. In: *The slow inward current and cardiac arrhythmias*. Eds: D.P. Zipes, J.C. Bailey & I. Elharrad, pp. 149-171. Martinus Nijhoff, Boston.

Danford, D.A., Huhta, J.C., Gutgesell, H.P. (1985) Left ventricular wall stress and thickness in complete transposition of the great arteries. *J. Thorac. Cardiovasc. Surg.* **89**, 610-615.

De Mello, W.C. (1983) The influence of pH on the healing-over of mammalian cardiac muscle. *J. Physiol.* **339**, 299-307.

De Mello, W.C. (1985) Intercellular communication in cardiac muscle: physiological and pathological implications. In: *Cardiac Electrophysiology and Arrhythmias*. Ed: D.P. Zipes, pp.

65-72. Grune & Stratton, New York.

De Mello, W.C. (1986) Interaction of cyclic AMP and Ca^{2+} in the control of electrical coupling in heart fibres. *Biochim. Biophys. Acta* **888**, 91-99.

De Mello, W.C. (1987a) Modulation of junctional permeability. In: *Cell-to-Cell Communication.* Ed: W.C. De Mello, pp. 29-64. Plenum Press, New York.

De Mello, W.C. (1987b) *Cell-to-cell communication.* Plenum Publishing Corp.,

DeBoer, L.V.W., Rude, R.E., Kloner, R.A., Ingwall, J.S., Maroko, P.R., Davis, M.A., Braunwald, E. (1983) A flow- and time-dependent index of ischemic injury after experimental coronary occlusion and reperfusion. *Proc. Natl. Acad. Sci. U. S. A.* **80**, 5784-5788.

Decker, M.L., Simpson, D.G., Lesch, M., Jones, J., Beyer, E., Decker, R.S. (1989) Reassembly of the intercalated disc in cultured adult cardiac myocytes. *J. Cell Biol.* **107**, 555a.

Delmar, M., Michaels, D.C., Johnson, T., Jalife, J. (1987) Effects of increasing intercellular resistance on transverse and longitudinal propagation in sheep epicardial muscle. *Circ. Res.* **60**, 780-785.

Delmar, M., Delgado, C., Chivalo, D., Michaels, D.C., Jalife, J. (1989) On the problem of anisotropic propagation in ventricular muscle. In: *Lethal Arrhythmias Resulting from Myocardial Ischemia and Infarction.* Eds: M.R. Rosen & Y. Palti, pp. 181-197. Kluwer Academic publishers, Boston.

Dermietzel, R., Traub, O., Hwang, T.K., Beyer, E., Bennett, M.V.L., Spray, D.C., Willecke, K. (1989) Differential expression of three gap junction proteins in developing and mature brain tissue. *Proc. Natl. Acad. Sci. U. S. A.* **86**, 10148-10152.

Délèze, J. (1970) The recovery of resting potential and input resistance in sheep heart injured by knife or laser. *J. Physiol. (Lond.)* **208**, 547-562.

Dillon, S.M., Allessie, M.A., Ursell, P.C., Wit, A.L. (1988) Influences of anisotropic tissue structure on reentrant circuits in the epicardial border zone of subacute canine infarcts. *Circ. Res.* **63**, 182-206.

Dolber, P.C., Beyer, E.C., Junker, J.L., Spach, M.S. (1992) Distribution of gap junctions in dog and rat ventricle studied with a double-label technique. *J. Mol. Cell. Cardiol.* **24**, 1443-1457.

Dolber, P.C., Spach, M.S. (1989) Structure of canine Bachmann's bundle related to propagation of excitation. *Am. J. Physiol. (Heart Circ. Physiol)* **257**, H1446-H1457.

Dupont, E., El Aoumari, A., Roustiau-Severe, S., Briand, J.P., Gros, D. (1988) Immunological characterization of rat cardiac gap junctions: presence of common antigenic determinants in heart of other vertebrate species and in various organs. *J. Membr. Biol.* **104**, 119-128.

Eberth, C.J. (1866) Die Elemente der gestreiften Muskeln. *Virchows Arch. A Pathol. Anat. Histopathol.* **37**, 100.

Ebihara, L., Beyer, E.C., Swenson, K.I., Paul, D.L., Goodenough, D.A. (1989) Cloning and expression of a *Xenopus* embryonic gap junction protein. *Science* **243**, 1194-1195.

El Aoumari, A., Fromaget, C., Dupont, E., Reggio, H., Durbec, P., Briand, J-P., Böller, K., Kreitman, B., Gros, D. (1990) Conservation of a cytoplasmic carboxy-terminal domain of connexin43, a gap-junctional protein, in mammalian heart and brain. *J. Membr. Biol.* **115**,

229-240.

Engelmann, T.W. (1875) Ueber die Leitung der Erregung im Herzmuskel. *Pfluggers Arch. Physiol.* **11**, 465-480.

Engelmann, T.W. (1877) Vergleichende Untersuchungen zur Lehre von der Muskel - und Nervenelektrizität. *Pfluggers Arch. Physiol.* **15**, 116-148.

Factor, S.M., Sonnenblick, E.H., Kirk, E.S. (1978) The histologic border zone of acute myocardial infarction - islands or peninsulas? *Am. J. Pathol.* **92**, 111-124.

Fallon, R.F., Goodenough, D.A. (1981) Five-hour half-life of mouse liver gap-junction protein. *J. Cell Biol.* **90**, 521-526.

Farmer, B.B., Mancica, M., Williams, E.S., Watanabe, A.M. (1983) Isolation of calcium tolerant myocytes from adult rat hearts: review of the literature and description of a method. *Life Sci.* **33**, 1-18.

Fishman, G.L., Hertzberg, E.L., Spray, D.C., Leinwand, L.A. (1991) Expression of connexin43 in the developing rat heart. *Circ. Res.* **68**, 782-787.

Flagg-Newton, J.L., Simpson, I., Loewenstein, W.R. (1979) Permeability of the cell-to-cell membrane channels in mammalian cell junction. *Science* **205**, 404-407.

Forbes, M.S., Sperelakis, N. (1982) Association between mitochondria and gap junctions in mammalian myocardial cells. *Tissue Cell* **14**, 25-37.

Forbes, M.S., Sperelakis, N. (1985) Intercalated discs of mammalian heart: a review of structure and function. *Tissue Cell* **17**, 605-648.

Fouron, J-C., Heitz, F., Carceller, A-M., Ducharme, G., van Doesburg, N.H., Davignon, A. (1988) Left ventricular function during the first month of life. *Biol. Neonate* **53**, 1-9.

Fozzard, H.A. (1977) Cardiac muscle: Excitability and passive electrical properties. *Prog. Cardiovasc. Dis.* **19**, 343-359.

Fozzard, H.A., Arnsdorf, M.F. (1992) Cardiac Electrophysiology. In: *The Heart and Cardiovascular System.* Eds: H.A. Fozzard, E. Haber, R.B. Jennings, A.M. Katz & H.E. Morgan, pp. 63-98. Raven Press Ltd., New York.

Fraser, S.E., Green, C.R., Bode, H.R., Bode, P.M., Gilula, N.B. (1988) A perturbation analysis of the role of gap junctional communication in developmental patterning. In: *Modern cell biology, (series ed. Birgit H. Satir) Vol.7, Gap junctions.* Eds: E.L. Hertzberg & R.G. Johnson, pp. 515-526. Alan R.Liss Inc., New York.

Friedman, W.F. (1972) The intrinsic physiologic properties of the developing heart. In: *Neonatal heart disease.* Eds: W.F. Friedman, M. Lesch & E.H. Sonnenblick, pp. 21-49. Grune & Stratton, New York.

Fromaget, C., El Aoumari, A., Dupont, E., Briand, J.P., Gros, D. (1990) Changes in the expression of connexin43, a cardiac gap junctional protein, during mouse heart development. *J. Mol. Cell. Cardiol.* **22**, 1245-1258.

Fromaget, C., El Aoumari, A., Gros, D. (1992) Distribution pattern of connexin43, a gap-junctional protein, during the differentiation of mouse heart myocytes. *Differentiation* **51**, 9-20.

Fujimoto, T., Peter, R., Hamamoto, H., Mandel, W.J. (1983) Electrophysiological observations during the spontaneous initiation of ischemia induced ventricular fibrillation. *Am. Heart J.* **105**, 189-197.

Furshpan, E.J., Potter, D.D. (1959) Transmission at the giant motor synapses of the crayfish. *J. Physiol.* **145**, 289-325.

Ganote, C.E., Nayler, W.G. (1985) Contracture and the calcium paradox. *J. Mol. Cell. Cardiol.* **17**, 733-745.

Geiger, B., Volk, T., Volberg, T. (1985) Molecular heterogeneity of adherens junctions. *J. Cell Biol.* **101**, 1523-1531.

Geiger, B., Volberg, T., Ginsberg, D., Bitzur, S., Sabanay, I., Hynes, R.O. (1990) Broad spectrum pan-cadherin antibodies, reactive with the C-terminal 24 amino acid residues of N-cadherin. *J. Cell Sci.* **97**, 607-614.

Gerdes, A.M., Kellerman, S.E., Moore, J.A., Muffly, K.E., Clark, L.C., Reaves, P.Y., Malec, K.B., McKeown, P.P., Schocken, D.D. (1992) Structural remodeling of cardiac myocytes in patients with ischemic cardiomyopathy. *Circulation* **86**, 426-430.

Gogol, E., Unwin, N. (1988) Organization of connexons in isolated rat liver gap junctions. *Biophys. J.* **54**, 105-112.

Goldstein, M.A., Sordahl, L.A., Schwartz, A. (1974) Ultrastructural analysis of the ventricular hypertrophy in rabbits. *J. Mol. Cell. Cardiol.* **6**, 265-273.

Gourdie, R.G., Green, C.R., Severs, N.J. (1988) The development of detergent-free methods for cardiac gap junction isolation. In: *Inst.Phys.Conf.Ser. (93). EUREM 88 Vol. 3.* Eds: H.G. Dickinson & P.G. Goodhew, pp. 139-140. IOP, Bristol.

Gourdie, R.G., Green, C.R., Thompson, R.P., Severs, N.J. (1990a) Three-dimensional reconstruction of gap junction arrangement in developing and adult rat hearts. *Trans. Roy. Microsc. Soc.* **1**, 417-420.

Gourdie, R.G., Harfst, E., Severs, N.J., Green, C.R. (1990b) Cardiac gap junctions in rat ventricle: localization using site-directed antibodies and laser scanning confocal microscopy. *Cardioscience* **1**, 75-82.

Gourdie, R.G., Green, C.R., Severs, N.J. (1991) Gap junction distribution in adult mammalian myocardium revealed by an antipeptide antibody and laser scanning confocal microscopy. *J. Cell Sci.* **99**, 41-55.

Gourdie, R.G., Green, C.R., Severs, N.J., Thompson, R.P. (1992) Immunolabelling patterns of gap junction connexins in the developing and mature rat heart. *Anat. Embryol.* **185**, 363-378.

Gourdie, R.G., Green, C.R., Severs, N.J., Anderson, R.H., Thompson, R.P. (1993) Evidence for a distinct gap-junctional phenotype in ventricular conduction tissue of the developing and mature avian heart. *Circ. Res.* **72**, 278-289.

Granger, B.L., Lazarides, E. (1979) Desmin and vimentin coexist at the periphery of the myofibril Z-disc. *Cell* **18**, 1253-1268.

Green, C.R. (1988) Evidence mounts for the role of gap junctions during development. *BioEssays* **8**, 7-10.

Green, C.R., Peters, N.S., Gourdie, R.G., Rothery, S., Severs, N.J. (1993) Validation of immunohistochemical quantification in confocal scanning laser microscopy: a comparative assessment of gap junction size with confocal and ultrastructural techniques. *J. Histochem. Cytochem.* **41**, 1339-1349.

Green, C.R., Severs, N.J. (1984a) Connexon rearrangement in cardiac gap junctions: evidence for cytoskeletal control? *Cell Tissue Res.* **237**, 185-186.

Green, C.R., Severs, N.J. (1984b) Gap junction connexon configuration in rapidly frozen myocardium and isolated intercalated disks. *J. Cell Biol.* **99**, 453-463.

Gros, D., Mocquard, J.P., Challice, C.E., Schrevel, J. (1978) Formation and growth of gap junctions in mouse myocardium during ontogenesis: a freeze-cleave study. *J. Cell Sci.* **30**, 45-61.

Gros, D., Mocquard, J.P., Challice, C.E., Shrevel, J. (1979) Formation and growth of gap junctions in mouse myocardium during ontogenesis: Quantitative data and their implications on the development of intercellular communications. *J. Mol. Cell. Cardiol.* **11**, 543-554.

Guiraudon, C.M., Guiraudon, G.M., Klein, G.J. (1988) "Nodal ventricular" Mahaim pathway: histologic evidence for an accessory atrioventricular pathway with an AV node-like morphology. *Circulation* **78(suppl. II)**, II-40.

Gustafson, R.A., Murray, G.F., Warden, H.E., Hill, R.C., Rozar, J (1988) Early primary repair of tetralogy of Fallot. *Ann. Thorac. Surg.* **45**, 235-241.

Guthrie, S.C., Gilula, N.B. (1989) Gap-junctional communication and development. *Trends Neuro. Sci.* **12**, 12-16.

Gülch, R.W. (1980) Alterations in excitation of mammalian myocardium as a function of chronic loading and their implications in the mechanical events. *Basic Res. Cardiol.* **75**, 73-80.

Han, J. (1971) The concepts of reentrant activity responsible for ectopic rhythms. *Am. J. Cardiol.* **28**, 253-262.

Harding, S.E., O'Gara, P., Jones, S.M., Brown, L.A., Vescovo, G., Poole-Wilson, P.A. (1990) Species dependence of contraction velocity in single isolated cardiac myocytes. *Cardioscience* **1**, 49-53.

Harding, S.E., MacLeod, K.T., Jones, S.M., Vescovo, G., Poole-Wilson, P.A. (1991) Contractile responses of myocytes isolated from patients with cardiomyopathy. *Eur. Heart J.* **12 (Suppl.D)**, 44-48.

Harfst, E., Gourdie, R.G., Severs, N.J., Green, C.R., Powell, T. (1988) Gap junctions from rabbit heart and dissociated myocytes — development of detergent-free isolation methods. *J. Mol. Cell. Cardiol.* **20(Suppl.5)**, S77.(Abstract)

Harfst, E., Severs, N.J., Green, C.R. (1990) Cardiac myocyte gap junctions: evidence for a major connexon protein with an apparent relative molecular mass of 70,000. *J. Cell Sci.* **96**, 591-604.

Harlow, E., Lane, D. (1988) *Antibodies: a laboratory manual.* pp. 1-726. Cold Spring Harbor, New York.

Harris, A.L., Spray, D.C., Bennett, M.V.L. (1983) Control of intercellular communication by voltage dependence of gap junctional conductance. *J. Neurosci.* **3**, 79-100.

Hellam, D.C., Studt, T.W. (1974) A core conductor model of the cardiac Purkinje fibre based on structural analysis. *J. Physiol.* **243**, 637-660.

Heller, G.V., Ahmed, I., Tilkemeier, P.L., Barbour, M.M., Garber, C.E. (1991) Comparison of chest pain, electrocardiographic changes and Thallium-201 scintigraphy during varying exercise intensities in men with stable angina pectoris. *Am. J. Cardiol.* **68**, 569-574.

Hiramatsu, Y., Buchanan, J.W., Knisley, S.B., Gettes, L.S. (1988) Rate-dependent effects of hypoxia on internal longitudinal resistance in guinea pig papillary muscles. *Circ. Res.* **63**, 923-939.

Hoffman, B.F., Dangman, K.H. (1987) Review. Mechanisms for cardiac arrhythmias. *Experientia* **43**, 1049-1056.

Hoffman, B.F., Rosen, M.R. (1982) Cellular mechanisms for cardiac arrhythmias. *Circ. Res.* **49**, 69-83.

Houghten, R.A. (1985) General method for the rapid solid-phase synthesis of large numbers of peptides: specificity of antigen-antibody interactions at the level of individual amino acids. *Proc. Natl. Acad. Sci. U. S. A.* **82**, 5131-5135.

Hoyt, R.H., Cohen, M.L., Saffitz, J.E. (1989) Distribution and three-dimensional structure of intercellular junctions in canine myocardium. *Circ. Res.* **64**, 563-574.

Hoyt, R.H., Cohen, M.L., Corr, P.B., Saffitz, J.E. (1990) Alterations of intercellular junctions induced by hypoxia in canine myocardium. *Am. J. Physiol. (Heart Circ. Physiol)* **258**, H1439-H1448.

Imanaga, I. (1974) Cell-to-cell diffusion of Procion yellow in sheep and calf Purkinje fibers. *J. Membr. Biol.* **16**, 381-388.

Imanaga, I. (1987) Cell-to-cell coupling studied by diffusional methods in myocardial cells. *Experientia* **43**, 1080-1083.

Inoue, S.I. (1989) Foundations of confocal scanned imaging in light microscopy. In: *The Handbook of Biological Confocal Microscopy*. Ed: J. Pawley, pp. 1-13. IMR press., Madison.

Jacobson, S.L., Piper, H.M. (1986) Cell cultures of adult cardiomyocytes as models of the myocardium. *J. Mol. Cell. Cardiol.* **18**, 661-678.

Jalife, J., Sicouri, S., Delmar, M., Michaels, D.C. (1989) Electrical uncoupling and impulse propagation in isolated sheep Purkinje fibres. *Am. J. Physiol.* **257**, H179-H189.

Janse, M.J. (1992) Reentrant Arrhythmias. In: *The Heart and Cardiovascular System*. Eds: H.A. Fozzard, E. Haber, R.B. Jennings, A.M. Katz & H.E. Morgan, pp. 2055-2094. Raven Press Ltd., New York.

Jongsma, H.J., Masson-Pévet, M., Tsjernina, L. (1987) The development of beat-rate synchronization of rat myocyte pairs in cell culture. *Basic Res. Cardiol.* **82**, 454-464.

Jongsma, H.J. (1993) Gap junctions: mediators of synchronisation and conduction of the cardiac impulse. In: *Proceedings XXXII Congress of the International Union of Physiological Sciences*. pp. 77. Glasgow.

Jongsma, H.J., Gros, D. (1991) The cardiac connection. *News Physiol. Sci.* **6**, 34-40.

Josephson, M.E. (1992) Electrophysiologic investigation: general concepts. In: *Clinical Cardiac Electrophysiology: Techniques and Interpretations*. Ed: M.E. Josephson, pp. 22-70. Lea & Febiger, New York.

Joyner, R.W. (1982) Effects of the discrete pattern of electrical coupling on propagation through an electrical syncytium. *Circ. Res.* **50**, 192-200.

Joyner, R.W. (1986) Modulation of repolarisation by electrotonic interactions. *Jpn. Heart. J.* **27**, 167-183.

Kadish, A.H., Spear, J.F., Levine, J.H., Moore, E.N. (1986) The effects of procainamide on conduction in anisotropic canine ventricular myocardium. *Circulation* **74**, 616-625.

Kannel, B. (1983) Prevalence and natural history of electrocardiographic left ventricular hypertrophy. *Am. J. Med.* **75(suppl)**, 4-11.

Kanter, H.L., Saffitz, J.E., Beyer, E.C. (1992) Cardiac myocytes express multiple gap junction proteins. *Circ. Res.* **70**, 438-444.

Kaufman, T.M., Horton, J.W., White, D.J., Mahony, L. (1990) Age-related changes in myocardial relaxation and sarcoplasmic reticulum function. *Am. J. Physiol. (Heart Circ. Physiol)* **259**, H309-H316.

Kawamura, K., Hayashi, K., Maekawa, M. (1964) Electron microscopy of myocardial fibrosis of unknown aetiology. In: *Proceedings of the 3rd Asian-Pacific Congress of Cardiology*. pp. 136-140. Kyoto, Japan.

Kawamura, K., Mitsui, H., Hayashi, K., Nohara, Y., Takayasu, M., Higasa, Y., Koie, H., Tsushimi, K., Abe, H. (1969) Electron microscopic studies of the human heart. III. The left atrial myocardium in mitral valvular disease. *Jpn. Circ. J.* **33**, 1141.(Abstract)

Kent, A.F.S. (1893) Researches on the structure and function of mammalian heart. *J. Physiol.* **14**, 233-254.

Kent, A.F.S. (1913) Observations on the auriculo-ventricular junction of the mammalian heart. *J. Physiol.* **7**, 193-195.

Kieval, R.S., Spear, J.F., Moore, E.N. (1992) Gap-junctional conductance in ventricular myocyte pairs isolated from postischemic rabbit myocardium. *Circ. Res.* **71**, 127-136.

Kirklin, J.K., Blackstone, E.H., Kirklin, J.W., Pacifico, A.D., Bargeron, J (1986) The Fontan operation: ventricular hypertrophy, age, and date of operation as risk factors. *J. Thorac. Cardiovasc. Surg.* **92**, 1049-1064.

Kistler, J., Christie, D., Bullivant, S. (1988) Homologies between gap junction proteins in lens, heart and liver. *Nature* **331**, 721-723.

Kleber, A.G. (1987) Review. Conduction of the impulse in the ischemic myocardium — implications for malignant ventricular arrhythmias. *Experientia* **43**, 1056-1061.

Klein, G.J., Hackel, D.B., Gallagher, J.J. (1980) Anatomic substrate of impaired antegrade conduction over an accessory atrioventricular pathway in the Wolff-Parkinson-White syndrome. *Circulation* **61**, 1249-1255.

Kléber, A.G., Riegger, C.B., Janse, M.J. (1987) Electrical uncoupling and increase of extracellular resistance after induction of ischaemia in isolated, arterially perfused rabbit papillary

muscle. *Circ. Res.* **61**, 271-279.

Kléber, A.G., Riegger, C.B. (1987) Electrical constants of arterially perfused rabbit papillary muscle. *J. Physiol.* **385**, 307-324.

Koteliansky, V.E., Shirinsky, V.P., Gneushev, G.N., Chernousov, M.A. (1985) The role of actin binding proteins vinculin, filamin, and fibronectin in intracellular and intercellular linkages in cardiac muscle. *Adv. Myocardiol.* **5**, 215-221.

Kowey, P.R., Friehling, T.D., Sewter, J., Wu, Y., Sokil, A., Paul, J., Nocella, J. (1991) Electrophysiological effects of left ventricular hypertrophy. Effet of calcium and potassium channel blockade. *Circulation* **83**, 2067-2075.

Kuo, C.S., Munakata, K., Reddy, C.P., Surawitz, B. (1983) Characteristics and possible mechanisms of ventricular arrhythmias dependent on the dispersion of action potential duration. *Circulation* **67**, 1356-1367.

Kyte, J., Doolittle, R.F. (1982) A simple method for displaying the hydropathic character of a protein. *J. Mol. Biol.* **157**, 105-132.

Laird, D.M., Puranam, K.L., Revel, J-P. (1990) Turnover and phosphorylation dynamics of connexin43 gap junction protein in cultured cardiac myocytes. *J. Cell Biol.* **111**, 155a.(Abstract)

Laks, M.L., Morady, F., Adomain, B.A., Swan, H.J.C. (1970) Presence of widened and multiple intercalated discs in the hypertrophied canine heart. *Circ. Res.* **27**, 391-401.

Lane, N.J., Swales, L.S. (1980) Dispersal of gap-junctional particles, not internalization, during the in vivo disappearance of gap junctions. *Cell* **19**, 579-586.

Langer, G.A., Brady, A.J., Tan, S.T., Serena, S.D. (1975) Correlation of the glycoside response, the force staircase, and the action potential configuration in the neonatal heart. *Circ. Res.* **36**, 744-752.

Larsen, W.J., Risinger, M.A. (1985) The dynamic life histories of intercellular membrane junctions. *Modern Cell Biology* **4**, 151-216.

Lesh, M.D., Pring, M., Spear, J.F. (1989) Cellular uncoupling can unmask dispersion of action potential duration in ventricular myocardium. *Circ. Res.* **65**, 1426-1440.

Levine, J.H., Moore, E.N., Weisman, H.F., Kadish, A.H., Becker, L.C., Spear, J.F. (1987) Depression of action potential characteristics and a decreased space constant are present in postischemic, reperfused myocardium. *J. Clin. Invest.* **79**, 107-116.

Lloyd, T.R., Baldwin, H.S. (1990) Emulation of conduction system functions in the hearts of early mammalian embryos. *Pediatr. Res.* **28**, 425-428.

Lochner, A., Sanan, D., Victor, J., Bester, R., Kotze, J.C.N., Van de Merwe, N., Schabort, I. (1986) Mitochondrial and sarcolemmal function and composition in myocardial ischaemia. *J. Mol. Cell. Cardiol.* **18(suppl.1)**, 344.

Loewenstein, W.R. (1981) Junctional intercellular communication: The cell-to-cell membrane channel. *Physiol. Rev.* **61**, 829-913.

Losay, J., Touchot-Kone, A., Bruniaux, J., Serraf, A., Lacour-Gayet, F., Planche, C., Binet, J.P. (1992) Immediate and medium term results of surgery for aortic stenosis in the neonatal period. *Arch. Mal. Coeur* **85**, 567-571.

Luke, R.A., Beyer, E.C., Hoyt, R.H., Saffitz, J.E. (1989a) Quantitative analysis of intercellular connections by immunohistochemistry of the cardiac gap junction protein connexin43. *Circ. Res.* **65**, 1450-1457.

Luke, R.A., Hoyt, R.H., Tolley, T.K., Saffitz, J.E. (1989b) Altered myocyte gap junction distribution in regions bordering healed infarcts. *Circulation* **80 II**, 499.

Luke, R.A., Saffitz, J.E. (1991) Remodeling of ventricular conduction pathways in healed canine infarct border zones. *J. Clin. Invest.* **87**, 1594-1602.

Maher, P.A., Cox, G.F., Singer, S.J. (1985) Zeugmatin: a new high molecular weight protein asssociated with Z-lines in adult and early embryonic striated muscle. *J. Cell Biol.* **101**, 1871-1883.

Makowski, L., Casper, D.L.D., Philips, W.C., Goodenough, D.A. (1977) Gap junction structures. II. Analysis of the X-ray diffraction data. *J. Cell Biol.* **74**, 629-645.

Makowski, L. (1988) X-ray diffraction studies of gap junction structure. *Advances Cell Biol.* **2**, 119-158.

Manjunath, C.K., Goings, G.E., Page, E. (1984) Detergent sensitivity and splitting of isolated liver gap junctions. *J. Membr. Biol.* **78**, 147-155.

Manjunath, C.K., Goings, G.E., Page, E. (1987) Human cardiac gap junctions: isolation, ultrastructure and protein composition. *J. Mol. Cell. Cardiol.* **19**, 131-134.

Manjunath, C.K., Page, E. (1985) Cell biology and protein composition of cardiac gap junctions. *Am. J. Physiol.* **248**, H783-H791.

Manjunath, C.K., Page, E. (1986) Rat heart gap junctions as disulphide-bonded connexon multimers: their depolymerization and solubilization in deoxycholate. *J. Membr. Biol.* **90**, 43-57.

Mankad, P.S., Severs, N.J., Lachno, D.R., Rothery, S., Yacoub, M.H. (1992) Superior qualities of University of Wisconsin solution for ex vivo preservation of the pig heart. *J. Thorac. Cardiovasc. Surg.* **104**, 229-240.

Matter, A. (1973) A morphometric study on the nexus of cardiac muscle. *J. Cell Biol.* **56**, 690-696.

Mazet, F., Wittenberg, B.A., Spray, D.C. (1985) Fate of intercellular junctions in isolated adult rat cardiac cells. *Circ. Res.* **56**, 195-204.

McCallister, L.P., Trapukdis, S., Neely, J.R. (1979) Morphometric observations on the effects of ischemia in the isolated perfused rat heart. *J. Mol. Cell. Cardiol.* **11**, 619-630.

McNutt, N.S. (1970) Ultrastructure of intercellular junctions in adult and developing cardiac muscle. *Am. J. Cardiol.* **25**, 169-183.

Mehra, R., Zeiler, R.H., Gough, W.B., El-Sharif, N. (1983) Reentrant ventricular arrhythmias in the late myocardial infarction period: 9. Electrophysiologic-anatomic correlation of reentrant circuits. *Circulation* **67**, 11-24.

Mehta, P., Bertram, J., Loewenstein, W.R. (1986) Growth inhibition of transformed cells correlates with junctional communication with normal cells. *Cell* **44**, 187-196.

Milks, L.C., Kumar, N.M., Houghten, R., Unwin, N., Gilula, N.B. (1988) Topology of the 32-kd liver gap junction protein determined by site-directed antibody localizations. *EMBO J.* **7**, 2967-2975.

Mines, G.R. (1914) On circulating excitations in heart muscles and their possible relation to tachycardia and fibrillation. *Trans. Roy. Soc. Cardiol.* **46**, 349-383.

Moreno, A.P., Eghbali, B., Spray, D.C. (1990) Voltage dependence of gap junction channels in cells stably transfected with connexin32 (Cx32) cDNA. *Biophys. J.* **57**, 243a.(Abstract)

Moreno, A.P., Eghbali, B., Spray, D.C. (1991a) Connexin32 gap junction channels in stably transfected cells. Equilibrium and kinetic properties. *Biophys. J.* **60**, 1267-1277.

Moreno, A.P., Eghbali, B., Spray, D.C. (1991b) Connexin32 gap junction channels in stably transfected cells: Unitary conductance. *Biophys. J.* **60**, 1254-1266.

Morré, D.J., Kartenbeck, J., Franke, W.W. (1979) Membrane flow and interconversions among endomembranes. *Biochim. Biophys. Acta* **559**, 71-152.

Mueller, T.M., Marcus, M.L., Ehrhardt, J.C., Chaudhuri, T., Abboud, F.M. (1976) Limitations of Thallium-201 myocardial perfusion scintigrams. *Circulation* **54**, 640-646.

Navaratnam, V., Kaufman, M.H., Skepper, J.N., Barton, S., Guttridge, K.M. (1986) Differentiation of the myocardial rudiment of mouse embryos: an ultrastructural study including freeze-fracture replication. *J. Anat.* **146**, 65-85.

Navaratnam, V. (1987) *Heart muscle: ultrastructural studies*. Cambridge University Press, Cambridge.

Neyton, J., Trautmann, A. (1985) Single-channel currents of an intercellular junction. *Nature* **317**, 331-335.

Neyton, J., Trautmann, A. (1986) Acetylcholine modulation of the conductance of intercellular junctions between rat lacrimal cells. *J. Physiol.* **377**, 283-295.

Nishimura, S., Mahmarian, J.J., Boyce, T.M., Verani, M.S. (1991) Quantitative Thallium-201 single-photon emission computed tomography during maximal pharmacologic coronary vasodilation with adenosine for assessing coronary artery disease. *J. Am. Coll. Cardiol.* **18**, 736-745.

Noma, A., Tsuboi, N. (1986) Dependence of junctional conductance on proton, calcium and magnesium ions in cardiac paired cells of Guinea pig. *J. Physiol.* **382**, 193-210.

Norwood, W.I., Dobell, A.R., Freed, M.D., Kirklin, J.W., Blackstone, E.H. (1988) Intermediate results of the arterial switch repair. *J. Thorac. Cardiovasc. Surg.* **96**, 854-863.

Oosthoek, P.W., Gros, D., Mijnders, T.A.M., Wessels, A., Vermeulen, J.L.M., Moorman, A.F.M., Lamers, W.H. (1990) Distribution of gap junctions in the human neonatal heart. (abstract). *Cell Biol. Int. Rep.* **14(suppl)**, 222.

Oosthoek, P.W., Van Kempen, M.J.A., Wessels, A., Lamers, W.H., Moorman, A.F.M. (1993) Distribution of the cardiac gap junction protein, connexin 43, in the neonatal and adult human heart. In: *Muscle and Motility. Vol.2.* pp. 85-90. Proceedings of XIXth European Conference in Brussels.

Öhnell, R.F. (1944) Preexcitation, a cardiac abnormality. *Acta Med. Scand.* **152**, 1-167.

Page, E. (1978) Quantitative ultrastructural analysis in cardiac membrane physiology. *Am. J. Physiol.* **235**, C147-C158.

Page, E. (1992) Cardiac Gap Junctions. In: *The Heart and Cardiovascular System.* Eds: H.A. Fozzard, E. Haber, R.B. Jennings, A.M. Katz & H.E. Morgan, pp. 1003-1048. Raven Press Ltd., New York.

Paul, D.L. (1986) Molecular cloning of cDNA for rat liver gap junction protein. *J. Cell Biol.* **103**, 123-134.

Pepper, J.R., Lockey, E., Cankovic-Darracott, S., Braimbridge, M.V. (1982) Cardioplegia versus intermittent ischaemic arrest in coronary bypass surgery. *Thorax* **37**, 887-892.

Peracchia, C. (1980) Structural correlates of gap junction permeation. *Int. Rev. Cytol.* **66**, 81-146.

Peters, N.S., Green, C.R., Poole-Wilson, P.A., Severs, N.J. (1993) Reduced content of connexin43 gap junctions in ventricular myocardium from hypertrophied and ischaemic human hearts. *Circulation* **88**, 864-875.

Pinto da Silva, P. (1987) Topology, dynamics and molecular cytochemistry of integral membrane proteins: a freeze-fracture view. In: *Electron Microscopy of Proteins. Volume 6. Membranous Structures.* Eds: J.R. Harris & R.W. Horne, pp. 1-39. Academic Press, London.

Poche, R. (1958) Submikroskopische Beiträge zur Pathologie der Herzmuskelzelle bei Phosphorvergiftung, Hypertrophie, Atrophie und Kaliummangel. *Virchows Archiv für Patholgische Anatomie und Physiologie und für klinische Medizin und Histopathologie* **331**, 165-248.

Poche, R., Ohm, H.G. (1963) Lichtmikroskopische, histochemische und elektronenmikroskopische Untersuchungen des Herzmuskels vom Menschen nach induziertem Herzstillstand. *Archiv für Kreislaufforschung; Beihefte zur Zeitschrift für Kreislaufforschung* **41**, 86-135.

Pogwizd, S.M., Hoyt, R.H., Saffitz, J.E., Corr, P.B., Cox, J.L., Cain, M.E. (1992) Reentrant and focal mechanisms underlying ventricular tachycardia in the human heart. *Circulation* **86**, 1872-1887.

Prod'hom, B., Pietrobon, D., Hess, P. (1987) Direct measurement of proton transfer rates to a group controlling the dihydropyridine-sensitive Ca^{2+} channel. *Nature* **329**, 243-246.

Pye, P.P., Cobbe, S.M. (1992) Mechanisms of ventricular arrhythmias in cardiac failure and hypertrophy. *Cardiovasc. Res.* **26**, 740-750.

Quan, W., Rudy, Y. (1990) Unidirectional block and reentry of cardiac excitation: a model study. *Circ. Res.* **66**, 367-382.

Quantk, M., Tchervenkov, C., Chiu, R.C-J. (1992) Unique responses of immature hearts to ischemia. *J. Thorac. Cardiovasc. Surg.* **103**, 927-935.

Rash, J.E., Hudson, C.S. (1979) *Freeze-fracture. Methods, artifacts and interpretation.* Raven Press, New York.

Reimer, K.A., Jennings, R.B. (1992) Myocardial ischemia, hypoxia, and infarction. In: *The Heart and Cardiovascular System: Scientific Foundations.* Eds: H.A. Fozzard, R.B. Jennings, E.

Haber, A.M. Katz & H.E. Morgan, pp. 1875-1973. Raven Press, New York.

Revel, J-P., Karnovsky, M.J. (1967) Hexagonal array of subunits in intercellular junctions of the mouse heart and liver. *J. Cell Biol.* **33**, C7-C12.

Richter, G.W. (1974) Ultrastructure of hypertrophied heart muscle in relation to adaptive tissue growth. *Circ. Res.* **34(supplII)**, II-27-II-32.

Rook, M.B., Jongsma, H.J., Van Ginneken, A.C.G. (1988) Properties of single gap junctional channels between isolated neonatal rat heart cells. *Am. J. Physiol. (Heart Circ. Physiol)* **255**, H770-H782.

Rosen, M.R., Legato, M.J., Weiss, R.M. (1981) Developmental changes in impulse conduction in the canine heart. *Am. J. Physiol. (Heart Circ. Physiol)* **240**, H546-H554.

Rüdisüli, A., Weingart, R. (1989) Electrical properties of gap junction channels in guinea-pig ventricular cell pairs revealed by exposure to heptanol. *Pflugers Arch.* **415**, 12-21.

Saffitz, J.E., Hoyt, R.H., Luke, R.A., Kanter, H.L., Beyer, E.C. (1992) Cardiac myocyte interconnections at gap junctions - role in normal and abnormal electrical conduction. *Trends Cardiovasc. Med.* **2**, 56-60.

Saffitz, J.E., Corr, P.B., Sobel, B.E. (1993) Arrhythmogenesis and ventricular dysfunction after myocardial infarction. Is anomalous cellular coupling the elusive link? *Circulation* **87**, 1742-1745.

Sáez, J.C., Nairn, A.C., Spray, D.C., Czernik, A.J., Hertzberg, E.L. (1990) Protein Kinase C-dependent regulation of heart connexin43. *J. Cell Biol.* **111**, 154a.(Abstract)

Schaper, J., Mulch, J., Winkler, B., Schaper, W. (1979) Ultrastructural, functional, and biochemical criteria for estimation of reversibility of ischemic injury. A study on the effects of global ischemia on the isolated dog heart. *J. Mol. Cell. Cardiol.* **11**, 521-541.

Severs, N.J., Slade, A.M., Powell, T., Twist, V.W., Jones, G.E. (1985) Morphometric analysis of the isolated calcium-tolerant cardiac myocyte: organelle volumes, sarcomere length, plasma membrane surface folds and intramembrane particle density and distribution. *Cell Tissue Res.* **240**, 159-168.

Severs, N.J. (1989a) Gap junction shape and orientation at the cardiac intercalated disk. *Circ. Res.* **65**, 1458-1461.

Severs, N.J. (1989b) Constituent cells of the heart and isolated cell models in cardiovascular research. In: *Isolated Adult Cardiomyocytes. volume 1.* Eds: H.M. Piper & G. Isenberg, pp. 3-41. CRC Press Inc., Boca Raton.

Severs, N.J., Shovel, K.S., Slade, A.M., Powell, T., Twist, V.W., Green, C.R. (1989) Fate of gap junctions in isolated adult mammalian cardiomyocytes. *Circ. Res.* **65**, 22-42.

Severs, N.J. (1990) Review. The cardiac gap junction and intercalated disc. *Int. J. Cardiol.* **26**, 137-173.

Severs, N.J., Slade, A.M., Powell, T., Twist, V.W., Green, C.R. (1990) Integrity of the dissociated adult cardiac myocyte: gap junction tearing and the mechanism of plasma membrane resealing. *J. Muscle Res. Cell Motil.* **11**, 154-166.

Severs, N.J., Gourdie, R.G., Harfst, E., Peters, N.S., Green, C.R. (1993) Review. Intercellular junctions and the application of microscopical techniques: the cardiac gap junction as a case

model. *J. Microsc.* **169**, 299-328.

Severs, N.J., Green, C.R. (1983) Rapid freezing of unpretreated tissues for freeze-fracture electron microscopy. *Biol. Cell* **47**, 193-204.

Severs, N.J., Hicks, R.M. (1979) Analysis of membrane structure in the transitional epithelium of rat urinary bladder. 2. The discoidal vesicles and Golgi apparatus: their role in luminal membrane biogenesis. *J. Ultrastruct. Res.* **69**, 279-296.

Shibata, Y., Nakata, K., Page, E. (1980) Ultrastructural changes during development of gap junctions in rabbit left ventricular myocardial cells. *J. Ultrastruct. Res.* **71**, 258-271.

Shibata, Y., Page, E. (1981) Gap junctional structure in intact and cut sheep cardiac Purkinje fibers: a freeze-fracture study of Ca^{2+} -induced resealing. *J. Ultrastruct. Res.* **75**, 195-204.

Sjöstrand, F.S., Andersson, E. (1954) Electron microscopy of the intercalated discs of cardiac muscle tissue. *Experientia* **9**, 369-371.

Slot, J.W., Geuze, H.J. (1984) Gold markers for single and double labeling of ultrathin cryosections. In: *Immunolabelling for Electron Microscopy*. Eds: J.M. Polak & I.M. Varndell, pp. 129. Elsevier Science Publishers, Amsterdam.

Smith, J.H., Green, C.R., Peters, N.S., Rothery, S., Severs, N.J. (1991) Altered patterns of gap junction distribution in ischemic heart disease. An immunohistochemical study of human myocardium using laser scanning confocal microscopy. *Am. J. Pathol.* **139**, 801-821.

Smith, S.H., McCaslin, M., Sreenan, C., Bishop, S.P. (1988) Regional myocyte size in two-kidney, one clip renal hypertension. *J. Mol. Cell. Cardiol.* **20**, 1035-1042.

Socolar, S.J., Loewenstein, W.R. (1979) Methods of studying transmission through permeable cell-to-cell channels. In: *Methods in Membrane Biology*. Ed: E.D. Korn, pp. 123-179. Plenum Press, New York.

Sommer, J.R., Jennings, R.B. (1986) Ultrastructure of cardiac muscle. In: *The heart and cardiovascular system*. Eds: H.A. Fozzard, E. Haber, R.B. Jennings, A.M. Katz & H.E. Morgan, pp. 61-100. Raven Press, New York.

Sommer, J.R., Scherer, B. (1985) Geometry of cell and bundle appositions in cardiac muscle: light microscopy. *Am. J. Physiol.* **248**, H792-H803.

Spach, M.S., Kootsey, J.M., Sloan, J.D. (1982a) Active modulation of electrical coupling between cardiac cells of the dog: a mechanism for transient and steady state variations in conduction velocity. *Circ. Res.* **51**, 347-362.

Spach, M.S., Miller, W.T.,III, Dolber, P.C., Kootsey, J.M., Sommer, J.R., Mosher, C.E.,Jr. (1982b) The functional role of structural complexities in the propagation of depolarization in the atrium of the dog. Cardiac conduction disturbances due to discontinuities of effective axial resistivity. *Circ. Res.* **50**, 175-191.

Spach, M.S., Dolber, P.C., Heidlage, J.F. (1988) Interactive roles of inhomogeneities of repolarisation and anisotropic propagation in atrial reentry. *Circulation* **78(supplII)**, II-413.

Spach, M.S., Dolber, P.C. (1986) Relating extracellular potentials and their derivatives to anisotropic propagation at a microscopic level in human cardiac muscle. *Circ. Res.* **58**, 356-371.

Spear, J.F., Michelson, E.L., Moore, E.N. (1983) Cellular electrophysiologic characteristics of

chronically infarcted myocardium in dogs susceptible to sustained ventricular tachyarrhythmias. *J. Am. Coll. Cardiol.* **1**, 1099-1110.

Sperelakis, N. (1979) Propagation mechanisms in the heart. *Annu. Rev. Physiol.* **41**, 441-457.

Spira, A.W. (1971) The nexuses in the intercalated disc of the canine heart: quantitative data for an estimation of its resistance. *J. Ultrastruct. Res.* **34**, 409-425.

Spray, D.C., White, R.L., Mazet, F., Bennett, M.V.L. (1985) Regulation of gap junctional conductance. *Am. J. Physiol. (Heart Circ. Physiol)* **248**, H753-H764.

Spray, D.C., Moreno, A.P., Eghbali, B., Chanson, M., Fishman, G.I. (1992) Gating of gap junction channels as revealed in cells stably transfected with wild type and mutant connexin cDNAs. *Biophys. J.* **62**, 48-50.

Spray, D.C., Sáez, J.C., Burt, J.M., Watanabe, T., Reid, L.M., Hertzberg, E.L., Bennett, M.V.L. (1993) Gap junctional conductance: Multiple sites of regulation. In: *Modern Cell Biology. vol.7. :Gap Junctions*. Eds: E.L. Hertzberg & R.G. Johnson, pp. 227-244. Alan R. Liss, New York.

Spray, D.C., Burt, J.M. (1990) Structure-activity relations of the cardiac gap junction channel. *Am. J. Physiol.* **258**, C195-C205.

St.John Sutton, M, Marier, D, Oldershaw, P, Sacchetti, R., Gibson, D (1982) Effect of age-related changes in chamber size, wall thickness, and heart rate on left ventricular function in normal children. *Br. Heart J.* **48**, 342-351.

Stewart, J.M., Page, E. (1978) Improved stereological techniques for studying myocardial cell growth: application to external sarcolemma, T-system, and intercalated discs of rabbit and rat hearts. *J. Ultrastruct. Res.* **65**, 119-134.

Sugiura, H., Toyama, J., Tsuboi, N., Kamiya, K., Kodama, I. (1990) ATP directly affects junctional conductance between paired ventricular myocytes isolated from guinea pig hearts. *Circ. Res.* **66**, 1095-1102.

Sulkin, M.N., Sulkin, D.F. (1965) An electron microscopic study of the effects of chronic hypoxia on cardiac muscle, hepatic and autonomic ganglion cells. *Lab. Invest.* **14**, 1523-1546.

Sun, S.C., Sohal, R.S., Burch, G.E., Chu, K.C., Colcolough, H.L. (1967) Coxsackie virus B_4 pancarditis in cynomolgus monkeys resembling rheumatic heart lesions. *Br. J. Exp. Pathol.* **48**, 655-661.

Sutton, J.M., Topol, E.J. (1991) Significance of a negative exercise Thallium test in the presence of a critical residual stenosis after thrombolysis for acute myocardial infarction. *Circulation* **83**, 1278-1286.

Swynghedauw, B. (1991) Remodeling of the heart in chronic pressure overload. *Basic Res. Cardiol.* **86 (suppl. I)**, 99-105.

Takeichi, M. (1990) Cadherins: a molecular family important in selective cell-cell adhesion. *Annu. Rev. Biochem.* **59**, 237-252.

TenEick, R.E., Houser, S.R., Bassett, A.L. (1989) Cardiac hypertrophy and altered cellular electrical activity of the myocardium: possible electrophysiological basis for myocardial contractility changes. In: *Physiology and Pathophysiology of the Heart*. Ed: N. Sperelakis, pp. 573-593. Kluwer Academic Publishers,

Tibbitts, T.T., Casper, D.L.D., Phillips, W.C., Goodenough, D.A. (1990) Diffraction diagnosis of protein folding in gap junction connexons. *Biophys. J.* **57**, 1025-1036.

Toshimori, H., Toshimori, K., Oura, C., Matsuo, H. (1987) Immunohistochemistry and immunocytochemistry of natriuretic polypeptide in porcine heart. *Histochemistry* **86**, 595-601.

Tritthart, H., Luedcke, H., Bayer, R., Stierle, H., Kaufmann, R. (1975) Right ventricular hypertrophy in the cat - an electrophysiological and anatomical study. *J. Mol. Cell. Cardiol.* **7**, 163-174.

Tsuboi, N., Kodama, I., Toyama, J., Yamada, K. (1985) Anisotropic conduction properties of canine ventricular muscles. Influence of high extracellular K^+ concentration and stimulation frequency. *Jpn. Circ. J.* **49**, 487-498.

Turin, L., Warner, A. (1993) Carbon dioxide reversibly abolishes ionic communication between cells of early amphibian embryo. *Nature* **270**, 56-69.

Unwin, P.N.T., Ennis, P.D. (1984) Two configurations of a channel-forming membrane protein. *Nature* **307**, 609-613.

Ursell, P.C., Gardner, P.I., Albala, A., Fenoglio, J.J., Wit, A.L. (1985) Structural and electrophysiological changes in the epicardial border zone of canine myocardial infarcts during infarct healing. *Circ. Res.* **56**, 436-451.

Van Hare, G.F., Hawkins, J.A., Schmidt, K.G., Rudolph, A.M. (1990) The effects of increasing mean arterial pressure on left ventricular output in newborn lambs. *Circ. Res.* **67**, 78-83.

Van Kempen, M.J.A., Fromaget, C., Gros, D., Moorman, A.F.M., Lamers, W.H. (1991) Spatial distribution of connexin43, the major cardiac gap junction protein, in the developing and adult rat heart. *Circ. Res.* **68**, 1638-1651.

Veenstra, R.D. (1990) Voltage-dependent gating of gap junction channels in embryonic chick ventricular cell pairs. *Am. J. Physiol. (Cell Physiol.)* **258**, C662-C672.

Veenstra, R.D. (1991) Comparative physiology of cardiac gap junction channels. In: *The Biophysics of Gap Junctions*. Ed: C. Peracchia, pp. 131-144. CRC Press, Boca Raton, Florida.

Veenstra, R.D., Wang, H.-Z., Westphale, E.M., Beyer, E.C. (1992) Multiple connexins confer distinct regulatory and conductance properties of gap junctions in developing heart. *Circ. Res.* **71**, 1277-1283.

Veenstra, R.D., Wang, H.-Z., Beyer, E.C., Brink, P.R. (1993) Differential permeability of connexin-specific gap junctions to fluorescent tracers. *Biophys. J.* **64**, A235.(Abstract)

Veenstra, R.D., DeHaan, R.L. (1988) Cardiac gap junction channel activity in embryonic chick ventricular cells. *Am. J. Physiol. (Heart Circ. Physiol)* **254**, H170-H180.

Verduyn Lunel, A.A. (1972) Significance of annulus fibrosus of heart in relation to AV conduction and ventricular activation in cases of Wolff-Parkinson-White syndrome. *Br. Heart J.* **34**, 1267-1271.

Viragh, S., Challice, C.E. (1973) The impulse generation and conduction system of the heart. ED -Challice,C.E. In: *Ultrastructure of the mammalian heart*. Ed: S. Viragh, pp. 43-89. Academic Press, London.

Volk, T., Geiger, B. (1986) A-CAM: a 135kD receptor of intercellular adherens junctions. I. Immunoelectron microscopic localization and biochemical studies. *J. Cell Biol.* **103**, 1441-1450.

Wackers, F.J., Sokole, E.B., Samson, G., van der Schoot, J.B., Lie, K.I., Liem, K.L., Wellens, H.J.J. (1976) Value and limitations of Thallium-201 scintigraphy in the acute phase of myocardial infarction. *N. Engl. J. Med.* **295**, 1-5.

Walsh, E.P., Rockenmacher, S., Keane, J.F., Hougen, J.T., Lock, J.E., Castaneda, A.R. (1988) Late results in patients with tetralogy of Fallot repaired during infancy. *Circulation* **77**, 1062-1067.

Warner, A.E., Guthrie, S.C., Gilula, N.B. (1984) Antibodies to gap-junctional protein selectively disrupt junctional communication in early embryos. *Nature* **322**, 127-131.

Weidmann, S. (1952) The electrical constants of Purkinje fibres. *J. Physiol. (Lond.)* **118**, 348-360.

Weingart, R. (1986) Electrical properties of the nexal membrane studied in rat ventricular cell pairs. *J. Physiol.* **370**, 267-284.

Weingart, R., Maurer, P. (1987) Cell-to-cell coupling studied in isolated ventricular cell pairs. *Experientia* **43**, 1091-1094.

Weingart, R., Maurer, P. (1988) Action potential transfer in cell pairs isolated from adult rat and guinea pig ventricles. *Circ. Res.* **63**, 72-80.

Wells, K.S., Sandison, D.R., Strickler, J., Webb, W.W. (1989) Quantitative fluorescence imaging with laser scanning confocal microscopy. In: *The Handbook of Biological Confocal Microscopy*. Ed: J. Pawley, pp. 23-35. IMR press, Madison.

White, J.G., Amos, W.B., Fordham, M. (1987) An evaluation of confocal versus conventional imaging of biological structure by fluorescence light microscopy. *J. Cell Biol.* **105**, 41-48.

White, R.L., Spray, D.C., Campos De Carvalho, A.C., Wittenberg, B.A., Bennett, M.V.L. (1985) Some electrical and pharmacological properties of gap junctions between adult ventricular myocytes. *Am. J. Physiol.* **249**, C447-C455.

Wibo, M., Bravo, G., Godfraind, T. (1991) Postnatal maturation of excitation-contraction coupling in rat ventricle in relation to the subcellular localization and surface density of 1,4-dihydropyridine and ryanodine receptors. *Circ. Res.* **68**, 662-673.

Wit, A.L. (1989) Anisotropic reentry: A model of arrhythmias that may necessitate a new approach to anti-arrhythmic drug development. In: *Lethal Arrhythmias Resulting From Myocardial Ischemia and Infarction*. Eds: M.R. Rosen & Y. Palti, pp. 199-213. Kluwer Academic Publishers, Norwell, Mass.

Wit, A.L., Janse, M.J. (1992) Basic mechanisms of arrhythmias. In: *The Ventricular Arrhythmias of Ischemia and Infarction*. pp. 1-160. Futura, New York.

Wood, F.C., Wolferth, C.G., Greckler, G.D. (1943) Histologic demonstration of accessory muscular connections between auricle and ventricle in a case of short P-R interval and prolonged QRS complex. *Am. Heart J.* **25**, 454-462.

Yamaguchi, M., Yamano, S., Muguruma, M., Robson, R.M. (1988) Polarity and length of actin filaments at the fascia adherens of the cardiac intercalated disc. *J. Ultrastruct. Mol. Struct. Res.* **100**, 235-244.

Yancey, S.B, John, S.A., Lal, R., Austin, B.J., Revel, J-P. (1989) The 43-kD polypeptide of heart gap junctions: immunolocalization, topology and functional domains. *J. Cell Biol.* **108**, 2241-2254.

Yancey, S.B., Nicholson, B.J., Revel, J-P. (1981) The dynamic state of liver gap junctions. *J. Supramol. Struct.* **16**, 221-232.

Yasui, H., Kado, H., Yonenaga, K., Hisahara, M., Ando, H., Iwao, H., Fukuda, S., Mizoguchi, Y., Sunagawa, H. (1989) Arterial switch operation for transposition of the great arteries, with special reference to left ventricular function. *J. Thorac. Cardiovasc. Surg.* **98**, 601-610.

Ypey, D.L., Clapham, D.E., DeHaan, R.L. (1979) Development of electrical coupling and action potential synchrony between paired aggregates of embryonic heart cells. *J. Membr. Biol.* **51**, 75-96.

Zak, R. (1974) Development and proliferative capacity of cardiac muscle cells. *Circ. Res.* **34(supplII)**, II-17-II-26.

Zhang, J-T., Nicholson, B. (1989) Sequence and tissue distribution of a second protein of hepatic gap junctions, Cx26, as deduced from its cDNA. *J. Cell Biol.* **109**, 3391-3401.

Zimmer, D.B., Green, C.R., Evans, W.H., Gilula, N.B. (1987) Topological analysis of the major protein in isolated intact rat liver gap junctions and gap junction-derived single membrane structures. *J. Biol. Chem.* **262**, 7751-7763.